NASA/CR—2005-213326

Low NO_x Combustor Development

J.A. Kastl, P.V. Herberling, and J.M. Matulaitis
General Electric Aircraft Engines, Cincinnati, Ohio

February 2005

The NASA STI Program Office . . . in Profile

Since its founding, NASA has been dedicated to the advancement of aeronautics and space science. The NASA Scientific and Technical Information (STI) Program Office plays a key part in helping NASA maintain this important role.

The NASA STI Program Office is operated by Langley Research Center, the Lead Center for NASA's scientific and technical information. The NASA STI Program Office provides access to the NASA STI Database, the largest collection of aeronautical and space science STI in the world. The Program Office is also NASA's institutional mechanism for disseminating the results of its research and development activities. These results are published by NASA in the NASA STI Report Series, which includes the following report types:

- TECHNICAL PUBLICATION. Reports of completed research or a major significant phase of research that present the results of NASA programs and include extensive data or theoretical analysis. Includes compilations of significant scientific and technical data and information deemed to be of continuing reference value. NASA's counterpart of peer-reviewed formal professional papers but has less stringent limitations on manuscript length and extent of graphic presentations.

- TECHNICAL MEMORANDUM. Scientific and technical findings that are preliminary or of specialized interest, e.g., quick release reports, working papers, and bibliographies that contain minimal annotation. Does not contain extensive analysis.

- CONTRACTOR REPORT. Scientific and technical findings by NASA-sponsored contractors and grantees.

- CONFERENCE PUBLICATION. Collected papers from scientific and technical conferences, symposia, seminars, or other meetings sponsored or cosponsored by NASA.

- SPECIAL PUBLICATION. Scientific, technical, or historical information from NASA programs, projects, and missions, often concerned with subjects having substantial public interest.

- TECHNICAL TRANSLATION. English-language translations of foreign scientific and technical material pertinent to NASA's mission.

Specialized services that complement the STI Program Office's diverse offerings include creating custom thesauri, building customized databases, organizing and publishing research results . . . even providing videos.

For more information about the NASA STI Program Office, see the following:

- Access the NASA STI Program Home Page at ***http://www.sti.nasa.gov***

- E-mail your question via the Internet to help@sti.nasa.gov

- Fax your question to the NASA Access Help Desk at 301–621–0134

- Telephone the NASA Access Help Desk at 301–621–0390

- Write to:
  NASA Access Help Desk
  NASA Center for AeroSpace Information
  7121 Standard Drive
  Hanover, MD 21076

NASA/CR—2005-213326

Low NO_x Combustor Development

J.A. Kastl, P.V. Herberling, and J.M. Matulaitis
General Electric Aircraft Engines, Cincinnati, Ohio

Prepared under Contract NAS3–25951

National Aeronautics and
Space Administration

Glenn Research Center

February 2005

Document History

This research was originally published internally as HSR053 in August 1997.

Note that at the time of writing, the NASA Lewis Research Center
was undergoing a name change to the
NASA John H. Glenn Research Center at Lewis Field.
Both names may appear in this report.

Available from

NASA Center for Aerospace Information
7121 Standard Drive
Hanover, MD 21076

National Technical Information Service
5285 Port Royal Road
Springfield, VA 22100

Available electronically at http://gltrs.grc.nasa.gov

TABLE OF CONTENTS

	Page
1.0 SUMMARY	1
2.0 INTRODUCTION	2
2.1 Background	2
2.2 Scope	2
3.0 SYSTEM DESIGN STUDIES	3
3.1 Cycle Selection	3
3.2 Ground Rules For Combustor System Designs	5
3.3 Candidate Combustor Configurations	8
3.3.1 Candidate Fuel-Air Mixer Configurations	9
3.3.2 Combustor Flowpath Development	10
3.3.2.1 Swirl-Jet Premixer	11
3.3.2.2 Lean Direct Injector	11
3.3.2.3 Cyclone Swirler Premixer	12
3.3.2.4 IMFH Premixer	12
3.3.3 Comparative Evaluation of the Various Combustor Layouts	12
3.4 Design of Fuel Staging System	17
3.5 Preliminary Combustor Mechanical Design	18
3.6 Chemical Kinetics Studies	19
3.7 Initial LPP/LDI Combustor Aero Design	20
4.0 SUBCOMPONENT TESTING AND EVALUATION	23
4.1 Swirl-Jet Premixer	24
4.1.1 Evaporation Characteristics	24
4.1.2 Concert 2-D Modeling	25
4.1.3 Single-cup Testing	25
4.1.3.1 Configuration 1 and 1A Testing	25
4.1.3.2 Configuration 2A and 2B Testing	27
4.1.3.3 High Pressure Single-cup Test	28
4.2 Lean Direct Injection (LDI)	30
4.2.1 Jet Mix CONCERT 3-D Analysis Using Design of Experiments	30
4.2.2 Jet Mix Cold Flow Spray Visualization Testing	31
4.2.3 Baseline Configuration Tests	31
4.2.3.1 Pressure Testing	32
4.2.4 Fuel Atomizer Improvements	33
4.3 IMFH Premixer	34
4.3.1 IMFH Config. 4 Testing at High Inlet Temperature & Pressure	35
4.3.2 IMFH Config. 5 Testing with Spent Cooling Air Injection	38
4.3.3 IMFH Config. 6A Testing - Alternate Spent Cooling Air Injection	40
4.3.4 Config. 6B Testing - Fuel Injection at the Mixer Tube Wall	41
4.3.5 Venturi IMFH Studies	42
4.4 Cyclone Swirler Premixer	43
4.4.1 Cyclone Swirler Fuel Injector Design	43
4.4.2 Atmospheric Test of Cyclone Swirler, Configuration 1	43
4.4.3 Pressure Test of Cyclone Swirler, Configuration 1	44
4.4.4 Cyclone Swirler with Spent Cooling Air Injection, Config. 2	46
4.4.4.1 Config 2 Cyclone Swirler Tests at Low Dome Ref.Velocity	47
4.4.4.2 Config 2 Cyclone Swirler Tests at Vref = 30 ft/s	48
4.4.4.3 Config 2 Cyclone Swirler Tests in Convectively-Cooled Liner	49

TABLE OF CONTENTS (continued)

	Page
4.4.4.4 Config 2 Cyclone Swirler Tests at High Pressure	50
4.5 Multiple-Venturi Swirler Mixer (Multiple-Venturi)	52
4.5.1 Multiple Venturi Single Module Testing	52
4.6 Supporting Cold Flow Mixing Experiments At CR&D	53
4.7 Laser Diagnostics at Pennsylvania State University	54
5.0 DISCUSSION OF SUBCOMPONENT TEST RESULTS	54
5.1 Comparative Evaluation of the Flametube Results	54
5.2 Selection of the Preferred Mixer Designs for Sector Testing	55
6.0 SECTOR COMBUSTOR DESIGN	55
7.0 CONCLUSIONS	61
8.0 REFERENCES	61
9.0 FIGURES	153
10. APPENDICES	153
A. Single-Cup Test Results	177
B. GE CR&D Final Report	207
C. Pennsylvania State University Final Report	

1.0 SUMMARY

The following was accomplished during the performance of Task 5 of the Aeropropulsion Technology Contract. The goal of these efforts was the development of an ultra-low emissions, lean-burn, combustor for the High Speed Civil Transport. The HSCT Mach 2.4 FLADE C1 Cycle was selected as the baseline engine cycle. A preliminary compilation of performance requirements for the HSCT combustor system was developed. The emissions goals of the program, the baseline engine cycle, and standard combustor performance requirements were considered in developing the compilation of performance requirements. Seven combustor system designs were developed. In order to control the flame temperature within the narrow limits required for good performance of lean-burn combustors, most of these combustor systems used fuel-staging. However, one combustor system design used air-scheduling, which in turn required the use of variable geometry. The development of the these system designs was facilitated by the use of spreadsheet-type models which predicted the performance of the combustor systems over the entire flight envelope of the HSCT. These models and their performance projections were refined as more design information and test data became available. A chemical kinetic model was developed for an LPP combustor and employed to study NOx formation kinetics and CO burnout. These kinetic predictions helped to define the combustor residence time. Five fuel-air mixer concepts were analyzed for use in the combustor system designs. One of the seven system designs, one using the Swirl-Jet and Cyclone Swirler fuel-air mixers, was selected for a preliminary mechanical design study.

Five fuel-air mixers were evaluated in subcomponent tests. Four types of single-cup rigs were used: atmospheric, 4 atmosphere and high pressure. The high pressure rig operated over the full range of HSCT combustor conditions. A major design innovation which came out these tests was the injection of spent cooling air into the flow exiting the fuel-air mixers. This helped resolve the conflict over using the available air to burn as lean as possible and to use it to cool the combustor materials. Two supporting studies of fuel-air mixing using advanced laser diagnostics were performed, one at GE's Corporate Research and Development Center and the other at Pennsylvania State University.

A LPP sector combustor was designed, fabricated and built up for evaluation in a follow-on contract. The sector combustor was sized for a subscale engine and was rectangular in configuration. The system design selected for the sector combustor used the IMFH and Cyclone Swirler fuel-air mixers. In this sector combustor, fuel-staging was relied upon for flame temperature control. A preliminary test plan was developed for the sector combustor evaluation.

2.0 INTRODUCTION

A key issue in the development of the next generation High Speed Civil Transport (HSCT) is environmental acceptability. Of particular concern is that the NOx emissions from HSCT engines operating at high altitude may have detrimental effects on the stratospheric ozone layer. This concern has led to significant efforts in atmospheric modeling, combustion research and development of low NOx gas turbine combustion systems.

2.1 Background

In previous studies, three combustion system concepts have been identified which yield low emissions in laboratory-scaled experiments. They are: Lean, Premixed, Prevaporized (LPP), Lean Direct Injection (LDI) and Rich Burn/Quick Quench/Lean Burn (RQL) combustors. The principle behind LPP combustor operation is simple -- provide a uniform mixture of prevaporized fuel and air that burns at a lean fuel/air ratio so that the flame temperature is low thereby minimizing NOx production. The LPP concept has disadvantages, some of which are narrow stability limits and the potential for autoignition and/or flashback into the premixing chamber. Lean fuel/air mixtures are also used in the LDI concept, but rather than being premixed, the fuel is injected directly into the combustion zone. The LDI concept may offer improvement in stability over the LPP concept and is found to yield emission levels that are comparable to the LPP concept. With LDI, there are no hazards of flashback and/or autoignition. In the RQL combustion concept, the approach is to burn the fuel in an oxygen-deficient first stage and add the remaining air in a rapid quench zone where the overall stoichiometry is brought quickly to a lean condition without simultaneously forming excess NO. The lean zone downstream of the rapid quench zone oxidizes the CO produced in the rich zone.

2.2 Scope

The efforts pursued during the performance of this Task evaluated, developed and tested concepts for the lean-burn ultra-low NOx combustor. Concepts for both types of lean-burn combustors; the Lean, Premixed, Prevaporized (LPP) and Lean Direct Injection (LDI); were considered in these studies. The specific goal of this task was to demonstrate the capability of advanced lean burning combustor concepts to reach the emission index goal of 5 g NOx/kg fuel at HSCT cruise conditions, while also having the capability to operate successfully over the full range of combustor inlet conditions. In pursuit of this cruise emissions goal, three technical subtasks were completed:

- Subtask I consisted of combustor design studies to define the overall combustion system features needed to meet the full range of operating requirements of the HSCT, while also meeting the NOx emission goals. Six system designs were considered.

- Subtask II consisted of single-cup development tests of five premixer design approaches.

- Subtask III completed the design, fabrication and buildup of a sector combustor for demonstration of the preferred combustor concept.

3.0 SYSTEM DESIGN STUDIES

This section discusses the selection of the engine cycle for this subtask, and describes pertinent cycle points used in the design and analysis of the combustor layouts. The section continues with the ground rules for the design and comparison of the combustor layouts. The four candidate combustor layouts are then described, and an evaluation of these designs is completed, culminating in the selection of a generic combustor design. Additional analysis of the fuel staging system, a detailed mechanical design of a representative generic combustor, and an analytical study to predict combustor emission characteristics using chemical kinetics relationships are discussed. This section concludes with a discussion of proposals for the future direction of HSCT combustion system designs.

3.1 Cycle Selection

The HSCT Mach 2.4 FLADE C1 cycle was selected as the baseline cycle for this task. Cycle conditions at key mission points are shown in Table 3-1. Table 3-2 depicts a typical HSCT mission profile.

Table 3-2 HSCT Preliminary Mission Profile

Flight Condition	Altitude (kft)	Mach Number	Duration (min)
Takeoff	~0	0.00 - 0.30	Seconds
Climb	3 - 55	0.50 - 2.40	~16
Supersonic Cruise	55 - 65	2.40	~202 (68% of Total)
Descent	65 - 15	2.40 - 0.55	~20
Climb	15 - 25	0.55 - 0.80	~1
Subsonic Cruise	25 - 15	0.80 and 0.5	~56

As shown in Table 3-2, the supersonic cruise leg of the mission accounts for nearly 70% of the entire mission flight time. The supersonic leg is flown at altitudes which place it within the ozone layer. The NOx emissions at these altitudes are therefore potentially the most detrimental. Three supersonic cruise conditions are shown: maximum or start cruise (55K), mid-cruise (60K) and minimum or end cruise (65K). The combustor fuel-air ratio and combustor inlet air temperature, T_3, stay very nearly constant during the entire supersonic cruise portion of the mission. Thus, the combustor can be optimized for low NOx emissions over the entire supersonic leg of the mission. Further minimizing the impact of NOx emissions on the ozone layer is the decrease in fuel burn rate (40%) as the altitude increases from 55K to 65K. The constant combustor conditions do not continue into the subsonic cruise portion of the mission, let alone, ground and flight idle conditions. The combination of narrow operating limits for lean-burn combustion and the wide range of HSCT combustor operating conditions requires some form of fuel staging or air scheduling.

Table 3-1. APT HSCT Baseline Cycle - Mach 2.4 GE21/FLA 1 Study C1.

Power Setting	Ground Idle	Takeoff (Std Day)	Max Cruise (Start Cruise)	Mid Cruise	End (Min) Cruise	Subsonic Max Cruise	Subsonic Min Cruise
Power Code	22	50		42.89	41.59	31.11	31.71
Altitude, kft	0	0	55	60	65	34	37
Thrust	3112	47412	15100	12488	9322	10578	9437
				~12500	~9300		
Mach Number	0	0	2.4	2.4	2.4	.95	.95
W3, pps	109.09	421.82	238.8	191.09	147.21	160.79	142.3
W36, pps	89.32	348.25	196.72	157.22	120.89	132.13	116.82
Pt3, psia	56.24	305.55	181.1	146.05	111.64	105.39	92.66
PS3, psia	51.30	283.38	166.13	134.11	102.42	97.34	85.6
T3, °R	815	1350	1662	1673	1662	1159	1141
T4, °R	1593	3018	3226	3286	3247	2526	2502
WF36, pph	3895.7	35036	19248	15915	11982	10344	9078
FAR4	.01212	.02795	.02718	.02812	.02753	.02175	.02159
PHI 4	.177	.407	.396	.410	.401	.317	.315
XM3.0	.36597	.33462	.36068	.35854	.3603	.3423	.3417
P4, psia	51.89	285.7	167.88	135.5	103.5	98.21	86.36

3.2 Ground Rules For Combustor System Designs

A list of criteria has been developed to facilitate the selection of premixer designs for the HSCT low NOx combustor. The criteria are separated by three major functional characteristics: performance, geometry and manufacturability.

Performance Related Attributes

Premixer performance can be classified further into two disparate characteristics: premixing and flame holding.

Premixing:

- Degree of vaporization and mixedness. This is comprised of the variation in the time-averaged profile of the mean and the variance of the fuel concentration across the premixer exit.
- Sensitivity of mixedness to the premixer pressure drop.
- Sensitivity of the flowfield inside the premixer to aerodynamic inlet conditions.
- Fuel spray characteristics and pressure drop across the fuel injector.
- Resistance to flashback and autoignition.

Table 3-3 summarizes the LPP design criteria that will be used in evaluating the LPP combustion system designs.

Flame holding:

- Mode of flame holding: either a swirl-induced central recirculation zone or a wake behind a bluff body.
- Range of operating dome reference velocities and their influence on combustor's lean blowout characteristics.
- Pressure drop across the flame holding device.

Geometrical and Manufacturability Attributes

- Premixer size, length, diameter.
- Complexity of combustor design and manufacture.
- Complexity of the fuel system design and manufacture.
- Sensitivity to thermal and mechanical deterioration .
- Assembly and maintenance ease.

Table 3-3. LPP Design Criteria.

CRITERION	LIMIT/GOAL	RATIONALE
Premixer Residence Time	≤1 ms	Avoid Autoignition
Effective Combustor Residence Time	≤2 ms	Post-Flame NOx
Liner Cooling Coverage	<50% of Current Levels	Premix Air Availability
Premixing Uniformity	<0.15 σ/mean	NOx Production
Premixing Evaporation	>90%	NOx Production
Premixer Velocity	250-300 f/s	Flashback
Flameholder-Blockage		Flame Stability
Unpiloted	>80%	
Piloted	>40%	
Dome Velocity		
Pilot	<30 f/s	Relight
Premixed Main	<100 f/s	Flame Stability
Premixer Duct Flow (Cruise)	85%	NOx Production
Pilot Airflow (Idle)	30%	Idle Emissions

Missing from this list of selection criteria, is any form of analysis of the stresses inherent in the mechanical design. This would require a detailed mechanical design which was outside the scope of the study.

In addition to the above general criteria, the following ground rules were established for design of the candidate combustor designs. These groundrules are based on established GEAE design practices as well as past experience with premixers.

1. Combustor flowpath and premixer designs were carried out for ground idle, SLTO and supersonic mid-cruise cycle conditions. The NOx emissions were evaluated at supersonic mid-cruise cycle conditions, and compared against the Emission Index (EI) goal of 5 g NOx/kg of fuel.

2. The following values were initially established as goals in development of these combustor system designs. Because of the exploratory nature of these system designs, the goals were not considered rigid requirements.

- Premixer Fuel/Air Equivalence Ratio - 0.50 at Supersonic Cruise
- Pilot Dome Average Reference* Velocity - 25 to 30 ft/sec at SLTO
- Main Dome Average Reference* Velocity - 70 ft/sec at SLTO
- Outer and Inner Passage Flow Velocity - less than 150 ft/sec at SLTO
- Combustion system pressure drops:
  - SLTO $\Delta P/P$ = 6.5%
  - Cruise $\Delta P/P$ = 7.2%
    - ΔP/Dump = 1.9%
    - ΔP/Dome = 5.3%
    - ΔP/Liner = 4.8%

*Reference Velocity is defined as the bulk velocity at the dome face, and is based on the combustor inlet conditions at SLTO.

3. The following geometric guidelines were also established for the combustor designs based on the baseline cycle. Figure 3-1 depicts a schematic of the hot section of a FLADE, cycle C1 engine with a double annular combustor for illustrative purposes only. As shown in the figure, the layout features the following compressor discharge and turbine inlet geometrical sizes.

Compressor Discharge		Turbine Inlet	
Tip	20.287 inches	Tip	23.063 inches
Pitch	19.483	Pitch	20.564
Hub	18.680	Hub	18.065

4. The preliminary performance requirements for the overall combustion system are shown below:

Requirement	Limit/Goal
Pattern Factor	<0.25
Profile Factor	Coordinate With Turbine Design
Average System $\Delta P/P$	6%
Airstart	>30,000 ft
Combustor Efficiency	>99.5%
SLS Emissions/Smoke	ICAO Limits

3.3 Candidate Combustor Configurations

A total of seven combustor configurations were considered. These are shown in Figures 3-2a through 3-2g. In general, these configurations could be classified into three major design categories single annular, double annular and triple annular.

Single Annular Configurations

Variable geometry for both the premixers and the secondary area (downstream of the dome) is a requisite for all single annular designs to operate successfully in the HSCT engine. The variable geometry would vary the air flow split between the premixers and the secondary air to maintain the primary zone fuel-air ratio and flame temperature within the required range.

Double Annular Configurations

Double annular configurations with the main stage comprised of a premixer and/or a bank of premixers and the pilot stage consisting of a conventional swirler dome were considered. Although of simpler nature, they may also require variable geometry to control the fuel-air ratio and primary zone flame temperature within the required range.

Triple Annular Configurations

A triple annular configuration was selected as the initial baseline design concept, since it had the potential of having enough stages so that no variable geometry might be required. At the time, there were not enough single-cup LPP combustor data to determine how many fuel stages would be required. However the estimates varied from 3 up to as many as 10. The selected configuration features a triple dome combustor with a central, fixed geometry Cyclone Swirler pilot dome. The pilot dome is used for ignition and for low power operation, and is designed for acceptable NOx at high power. The inner and outer domes are equipped with low NOx premixers and are operational during high power operating conditions. This configuration has the advantage of minimal risk in terms of the need for variable geometry, and also provides maximum flexibility in arrangement of the premixers.

Figure 3-3 depicts flow splits for the initial baseline triple annular combustor operating at supersonic cruise. These flow splits are presented as a percentage of the total combustor airflow (W_3). All three stages of the combustor were initially sized with these flow splits. Table 3-4a lists the critical parameters corresponding to inner, outer and pilot stages, while Table 3-4b lists the outer and inner passage cooling flow requirements.

Table 3-4a. Characteristic Geometrical Parameters.

Cycle Point	Outer LPP Main Stage Dome Height (in)	Outer LPP Main Stage Dome Velocity (ft/s)	Outer LPP Main Stage Dome Φ	Inner LPP Main Stage Dome Height (in)	Inner LPP Main Stage Dome Velocity (ft/s)	Inner LPP Main Stage Dome Φ
30%	5.97	45.14		4.85	53.98	
Hot Day T/O	5.97	49.30		4.85	55.10	
Bucket Cruise	5.97	70.00	0.575	4.85	70.00	0.575
		Pilot Stage				
30%	4.265	22.60	0.520			
Hot Day T/O	4.625	25.00				

Table 3.4b. Cooling Flow Requirements.

Cycle Point	Outer Passage Flow (pps)	Outer Passage Velocity (ft/s)	Inner Passage Flow (pps)	Inner Passage Velocity (ft/s)
30%	16.0	138.0	21.3	137.9
Hot Day T/O	31.7	153.0	42.1	153.0
Bucket Cruise	17.3	194.0	22.2	187.2

3.3.1 Candidate Fuel-Air Mixer Configurations

Five fuel-air mixers were analyzed for mixing and flame holding potential. The fuel-air mixer studies made use of all the available existing information. The mixers studied were:

1. Swirl-Jet Premixer
2. Lean Direct Injector (Jet Mix)
3. Integrated Mixer Flame holder (IMFH)/Venturi IMFH
4. Cyclone Swirler
5. Lean Direct Multiple-Venturi

Figure 3-4 depicts a schematic of the Swirl-Jet premixer design. As shown, the design features a radial swirler with an airblast fuel injector on the centerline. The fuel exiting from the injector atomizes, vaporizes and mixes with the swirling air in the premixing tube. An annular passage around the fuel injector tube introduces air to prevent a centerline recirculation zone from forming which would increase local residence time and increase the potential for autoignition. A second swirler is installed downstream to further enhance mixing and to ensure that fuel does not contact the premixer wall. The premixed fuel-air mixture exits the premixer and is ignited in the flame holding region downstream of the flame holder/dome plate.

Figure 3-5 depicts a schematic of a Lean Direct Injector. In the design shown, 80% of the airflow passes through an outer ring of eight mixing holes with the remainder being mixed with radially injected fuel in the inner annulus. This fuel-air mixture is injected radially into the jet shear layer formed by the outer ring of mixing holes. Rapid mixing of the fuel-rich radial jets and the axial air jets produces a well mixed fuel/air mixture at the flame front for combustion. This scheme is also expected to provide intense mixing with the stability of a conventional combustor.

The Cyclone Swirler (Figure 3-6) is a radial inflow swirler in which fuel is injected from a number of plain-jet airblast atomizers radially outwards into the swirler. The atomizers are contained in a large centerbody which is sized to block the formation of a central recirculation zone due to the strong swirl. The end of the centerbody is air-cooled. The swirler is fabricated by cutting narrow slots at an angle to the radius in a metal cylinder. The dimensions of the swirler are selected to yield an average residence time inside the swirler of about 0.3 to 0.4 milliseconds.

The Integrated Mixer Flame Holder (Figure 3-7) is a lean premixed prevaporized system designed to meet low NOx requirements at high supersonic cruise inlet temperatures. Fuel is injected into high velocity air which atomizes, vaporizes and mixes with it. The high air velocity minimizes mixer residence time to reduce the risk of autoignition and prevents the formation of low velocity regions which could promote flashback into the mixer tube. Mixer length is sufficient for fuel evaporation and fuel air premixing. Dome cooling air is introduced into the mixer tube near its discharge to include the air as a combustion reactant. The fuel-air mixture burns downstream of the mixer discharge where the flame is stabilized by IMFH blockage recirculation regions. Initial development of this mixer, under contract NAS3-25552, demonstrated 4.1 EI NOx and 99.7% combustion efficiency at a 3593 R (1996 K) flame temperature for inlet conditions of 1626 R (903 K) and 4 atmospheres.

The Multiple-Venturi (Figure 3-8) is a lean direct injection concept developed at NASA's Lewis Research Center and Textron, Inc. The device consists of a small axial swirler, and a miniature simplex atomizer located at the throat of a sharp edged venturi. The swirler is designed to provide a strong swirling flow which aids fuel atomization, vaporization and mixing. In addition, the swirling flow produces a recirculation zone which provides flame stabilization. The miniature simplex atomizer produces small droplets which evaporate quickly in the strongly swirling flow. The device is designed to produce low NOx, high combustion efficiencies and wide stability limits.

3.3.2 Combustor Flowpath Development

The first step in developing the design of a combustor system is a preliminary definition of the flow path. Although these combustor flow paths, as presented, are specific to a particular premixer, the flow paths are sufficiently generic so that the premixers could be interchanged among them. Each of these designs is based on the baseline triple annular design initially selected for development. Since the Multiple-Venturi concept was introduced late in the contract, no flowpath development was completed.

A mixer's physical size can be the controlling factor in determining the combustor's dome velocities. Because of the very high dome airflows required for lean combustion, higher dome velocities were used in the main stages of these conceptual layouts to reduce the dome height/combustor length ratio and the volume of the combustors to an acceptable level.

The following unconventional methods were used to optimize the packing density of the mixer combinations. Mixer diameters (and effective areas) were varied in proportion to their radial position from the engine axis. Mixer numbers on an annulus were varied relative with radial position from the engine axis. Mixer circumferential positions were staggered on the annuli so that their radial positions could overlap. Though none of these methods are desirable, they were resorted to the degree required to establish a reasonable trade-off with other design objectives. HSCT combustor volumes are slightly higher than desired due to these packing density constraints.

3.3.2.1 Swirl-Jet Premixer

Figure 3-9 depicts a schematic of the Swirl-Jet combustor design. As shown, this design features three annular domes. The inner and outer domes are equipped with the Swirl-Jet premixers, while the central (pilot) dome is equipped with a conventional radial swirler. The figure also shows some of the pertinent geometrical dimensions. For example, the innermost radius of the combustor dome is 14 inches, while the outermost radius is 25 inches, resulting in a dome height of 11 inches. The combustor length downstream of the premixers is 6 inches which results in combustion residence time of about 3.4 milliseconds at supersonic mid-cruise conditions. Figure 3-9 also exhibits the geometrical details of the Swirl-Jet premixers. As shown, the swirl cup has an outer diameter of 3.6 inches with the premixer tube being 2 inches in diameter at the exit. At the design pressure drop of 4.5%, this design results in a flow area of 2.3 in^2 yielding an average main dome velocity of 62 ft/sec at supersonic mid-cruise conditions.

Figure 3-10 shows the packing scheme for the premixers and the pilot radial swirlers. As shown, there are 36 cups in the outer and central annuli and 24 cups in the inner annulus

3.3.2.2 Lean Direct Injector

Figure 3-11 depicts a schematic of the combustor design which is based on the design of Ali and Andrews [1]. As shown, this design features three annular domes. The outer dome and the inner dome are each equipped with 60 Lean Direct Injectors (LDI), while the pilot dome is equipped with 30 fixed geometry Cyclone Swirlers. The overall main dome (LDI) cup diameter is 2 inches, with the jet mix to cup area ratio being 0.421. This cup design results in an effective flow area of 0.812 in^2. This yields an average dome velocity of 87 ft/sec at supersonic mid-cruise conditions and a pressure drop of 5.3%.

Figure 3-12 depicts a fuel flow staging schedule proposed for the 60-30-60 (outer-pilot-inner cups) LDI design. The staging schedule is devised to assure fuel modulation such that various extreme HSCT program goal limits (e.g., NOx EI, LBO limit, etc.) are met during the full range of cycle operating conditions. The plot depicts the computed flame temperature as a function of turbine inlet temperature (T_4) for the various fuel stages. The plot also shows

three horizontal lines corresponding to EI NOx <5.0, 0.50% combustion inefficiency, and the estimated LBO limit. As shown in the figure, the combustor stage fuel-air ratio is increased (increase in T_4) until the smoke limit and/or high T_f limit is reached. At this point, in addition to the pilot, the inner and outer main stages begin to flow with 25% of the main stage fuel flow through them. The combustor operation now follows the stage-2 line until the upper flame temperature limit is reached. Next, fuel flow through the main stages is increased to 50% in each. At this point, the combustor follows the stage-3 line until the upper temperature limit is reached. The next two stages, stage 4 and stage 5, include a fully fueled outer dome and 75% fueled inner dome (stage 4) and all three domes fully fueled (stage 5). In each case, the combustor operation follows the corresponding stage line until the 0.5% combustion inefficiency limit (at the lower end) or the EI NOx limit (at upper end) is reached.

3.3.2.3 Cyclone Swirler Premixer

In the system design selected for the layout, the combustor flowpath used four annular rows of mixers. The two inner annuli will have 45 Cyclone Swirlers each with effective areas of 0.55 in^2. The two outer annuli will have 45 Cyclone Swirlers each with effective areas of 0.96 in^2. The pilot stage will be the innermost stage, with the sequence continuing from the inner to the outer annuli. Variable dilution area is required to trim the fuel-air ratio. The benefit of modulating the airflow in this way is good control of combustor flame temperature without significant combustor pressure drop variations.

3.3.2.4 IMFH Premixer

A mechanical design layout of an IMFH combustor is shown in Figures 3-13 and 3-14. This design features three annuli where the inner and outer annuli consist of several rows of premixer tubes, while the central annulus is a pilot stage that uses Cyclone Swirlers. As shown in Figure 3-14, the premixing outer main stage consists of four rows of 120 premixing tubes, while the premixing inner main stage has three rows of 120 premixing tubes. The IMFH premixers are shown with coaxial fuel injectors. The central pilot stage consists of one row of 60 Cyclone Swirlers.

3.3.3 Comparative Evaluation of the Various Combustor Layouts

In order to comparatively evaluate the mechanical complexities and NOx reduction potential of each of the premixer/combustor concepts (IMFH, Swirl-Jet, Cyclone Swirler and Jet Mix), the pertinent geometry (Table 3-5), aero (Table 3-6) and combustor performance (Table 3-7) parameters of the concepts are reviewed below.

Out of the four, the Swirl Jet concept employs the least number of premixers (Table 3-5) with relatively large mixer effective area. In contrast, the IMFH concept features the largest number of small size premixing tubes. These system design studies are very preliminary, and very little actual test data for emissions performance of the fuel-air mixers is available. Thus, the number of fuel stages shown are only a preliminary estimate, and thus, not very meaningful. The overall external dimensions (length and dome height) of all the four concepts are nearly the same and reflect the following design philosophies:

- All of the designs feature multi-annular domes in order to provide the large dome flow area for the lean combustor.

- The airflow distribution is highly biased to the main stages in order to reduce both idle and high power emissions.

- The pilot dome is designed for a low dome velocity (about 30 feet/second) to provide sufficient flame stability.

- At high power conditions, most of the fuel is supplied to the main stages. In the main stage, the combustion residence times are very short (main stage reference velocities range from 60 to 90 ft/sec), and fuel burns at lean fuel-air ratios in order to minimize NOx emissions.

Table 3-6 depicts the corresponding aero parameters. As pointed out earlier, the airflow distribution is highly biased towards main stages (~68%) with the remainder distributed almost evenly between the pilot stage and cooling/dilution flow requirements. The premixer flow velocities are high with residence times less than 1 millisecond. Both of these parameters are selected to prevent flashback and autoignition. The parameter with the most variation among the four concepts is the combustor residence time. It is the lowest for the IMFH concept (1.7 ms) compared to 3.4 ms for the LDI design. This variation in residence time primarily reflects the challenge of designing a combustor with the combination of high dome airflow and a short combustor residence time. The IMFH has the advantage because the mixer does not require radial flow (swirlers) and is therefore more compact. Nevertheless, in all of the designs, the goal was to keep the combustor residence time at about 2 milliseconds in order to minimize NOx production.

A comparison of the various layouts leads to the following observations:

- All of the designs will need a multi-annular dome with at least two main stages and one pilot stage. This in itself offers several combustor system design challenges. For example, from the aero standpoint, a multi- passage diffuser with significant pressure recovery (in each passage) will be required in order to feed air into each of the stages.

- The effective areas of the swirlers/premixers are generally smaller than the conventional mixers in large aircraft turbines to date. This may require more stringent manufacturing tolerances resulting in more complex and careful manufacturing practices.

- The IMFH/Cyclone Swirler concept features a total of 900 premixers. This adds to the fuel preparation, thermal protection and staging complexities.

- In order to maintain sufficiently lean fuel-air ratios (in the main stage) at high power conditions, minimal air will be available for combustor liner cooling. This indicates a need for development of highly efficient liner cooling schemes and high temperature materials for each of the four concepts.

- The use of multiple fuel stages will require development of a complex fuel staging control system.

Table 3-5. Geometry for Lean Burn Combustor Systems.

	IMFH	SJ	CYCLONE	LDI
Total Number of Mixers	900	96	180	150
Number of Casing Fuel Penetrations	120	48	180	60
Combustor External Length (in)	9.2	10.8	10.0	9.3
Combustor External Dome Height (in)	9.4	11.0	9.4	12.7
Effective Area of Each Pilot Mixer (in^2)	0.40	0.68	0.54	0.93
Effective Area of Inner Mixers (in^2)	0.18	1.85	0.54	1.23
Effective Area of Outer Mixers (in^2)	0.18	1.85	0.96	0.85

Table 3-6. Aero Parameters for Lean Burn Combustor Systems.
Supersonic Mid-Cruise Unless Stated Otherwise.

	IMFH	SJ	CYCLONE	LDI
Premixer Residence Time (ms)	0.8	0.9	0.5	-
Premixer Exit Velocity (ft/s)	534	392	330	-
Combustor Residence Time (ms)	1.7	3.2	2.9	3.4
Pilot Dome V_{ref}, SLTO (ft/s)	40	36	35	26
Main Dome V_{ref}, (ft/s)	90	62	66	80
Pilot Stage Flow Split (%)	14.7	14.7	14.8	15.5
Total Main Stage Flow Split (%)	67.2	67.2	67.2	69.2
Cooling/Dilution Flow Split (%)	18.1	18.1	18.0	15.3

Table 3-7. Predicted NOx EI for Lean Burn Combustor Systems.
(Mach 2.4 GE21/FLA 1 Study C1 Cycle)

	IMFH	SJ	CYCLONE	LDI
Standard Day Takeoff	(8)*1.1	(4) -	(4) 3.5	(4) 3.7
Supersonic Max Dry Climb	(8) 4.8	(4) -	(4) 5.1	(5) 8.4
Supersonic Max Cruise	(8) 2.0	(4) 5.2	(4) 4.1	(5) 3.4
Supersonic Mid-Cruise	(8) 2.4	(4) 2.9	(4) 4.1	(5) 4.1
Supersonic End Cruise	(8) 2.1	(3) 3.6	(4) 4.1	(5) 3.6
Supersonic Bucket Cruise	(5) 2.0	(3) -	(3) 4.1	(3) 5.4

*Numbers in brackets represent number of operating fuel stages.

3.4 Design of Fuel Staging System

Control of the fuel-air ratio of the mixture within the constraints dictated by combustor stability, emissions, combustion efficiency, and material temperature limits is one of the major challenges of the LPP/LDI approaches to a low emissions HSCT combustor. Fuel staging is the primary means being employed to control the premixer fuel-air ratio, although variable geometry is also being investigated. The fuel staging analysis for the four combustor system designs presented above were performed by considering 18 discrete cycle points of the baseline HSCT engine cycle. The performance of a given staging design was then predicted by calculating the fuel-air ratios and flame temperatures. In lieu of actual subcomponent data for emissions, available correlations were then used to estimate emissions and stability for combustors. The disadvantage of the discrete analysis was that the evaluation was not made over all the possible combustor operating conditions in the HSCT's flight envelope.

An additional constraint due to combustor liner material temperature is given consideration using a simple cooling effectiveness model. The design point for the combustor is mid-supersonic cruise where the flame temperature is determined by the NOx EI goals, say at 3600 R (2000 K). The most severe cycle point in terms of combustor fuel-air ratio and NOx emissions (fully staged) is top of climb. If a simple heat transfer analysis is applied to the combustor at each of the discrete cycle points, a required cooling effectiveness can be calculated based on the most severe point (usually top of climb);

$$\varepsilon_c = \frac{T_f - T_{ml}}{T_f - T_3}$$

where T_f is the flame temperature. For example, using the baseline cycle, the result is $\varepsilon_c = 0.48$, assuming a material temperature limit, T_{ml}, of 2860 R (1589 K). Nothing is being assumed about the cooling design, only that this cooling effectiveness must be attained with the available cooling air for the assumed material temperature limit. Generally, at lower power, as T_3 decreases, a higher T_f is used because it is required to maintain stability.

If the NOx constraint is relaxed at all partially staged conditions (none of which are supersonic cruise points) and the material temperature constraint used instead the NOx emissions, some very encouraging tentative projections can be made. First, at low engine power, the material temperature constraint on the upper flame temperature is not restrictive when operating near stoichiometric on the pilot stage only and possibly even during operation on the second stage. (Slightly rich combustion was already being used for stability at idle in the system designs. This analysis indicates it is feasible.) Second, NOx emissions are not appreciably affected at supersonic cruise. Third, the NOx emissions at subsonic cruise are acceptable. This performance appears to be attainable with only four or five fuel stages with reasonable control margins.

3.5 Preliminary Combustor Mechanical Design

The Swirl-Jet combustor concept was selected for a more detailed preliminary design study to assure mechanical and heat transfer feasibility of the LPP/LDI concepts. Figure 3-15 shows a schematic of the revised Swirl-Jet combustor design for the HSCT C1 cycle. This design differs from the layout reported above in the following ways:

- This combustor uses a dome configuration with 30 cups each in each of the three annuli. In contrast, the earlier design featured 36 cups each in the outer and middle annuli, with 24 cups in the inner annulus.

- This combustor uses a fixed-area Cyclone Swirler vaporizer as a pilot in contrast to the conventional pilot swirler proposed in the earlier layout.

There are several advantages with this layout. For example, the revised layout allows for a reduced number of fuel nozzles (30) and only one fuel stem type. The mechanical complexity and the number of fuel nozzle penetrations are reduced with the same number of cups in each annulus. However, a prime disadvantage of this design is the fact that it requires two Swirl-Jet premixer configurations with distinctly different effective areas. The per cup effective area of outer mixers will be 2.22 in^2 (compared to 1.85 in^2 in the earlier design), while the effective area of the inner mixers will be 1.48 in^2 (compared to 1.85 in^2 in the earlier design). The pilot cups are also slightly larger in this design. The per cup effective area of the pilot mixers is 0.82 in^2 compared to 0.68 in^2 in the earlier design. The total dome effective area is fixed at 136 in^2. Among other pertinent features, the pilot dome reference velocity in this design is 39 fps compared to 36 fps in the earlier design. The pilot dome reference velocity was recognized as being considerably above the goal.

Figure 3-16 shows a frontal view of the combustor, while Figures 3-17 and 3-18 show side views. Figure 3-17 is a cross-sectional view through the dome structure, while Figure 3-18 is a cross-sectional view between swirlers. This combustor (Figure 3-15) uses advanced CMC material for the liners and also for dome heat shields. The liners and heat shields are backside impingement cooled, where the spent impingement air is discharged at the liner aft end to trim the exit temperature profile. The impingement cooling air for the dome heat shields is discharged as cooling film for the premixer trailing edge and as film for the pilot liners.

The dome structure consists of three one-piece, C-shaped metal rings which form the domes. Each C-shaped ring consists of a radial disk with equally spaced holes for the swirlers. The swirlers slide partially through the holes and then bear against the disk to support the swirler for axial loading. The interface between the swirler and disk is used as a braze joint to secure the swirler for tangential loading (swirl) and for all other loads. Each dome disk has a cylindrical flange at the outer and inner diameter to connect to the adjacent domes and cowls by radial bolts. The dome assembly is reinforced by 30 radial struts between swirlers, in addition to the bolted cylindrical flanges, to minimize deflection of the dome. The metal dome assembly is secured axially and radially by an inner mounting ring.

A major feature of the design is the use of CMC (ceramic matrix composite) material for the liners and dome aft-face heat shields. This material

has a high temperature capability, which reduces film cooling air requirements for the liners and heat shields. Combustion efficiency is also enhanced (HC and CO emissions reduced) by this reduction in film cooling airflow.

The metal dome structure is protected from the combustion heat load by three one-piece, C-shaped CMC heat shields, which also serve as bluff body flame holders. The C-shaped shield consists of a radial disk, located at the downstream face of the dome, which serves as the flame holder. Extending forward from the outer and inner diameters of the disk are cylindrical rings. The heat shields are secured by radial pins at the cooler forward ends of these cylindrical rings. The cylindrical CMC rings adjacent to the pilot primary zone serve as pilot liners.

The outer and inner liners are one-piece CMC cylindrical shells secured at the forward end by radial pins. Like the CMC heat shields, the CMC liners are with a radial gap between the metal structural rings and the CMC rings to avoid interference due to radial growth differences. The radial gaps are sealed to prevent air leakage. All five CMC parts are cooled by impingement metal liners. Sufficient radial gap is provided between the impingement liners and the CMC liners to prevent thermal interference. The impingement liners carry the majority of the pressure load across the liner thereby reducing the hoop and buckling loads on the CMC shells. The CMC parts are suspended from the metal structures, carry no structural loads and carry minimal pressure loads.

The fuel nozzle assembly is a radial structure bolted to the outer casing. The radial positions of the three fuel nozzle tips will be designed to be centered with the swirlers at supersonic cruise conditions. There will be radial movement of the fuel nozzles relative to the swirlers, due to thermal growth differences at other power settings and also due to manufacturing tolerances.

3.6 Chemical Kinetics Studies

A combustor kinetics model has been used to predict CO and NO emissions from the HSCT combustor. The model was developed using the CHEMKIN subroutine library. The model consists of a well-stirred reactor followed by a plug flow reactor. The former simulates the flame holding region of the combustor while the latter simulates the non-recirculating flow region of the combustor. The propane-air chemical kinetics model of Nguyen, Bittker and Niedzwiecki[2] with a few modifications was used. The model has 98 chemical kinetic reactions including propane oxidation, thermal NO production and prompt NO production. The single adjustable parameter in the model (the residence time of the well-stirred reactor) was adjusted using stability as a criterion. The predicted NO and CO emissions were in good agreement with IMFH emissions measurements for flame temperatures ranging from 3420 R to 3960 R (1900 K to 2200 K).

Two important design issues for the HSCT combustor have been addressed using the model. The first question is whether further CO oxidation will occur during the turbine nozzle expansion at higher T_4's, when equilibrium CO exiting the combustor is high. Two cycle conditions, mid-cruise and top of climb, were considered. Equilibrium CO was assumed at the combustor exit before entering the nozzle. A typical transient temperature and pressure for nozzle expansion was imposed. It was found that during mid-cruise, no further CO oxidation occurred. However, during top of climb CO decreased by

12%. The nozzle cooling air was assumed not to mix with combustion gases for these calculations. A further decrease of CO in the HP turbine rotor was also predicted. However, there, the CO is more likely to be quenched by mixing with the cooling air in the turbine, which was not considered in the calculations.

The second issue addressed in another series of calculations was the relation between NO and CO emissions, combustor flame temperature and combustor residence time. A flame temperature of 3600 R (2000 K) had previously been tentatively selected for the combustor design point of mid-cruise. The high T_4 of 3287 R (1826 K) at mid-cruise and the requirement for some cooling air prevent a choice much lower than 3600 R (2000 K). Higher flame temperatures would be expected to produce higher NO emissions, unless shorter residence times could offset this effect. Shorter residence times complicate the challenges of high aspect ratio of dome height to combustor length (already as high as 3 to 1), but also decrease liner cooling air requirements (because the liner area would be smaller).

The model computations roughly confirm the choice of 3600 R (2000 K) as the design point flame temperature. A way of clearly presenting all the combustor design tradeoffs to arrive at a more precise optimum would require detailed submodels for the entire combustor system. However, from the kinetic model results shown in Figure 3-19, it is apparent that combustor designs with residence times longer than about 2.5 or 3.0 milliseconds will significantly increase NO emissions whenever the flame temperature is allowed to increase much over 3600 R (2000 K). With the most practical fuel staging designs, which use as few as four fuel stages, flame temperatures would be high at some partially staged conditions. NOx emissions would also be high at these partially staged conditions, unless the combustor residence time is kept as short as possible.

3.7 Initial LPP/LDI Combustor Aero Design

The initial design process for a fuel-staged combustor entails selecting the total effective air flow area for the combustor to meet pressure drop requirements and then selecting the size and number of the fuel stages. The size of a fuel stage is characterized by the combined effective air flow area of the fuel-air mixers being fueled by that fuel stage. The stages are numbered in order of their use with increasing engine power. The flow area of a given stage includes the flow areas of all the lower stages. To a good approximation, the combustion zone's fuel-air ratio is determined by multiplying the overall combustor fuel-air ratio by the ratio of the total combustor flow area divided by the stage flow area. This assumes that all the operating pilot and main stage mixers are at the same fuel-air ratio.

In these designs, the total effective flow area for the combustor which met the pressure drop requirements was determined to be 178 in^2. The total effective air flow area for all the combustor's fuel-air mixers was 142 in^2. At the design point (supersonic mid-cruise), this yielded a fuel-air ratio corresponding to a 3600 R (2000 K) flame temperature. This flame temperature and combustor volume (which sets the residence time) determine the NOx emissions at the design point.

The pilot stage effective flow area is selected to yield good stability at the low combustor fuel-air ratios which occur at flight and ground idle conditions. The area used in this design is 30 in^2. NOx emissions during pilot-only operation were not considered since the Roffe and Venkataramani (1) correlation does not apply near stoichiometric operation (and consequent very high flame temperatures) and with poor prevaporization which will occur at the low inlet temperatures.

Selection of the effective air flow area to be fueled during subsonic cruise was a three-way trade-off between emissions performance, operability and system complexity. Based on the current limited emissions data base, there were several possible fuel-staging system design choices. The subsonic cruise effective air flow area could be selected to minimize subsonic cruise emissions. This would involve a trade-off between CO, UHC and NOx emissions. Based on the IMFH emissions data obtained so far, the best choice for the flame temperature would be at least 3690 R (2050 K), or higher than the supersonic mid-cruise design point. The corresponding stage flow area would leave very large stage area gaps in a three stage design. Therefore, it is unlikely that the fuel-air ratio operating range of a premixer would allow as few as three fuel stages for the combustor system design for this engine cycle. A five stage design would result if at least one additional stage above and one stage below the subsonic stage would be needed for the necessary operability.

A system design with as few as four fuel stages appears to be a possibility, if the stage areas were based on operability considerations alone. The subsonic cruise point could be included in the second stage if its area was increased relative to a five stage design, the third stage of the five stage design was eliminated, and the third stage (the old fourth stage) had a reduced area. 72 and 107 in^2 were selected for the second and third stages areas of this four stage design. Higher subsonic cruise flame temperatures, good combustion efficiency and acceptable NOx emissions would result.

Once the air flow areas of the fuel stages are determined, the cycle points can be allocated among the stages. The combustion fuel-air ratio, flame temperature, combustion efficiency and NOx emissions can be estimated. The allocation is based upon a correlation for the minimum flame temperature for 99% combustion efficiency as a function of combustor inlet temperature. In the past, a 99% combustion efficiency correlation was contrived from a stability correlation due to Roffe and Venkataramani [3] by adding a constant temperature. This interim combustion efficiency correlation did have the expected trend with combustor inlet temperature. Part way through the system design effort, a correlation for the required flame temperature (for 99% combustion efficiency) based upon actual IMFH data at three inlet temperatures was adopted. This correlation is a nonlinear function of inlet temperature and reflects the higher sensitivity of the IMFH's efficiency to inlet temperature compared to the previous correlation (which was based on the premixing and combustion of gaseous propane).

Other considerations during the design included the maximum possible flame temperature as constrained by the combustor liner material temperature limit. A simple heat transfer model is used to relate maximum flame temperature to the combustor inlet temperature.

The results of this design in terms of flame temperatures plotted versus combustor inlet temperature for 29 engine cycle points is shown in Figure 3-20. Also shown in the plot are: the 99% combustion efficiency limit, the flame temperature corresponding to a measured NOx EI of 5 for the IMFH, and the flame temperature limit for a 2860 R (1589 K) liner material temperature. The points violating the IMFH's 99% combustion efficiency limit are for the pilot only stage, whose mixers will be required to demonstrate wider operating limits for inlet temperature than the IMFH. The resulting estimates for the NOx emissions (from the correlation and interpolated from IMFH data) and combustion efficiency for some important cycle points are shown in Table 3-8. A diagram which plots the flame zone equivalence ratio versus overall combustor fuel-air ratio is shown in Figure 3-21. The linear relationships reflect their dependence on fuel-stage air flow area described above. The large gap between the pilot and second stages resulting from shifting the intermediate stage areas upwards is apparent.

Table 3-8

Combustor System Using Four Fuel Stages
Design Based on Actual IMFH Configuration 5 Emissions Data (Preliminary)
Baseline HSCT LPP/LDI Cycle

	Stages (#)	T_{flame} (R)	ø	EI_{NOx} GASL (g/Kg)	EI_{NOx} IMFH (g/Kg)	Comb. Ineff. (%)
Take-off	4	3372	0.51	1.8	2	0.06
Subsonic climb	4	3449	0.56	2.4	2	0.6
Max. climb	4	3898	0.59	7.1	5	0.3
Supersonic cruise	4	3600	0.51	3.6	3	0.2
Supersonic idle	1	4140	1.27	-	-	-
Subsonic cruise	2	4029	0.78	10.7	7	0.4
Subsonic idle	1	4156	1.09	-	-	-
Approach	2	3490	0.61	3.1	2	1.0
Ground idle	1	4231	1.04	-	-	-

The relative contributions to NOx emissions of three flight conditions above 42,650 feet (13 km) can be estimated. These estimates for a 5000 mile mission are shown in Table 3-9. The NOx EI estimate shown in the table for descent is probably high. The fuel-air ratio is too high for the Roffe-Venkataramani correlation to be applied. A conservative (high) estimate of the NOx EI was used. In any case, its contribution to the total is negligible.

Table 3-9

Preliminary Estimates of NOx Emissions above 13 Kilometers
5000 Mile Mission

Cycle Point	Time (min.)	Fuel flow (lb/engine hr)	NOx EI (g/kg fuel)	NOx (lb)	NOx (% of total)
Climb	4.0	26,308	7.1	50	6.7%
Start Cruise	67.3	19,248	3.0		
Mid Cruise	67.3	15,915	3.6	686	91.8%
End Cruise	67.3	11,982	3.1		
Descent	4.8	1,697	20*	11	1.5%

*Estimate

It should be emphasized that these system design results are preliminary based on the small effort invested in optimizing the design parameters. A more accurate analysis will require a larger emissions performance data base for the fuel-air mixers. Some design aspects have not yet been proven to be feasible; most notably the heat transfer design for the combustor liner, the 2860 R (1589 K) liner material and the pilot stage mixer low inlet temperature operability.

4.0 SUBCOMPONENT TESTING AND EVALUATION

This section discusses the development and testing completed on the five mixer concepts selected for further development in section 3.3.1 above:

1. Swirl-Jet Premixer
2. Lean Direct Injector (Jet Mix)
3. Integrated Mixer Flame Holder (IMFH)/Venturi IMFH
4. Cyclone Swirler
5. Multiple-Venturi

This section concludes with a summary of the IMFH cold flow mixing activities completed at GE's Corporate Research and Development Center (CR&D) and the IMFH Laser diagnostic activities completed at Pennsylvania State University. The complete reports are contained in Appendices 9.2 and 9.3, respectively.

Figure 4-1 exhibits a schematic of the low-pressure single-cup test rig. A salient feature of this rig is the use of cast-in-place ceramic liners (based on practice at NASA's Lewis Research Center) for the combustor. The use of a ceramic liner allows combustor walls to operate at high temperatures resulting in hotter thermal boundary layers; which are representative of the actual proposed combustor in which the liners are expected to be backside cooled. The dome/rig interface was designed for quick installation/removal of the test piece by using a common interface for all dome configurations.

4.1 Swirl-Jet Premixer

This section discusses the design and development of the Swirl-Jet premixer. The Swirl-Jet premixer was an attempt to increase the IMFH concept's scale while maintaining the IMFH's low NOx and high combustion efficiency characteristics. This would have the potential of decreasing the number of fuel injection points. Swirl was used to enhance the fuel/air uniformity in the large premixer. The predicted droplet evaporation characteristics, 2-D CFD model results, as well as low and high pressure (4 and 18 atmospheres respectively) single-cup test results of the Swirl-Jet premixer are discussed.

4.1.1 Evaporation Characteristics

A short description of the Swirl-Jet premixer concept has been given in Section 3.3.2.1. A schematic of the Swirl-Jet premixer is shown in Figure 3-4. The rather complex combination of swirlers used in the Gen 1 Swirl-Jet design are used to promote a moderate amount of shear and mixing in the radial direction both inside the premixing chamber to generate a more uniform premixture leaving the premixer. The shear and radial mixing occurring inside the jet as it exits into the combustion chamber also promote burning across the jet and help to keep the flame length short.

A one-dimensional vaporization model was used to provide some insight into the vaporization processes involved and to give first order estimates of the evaporation time scales for a premixer of this type. These evaporation calculations were carried out using the HOWLEVAP code to calculate drop trajectories, velocities, instantaneous drop sizes and temperatures. The fuel vapor fraction was computed for the developed spray downstream of the fuel injector. The fuel was assumed to be single component JP-5 for these computations fuel with the properties calculated at the 50% distillation point of the fuel.

One of the HOWLEVAP code inputs is the Rossin-Ramler exponent for the spray distribution. This exponent was assumed to be 1.3 for all of the computations. The SMD at various operating conditions was computed using the following correlation due to Rizkalla and Lefebvre (2).

$$SMD = 0.95 \cdot \frac{(\sigma \cdot m_L)^{0.33}}{U_R \cdot \rho_L^{0.37} \cdot \rho_A^{0.30}} \cdot \left[1 + \frac{1}{ALR}\right]^{1.70} + 0.13 \cdot \frac{(\mu_L^2 \cdot d_0)^{0.50}}{\sigma \cdot \rho_L} \cdot \left[1 + \frac{1}{ALR}\right]^{1.70}$$

Table 4-1 depicts the computed values of the initial droplet SMD's at four conditions: mid-cruise, ground idle, standard day takeoff and subsonic max.-cruise. As shown in the table, the droplet diameters range form 31 microns to 44 microns at these conditions.

Table 4-1. COMPUTED SMD's FOR AN AIRBLAST ATOMIZER (JP-5 FUEL)

Cycle Point	P_3 (atm)	T_3 (R)	SMD (microns)
Mid-Supersonic Cruise	10	1660	37.12
Ground Idle	3.5	815	43.96
Standard Day Take-off	19.27	1350	30.62
Subsonic Maximum-Cruise	6.63	1159	37.39

Figure 4-2 depicts the computed fuel spray distribution for 30 and 50 micron sprays. Both the sprays demonstrate that only about 25% of the droplets are centered around the SMD, with a larger number of the fraction being distributed over other droplet size range. Figure 4-3 depicts the vaporization history of the 30 and 50 micron size droplets. These computations assume that the spray is injected into the 1660 R (922 K) air stream with the mean airspeed of 500 fps. As shown in the figure, 50 micron spray takes about 2.5 msec to fully vaporize, while the 30 micron spray takes about 0.80 msec to vaporize fully. An important observation from this figure is that most of the 30 micron spray (>90%) vaporizes in less than 0.50 msec.

It should be emphasized that, in the model, these sprays are injected into an uniform air stream where no further atomization of the spray is effected by the flow field. In the Swirl-Jet premixer concept, shear gradients (jet entrainment boundary and recirculation zone) exist which may cause further significant atomization of the fuel droplets.

4.1.2 Concert 2-D Modeling

Figures 4-4a and 4-4b show the computed velocity vectors for two conditions: 1) no flow through the central jet; and 2) central jet flowing with a plug flow velocity profile at the exit of the jet. As shown in Figure 4-4a, a weak central toroidal recirculation zone is established on the centerline, which disappears with the introduction of the central jet (Figure 4-4b).

Figure 4-5 shows the droplet trajectory history of the spray injected at the X = 0 location. The conditions are an air inlet air temperature of 1660 R (922 K), a main air stream swirl angle 60°, and droplet sizes ranging from 5 to 60 microns. As shown in the figure, most of the spray vaporizes within the first 65% of the premixer length downstream of the fuel injector. This corresponds to a predicted droplet evaporation time of 1.2 msec.

4.1.3 Single-cup Testing

Five single-cup tests on the swirl jet concept were completed, and are described below.

4.1.3.1 Configuration 1 and 1A Testing

The pertinent features of configurations 1, 1A and 2, fuel injector type and swirler vane configuration, are given in Table 4-2. Configuration 1 used a 180° spray angle fuel nozzle while configuration 1A used a 60° spray angle and a flow number 14 fuel nozzle. Configurations 1 and 1A were tested at the operating conditions shown in Table 4-3a.

Table 4-2. Swirl-Jet Configurations.

Config. Number	Number of Primary Vanes	Number of Secondary Vanes	Fuel Injector Type	Configuration
1	20	14	Peanut Nozzle 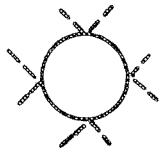 Located Upstream in Venturi	Counter-Rotate
1a	20	14	Peanut Nozzle Located Downstream in Venturi	Counter-Rotate
2	20	14	Spraybar Ring	Co-Rotate

Table 4-3a. TEST CONDITIONS FOR SWIRL JET CONFIG 1

Configuration	1	1A
P_3, psia	17 - 60	17 - 60
T_3, R	910 - 1360	910 - 1490
ΔP, % P_{inlet}	4, 6, 8	2, 4, 6, 8
Combustor T_{res}, ms	2.3 - 4.0	1.8 - 4.4

Figure 4-6 shows measured NOx EI as a function of calculated flame temperature, corrected by the measured inefficiency for configurations 1 and 1A. The program goal of achieving less than 5 EI NOx at FLADE C1 cycle conditions, was achieved with configuration 1A for inlet temperatures of 1110 R (617 K) and higher. Some of the measured data fell within the boundaries of the previously published LPP data. Although the ΔP across the cup was varied from 4% to as high as 8%, no discernible influence on measured NOx was documented at these conditions. The low NOx emissions measured at low inlet temperatures are a consequence of low test flame temperatures due to the high combustion inefficiencies measured at these conditions. This was especially the case for Configuration 1.

Figure 4-7 shows the measured combustion inefficiency plotted versus the flame temperature calculated from the gas analysis of the emissions sample, including a correction for combustion inefficiency. For Configuration 1A, as the pressure drop, across the premixer is increased, there is a slight improvement in the measured combustion efficiencies. Combustion inefficiency for configuration 1A is much more sensitive to T_3. Ignoring any effect of pressure drop, as T_3 is increased from 910 R (506 K) to 1110 R (617 K), for configuration 1A at P_3=17 psia, the inefficiency was reduced by about 90%. Configuration 1A achieved to program goal of at least 99% combustion efficiency at FLADE C1 cycle conditions (Figure 4-7) for a limited set of test conditions. Combustion inefficiencies for Configuration 1 were unacceptable.

The performance deficiencies of Configurations 1 and 1A are probably due to non-uniform mixing. A cold flow visualization test was carried out on Configuration 1. The fuel nozzle was placed in the entrance region of the central jet at the same location as it was during the combusting test. Despite the 180° spray angle, the spray bends almost immediately downstream of the fuel nozzle and enters the swirler in the form of a concentric stream tube. It is apparent that fuel , once atomized, does not penetrate a high velocity air stream.

4.1.3.2 Configuration 2A and 2B Testing

A new fuel injector was designed to distribute fuel more uniformly in the Swirl-Tube's premixing chamber. This injector consisted of four radial fuel spray bars which were placed at the exit of the venturi. This spraybar arrangement provides multiple injection points and with more uniform fuel distribution. As shown in Figure 4-8, this spraybar fuel injector design was used for Configurations 2a and 2b. The flow number of the spraybar fuel injector was measured to be 14.60. Pertinent features of Configuration 2 are given in Table 4-3. Configurations 2a and 2b were distinguished by their swirlers:

Configuration 2a	Co-rotating Swirlers
Configuration 2b	Counter-rotating Swirlers

The test conditions for Configurations 2a and 2b were nearly the same as those for Configurations 1 and 1a. The test conditions for Configurations 2a and 2b are shown in Table 4-3b.

Table 4-3b. TEST CONDITIONS FOR SWIRL JET CONFIG 2

Configuration	2a	2b
P_3, psia	17 - 60	60
T_3, R	910 - 1460	910 - 1460
ΔP, % P_{inlet}	2 - 7	2 - 7
Combustor T_{res}, ms	1.8 - 4.0	2.3 - 4.2

Figure 4-9 compares the measured NOx EI as a function of flame temperature for co-rotating and counter-rotating configurations. The open symbols correspond to co-rotation, while closed symbols correspond to counter-rotation. In general, co-rotation resulted in higher NOx and poorer combustion efficiencies, causing most of the co-rotation data points to fall outside of the previously measured data set. There was no significant influence of pressure drop on measured NOx values. Configuration 2b (counter-rotating swirlers) yielded NOx values far below the desired program goal of 5 EI. In particular, at 3600 R (2000 K) flame temperature, the measured average NOx emissions value was a little over a 1.20 EI. However, low NOx emissions with acceptable combustion inefficiencies were only attained with Configuration 2b for inlet temperatures of 1410 R (783 K) or more.

Figure 4-10 compares the combustion inefficiency data for counter- and co-rotating configurations. The influence of inlet temperature (T_3) on combustion inefficiency is quite evident. As T_3 is increased from 1110 R (617 K) to 1460 R (811 K), the inefficiency was reduced significantly. Configuration 2b is seen to yield combustion inefficiencies in the range of 4% to 2% at low temperature (T_3=1110 R, 617 K) conditions. Also, counter-rotation is seen to result in improved combustion inefficiencies compared to co-rotation, except at T_3=1460 R (811 K). The inefficiency is affected by two counter-balancing factors: mixing and residence time. Counter-rotation yields high turbulence intensities than co-rotation which could have resulted in better mixing and improved combustion efficiency.

4.1.3.3 High Pressure Single-cup Test

Pertinent values of the parameters for the high pressure test of the Swirl Jet and the configuration are shown in Table 4-3c.

Table 4-3c. CONDITIONS FOR HIGH PRESSURE SWIRL JET TEST

P_3, psia	60 - 268.7 psia
T_3, R	1410 R - 1627 R
ΔP, % of P_{inlet}	5
Combustor T_{res}, ms	2.2 - 3.4
Equivalence Ratio	0.27 - 0.55
Swirlers	Counter-Rotating
Fuel Injector	Crossed Spraybar mounted at Venturi Exit

Table 4-4. Cell 5 Test Conditions and Measured Emissions Data for the Swirl Jet.

Test No.	P_3 psia	T_3 °F	Delta P Percent	NO_x EI	PHI	CO EI	Eff. (T_4, °R)
1	60	950	5.0	0.75	0.47	14.52	98.78 (3249)
2	60	950	5.0	2.19	0.55	3.87	99.90 (3559)
3	145	950	5.0	6.90	0.27	76.65	98.14 (2493)
4	145	950	5.0	9.16	0.30	25.67	99.39 (26 43)
5	145	950	5.0	11.25	0.38	0.76	99.98 (29 63)
6	250	1140	5.0	23.93	0.33	0.83	99.98 (2925)
7	250	1140	5.0	25.62	0.48	1.53	99.96 (3471)
8	267	1167	5.0	25.64	0.36	0.67	99.98 (3661)

Table 4-4 lists the combustion efficiency and the NOx emissions data for the high pressure single-cup test of the Swirl Jet. The combustion efficiencies are 99% and above for most of the test conditions. However, the measured NOx levels are high, especially at the higher pressures (P_3 = 150 and 260 psia). Figure 4-11 contrasts two measured fuel-air ratio profiles acquired at 60 psia and at 267 psia. As shown, the profile at 60 psia (Profile A) is uniform with maximum variation in fuel-air ratio being about 5%. The profile at 267 psia (Profile B) shows significant radial variation in the measured fuel-air ratio profile and could be as high as 22%. This variation in the fuel-air ratio profile at the measurement plane could be the cause of high NOx at high pressure conditions.

Post-test inspection of the hardware did not reveal any signs of hardware damage, indicating autoignition and flashback-free operation of the combustor, even at the most severe test point (267 psia, 1627 R, 904 K).

4.2 Lean Direct Injection (LDI)

Lean direct injection has been found to yield NOx levels which are comparable to LPP and yet offer the stability of conventional combustor design. The LDI concept selected for development was originally developed by Gordon Andrews and his co-workers. Figure 4-12 shows a schematic of this single-cup Jet Mix premixer. This section describes the initial development of the premixer via an innovative combination of CFD modeling and Design of Experiments (DOE). A discussion of the initial atmospheric and high pressure test results is then presented. An attempt to enhance the emissions performance of the mixer by improving the fuel atomizer concludes this section.

4.2.1 Jet Mix CONCERT 3-D Analysis Using Design of Experiments

A CONCERT 3-D model of the Jet Mix concept was created to study the effects of various design parameters on NOx formation. An experimental design using DOE methodology was then created which utilized this CONCERT 3-D model. The basic 8-run "analytical experiment" indicated that several design variables can have a significant impact on calculated NOx results. In order to separate the main effects from possible two factor interactions, a reflected study of 8 runs was done. By combining these two studies it was possible to separate two factor interactions from the single factor effects. In addition, the second study independently confirmed that the active factors seen in the initial study were in fact real effects and not random variations. The factors considered in the study are shown in Table 4-5.

The factors found to have a significant effect on NOx were radial hole airflow, the interaction between radial hole airflow and axial hole position (factors A and C), the interaction between axial hole position and cup length (factors C and G) and the interaction between axial hole position and fuel injector diameter (C and F). The optimum combination of these factors (for low NOx) occur when factors A, F and G were at the high level (1), and factor C was at the low level (0).

It should be noted that although the CONCERT3D code computes NOx values which appear to be of reasonable magnitude, the absolute levels may not replicate the levels emitted under actual test or flight conditions. However, the relative changes in NOx values are believed to be representative.

Table 4-5 - DOE Factors and Levels

Label	Factor	Levels 0	Levels 1	
A	Radial Hole Airflow as a Percentage of the Axial Hole Airflow	8.00	20.00	%
B	Fraction of Hole Area to Cup Area	0.300	0.403	
C	Radial Location of the Axial Hole (from Fuel Injector [0] / from Cup Wall [1])	0.0625	0.0625	in.
D	Circumferential Location of the Axial Hole	0.0	22.5	deg.
E	Axial Location of the Radial Jet (from the Forward Cup Wall)	0.015	0.250	in.
F	Fuel Injector Diameter	0.682	1.023	in.
G	Cup Length	2.17	1.08	in.

4.2.2 Jet Mix Cold Flow Spray Visualization Testing

Cold flow visualization tests have shown acceptable levels of fuel atomization in the cup, but show a need for improved atomization in the fuel nozzle. Figure 4-13 show results of some of the spray flow visualization studies. They correspond to the same pressure drop across the dome, but for different fuel flow rates (26 pph and 50 pph). For both cases, the fuel distribution quality is good, with nearly uniform fuel distribution achieved at the premixer exit, but with some rather large droplets at the edge of the cup.

4.2.3 Baseline Configuration Tests

The relevant parameters for the cold flow visualization tests are shown in Table 4-6.

Table 4-6. PARAMETERS FOR COLD FLOW VISUALIZATION TESTS

Cup ID	= 2.16 in.	Cup Length	= 2.16 in.
Axial Hole Dia.	= 0.3946 in.	Number of Axial Holes	= 8
Radial Hole Dia.	= 0.1387 in.	Number of Radial Holes	= 8
Fuel Tube Hole Dia.	= 0.0125 in.	Number of Fuel Tube Holes	= 8
Fuel Injector Dia.	= 0.682 in.	Combustor Dia.	= 2.75 in.

Effective Area - Axial Holes	= 0.7798 in^2
Effective Area - Radial Holes	= 0.1031 in^2
Cup Discharge Coefficient	= 0.8032
Axial Hole Flow Split	= 88.32%
Radial Hole Flow Split	= 11.68%
Dome Reference Velocity @ T = 1360R and 5% DP/P	= 61 ft/s

Four configurations were tested under atmospheric inlet pressures and inlet temperatures from ambient to 1260 R (700 K). Configurations 1 and 2 were distinct from configurations 3 and 4 in that configurations 1 and 2 had the fuel injection holes aligned with the axial air jets (Figure 4-12), whereas configurations 3 and 4 did not. In addition, configurations 1 and 3 had the forward edge of the radial holes positioned within 1/16 inch of the backplate of

the cup, whereas configurations 2 and 4 had the radial holes positioned approximately 1 inch from the backplate of the cup.

Figures 4-14 through 4-17 show the lean stability limits for each configuration versus inlet temperature for three dome pressure drops. Note that at some conditions, the device demonstrated stability below the measurement capability of the test facility flowmeter, hence the LBO points at zero fuel flow. Visual observations indicate that at these points the device burned whatever fuel was draining out of the fuel lines once the fuel valve was turned off completely. Much of this combustion was occurring near the hot wall ceramic liners, which seemed to greatly enhanced stability.

At inlet temperatures above 910 R (506 K), configurations 1, 3 and 4 had combustion inside the cup and stabilized off the fuel injector. Visual observation revealed a flat flame which burned very close to the cup. Configuration 2 had no in-cup combustion at any inlet temperature. It had the flame stabilized off the dome dump at the exit of the cup. The flame appeared to have an unburned core of fuel-air mixture in the center of the cup which burned approximately half way down the combustor.

Post test observation of configurations 3 and 4 revealed black streaks left on the combustor walls in the plane opposite the radial holes. This was due to the fuel injection holes being purposely misaligned with axial jets. This allowed the fuel to penetrate further radially into the air stream and impinge on the cup sides. Configurations 1 and 2 did not show any black streaks since the radial holes were aligned with the axial holes. This allowed the fuel droplets to vaporize and mix better with the axial air jets.

4.2.3.1 Pressure Testing

Jet Mix configuration 1 was tested at inlet pressures up to 60 psia and inlet temperatures ranging from 660 R (367 K) to 1360 R (756 K). Figure 4-18 shows the combustion efficiency data plotted as a function of metered equivalence ratio for different inlet temperature conditions. All of the data points correspond to 60 psia inlet pressure except the points corresponding to an inlet temperature of 660 R (367 K). At this temperature the inlet pressure was maintained at 17 psia in order to simulate the low power cycle condition. As the figure shows, the combustion efficiency dropped from 99.5% to 57% as the metered equivalence ratio was increased from about 0.48 to 1.06. At the same equivalence ratio, higher inlet temperatures were found to result in higher combustion efficiency.

The poor combustion efficiency beyond the equivalence ratio of 0.6 is attributed to inefficient fuel-air mixing at the exit of the premixing cup. Post-test inspections of the hardware revealed formation of black carbon on the cup walls directly opposite the radial fuel holes, indicating impingement of fuel on the walls. As the fuel jet velocity increased, the relative velocity of the fuel jet and air velocity through the radial holes decreased. This reduced fuel atomization resulted in poor vaporization and mixing. In addition, as the fuel jet velocity increased it penetrated through the axial air stream, impinged on the outer hot wall, and concentrated there. This caused a rich zone near the outer rim and a very lean inner core. The non-uniform fuel-air profile at the mixer cup exit resulted in wide combustion stability limits; but poor combustion efficiency and high NOx emissions.

Figure 4-19 shows variation of NOx EI versus corrected flame temperature, for configuration 1. As shown in the figure, the measured NOx data is found to vary from an EI of 1 g/kg at 17 psia and 710 R (394 K) inlet temperature to EI of about 12 g/kg at 60 psia and 1360 R (756 K) inlet temperature. The data show that the NOx EI is relatively independent of the corrected flame temperature and is sensitive to inlet temperature. This is characteristic of a highly non-uniform fuel-air distribution.

Subsequent tests showed that the pressure drop across the radial holes is less than expected due to the constrictions in the annular passage leading up to the radial holes. The pressure drop across the radial holes was 3.7% compared to 5% across the axial holes. The fuel injector support that caused the constriction has since been removed, increasing the pressure drop across the radial holes to 4%.

4.2.4 Fuel Atomizer Improvements

The results of the pressure test indicated that the fuel jets were passing through the radial/axial jet interaction without being vaporized, and impinging on the cup wall opposite the radial holes. A remedy for this problem is to decrease the fuel/radial air momentum ratio to below 100 by increasing the diameter of the fuel holes. This in turn should decrease penetration of the fuel jet, allowing the turbulence created by the axial/radial jet interaction to atomize the spray. This approach should increase mixture uniformity, lower local flame temperatures and improve combustion efficiency and NOx emissions.

Fuel tubes with larger holes (diameter of 0.0313 inch), designed to reduce fuel penetration were evaluated with water spray testing. Based on these tests, the spray quality of the fuel tubes is acceptable. Experimentation with inserting smaller diameter tubing inside the fuel tube to change the characteristics of the fuel flowfield as it approaches the hole in order to improve atomization was also completed using water spray testing. Inserting 0.072 inch OD tubing into the fuel tubes with 0.0125 inch diameter radial holes improved radial jet atomization the most over the baseline of no inner tube. Repeating the test with the fuel tube having the 0.0313 inch diameter holes resulted in a degradation of the discrete jet characteristics.

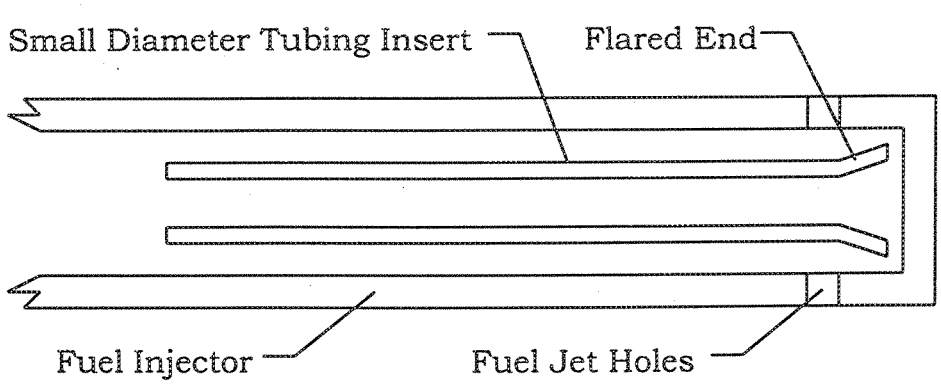

Testing of the two best fuel tube concepts for radial fuel jet penetration was completed in the single-cup rig. Testing consisted of spray visualization

testing at ambient temperature and pressure, 5% pressure drop and 50 pph fuel flow. Both configurations demonstrated acceptable penetration. The large radial fuel hole (0.0313 inch radial holes in a 0.125 inch diameter tube with no inner tube) concept showed the best results with no visible jets, significant jet breakup and atomization in the axial/radial air interaction zone. The small radial fuel hole, tube-in-a-tube concept (0.0125 inch diameter fuel holes in a 0.125 inch diameter fuel tube with a 0.072 inch in OD flared end inner tube) did show some discrete jets within the axial/radial jet interaction zone. However, these jets were atomized and turned downstream by the axial jet before they reached the cup wall.

Configuration 6 consisted of configuration 1 (fuel module radial holes close to and in-line with the cup axial holes) with a 0.125 inch OD central fuel tube with eight 0.0313 in diameter holes in line with the radial air holes. Configuration 7 was similar except the central fuel tube was replaced with one containing eight 0.0125 in diameter holes and a 0.072 in OD flared end inner tube. Each configuration was tested at inlet conditions of 4 atmospheres pressure and inlet temperatures of 910 R, 1120 R, and 1410 R. As shown in Figure 4-1, both the configurations were tested using the 4.89 inch diameter cast ceramic liner, with the emissions probe 2.62 inches downstream of the cup exit. This configuration yielded a bulk dome velocity of 22.7 ft/s and a combustor bulk residence time of 3.2 ms, based on an inlet temperature of 1360 R (756 K), a flame temperature 3600 R (2000 K), an inlet pressure of 60 psia, and a dome pressure drop of 5%. In contrast, configuration 1 used the 2.8 inch diameter liner with the emissions probe 7.42 inches downstream from the cup exit. This configuration yielded a bulk residence time of 3.1 ms and a bulk dome velocity of 69.2 ft/s at the above conditions. The reason for the change to the larger combustor diameter in the later tests stem from the decision to evaluate the Jet Mix at bulk velocities representative of a pilot dome, instead of a main dome.

The NOx emissions indices for Jet Mix configurations B6 and B7, two Multiple-Venturi premixer configurations tested at GEAE and IMFH premixer Configuration 5A are compared in Figure 4-20. As shown in the figure, at inlet temperatures near 910R, the results plotted in Figure 4-20a show that all three mixer designs have similar NOx emissions. At combustor inlet temperatures near 1120 R (622 K), the results plotted in Figure 4-20b show that the NOx EI of Jet Mix follows closely that of Multiple-Venturi, and is higher than IMFH at design flame temperature below 3600 R. As the inlet temperature is increased to 1410 R (783 K), the results plotted in Figure 4-20c show that the NOx EI of Jet Mix is significantly higher than either the IMFH or Multiple-venturi for flame temperature below 3600 R (2000 K), and is similar to the IMFH and Multiple-Venturi above flame temperatures of 3600 R.

Figure 4-21 compares the combustion inefficiencies for the same configurations of the three premixer designs. For the sake of simplicity, the figure only compares the measured inefficiencies at the lowest and highest inlet temperatures. In general, the Jet Mix has higher combustion inefficiency than either Multiple-Venturi or the IMFH, with the exception that at 910 R (506 K) inlet temperature, the IMFH data show higher inefficiency than either the Multiple-Venturi or the Jet Mix.

4.3 IMFH Premixer

The Integrated Mixer Flame Holder (IMFH) was initially developed under contract NAS3-25552 during which IMFH Configurations 1 through 3 were tested. Low emissions (4.1 EI NOx and 99.7% combustion efficiency at a 3593 R (1996 K) flame temperature) were demonstrated in flame tube tests for near design inlet temperatures (1626 R, 903 K) but at low inlet pressure (4 atm). The contract concluded with the design, procurement, and assembly of IMFH high pressure test rig and mixer (Configuration 4) hardware to evaluate emissions and the potential for autoignition and flashback near design conditions.

IMFH design efforts in this contract were initiated with high inlet temperature and pressure flame tube testing of IMFH Configuration 4. Dome cooling air flow introduction into the mixer air flow was developed in Configuration 5. This key design feature was necessary to allow incorporation of the IMFH into combustor dome designs. An alternate dome cooling air insertion design, as well as injector immersion effects were evaluated in Configuration 6. A summary of the major design parameters varied for IMFH Configurations 1 through 6 is shown in Table 4-7. Alternate IMFH designs, such as the venturi IMFH (discussed below) were also studied.

IMFH development has continued under contracts NAS3-26617 and NAS3-27235 with sector and flame tube tests evaluating fuel injector and mixer tube design variations to better implement an IMFH combustor main dome.

4.3.1 IMFH Configuration 4 Testing at High Inlet Temperature & Pressure

Integrated Mixer Flame Holder (IMFH) Configuration 4 successfully operated at 145 psia and 1600 R (889 K) inlet conditions with 5% and 3% combustor dome pressure drop. This is the design engine cycle mid-cruise inlet pressure and approaches the mid-cruise inlet temperature of 1675 R (931 K). NOx emissions were below HSCT goals and combustion efficiencies were 99.8% and higher. At 5% pressure drop, NOx emissions ranged from 0.7 to 6.3 EI for averaged gas sample equivalence ratios of 0.41 to 0.57 corresponding to efficiency corrected flame temperatures of 3207 R to 3774 R (1782 K to 2097 K). Combustion efficiency ranged from 99.93 to 99.80%. NOx emissions at 3% dome pressure drop (lower velocity and subsequently longer combustion residence time) were 1.8 and 5.1 EI NOx for 0.44 and 0.51 sample equivalence ratios (3335 R & 3568R, 1853 K & 1982 K flame temperatures). These results compared favorably with those of previous IMFH configurations as shown in Figure 4-22.

The high pressure and temperature test point schedule which encompasses a range of pressures and temperatures emulating HSCT cycle operating ranges is summarized in Table 4-8. The maximum combustor inlet pressure and temperature (at supersonic cruise, cycle C1) correspond to 220 psia and 1675 R (931 K). The combustor inlet temperature at SLTO is 1350 R (750 K). Cell 5 testing was carried out at the test conditions of 4 atm and 1410 R (783 K) to 10 atm and 1600 R (889 K) to emulate these cycle points within the constraints of the cell facility. The results of these tests are described below.

Table 4-7. IMFH Test Configurations for Contracts NAS3-25552 and NAS3-25951.

INTEGRATED MIXER FLAMEHOLDER DEVELOPMENT HISTORY

Boxed information indicates a change from previous configuration

Conf #	Test Date	Mixer Tube: Description	Mixer Tube #	Exit Diam. in.	Total Length in.	Mixing Length in.	Inlet Radius in.	Dome Cooling Air	Injector: Type	Each Inj. Flow #	Injector Discharge #	I.D., in.	O.D., in.	Axial Dist from inlet	Immers. %	Combustor Liner: Type	Diam., in.	Dist.to Sample Probe,in.	Test Type: High pressure Low pressure Atms.dsch.
Developed under NAS3-25552:																			
1	05-91	0.769" ID Straight mixer tube	7	0.769	5.100	4.500	20 deg.flare	Bypass comb.	Large ID,transverse tube	1.5	1	0.069	0.125	0.600	50	Metal:H2O Cooled	4.300	6.800	Atm.& Low p.
2	07-91	0.769" ID Straight mixer tube	7	0.769	5.100	4.500	20 deg.flare	Bypass comb.	Transverse tube with 4 injection holes	1.4	4	0.008	0.125	0.600	30 & 70	Cast ceramic with air passages	4.300	6.800	Low pressure
3A1	09-91	0.560" ID Straight mixer tube	7	0.560	5.100	4.500	20 deg.flare	Bypass comb.	Transverse tube with 2 injection holes	1.3	2	0.008	0.125	0.600	50	Cast ceramic with air passages	4.300	6.800	Low pressure
3A2	09-91	0.560" ID Straight mixer tube	7	0.560	5.100	4.500	20 deg.flare	Bypass comb.	Transverse tube with 2 injection holes	1.3	2	0.008	0.125	0.600	50	Cast ceramic with air passages	4.300	3.625	Low pressure
																	Half comb.res. time of 3A1		
3B	09-91	0.560" ID Straight mixer tube	7	0.560	5.100	4.500	20 deg.flare	Bypass comb.	Fine tube angled 15 deg.	1.2	1	0.020	0.040	0.600	50	Cast ceramic with air passages	4.300	6.800	Low pressure
4A	11-91	0.495" ID Straight mixer tube	13	0.495	5.500	4.500	0.188	Exit: 90 holes 0.086"diam.at dome ring	Fine tube angled 15 deg.	1.3	1	0.020	0.040	1.000	50	Cast ceramic with backside air cool.	4.500	9.450	High presssure
Developed under NAS3-25951:																			
4B	01-92	0.495" ID Straight mixer tube	13	0.495	5.500	4.500	0.188	Bypass comb.	Fine tube angled 15 deg.	1.3	1	0.020	0.040	1.000	50	Cast Ceramic with air passages	4.888	7.423	Low pressure
5A	03-92	0.495" ID with dome cool.air inj.into aft end of mixer tube	13	0.495	5.500	4.500	0.188	Inj. into mixers 6x 0.090" holes	Fine tube angled 15 deg.	1.3	1	0.020	0.040	1.000	50	Cast Ceramic with backside air cool.	4.888	7.423	Atm.& Low P.
5B	07-92	0.495" ID with dome cool.air inj.into aft end of mixer tube	13	0.495	5.500	4.500	0.188	Inj. into mixers 6x 0.090" holes	Fine tube angled 15 deg.	1.3	1	0.020	0.040	1.000	50	Cast Ceramic	4.500	9.450	High presssure
6A	10-92	0.560" ID with dome cool.air inj.thru dome near mixer exit	7	0.560	5.100	4.500	20 deg.Flare	Through dome 6x 0.100" holes	Fine tube angled 15 deg.	1.3	1	0.020	0.040	1.000	50	Cast Ceramic	4.300	6.800	Low pressure
6B	01-93	0.560" ID with dome cool.air inj.thru dome near mixer exit	7	0.560	5.100	4.500	20 deg.Flare	Through dome 6x 0.100" holes	Fine tube wall injection	1.3	1	0.020	0.040	1.000	0	Cast Ceramic	4.300	6.800	Low pressure

Table 4-8. IMFH High Pressure Test Conditions.

INLET TEMP. deg.F	INLET PRES-SURE ata	% DOME PRES-SURE DROP	COMBUSTOR AIRFLOW pps	COMBUSTOR EQUIV. RATIO	COMBUSTOR FLAME TEMP. K	MIXER AIRFLOW pps	MIXER EQUIV. RATIO	MIXER FLAME TEMP. K	
900	4.0	5.0%	.97	.468	1800	.85	.536	1929	
900	4.0	5.0%	.97	.520	1900	.85	.596	2037	
900	4.0	5.0%	.97	.575	2000	.85	.659	2146	
900	4.0	5.0%	.97	.632	2100	.85	.724	2252	
									LOW PRESSURE TEST POINTS
900	4.0	7.0%	1.15	.468	1800	1.00	.536	1929	
900	4.0	7.0%	1.15	.520	1900	1.00	.596	2037	
900	4.0	7.0%	1.15	.575	2000	1.00	.659	2146	
900	4.0	7.0%	1.15	.632	2100	1.00	.724	2252	
900	9.9	5.0%	2.39	.468	1800	2.09	.536	1929	
900	9.9	5.0%	2.39	.520	1900	2.09	.596	2037	
900	9.9	5.0%	2.39	.575	2000	2.09	.659	2146	
900	9.9	5.0%	2.39	.632	2100	2.09	.724	2252	
900	9.9	7.0%	2.83	.468	1800	2.47	.536	1929	
900	9.9	7.0%	2.83	.520	1900	2.47	.596	2037	
900	9.9	7.0%	2.83	.575	2000	2.47	.659	2146	
900	9.9	7.0%	2.83	.632	2100	2.47	.724	2252	
1150	9.9	5.0%	2.20	.412	1800	1.92	.472	1918	
1150	9.9	5.0%	2.20	.462	1900	1.92	.530	2028	
1150	9.9	5.0%	2.20	.515	2000	1.92	.590	2137	
1150	9.9	5.0%	2.20	.569	2100	1.92	.652	2245	
1150	9.9	7.0%	2.60	.412	1800	2.27	.472	1918	
1150	9.9	7.0%	2.60	.462	1900	2.27	.530	2028	
1150	9.9	7.0%	2.60	.515	2000	2.27	.590	2137	
1150	9.9	7.0%	2.60	.569	2100	2.27	.652	2245	HIGH PRESSURE TEST POINTS
1150	9.9	3.0%	1.70	.412	1800	1.49	.472	1918	
1150	9.9	3.0%	1.70	.462	1900	1.49	.530	2028	
1150	9.9	3.0%	1.70	.515	2000	1.49	.590	2137	
1150	9.9	3.0%	1.70	.569	2100	1.49	.652	2245	
1150	13.6	5.0%	3.03	.412	1800	2.65	.472	1918	
1150	13.6	5.0%	3.03	.462	1900	2.65	.530	2028	
1150	13.6	5.0%	3.03	.515	2000	2.65	.590	2137	
1150	13.6	5.0%	3.03	.569	2100	2.65	.652	2245	
1150	13.6	7.0%	3.59	.412	1800	3.13	.472	1918	
1150	13.6	7.0%	3.59	.462	1900	3.13	.530	2028	
1150	13.6	7.0%	3.59	.515	2000	3.13	.590	2137	
1150	13.6	7.0%	3.59	.569	2100	3.13	.652	2245	
1150	13.6	3.0%	2.35	.412	1800	2.05	.472	1918	
1150	13.6	3.0%	2.35	.462	1900	2.05	.530	2028	
1150	13.6	3.0%	2.35	.515	2000	2.05	.590	2137	
1150	13.6	3.0%	2.35	.569	2100	2.05	.652	2245	

There were no apparent signs of flashback or autoignition during the test. The most likely test conditions for autoignition were 10 atm and 1600 R (889 K), with 3% pressure drop across the premixer. At these conditions, the average mixer tube residence time was approximately 20% of the estimated autoignition time.

Figure 4-23 depicts NOx EI (normalized by residence time) plotted as a function of flame temperature for Configurations 3b and 4 (4 atm and 10 atm). Roffe-Venkataramani's [3] premixed NOx correlation for propane is also plotted on the figure for comparison. The test data collapse onto a single curve and replicate Roffe-Venkataramani's correlation reasonably well, indicating near-ideal vaporization/mixing achieved for these two configurations. Configuration 4 test data at 4 atm and 1350 R (750 K) inlet temperature show significantly higher NOx emissions compared to the above two configurations. Figure 4-24 shows a plot of combustion inefficiency as a function of NOx emissions index for the same configurations. As shown in the figure, Configuration 4 at 4 atm has resulted in inefficiency as high as 14% to 21% compared to less than 0.25% for Configuration 4 at 10 atm. In comparison, Configuration 3b combustion inefficiencies dropped from a maximum of only 2.2% at a 1360 R (756 K) inlet to 0.4% and less at a 1630 R (906 K) inlet. Configuration 4 differed from previous IMFH configurations in that the spent flameholder cooling air was dumped as a film into the flame tube. Evidently, the low temperature spent dome cooling air discharged near the flame tube walls resulted in higher combustion inefficiencies due to CO quenching in the reaction zone.

An alternate spent cooling air discharge scheme was designed and tested to evaluate the influence of cooling air on combustion efficiency. Figure 4-25 depicts flameholder cooling air discharge schemes for Configurations 4 and 4b. As shown in configuration 4, the spent air discharged directly into the primary zone, while in Configuration 4b, the spent air was rerouted around the combustor through discharge slots in the ceramic liner. Configuration 4b NOx emissions plotted as a function of flame temperature in Figure 4-26 fall within the band of measured NOx EI for the earlier configurations. Figure 4-27 compares the measured inefficiencies for Configurations 4 and 4b at the low inlet temperatures troublesome for Configuration 4. Redistributing the spent cooling air significantly reduced combustion inefficiency. This demonstrates the CO quenching effect of the spent air in Configuration 4.

Configuration 4b test data show the effects of mixing and evaporation on combustion efficiency. Figure 4-28 shows the influence of increased pressure drop on combustion efficiencies. As pressure drop across the premixer is increased from 1.60% to 6.2%, better mixing is achieved, resulting in improved measured efficiencies. Figure 4-29 shows the inlet temperature (evaporation) influence on combustion inefficiency. As the inlet temperature is increased from 910 R (506 K) to 1419 R (788 K), the measured efficiency values improve significantly due to enhanced droplet evaporation and more rapid reaction achieved at higher temperatures.

4.3.2 IMFH Configuration 5 Testing with Spent Cooling Air Injection

A novel design approach that injects spent dome impingement cooling air into the IMFH premixing tubes was demonstrated to reduce NOx by providing more combustion airflow to lean-out the mixer, and also to reduce CO by

eliminating the cooling air film which quenches combustion reactions. Figure 4-30 shows a schematic of the flameholder cooling air injection design of Configuration 5, where spent cooling air is injected into the premixer just before the premixer exit.

The measured combustion inefficiency and NOx emissions for Configurations 4 (no spent air addition in premixer) and 5 (spent air addition in premixer) are compared in Figures 4-31 and 4-32. The data demonstrate no detrimental effect of the spent air injection on high inlet temperature combustion inefficiency and NOx emissions. These tests showed combustion inefficiency and NOx levels substantially below program goals over a wide range of operating conditions. As shown in Figure 4-33, the spent air injection showed lower combustion inefficiency at 1110 R (617 K) inlet temperatures and high flame temperatures.

Possible impacts of the spent air addition in the premixer include improved stability due to increased mixing of recirculated combustion gases at the point where they first come in contact with the premixed fuel-air mixture. As well as improved performance at low inlet temperatures due to the air jets reatomizing unvaporized fuel as it exits the IMFH tubes. A risk of the added air was that it would result in a greater variation in the premixer fuel-air ratio. Wide variations in premixed fuel-air ratios have generally been related to higher thermal NOx production for a given average fuel-air ratio. There has been no evidence of this by the IMFH test data. It might be that the small-scale of the IMFH creates small scale nonuniformities which mix out before the integrated effect of the hot spots can impact the NOx emissions.

The IMFH Configuration 5B test was a major success with stable operation demonstrated over a range of test conditions from 1410 R (783 K) and 4 atm to 1656 R (920 K) at the design point inlet pressure of 10 atmospheres. This test also demonstrated autoignition/flashback-free steady state operation of IMFH Configuration 5B for most of the HSCT steady state design cycle conditions by running up to 1631 R (906 K) and 17 atm inlet conditions with as little as 3.6% dome pressure drop. The test results supported use of this dome cooling air injection into the mixer tubes design for the first sector design.

Key Configuration 5B test result data trends are readily apparent in the following figures which compare Configuration 4, 4B, 5A and 5B results. Note that the emissions data are arithmetic averages of five samples taken during a radial traverse. Also recall the differences between Configurations 4, 4B, 5A and 5B which are summarized in Table 4-9.

Table 4-9. IMFH CONFIGURATIONS SUMMARIZED

Configuration	Facility (Rig)	Dome Cooling Air Discharge	Fuel Injectors
4	Cell 5	As Liner Film	Original Hypo Injectors
4B	306	Around Combustor	Same as 4
5A	306	Into Mixer Tubes	Same as 4 and 4B
5B	Cell 5	Into Mixer Tubes	New Set Like 4, 4B, & 5A

NOx emissions data are presented as a function of corrected flame temperature in Figure 4-34. Configuration 5B NOx emissions were below goal at the design flame temperature, within the range of previous results and followed similar trends. There was little difference between Configurations 5B and 5A NOx emissions, although the combustion zone residence times of Configuration 5B (4.1 to 5.7 ms) are longer than those of Configuration 5A (2.6 to 3.9 ms).

In Figure 4-35, the influence of combustor residence time has been eliminated by dividing NOx emissions by the residence time. Most of the Configuration 5B data falls at or just below the Roffe-Venkataramani LPP propane combustion correlation line. With the exception of the low pressure (4 atm) Configuration 4 data, the NOx emissions followed very consistent trends. Thus, the differences between Configuration 4B, 5A and 5B had no impact on NOx emissions.

Figure 4-36 shows the low combustion inefficiencies, well below the goal, demonstrated for a wide range of flame temperatures (~3150 R - 4320 R, 1750 K - 2400 K). At the same inlet pressure (4 atm), differences between Configuration 4B, 5A and 5B had no impact on combustion inefficiency despite 30 to 40% difference in combustor residence time. It is therefore expected that Configuration 5B would maintain low combustion inefficiencies with combustor residence times reduced to Configuration 5A test levels (30 to 40%). Combustion inefficiencies decreased at the elevated pressures tested with Configuration 5B. One of the 1650 R (917 K) and 10 atm Configuration 5B test points doesn't even appear on the plot due to its very low emissions.

Figure 4-37 shows combustion inefficiency plotted as a function of NOx emission index. The data follow the trends of the previous figures with reduced inefficiency at elevated pressures and a majority of the data satisfying both NOx and combustion inefficiency goals.

4.3.3 IMFH Configuration 6A Testing - Alternate Spent Cooling Air Injection

The objective of this test was to identify any compromises in combustion efficiency, flame stability, and/or NOx emissions due to a shift in dome cooling air discharge location to the face of the flame holder in Configuration 6 rather than into the mixer tubes as in Configuration 5. The benefit of this new discharge hole location would be reduced IMFH mixing tube air flow blockage. Mixer tube flow blockage is concerning since it reduces the air velocity and flow past the injectors (reducing fuel atomization) and increases the residence time in the premixer (increasing the possibility of autoignition).

A schematic of IMFH Configuration 6 is shown in Figure 4-38. It used Configuration 3B hardware (7 mixer tubes with 0.560 inch inner diameters and hypodermic injectors) modified to inject flame holder cooling air through the face of the flame holder. Figure 4-30 shows a schematic of Configuration 5 to allow a comparison of dome cooling air injection methods. Configuration 6 had larger mixer tube inner diameters (0.560" vs. 0.495"), smaller length to tube diameter ratios (8.0 vs. 9.1) and a larger dome blockage (88% vs. 83%) than Configuration 5.

IMFH Configuration 6A was tested in the low pressure test facility at inlet temperatures ranging from 910 R (506 K) to 1410 R (783 K), and at pressure

drops ranging from 3.5% to 6.5%. The combustor inlet pressure was maintained constant (at 4 atm) for all the test conditions. Low inlet temperature performance, as indicated by lightoff equivalence ratio, was slightly worse for Configuration 6 than for Configuration 5. Emission measurements were made over the flame temperature range of 2920 R to 4360 R (1622 K to 2422 K). As shown in Figure 4-39, the NOx emissions were higher for Configuration 6A than for Configuration 5A at 1410 R (783 K) inlet temperature and flame temperatures greater than ~3450 R (1361 K). At 1110 R (617 K) inlet temperature, Configuration 6A NOx emissions were comparable to those of Configuration 5A. Configuration 6A combustion inefficiency results were comparable to Configuration 5A at the higher inlet temperatures (Figure 4-40).

Figure 4-41 compares the emissions data (normalized by residence time) corresponding to flameholder discharge of spent air (Configuration 6A), with no dome cooling air discharge (Configuration 3B). As shown, the NOx emissions for Configuration 6A were significantly higher than those of Configuration 3B for inlet temperatures near 1400 R (778 K) and flame temperatures above 3600 R (2000 K). However, as shown in Figure 4-42, Configuration 6A inefficiencies were at least an order of magnitude less than those of Configuration 3B indicating that the improvements in combustion inefficiency due to flameholder discharge of spent dome cooling air were made at the expense of higher NOx emissions. In contrast, the injection of spent dome cooling air into the mixer tubes reduced NOx emissions without significantly impacting combustion inefficiency. This can be seen by comparing the 910 R, 1110 R and 1410 R (506 K, 617 K, and 783 K) inlet temperature EI NOx/ms data in Figure 4-43 with the combustion inefficiency data of Figure 4-44.

Among other observations, it was inconclusive whether Configuration 6A was much more difficult to light than Configuration 5A at 910 R (506 K). The minimum equivalence ratio for stable operation of Configuration 6A was 0.89 compared to 0.77 for Configuration 5A at this inlet temperature. It should be noted that flameholder discharge of dome cooling air reduced the minimum inlet temperature needed for stable operation of Configuration 3B.

4.3.4 Configuration 6B Testing - Fuel Injection at the Mixer Tube Wall

Configuration 6B had hypo tube fuel injectors discharging perpendicular to the airflow at the mixer tube walls, as shown in Figure 4-45 in contrast to configuration 6A which had hypo tube fuel injectors discharging nearly perpendicular to the airflow at the mixer tube centerline.

Combustion inefficiencies were significantly higher for Configuration 6B than those of Configuration 6A as shown in Figure 4-46. Even at 1420 R (789 K) inlet temperatures, Configuration 6B combustion inefficiencies were 0.7 to 9.2% compared to 0.02 to 1.6% for configuration 6A. This is attributed to poorer fuel atomization and mixing with air for wall injection. Indications of this were high levels of unburned hydrocarbons at high inlet temperatures (1420 R, 789 K), fuel streaks aft of the injectors observed in the mixer tubes during the post test inspection, and a stagnation zone observed aft of the injectors in an unfired post run test. Unburned hydrocarbons have typically been less than 0.1 EI at 1420 R (789 K) inlet temperatures for IMFH Configuration 4B, 5, and 6A. In comparison, Configuration 6B unburned hydrocarbons ranged from 3 to 93 EI at these conditions.

Configuration 6B NOx emissions are compared to those of Configuration 6A in Figure 4-47. Though the Configuration 6B NOx emissions are lower than those of Configuration 6A for calculated flame temperatures greater than 3400 R (1889 K), the slope of the data as well as the high concentration of unburned hydrocarbons are more indicative of a poorly mixed flame. As a consequence of these results, the hypo tube injector discharge flush with mixer tube walls was dropped from consideration in the IMFH.

4.3.5 Venturi IMFH Studies

The velocity of the air in the IMFH plays a crucial role in atomizing the fuel in the IMFH. Changing the straight tube geometry of the IMFH premixer to a venturi to increase the air velocity at the point of fuel injection could improve performance. To better understand the potential for performance improvement, an analytical model of a venturi IMFH was developed and effect of venturi throat diameter on IMFH performance was studied. Mixer tube residence time, autoignition time, fuel mean droplet size, evaporation time and pressure drop losses due to friction and the premixer dump were calculated as a function of the throat diameter. A constant mass flow rate and a constant discharge coefficient (which implies a constant exit diameter) were assumed for a given flight condition. Other assumptions were an isentropic inlet, a straight tube section with friction and an isentropic diffuser section. The straight tube section was shortened as the throat diameter decreased. Part of the decrease was due to the diffuser getting longer, but additional length was taken out to maintain the pressure drop constant despite the increase in friction with increasing velocity. The fuel was injected at the inlet of the straight section. The diffuser section was assumed to be conical in shape to simplify the residence time calculations.

As shown in Figure 4-48, the predicted ratio of residence time in the premixing length of the tube to autoignition time was substantially reduced for the supersonic maximum climb and supersonic mid-cruise flight conditions by decreasing the throat diameter of the venturi. This was due to higher velocity within the premixer section leading to lower static temperatures and a corresponding increase in autoignition time. With a decrease in throat diameter, the predicted ratio of tube residence time to fuel vaporization time was significantly increased (Figure 4-49). The increased velocity at the throat decreases the fuel mean drop size, thereby lowering the vaporization time and giving fuel droplets a greater margin for evaporation within the premixer tube assembly.

These plots suggest that the utilization of a venturi tube within the IMFH will enhance performance by providing better atomization, lower residence and vaporization times and longer autoignition times. The beneficial results of the smaller venturi throat is mainly an effect of the improved atomization due to the higher air velocities. These predicted benefits are only as good as the correlation used for predicting the effect of velocity on drop size. Caution should be taken, however, for all of the parameters have not been studied in this analysis. Though atomization and fuel evaporation improve with the decrease in throat diameter, the effect on mixing is unknown. The reduction of the premixer length with decreasing throat diameter may compromise mixing performance. Additionally, the low velocity within the larger boundary layer in the diffuser section of the venturi IMFH premixer assembly may induce

autoignition or flashback within the boundary layer. Though there may appear to be drawbacks to the venturi IMFH setup, the benefits warrant further analysis and/or experimentation.

4.4 Cyclone Swirler Premixer

The Cyclone Swirler Premixer was chosen as a candidate fuel-air mixer for the LPP combustor's pilot stage based on previous experience with various versions the concept at GEAE. It is a radial swirler with the fuel injector incorporated into a centerbody on the axis of the radial swirler.

4.4.1 Cyclone Swirler Fuel Injector Design

The fuel injector for the HSCT version was patterned after the fuel injector used in Gordon Andrew's LDI concept discussed in Section 4.2, except that the air flow was significantly reduced. Two versions of the centerbody/injector were fabricated, an eight injector and a twelve injector design, both with the same physical flow area. The assembly drawing of the eight hole version of the nozzle is shown in Figure 3-6. In qualitative spray tests the eight hole version worked better than the twelve hole version, but even the eight hole version was not satisfactory. Because the air flow was reduced from Anderson's design, the air holes through which the fuel must pass is smaller. As a result, fuel is more likely to contact the surface of the air hole and dribble off the nozzle. The observations confirmed this expected trend. In early sketches of this nozzle, extensions were included on the fuel tubes to guide the fuel to the entrance of the air holes, but they were eliminated in the first fabricated versions to simplify the design. The extensions proved to be necessary and were added back in the form of 0.012 inch I.D., 0.020 inch O.D. hypodermic tubing extensions about 0.2 inches long. Spray tests of the modified injector then resulted in good quality fuel sprays. Although the extensions add to the complexity of the design, they have the advantage of making each injector tube and air hole or air nozzle equivalent to a plain-jet airblast atomizer as studied by Lorenzetto and Lefebvre [4, 5]. The correlations resulting from those studies can be used to predict and optimize the performance of the injector.

Besides Lefebvre's study and the study of G.E. Andrews [6] in support of his LDI concept, there are other published studies of airblast fuel nozzles with geometries similar to the that used in the Cyclone Swirler. These results provide guidance to further optimizing the fuel injector's performance. The experimental conditions in a study performed by H.F. Hrubecky appear to be relevant [7]. These studies suggest that 20 micron droplet fuel sprays should be attainable in the airblast fuel injector.

The basic design of the injector appears to be very well suited for the Cyclone Swirler premixer. The advantage of the design is that it has the simplicity of a single nozzle assembly located at the axis of the Cyclone Swirler. The fuel is injected towards the Cyclone Swirler wall in discrete jets which can penetrate through the main air flow (which is moving inwards opposite to the jets) to the wall of the Cyclone Swirler.

4.4.2 Atmospheric Test of Cyclone Swirler, Configuration 1

The first HSCT Cyclone Swirler design (Configuration 1) had an effective flow area of 0.65 in^2, a residence time of about 0.4 milliseconds, and a calculated swirl number of 0.94. Its first fired test was at atmospheric pressure. Combustor inlet temperatures were varied from ambient to 1405 R (781 K). Pressure drops of 5% and 7% were investigated. The corresponding combustor reference velocities were 53 and 62 ft/sec. Results for ignition and lean blow out were obtained and the appearance of the flame recorded with a video camera. At these reference velocities, the Cyclone Swirler would not ignite at ambient inlet temperature. However, the fuel spray within the combustion chamber appeared normal; i.e., there was no chugging or loading with fuel which can occur with Cyclone Swirler designs at low inlet temperatures. This was by design, although the pilot application of Configuration 1 was not certain at the time of its design. Smooth ignition did occur at 710 R (394 K). These ignition results have to be considered in light of the higher than normal reference velocity for a pilot stage (which degrades ignition performance) and the use of a torch rather than a spark ignitor (which favors ignition performance).

Lean blow out results were very repeatable and varied linearly from an equivalence ratio of 0.55 at a T_3 of 735 R (408 K) to 0.21 at 1405 R (781 K). These results were insensitive to pressure drop.

Combustion oscillations were observed at very lean or very rich conditions at the higher inlet temperatures. The conditions appear to be outside the planned operating envelope for the pilot. Also, the acoustic characteristics of the single-cup combustor geometry are considerably different from the HSCT combustor. In particular, the single-cup combustor corresponds to axial acoustic half-wavelength of about 14 inches, well above the intended HSCT combustor length.

4.4.3 Pressure Test of Cyclone Swirler, Configuration 1

The first pressure test of the Cyclone Swirler premixer was performed at four atmospheres. Combustor inlet temperatures were varied from 710 R (394 K), the minimum temperature at which it would ignite, to 1420 R (789 K). Pressure drops ranged from 4.9 to 7.6%. The combustor reference velocities ranged from 36 to 70 ft/sec. Emissions data were obtained at the nominal inlet temperatures of 910 R (506 K), 1110 R (617 K) and 1410 R (783 K). Combustion oscillations were observed at about one-half of the conditions tested. Generally, the oscillations occurred at the lower inlet temperatures.

Emissions were determined at thirteen test points. The air flow rate could not be measured because part of the air was being vented after the metering section to maintain the indirect preheater within its design flow range. The sample fuel air ratio calculated from the gas analysis was used to calculate the air flow rate from the fuel flow rate. The results are plotted versus the flame temperature calculated from the sample fuel air ratio. Three of the thirteen test points had to be discarded because the CO emissions greatly exceeded the reliable range of the analyzer's calibration. Without a reliable CO analysis, sample fuel air ratio and flame temperature could not be calculated for these three points. These three discarded points had equivalence ratio's of about 1.4 or greater (estimated using airflows calculated from the combustor pressure drop), so inefficient combustion was expected.

There was a concern that the combustion oscillations, when they occurred, would affect emissions. If so, these test results would have to be discarded or at least correlated separately. The smooth trends in the data are an indication that this did not happen. As seen below, the ten remaining data points, including those with combustion oscillations (not indicated, but generally the 910°R inlet temperature points), yield smooth trends in all the plots versus flame temperature.

The NOx emissions index is plotted versus flame temperature in Figure 4-50. The NOx EI is only slightly higher than the previous results for the IMFH (not shown) and the boundary of the published LPP data compiled by NASA (indicated by the dashed perimeter). The NOx emissions index at the mid-supersonic cruise design point for the combustor is estimated to be 5.8 g/kg fuel (calculated from the third order polynomial best fit of the data at a flame temperature of 3600 R or 2000 K). Thus, the first configuration of the Cyclone Swirler nearly meets the program goal of 5 g/kg for the NOx emissions index. Based on the results of this evaluation, it appears the Cyclone Swirler can be considered as a potential candidate for a premixer for the main stage of the HSCT's combustor. This NOx emissions performance in this 4 atmosphere test is excellent for a mixer that is also expected to meet the special operability requirements of the pilot stage. Although all the performance requirements for the pilot stage are far from being demonstrated, there are some promising results as shown below.

The calculated combustor residence times of the ten test points ranged from 2.4 to 3.8 milliseconds. This is on the high side of the intended design range for the HSCT engine combustor. Plotting the NOx emissions index normalized by the residence time can be done in an attempt to account for differences in combustor residence times, the implication being that the source of the NOx is primarily thermal rather than prompt. Plotting the data in this way also allows comparison with the correlation of Roffe and Venkataramani, which is a convenient baseline for comparison of NOx emissions. The form of the correlation also implies by its linear dependence on residence time that all the NOx is thermal. The correlation is referred to here as the GASL correlation. The GASL NOx emissions data were for premixed propane and air flames. The comparison is shown in Figure 4-51. The Cyclone Swirler NOx emissions are only 10 to 20% higher than the correlation, except at flame temperatures over about 4000 R (2222 K).

That the NOx emissions are at the high end of the compilation of literature data in Figure 4-50 and higher than the GASL correlation in Figure 4-51 suggests that the flame produced by the Cyclone Swirler may not be uniformly premixed. Depending on the degree of this unmixedness, this could result in a further increase in NOx emissions as pressure is increased from 4 atmospheres. However, significant diffusion burning should also result in the NOx emissions being sensitive to inlet temperature, and no inlet temperature sensitivity is seen in Figures 4-50 and 4-51.

The CO emissions index is plotted versus the calculated flame temperature in Figure 4-52. At calculated flame temperatures as low as 3084 R (1713 K), the CO emissions are essentially at their equilibrium values. There is no indication that the kinetics of CO burnout is limiting combustion efficiency at this temperature, even though the residence time is only 3.2 milliseconds. However, at the lowest inlet temperature of 910 R, the trend is

for the CO to increase above equilibrium as the flame temperature increases to 3814 R (2119 K). At the high inlet temperature of 1410 R, the measured CO crosses below equilibrium as the flame temperature increase, indicating the probe is not fully quenching the sample at these conditions. This is often seen in combustor tests, but the cross-over occurs at a lower temperature than in other tests in this program. Only for the intermediate inlet temperature of 1110 R is the CO just above equilibrium at a high flame temperature.

In Figure 4-53, combustion inefficiency is plotted versus flame temperature. The plot generally reflects the trends in CO emissions in Figure 4-52, as the CO is the principal source of the combustion inefficiency. The only exception is the 910 R inlet temperature, 3084 R (1713 K) flame temperature point for which the hydrocarbon emissions index of 0.72 g/kg exceeded the CO emissions index of 0.30 g/kg. Both of these EI's are extremely low. At this low inlet temperature, that the combustion inefficiency increases so fast with increasing flame temperature is a cause for some concern. However, this observation is based on a single data point. In any case, based on the current combustor system designs for the FLADE C1 cycle at engine flight idle, the pilot will have to operate with reasonable efficiency at inlet temperatures as low as about 660 R (367 K) and flame temperatures around 4200 R (2333 K).

Based on these results, it appears this Cyclone Swirler design will function as a workable pilot in the first HSCT sector combustor, as planned.

4.4.4 Cyclone Swirler with Spent Cooling Air Injection, Configuration 2

In the IMFH, the spent cooling air has been injected at near the exit of the IMFH tubes. The air jets have been aimed towards the axis of the exiting jet. For the IMFH, this flow did not have any detrimental effect on performance. For swirlers, which depend on the axial recirculation zone for stability, the jets could affect stability, since the jets tend to be counter to the recirculation flow. However, the hope is that velocity and the mass flow rate of the jets will be too small to impact the recirculation.

Another risk in extrapolating the success of spent dome cooling air injection in the IMFH to the Cyclone Swirler or the other mixers is that the scale of the jets needs to be larger in the Cyclone Swirler, so the nonuniformities will not mix out as quickly and thermal NOx production will increase.

To discharge the spent dome cooling air, 20 holes, each 0.122 inches in diameter, were added to the trailing edge of the conical discharge throat from the Cyclone Swirler. The holes pass the spent cooling air from the chamber between the baffle and the dome to the throat of the Cyclone Swirler. The holes have a smaller total physical area than the holes they replaced which bypassed the spent cooling air around the combustion zone. Thus the original impingement cooling airflow was higher, resulting in a more conservative cooling design. The physical area of the new holes was reduced to closely simulate the cooling design planned to be used in the sector combustor and also to increase the jet velocity so the jets penetrate and mix well with the discharge from the Cyclone Swirler. The sector combustor cooling design is developed such that it just meets material temperature requirements at the simulated maximum supersonic combustor test point. This was done to

minimize the air injected into the combustion zone and to minimize the airflow crossing the impingement jets. The ratio of physical area of the impingement baffle holes to the physical area of the discharge holes in the original configuration of the single-cup Cyclone Swirler was 0.15. In the current configuration it is 0.67. The modified Cyclone Swirler was designated Configuration 2.

4.4.4.1 Configuration 2 Cyclone Swirler Tests at Low Dome Reference Velocity

Configuration 2 was tested in an open rig at atmospheric pressure. The combustor rig hardware available at the time (4.84 inch liner inner diameter) dictated that the first tests be performed at a nominal dome reference velocity of 18 feet/second, which is below typical pilot dome values. The open rig allowed visual inspection of the flame characteristics during the stability tests. In this atmospheric test, the stability of the new configuration was excellent. Video tapes comparing the appearance of the flame in the two configurations showed no significant difference. Lean blowout occurred well below an equivalence ratio of 0.15 at 910 R and 1110 R (506 K and 617 K) inlet temperatures. Also, for the first time, Cyclone Swirler ignition was accomplished at ambient inlet temperatures, albeit at very high fuel flows. The very low dome reference velocity has to be taken into account, when considering the good stability and ignition results of this test.

Two pressure tests of Configuration 2 of the Cyclone Swirler were performed at 4 atmospheres. Excellent flame stability was observed in these tests. These tests were also performed at a nominal dome reference velocity of 18 feet/sec. The NOx emissions results in these two pressure tests were at the same level as those for Configuration 1. As seen in Figure 4-54, there is indication of the inlet temperature having an effect on the NOx emissions, suggesting that the fuel-air mixing is not completely uniform.

As shown in Figure 4-55, the measured CO emissions index were below, but generally close to, the calculated equilibrium CO concentrations. Normally, this would be an indication that the probe is not quenching the sample very well. However, since the deviation below equilibrium remains small and constant over a very wide range of flame temperatures, it is more likely that the CO is in fact at equilibrium and there is small consistent error in the calculated flame temperatures. The evidence that there is a small consistent error is strongest for the CO emissions point at 2800 R (1556 K). It is below the equilibrium line by the same amount as at flame temperatures up to 4200 R (2333 K). The probe should not have any difficulty in quenching the 2800 R sample. The ability of the probe to quench the sample should be a strong function of flame temperature. There is no evidence that the ability of the probe to quench the sample is changing as the flame temperature increases.

Only at flame temperatures below 2800 R (1556 K) does the CO combustion become kinetically limited. The excellent CO emissions performance of the Cyclone Swirler may be partly due to the long combustor residence time in these tests. The sampling plane was 7 inches downstream of the pilot dome resulting in a nominal value of the combustor residence time of 10 milliseconds. Constraints in the rig hardware available at the time of the test prevented obtaining a shorter residence time at the 18 ft/sec reference velocity being tested.

Judging from the noise levels, the dynamic pressure continue to be much lower than the Configuration 1, which had no spent cooling air injection.

In these two pressure tests of Configuration 2, the ignition characteristics have been considerably improved over Configuration 1. Ignition is reliable at ambient as well as higher inlet temperatures. Air injection had a similar beneficial effect on the ignition characteristic of the IMFH.

4.4.4.2 Configuration 2A Cyclone Swirler Tests at Vref = 30 ft/s

Two additional pressure tests were completed with the Configuration 2 HSCT Cyclone Swirler single cup hardware. These tests were performed at four atmospheres pressure in a new castable ceramic combustor liner with a 3.67 inch diameter. These tests are referred to as configuration 2A due to the different liner used. The new combustor liner yields the same reference velocity as the pilot stage of the sector combustor (about 30 feet/second) and with the sampling plane at 7 inches yields a nominal combustor residence times of about 6 milliseconds. The results were in general agreement with previous Cyclone Swirler test results.

The NOx emissions index results are plotted versus calculated flame temperature in Figure 4-56. The observed values of the NOx emissions index meet requirements for the low NOx combustor. However, as in previous tests, the NOx EI exhibits some evidence of a dependence on inlet temperature which suggests that the fuel is not totally premixed with the air. If this inference is correct, then there should also be a pressure effect.

The CO emissions index is plotted versus calculated flame temperature in Figure 4-57. The break point, where the measured CO emissions suddenly increases from calculated equilibrium CO as flame temperature is decreased, occurs in the range of 3100 R to 3400 R (1722 K to 1889 K), depending on the inlet temperature. This is higher than in the previous tests, where the breakpoint was observed within the acceptable limits. For comparison, in the previous test of the Cyclone Swirler, at a reference velocity of about 18 feet/second and a combustor residence time of 10 milliseconds, the observed CO break point temperature was about 2800 R (1556 K).

4.4.4.3 Configuration 2 Cyclone Swirler Tests in Convectively-Cooled Liner

An atmospheric pressure test of Configuration 2 of the Cyclone Swirler was performed in a convectively cooled liner. This liner was especially designed to address the concern that the cast ceramic liner being used in the single-cup tests is yielding misleading stability results. This is because of the ceramic liner's high temperature combined with a very long time constant for transient thermal response. As a result, lean-blow-out results using the cast ceramic liner have almost certainly been optimistic to some degree. The cooled liner was purposely designed to be "over-cooled" and therefore the results represent a worst case for stability. The only exception to the liner being a worst case is that the convectively cooled liner is square in cross-section so that its stability does have the benefit of the corner circulation zones.

Three sets of LBO results obtained for the HSCT Cyclone Swirler to date are compared in a plot versus Lefebvre's LBO correlating parameter in Figure

4-58. The single low out-lier point on the plot might be due to the hot ceramic liner stabilizing the combustor. Lefebvre's correlating parameter used in the plot is given by [8]:

$$\Theta = \left[\left(\frac{V_{ref}}{P_4^{0.25}} \right) \cdot T_3 \cdot e^{\left(\frac{T_3}{270} \right)} \right]^{0.16}$$

The three curves in the figure are quadratic best fits of each of the three data sets. The results for the three different configurations are roughly correlated by Lefebvre's parameter, even though there are some differences in the combustor configurations not even indirectly taken into account by the parameter (the hot ceramic liner, the corner circulation and cold walls of the square convectively cooled liner used in the third set of LBO data). The first set of LBO data were taken prior to the spent dome cooling air injection holes being added (Configuration 1). The spent cooling air injection is taken into account only indirectly through the Vref term. Apparently, none of these configuration changes significantly affect the stability of the Cyclone Swirler. There is some evidence of a trend towards better stability at high values of the correlating parameter for the square combustor liner.

For comparison, the actual pilot operating conditions for a combustor system design for the A5B mixed flow turbofan cycle are also plotted in Figure 4-58. The A5B plot conditions cover the entire power range of the engine: including ground and flight idle, subsonic and supersonic cruise, as well as take off and climb. As can be seen in the Figure, there is a wide stability margin over the whole power range, amounting to two or three tenths of equivalence ratio.

A weakness of the comparison between the LBO data and the pilot conditions for the combustor system design is that these LBO data were all obtained at atmospheric pressure. However, the atmospheric LBO data appears to be consistent with the available 4 atmosphere pressure data for CO emissions. As the flame temperatures are decreased in the four atmosphere tests, CO emissions were observed to rise above equilibrium. This indicates that the combustion efficiency is becoming limited by the chemical kinetic reaction rates because of the low flame temperatures and that the combustor is approaching LBO. Four of these points, in three different tests of the Cyclone Swirler Configuration 2 (with spent dome cooling air) are plotted in Figure 4-59. They are very consistent with each other and the atmospheric LBO data.

One CO breakpoint found for configuration 1 (without spent dome cooling air injection) is not plotted in Figure 4-59. It falls in the grouping of the atmospheric LBO data. This point is not consistent. It indicates the Cyclone Swirler has better stability with the spent cooling air injection. Also there were a series of tests of Configuration 2 in which the stability was not good at higher reference velocities. No CO break points were observed in those tests. The sudden flame outs at high flame temperatures are not consistent with Figure 4-59. At least one of those tests was discounted because of high gas sample probe purge flows. The correlation in Figure 4-59 suggests that the Cyclone

Swirler would easily run at a Vref of 60 feet/second. (Doubling the approximately 30 feet/second reference velocity of the A5B pilot points to 60 feet/second only increases Lefebvre's parameter by $2^{0.16}$= 1.12 or 12%.) This is not consistent with the observations in those early tests in Configuration 2. Perhaps high probe purge was also being used in the other inconsistent point, or there was some other problems such as rig quench water getting in the flame zone.

Overall, the available information on the stability of the Cyclone Swirler indicates very good performance.

4.4.4.4 Configuration 2 Cyclone Swirler Tests at High Pressure

Configuration 2 of the HSCT Cyclone Swirler was tested in the Cell 5 high pressure single-cup rig. The high pressure rig's combustor was a castable ceramic liner with a 3.67-inch diameter. This resulted in a nominal reference velocity of about 30 feet/second, about the same as the pilot stage of the sector combustor. The gas sample probe was traversed along a diameter 4.5 inches downstream of the dome yielding a nominal residence time of about 4 milliseconds. The profiles were fairly uniform, so only 4 points were sampled on the diameter.

The NOx emissions index results are plotted versus calculated flame temperature in Figure 4-60. The CO emissions index results are plotted versus calculated flame temperature in Figure 4-61. For reference, the combustor exit temperature at supersonic cruise for the A5B engine cycle is shown in Figure 4-60. This represents the minimum possible flame temperature during supersonic cruise, corresponding to all the combustor air being premixed with the fuel. In Figures 4-60 and 4-61, there are 4 series of data and their curve fits corresponding to 4 combinations of combustor pressure and inlet temperature; 60 psia and 1310 R (728 K), 150 psia and 1310 R (728 K), 150 psia and 1620 R (900 K), and 275 psia and 1620 R (900 K).

The 60 psia, 1310 R (728 K) series of data in this test duplicated pressure, inlet temperature, and reference velocity for an earlier set of data obtained at 4 atmospheres pressure in the low pressure single-cup test facility. These data have already been discussed above. In the earlier test, the probe traverse was made 7 inches downstream instead of 4.5 inches. The Cyclone Swirler's configuration was identical, except the fuel injector in the high pressure test was new. The design of the injector allows the position of the eight fuel injector hypo tubes to be axially and circumferentially adjusted relative to the radial air nozzles at assembly and the alignment of the injector tubes may not have been identical in the two tests. The NOx emissions results at 60 psia and 1310 R in the high pressure test are slightly lower than the earlier results in the low pressure rig. This may be due to the shorter combustor residence time in the high pressure rig or differences in fuel nozzle or alignment in the two tests. The lowest fuel-air ratio point in the 4 atmosphere series of data, plotted at a flame temperature of 3140 R (1744 K), had the lowest fuel flow of the entire test and was the most severe in terms of heat transfer to the fuel. During this point, the measured flow number of the fuel injector system dropped from 7 to 5, the only time this occurred during the entire test. This is evidence that the fuel was partially vaporizing in the fuel system during this test point.

For the next series of data, the pressure was brought up to nominal supersonic cruise conditions of 150 psia. The NOx emissions are slightly higher than at 60 psia, possibly indicating less than perfect premixing. At the lowest equivalence ratio and flame temperature on the test point schedule, the combustion efficiency was still 99.97%. At this point, the calculated flame temperature was 2932 R (1629 K) and the NOx EI was 0.55 g/kg. The decision was made to go lower in equivalence ratio to find the CO breakpoint. The equivalence ratio was dropped to 0.37 corresponding to a calculated flame temperature of 2840 R (1578 K). The NOx EI went up to 3.35 and the combustion efficiency increased to 99.99%. Both results were contrary to the expected trends. The emissions panel operator reported that the calibration of CO analyzer was slightly off, so a recalibration was performed. The point was repeated, with essentially identical results for the NOx emissions. The CO EI increased from 0.18 to 0.50 g/kg, the latter still corresponding to 99.99% combustion efficiency. The decision was made to revert to the original test point schedule and the inlet temperature was increased to 1620 R (900 K), nearly up to supersonic cruise conditions of 1680 R (933 K). As shown in Figure 4-60, the NOx emissions increased to a significantly higher levels for this series and the next series 1620 R (900 K) and 275 psia.

The conditions at which the anomalous high NOx emissions were first observed (1620 R or 900 K, and 150 psia and low equivalence ratios) was repeated before ending the test. During the reduction in inlet conditions, the combustor flamed out, but was immediately reignited by the hot ceramic liner when the fuel flow was increased (the ignitor torch will not operate over 30 psia). Emission readings which yielded NOx EI's of 0.90 and 0.62 g/kg. These values are very close to the original low value of NOx EI of 0.55 g/kg.

After opening up the rig, but before disturbing the fuel-nozzle, it was observed that only 4 of the 8 fuel jets properly passed through the air nozzles (with no air flow). Upon removal of the fuel injector, it was found that the 1/4-inch fuel tube was warped about 0.1 inch radially. Three of the eight injector tips were severely bent and a fourth was plugged (the plug was temporary as all the tips were open when checked again). The exterior cylindrical surface near the end of the centerbody where the centerbody cooling air is ejected was also found to be oxidized. No other clear evidence of high material temperatures was found.

It is not clear what caused the fuel injector damage, nor is it certain when it occurred. As stated above, it appeared to be operating properly after assembly. According to reports, the damage did not occur during disassembly. Assuming that at least some of the damage occurred just before the abnormally high NOx emissions were measured, then the higher than expected NOx emissions can be attributed to poor atomization. Based on experience gained during nozzle spray tests, much of the fuel must have been running along the centerbody after the damage. This would explain the oxidation at the cooling air ejection holes. The fuel running along the centerbody apparently stabilized a flame at the air ejection holes. This may also help explain why the last two NOx emissions readings dropped back down to nearly the lowest value. When the nozzle damage occurred, the NOx emissions increased for two reasons, poor atomization and the flame moving upstream to the air ejection holes. At this time, the material became hot and it continued to hold the flame at the holes, until the blowout occurred. By the time relight had occurred, the material had cooled and the flame stabilized further downstream, yielding an intermediate

increase in NOx. During the test at the most severe inlet conditions, with this scenario in mind, some consideration was given to purposely putting out the fire and relighting with the hot liner to see if a new flame position and lower NOx emissions resulted. Unfortunately, this was not done.

The CO emissions in Figure 4-61 are in good agreement with previous results. They are close to equilibrium levels down to flame temperatures of 2800 R (1556 K) or below. System designs for the HSCT combustor have always maintained the design flame temperature above about 3200 R (1778 K) for a minimum of a 400 R (222 K) stability margin.

In summary, the primary goals of this test were only partly accomplished. The HSCT Cyclone Swirler's NOx emissions were shown to be acceptable at supersonic cruise pressure. For the more severe conditions, the NOx emissions results are inconclusive because of the damage to the fuel injector. Combustion efficiencies were always excellent. Adequate margins for lean stability continues to be seen. The combustor exit profile continues to be relatively flat. Some flame holding within the throat of the Cyclone Swirler is evident. This will have to be addressed, but there are a number of known design modifications that can be employed if this burning at the centerbody cooling air injection holes continues to be a problem, all of them with very minor trade-offs. There continues to be limited evidence of dynamic pressures.

4.5 Multiple-Venturi Swirler Mixer (Multiple-Venturi)

This section describes the results of two 4 atmosphere single module tests of the Multiple-Venturi mixer concept developed at NASA's Lewis Research Center. The module (Figure 4-62) consists of seven small swirlers arranged in a hexagonal pattern (one in the center). The fuel injection device is a miniature simplex atomizer developed by Textron Fuel Systems. This device had previously been tested at both Textron and NASA's Lewis Research Center.

4.5.1 Multiple Venturi Single Module Testing

The initial four atmosphere pressure test (Configuration G1) simulated the most stable configuration of the device found during atmospheric combusting tests at Textron. As shown in Figure 4-62, the fuel injector tips were positioned approximately 1/16th inch downstream of the venturi throats. The large, 4.89 inch, dome diameter was used. The resulting dome velocities (10-15 feet per second) were low, at approximately half of typical design pilot dome velocities.

Configuration G1 ran successfully at inlet temperatures ranging from ambient (515 R, 286 K) to 1115 R (619 K) and combustor dome pressure drops from 5 to 7 percent. Lightoffs were easily achieved at all conditions. Blowout data was not obtained since fire continued to burn in the combustor even after fuel flow was turned off in several instances. Such occurrences and the difficulty in stabilizing the flame during Textron tests in which there was no abrupt step at the dome discharge suggest that the flame is not swirl stabilized but rather bluff body stabilized.

Configuration G1 NOx emissions were comparable to the NASA multiple-venturi data as shown in Figure 4-63. Combustion inefficiency measurements were very consistent for Configuration G1, as seen in Figure 4-64, with inlet

temperature and dome pressure drop variations having no effect. Note that emissions data comparisons were made only against the NASA Multiple-Venturi data having a 1.8-2.5 millisecond combustor residence times. Configuration G1 combustor residence times were roughly twice that, at 2.4-4.4 milliseconds. Differences in measured combustion inefficiencies between the GEAE test and NASA data could be attributed to the longer residence times of Configuration G1 and the significantly higher dome velocities (57-70 ft/sec) of the NASA tests.

Multiple-Venturi mixer Configuration G2 was tested at high pressure conditions (4 atmospheres). Configuration G2 has the same axial fuel injector positions as Configuration G1 with the injector tips extended 1/16th inch downstream of the venturi throats as shown in Figure 4-62. However, Configuration G2 had a reduced dome height relative to Configuration G1 (3.67 inches compared to 4.89 inches), which resulted in dome velocities which were typical of a pilot stage design, 22 to 35 feet per second.

Figure 4-63 depicts a comparison of NOx data between Configuration G2 tested at GEAE and at NASA's Lewis Research Center. As shown in the figure, the measured Configuration G2 NOx values range from 4-5 EI at 3600 R (2000 K) flame temperature, and in general, are comparable to the NASA-Lewis data. Configuration G2 NOx emissions were also lower than those of Configuration G1, as Configuration G2 combustor residence times were roughly half of Configuration G1. Figure 4-64 compares the combustion inefficiency results between the GEAE and the NASA-Lewis tests. As shown in the figure, the G2 combustion inefficiencies were lower than the NASA-Lewis data and slightly higher than Configuration G1 data at 1140R (633K) inlet temperature. The difference between the Configuration G1 and Configuration G2 inefficiency data is also consistent with the residence time difference of the two configurations.

4.6 Supporting Cold Flow Mixing Experiments At CR&D

A full report of these activities is contained in Appendix 9.2. Thus, only a summary of the cold flow mixing experiments is given here. The non-intrusive laser-based diagnostic technique of Spontaneous Raman/Raleigh scattering was successfully extended to elevated pressures to measure the scalar flowfield downstream of a single IMFH (Integrated Mixer Flame Holder) tube at elevated pressures up to 150 psia (10.2 atm). This study represents the first practical application of Raman/Raleigh scattering at elevated pressures. A single IMFH tube was mounted in an 8 inch combustion tunnel with large optical access build specifically for the purpose. Detailed measurements of mean and rms of temperature and major species were made at three axial locations downstream of the burner exit in a premixed flame region with liquid fuel (both kerosene and Jet-A) to demonstrate the enhanced capabilities of the technique. Provision was made to account for laser-induced fluorescence and flame generated luminescence anticipated in this application. Measured data, however, showed that the interference from laser-induced fluorescence and flame generated luminescence were minimal and easily accounted for under the conditions examined in this study. The results showed the measured temperature and scalar profiles to be representative of flow fields established by a premixed fuel/air jet issuing into a recirculating product field downstream of the exit. The expertise and experience gained from this technique is expected to be applicable to all such applications at elevated pressures. The

major goal of the program to demonstrate the feasibility of such measurements has been successfully met.

4.7 Laser Diagnostics at Pennsylvania State University

A full report of these IMFH fuel-air mixing studies is contained in Appendix 9.3. Thus, only a summary of the laser diagnostics activities at Pennsylvania State University is given here. Experimental measurements were carried out in two phases to achieve the overall goals of determining the effects of incomplete fuel-air mixing and vaporization on the lean limit and emissions characteristics of a lean, prevaporized, premixed combustor. In the first phase, two-dimensional exciplex florescence was used to characterize the degree of fuel vaporization and mixing at the combustor inlet under non-combusting conditions. Tests were conducted at 4 atmospheres pressure, an inlet temperature of 1140 R (360 C), a mixer tube velocity of 100 m/s (328 ft/s), and an equivalence ratio of 0.8 using a mixture of tetradecane, 1-methylnapthalene, and TMPD as a fuel simulant. Two transverse injection geometries (with the fuel discharge on the centerline and at the wall) were investigated. In both cases, there was a significant amount of unvaporized fuel at the mixer discharge. Centerline injection exhibited a very non-uniform distribution of the fuel liquid and vapor, while wall injection yielded a much more uniform distribution of fuel across the width of the mixer discharge.

In the second phase, the combustion lean limit and emissions were measured over a range of inlet temperatures at 4 atmospheres pressure for combusting flows using Jet-A as the fuel and employing both fuel injection geometries. Contrary to expectations, wall injection produced better mixing and yielded leaner operating limits. For a given equivalence ratio and inlet temperature, the two injection geometries also unexpectedly yielded comparable NOx emissions; however, wall injection allowed operation at leaner equivalence ratios, thus yielding lower NOx levels. These results were contrary to the GEAE flame tube tests of IMFH Configurations 6A and 6B in which fuel discharge at the wall resulted in significantly worse performance as was shown in Figure 4-46.

5.0 DISCUSSION OF SUBCOMPONENT TEST RESULTS

5.1 Comparative Evaluation of the Flametube Results

Because of the uncertainties in the development of a mechanical design for the LPP sector combustor, the design needed to be initiated early in the Task 5 schedule. This required making a down-select from the fuel-air mixers be developed very early in their development and evaluation. Although the Swirl-Jet concept had been chosen as the favored approach for the preliminary mechanical layouts for the studies full size engine combustor, the available Swirl-Jet test data did not support using that mixer for the sector combustor. A tentative decision was made to use the Cyclone Swirler for the pilot stage and the IMFH for the main stage. At the time, given the available data, the choice was an obvious one. These two concepts both had demonstrated very good performance for the proposed applications very early in their development. The selections were made with the understanding that they might be changed if the performance of one of the other fuel-air mixer concepts improved and the sector combustor design was not too far along. It was also understood that

this selection of fuel-air mixers for the sector combustor did not necessarily commit the long term LPP combustor development to these two concepts.

5.2 Selection of the Preferred Mixer Designs for Sector Testing

The fuel-air mixers for the sector combustor design were selected based on their demonstration of low NOx emissions and high combustion efficiency performance over a range of operating conditions. Ideally, the fuel-air mixers will maintain their relatively low NOx emissions even at flame temperatures higher than the supersonic cruise design point of 3600 R (2000 K) and maintain acceptable levels of combustion efficiency for relatively low flame temperatures, and do this over a wide range of combustor inlet pressures and temperatures. Meeting these requirements, would allow the fewest number of fuel stages. As a first-order indication of flexibility of the mixers in this regard, their acceptable performance range was quantified by the ratio of equivalence ratio for 5 EI NOx emissions divided by the equivalence ration at which combustion efficiency dropped to 99%. These ratios are tabulated in Table 5-1 for the mixers in this study.

Table 5-1. LPP/LDI Comparative Performance

Mixer Design	Single Cup Test at P3 (atm)			$\frac{\Phi\ (NOx\ EI = 5)}{\Phi\ (Comb.\ Eff. = 0.99)}$	P_4 (atm) / T_3 (R)
	1	4	14-17		
IMFH	X	X	X	1.4	10 /1410
Swirl IMFH	X	X		1.3	4 / 1410
Cyclone Swirler	X	X	X	1.6	10 / 1310
Swirl Jet 1	X	X	X	1.2	4 / 1460
Swirl Jet 2	X				
LDI Jet Mix	X	X		1.1	4 / 1400
LDI Multiple-Venturi	X	X	X	1.3	14 / 1520

The IMFH was selected for the sector combustor's main stage since it generated the lowest NOx emissions at high flame temperatures with acceptable combustion efficiencies for a reasonable range of equivalence ratios. The use of a different fuel-air mixer for the pilot stage was required because the IMFH's emissions performance was unacceptable at low power conditions. The Cyclone Swirler mixer was selected for the pilot stage due to its stable operation over a wide range of equivalence ratios with reasonably low NOx emissions.

6.0 SECTOR COMBUSTOR DESIGN

The HSCT LPP sector combustor design was initiated with the IMFH concept for the main stage premixer and the Cyclone Swirler for the pilot stage. The mixers were selected based on the test data collected during this contract.

A study investigating the influence of IMFH mixer tube cant angle on mixing was carried out as part of the five-cup sector rig design and development effort. Table 6-1 lists the configurations studied and the mixing length required to achieve a uniform temperature profile. As outlined in the table, the compound cant angle configuration resulted in shorter mixing length. However, mechanical and packaging considerations excluded the use of mixer tube angling in the sector design.

The success of IMFH Configuration 5 tests significantly impacted the sector combustor design, particularly the dome design. Previously, 13% of the dome air was used in the flametube tests for dome cooling and it was expected that a comparable level of cooling would be required for the sector dome. Configuration 5 flametube tests demonstrated that this air can be injected into the mixer tubes with acceptable combustion efficiency and NOx emissions. Since a portion of the IMFH fuel-air premixers' air to be used to burn the fuel could now be used to also cool the domes, the previously separate allotment of dome cooling air became available for liner cooling. A similar dome cooling air injection scheme was incorporated into the Cyclone Swirler pilot dome. Preliminary heat transfer analyses of sector combustor main dome cooling requirements indicate that the projected maximum material temperatures would be acceptable using cooling air amounts comparable to levels already demonstrated in the Configuration 5 flametube tests at low and high pressure.

The HSCT combustor system design layouts developed in Section 3.3.2.4, assumed the use of advanced high temperature materials. Since these materials were not yet available, an alternate liner cooling design was utilized. Film cooling was known to be undesirable based on the experience of spent dome cooling air discharge during IMFH subcomponent tests. Backside impingement cooled metal liners were selected to accommodate these design constraints. The cooling air discharge of these TBC coated liners and side panels was located downstream of the gas sampling plane to best simulate the emissions of an actual HSCT combustor design. As much cooling air as required to insure a reliable test vehicle could be used without impacting dome flame temperatures and combustor sector emissions. The sector was designed in this manner to evaluate the dome characteristics in isolation from liner cooling and sector cooling effects. An option to block the liner aft end cooling flow discharge and to redirect the flow through the liners is open for subsequent tests. If this option is exercised, the emissions samples would be affected by the liner cooling flow levels. Meanwhile, the emissions data that is obtained without the confounding effects of liner cooling air injection can easily be scaled to any level of liner cooling air along with its impact on dome fuel-air ratio. All this assumes spent liner cooling air is not returned to the dome and injected at the exit of the premixers. This is always an option, but will involve tradeoffs with mechanical complexity, as well as some areas of aerothermal performance.

Table 6-1 IMFH Mixer Tube Cant Angles.

CONFIGURATION	UNCANTED	RADIAL CANT ANGLE	TANGENTIAL CANT ANGLE	COMPOUND CANT ANGLE
IMFH DISCHARGE FLOW DIRECTION: END VIEW				
SIDE VIEW				
DISTANCE FROM DISCHARGE FOR "UNIFORM" TEMPERATURE (MAX - MIN $\leq$ 50 ^{o}F)	3.4"	2.6"	2.0"	1.9"

Although the scale of the five-cup sector combustor is much smaller than the baseline combustor HSCT engine, many characteristics of the sector combustor are similar to full size HSCT combustor designs. Among the sector parameters that will be closely matched to the full size HSCT combustor design are the IMFH tube dimensions, the dome reference velocities, the combustor residence time and the pressure drop.

The sector combustor design has three domes. The initial combustor sector design is shown in Figure 6-1. The sector was sized to an existing 60° sector test rig with a turbine pitch (average combustor exit) radius of 12.6 inches. The center dome has five Cyclone Swirlers for the pilot stage while the outer and inner domes have 30 and 20 IMFH mixers, respectively for the main stages. The pilot dome was designed for a variety of axial positions to determine the optimum pilot dome recess relative to the IMFH domes for pilot stability (Figure 6-2). The sector has a dome height of 7.8 inches.

The sector design was changed to a rectangular cross-section as shown in Figure 6-3 to simplify the design of several sector parts and reduce cost. (Note that Figure 6-2 still accurately represents a side view of the combustor sector.) The rectangular sector retained five pilot Cyclone Swirler mixers fueled from a common fuel manifold. The number of IMFH tubes was reduced from 50 to 48. The sector was scaled down slightly to accommodate this change in flow area. The now identical outer and inner domes each have two rows of 12 mixer tubes each. Every six injectors in a row are fed by a single internal fuel manifold and fuel manifolds are mounted onto the dome structure (two manifolds per mixer tube row). The multiple main stage dome fuel manifolds allow for greater flexibility in investigating various fueling modes. Radial staging would be simulated by fueling selected manifold rows while sector staging would be simulated by fueling the left or right manifolds in a mixer tube row(s). IMFH fuel injector differential thermal growths and fuel line thermal protection to prevent fuel coking were incorporated in the sector design.

The sector combustor design addresses the stresses generated by differential thermal expansion between combustor components. Some combustor parts will operate near T_3, or roughly at 1660 R (922 K). These include the IMFH tubes, Cyclone Swirler, impingement baffles and flanges. The combustor liner adjacent to the combustion zone will operate at temperatures that may exceed 2160 R (1200 K). Where these parts that will operate at widely different temperatures are attached or in close proximity, the design allows for differential movement of the parts. Over the 13 inch "circumferential" length of the sector, differential movement is projected to be about 0.08 inches. At the same time, air leakage at the sealing surfaces between these parts are kept to a minimum to prevent air quenching of combustion reactions which would reduce combustion efficiency.

The combustor sector flow splits, based on the design flow areas, are shown schematically in Figure 6-4. Flows are presented as a percentage of the total dome flow, as a percentage of the combustor flow and as a percentage of the sector flow. Although both the liner and side-panel flows do not go through the dome, they are expressed as percentages of the total dome flow to more easily gauge their relative magnitude. Likewise, the side-panel flows are presented as a percentage of combustor airflow to help keep them in perspective.

The combustor sector test plan has the following three objectives:

A. Obtain emissions, crossfire, and lean blowout (LBO) data characteristic of the IMFH/Cyclone Swirler 2D sector,
B. Demonstrate low NOx emissions and low combustion inefficiency,
C. Assess the impact of fuel split variations and staging on emissions.

To demonstrate these objectives, the combustor sector will be operated at combustor inlet pressures representative of supersonic and subsonic cruise, sea-level takeoff (SLTO), and idle conditions. Combustor inlet temperatures will correspond to the inlet pressures up the current facility's maximum of 1560 R (867 K). The key inlet temperatures are presented in Table 6-2. Combustor flame temperatures will be varied by adjustments to combustor fuel-air ratio from at least a lean 99% combustion efficiency level to a 5 EI NOx level. Stage to stage flame temperature (equivalence ratio) variations will be investigated.

Table 6-2. Principal LPP Sector Combustor Inlet Test Conditions

Flight Condition	Pressure (psia)	Temperature (R)
Supersonic Cruise	169	1560 *
Supersonic Max. Climb	184	1560 *
Sea-Level Takeoff	301	1385
Subsonic Cruise	88	1065
Idle	35	702

*Facility Maximum in 1993

The planned test sequence is broken down into the following five planned test days:

1. Collect data during a slow ramp to and at supersonic cruise conditions. Perform fired system checkouts.
2. Collect data at supersonic cruise conditions with baseline and varied flame temperature and fuel splits.
3. Collect data at sea-level takeoff conditions.
4. Collect data at subsonic cruise conditions. Investigate staging and cross-fire variations.
5. Conduct pilot only studies at idle conditions.

Emissions data will be collected using four gas sample rakes each with five sampling elements. Individual as well as ganged rake sample will be taken.

The test plan to assess the cycle emissions for the first HSCT sector is divided into five test days per test. During each day, conditions will be changed, fuel staging and local equivalence ratio (flame temperature) will be varied, and emissions samples collected in the sequences of Table 6-3. Combustor flame temperatures will be varied by adjustments to combustor fuel-air ratio from at least a lean 99% combustion efficiency level to a 5 EI NOx level. Also, the then current facility's maximum inlet temperature was 1560 R

Table 6-3. IMFH/Cyclone LPP Combustor Test Sequence.

DAY 1: Slow ramp to supersonic cruise condition:
Design: T = 1671 R, P = 169 psia
Cell 3: T = 1560 R, P = 169 psia

* Pretest checkout.
* Pilot lightoff at Idle: T = 702 R, P = 35 psia. Fired checkout.
All premixer lightoff at 910 R. Full Fired checkout.
* Intermediate point checkout 1360 R.
* Supersonic cruise condition flame temperature variations.
* Shutdown along similar condition schedule.

DAY 2: Supersonic cruise condition variations
(Flame temperature and fuel flow splits):

* Repeat day 1 start-up procedure with fewer check points.
* Supersonic cruise condition flame temperature variations.
* Supersonic cruise condition dome fuel split variations.

* Supersonic Maximum Climb option:
Design: T = 1709 R, P = 184 psia
Cell 3: T = 1560 R, P = 184 psia

DAY 3: High Pressure SLTO condition:
Design: T = 1385 R, P = 302 psia
Cell 3: T = 1385 R, P = 250-280 psia
(pressure limited to remain on 20 atm air supply).

* Repeat day 1 start-up procedure with fewer check points.
* SLTO condition flame temperature variations.
* SLTO condition dome fuel split variations.

DAY 4: Subsonic cruise condition staging & crossfire variations
Design & Cell 3: T = 1048 R, P = 88 psia

* Pilot lightoff at Idle: T = 702 R, P = 35 psia
Selected premixer lightoff at 910 R. Fired checkout.
Staging variations. Flame temperature and fuel split variations
at 1048 R, P = 88 psia.

DAY 5: Idle: Pilot only studies

* Pilot lightoff at Idle: T = 702 R, P = 35 psia. Fired checkout.
Blowout studies. Supplemental points from day 1-4 schedules.

(867 K). Subsequent sector combustor tests, starting in 1995 and beyond, will be able to operate in a new combustor test facility with inlet air temperatures exceeding the maximum HSCT combustor inlet temperatures.

7.0 CONCLUSIONS

The goals for this program have been achieved. Combustion system performance goals needed to meet the operating requirements of the HSCT over its flight envelope, while also meeting the HSR Program NOx emission goals, have been defined. Preliminary combustor system designs are proposed. These designs include features that allow the combustor system designs to meet the combustor performance goals.

Flame tube evaluation tests of the Swirl-Jet Premixer, Lean Direct Injector (Jet Mix), Integrated Mixer Flame Holder (IMFH)/Venturi IMFH, Cyclone Swirler, and the Multiple-Venturi Lean Direct Injection fuel-air mixers have been conducted. Of these, the Cyclone Swirler and IMFH premixer designs had the best performance and were selected for incorporation into a sector combustor.

A three-dome 5-pilot-cup sector combustor with a Cyclone Swirler pilot stage and IMFH main stage has been designed, fabricated and built up for evaluation tests (performed under the follow-on contract, NAS3-26617).

8.0 REFERENCES

[1] Ali, A.F. and Andrews, G.E., "Conical Grid Plate Flame Stabilizers: Stability and Emissions for Liquid Fuels," Int. J. of Turbo and Jet Engines, Vol. 3, 1986.

[2] Nguyen, H. Bittker, D. and Niedzwiecki, R., "Investigation of Low NOx Staged Combustor Concept in High Speed Civil Transport Engines," AIAA 89-2942 (1989).

[3] Roffe, G., and Venkataramani, K.S., "Emission Measurements for a Lean Premixed Propane/Air System at Pressures Up to 30 Atmospheres," NASA-CR-159421, June 1978.

[4] Lorenzetto, G.E. and Lefebvre, A.H.; "Measurements of Drop Size on a Plain Jet Airblast Atomizer," AIAA J., Vol. 15, No. 7, 1977, pp. 1006-1010.

[5] Lefebvre, A.H.; Atomization and Sprays, Hemisphere Publishing Co., New York, 1989, pp. 238-244.

[6] Ahmad, N.T. and Andrews, G.E., "Emissions from Enclosed Swirl Stabilized Premixer Flames", Int.J. of Turbo and Jet Engines, Vol. 3, pp. 147-158 (1986).

[7] H.F. Hrubecky, Experiments in Liquid Atomization by Air Streams, Journal of Applied Physics, 29, Number 3, p. 572-578 (March, 1958).

[8]. Lefebvre, A.H., "Gas Turbine Combustion", Hemisphere Publishing, New York (1983).

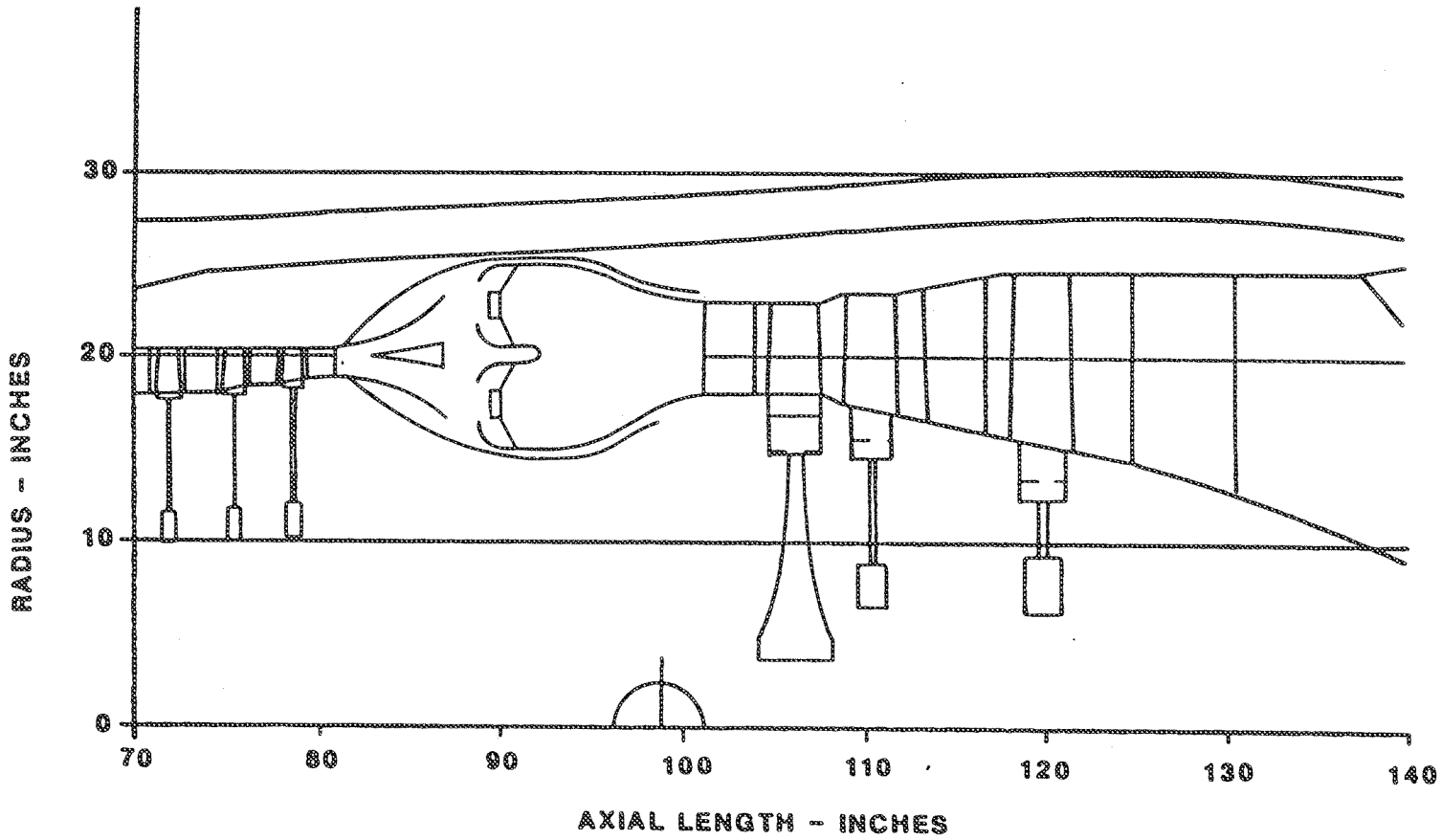

Figure 3-1. Schematic of a FLADE Cycle C1 Engine.

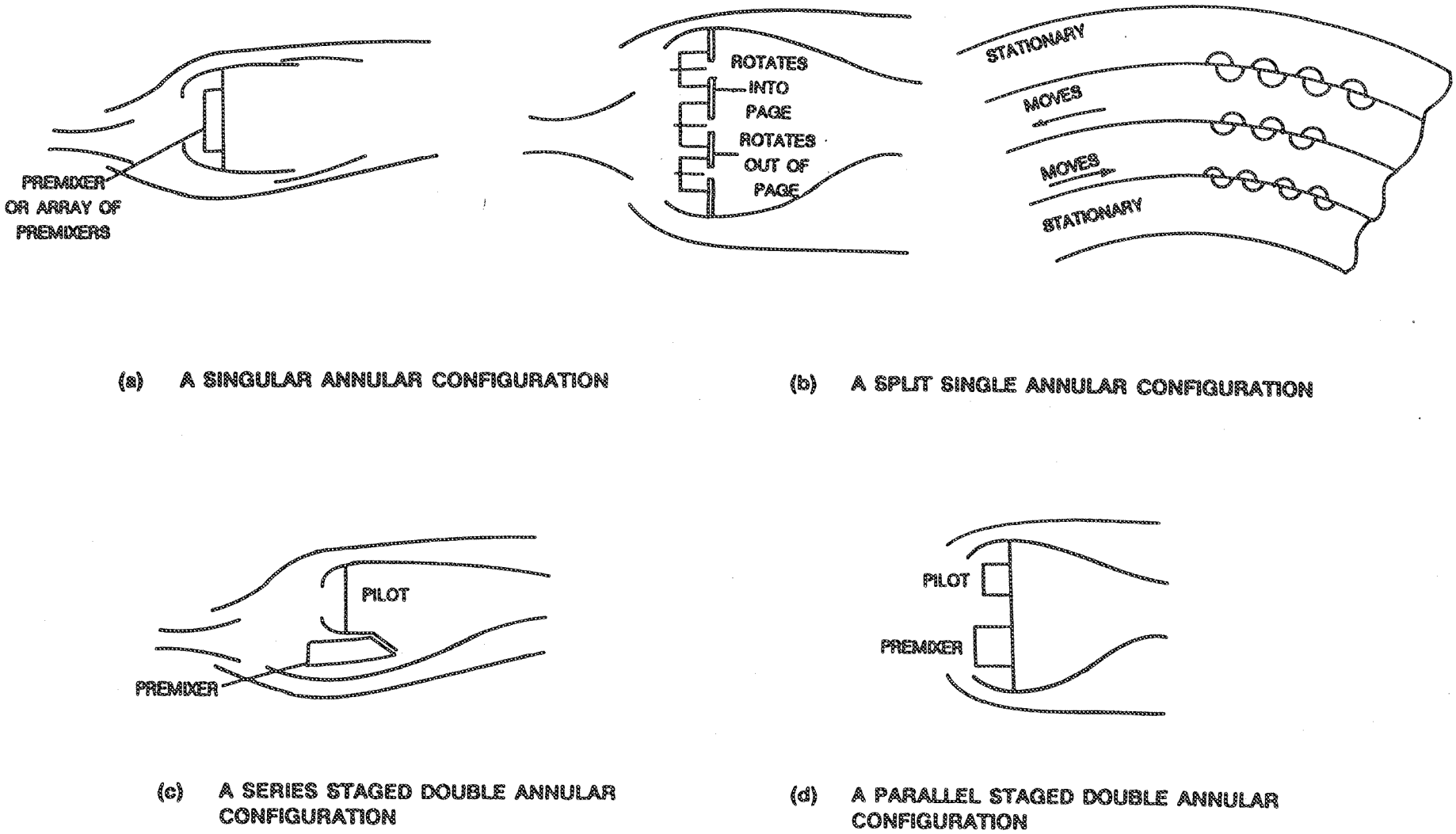

(a) A SINGULAR ANNULAR CONFIGURATION

(b) A SPLIT SINGLE ANNULAR CONFIGURATION

(c) A SERIES STAGED DOUBLE ANNULAR CONFIGURATION

(d) A PARALLEL STAGED DOUBLE ANNULAR CONFIGURATION

Figure 3-2. Schematics of Candidate Combustor Configurations.

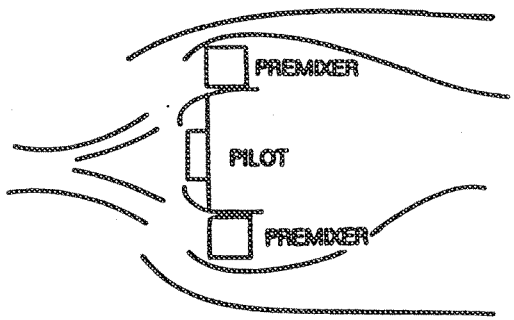

(e) TRIPLE ANNULAR CONFIGURATION WITH CONVENTIONAL PILOT

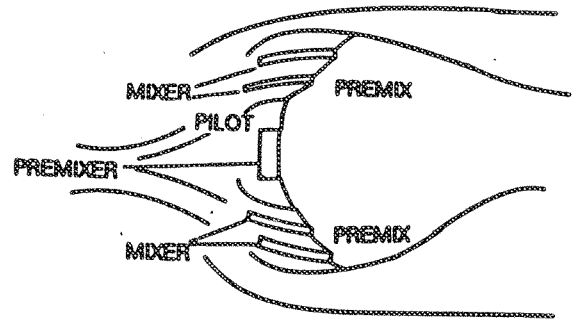

(f) TRIPLE ANNULAR CONFIGURATION WITH PREMIXED PILOT

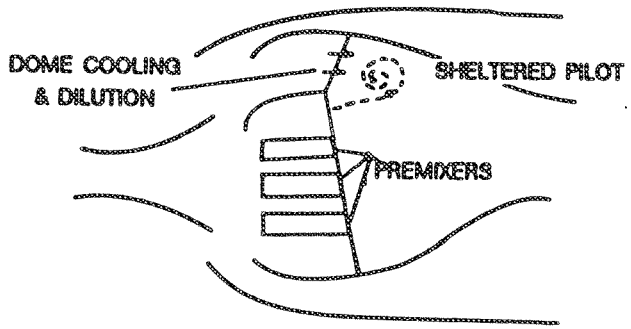

(g) STEP COMBUSTOR

Figure 3-2a. Schematics of Candidate Combustor Configurations (Continued).

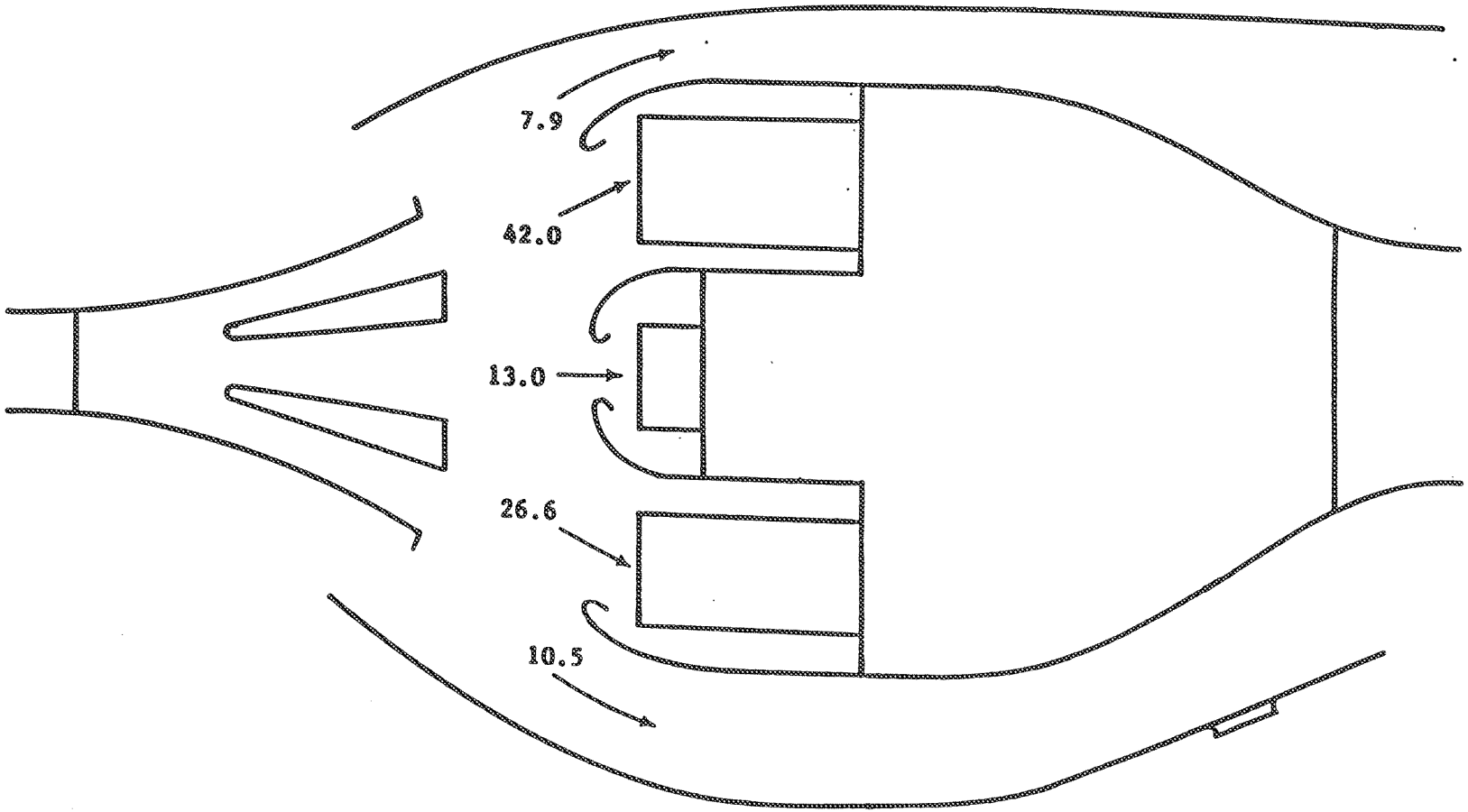

Figure 3-3. Flow Splits for a Triple Annular Combustor Design.

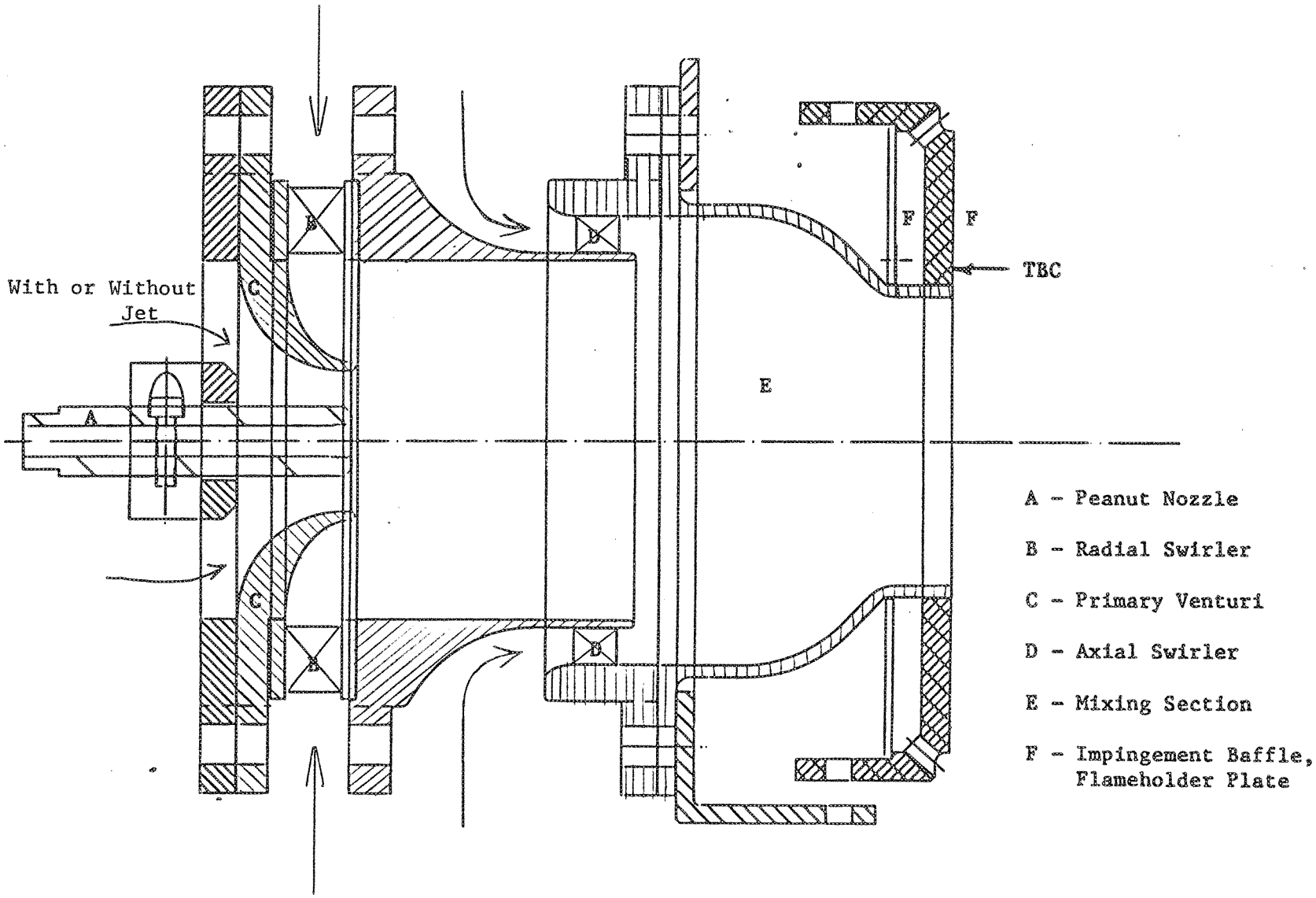

Figure 3-4. Schematic of the Swirl-Jet Premixer.

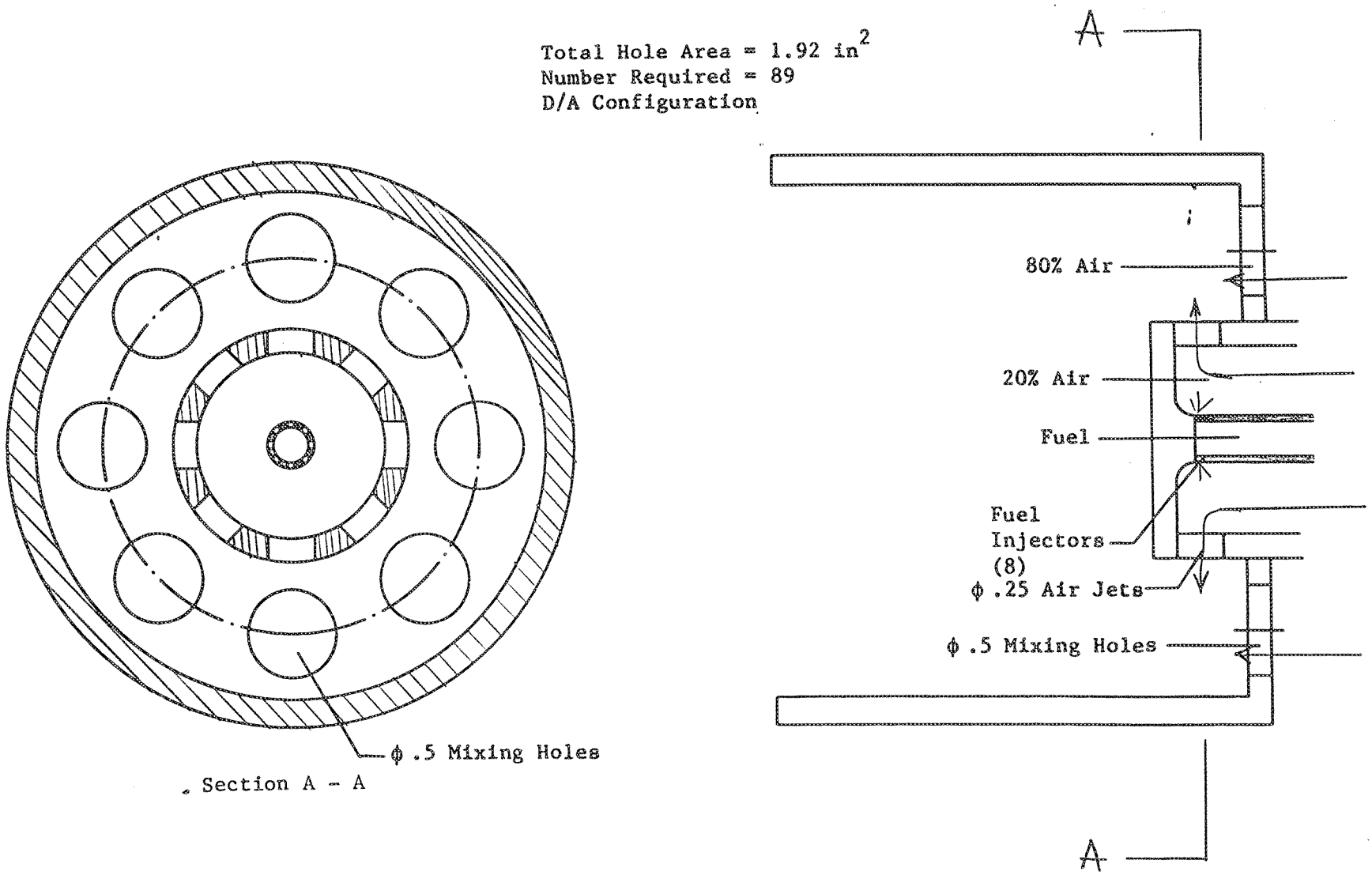

Figure 3-5. Schematic of the Jet Mix LDI Mixer.

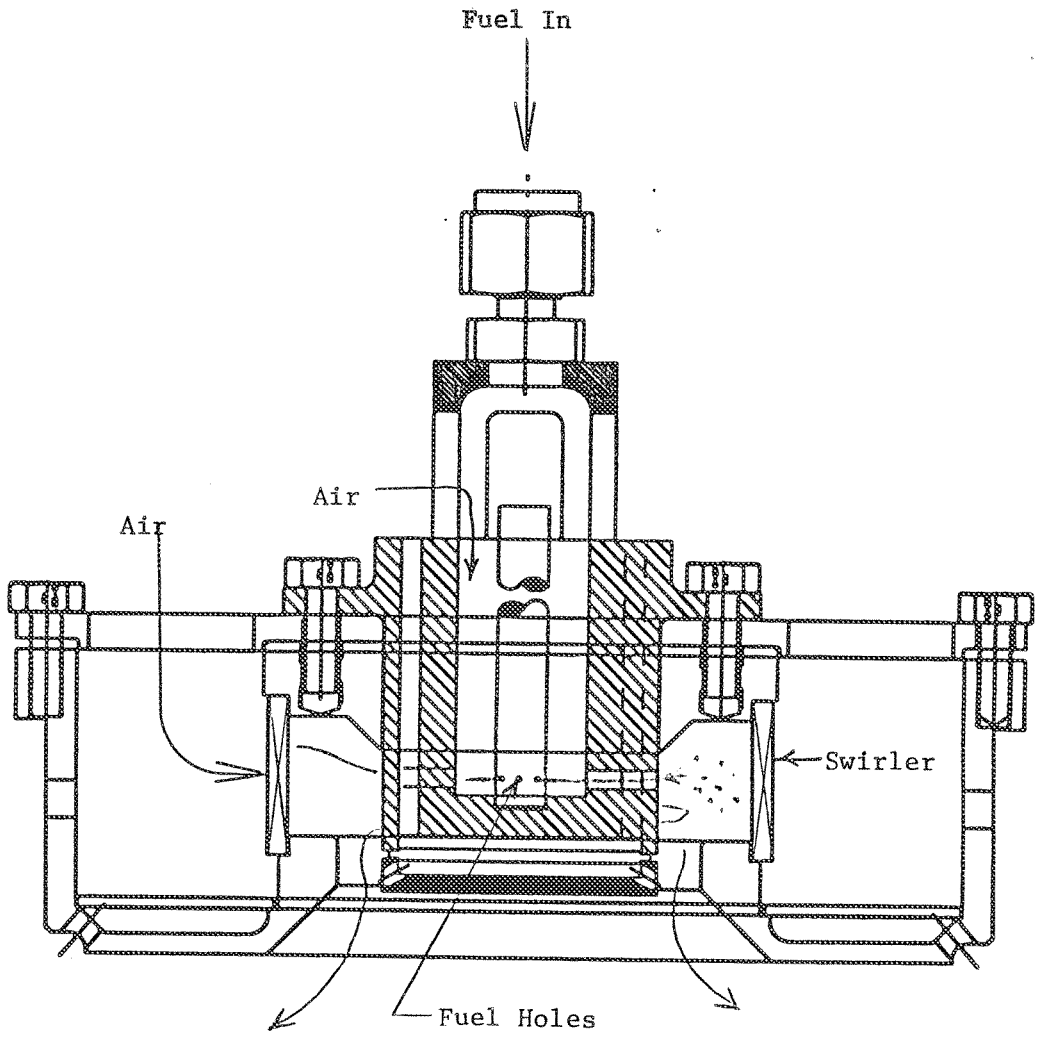

Figure 3-6. Schematic of the Cyclone Swirler Premixer.

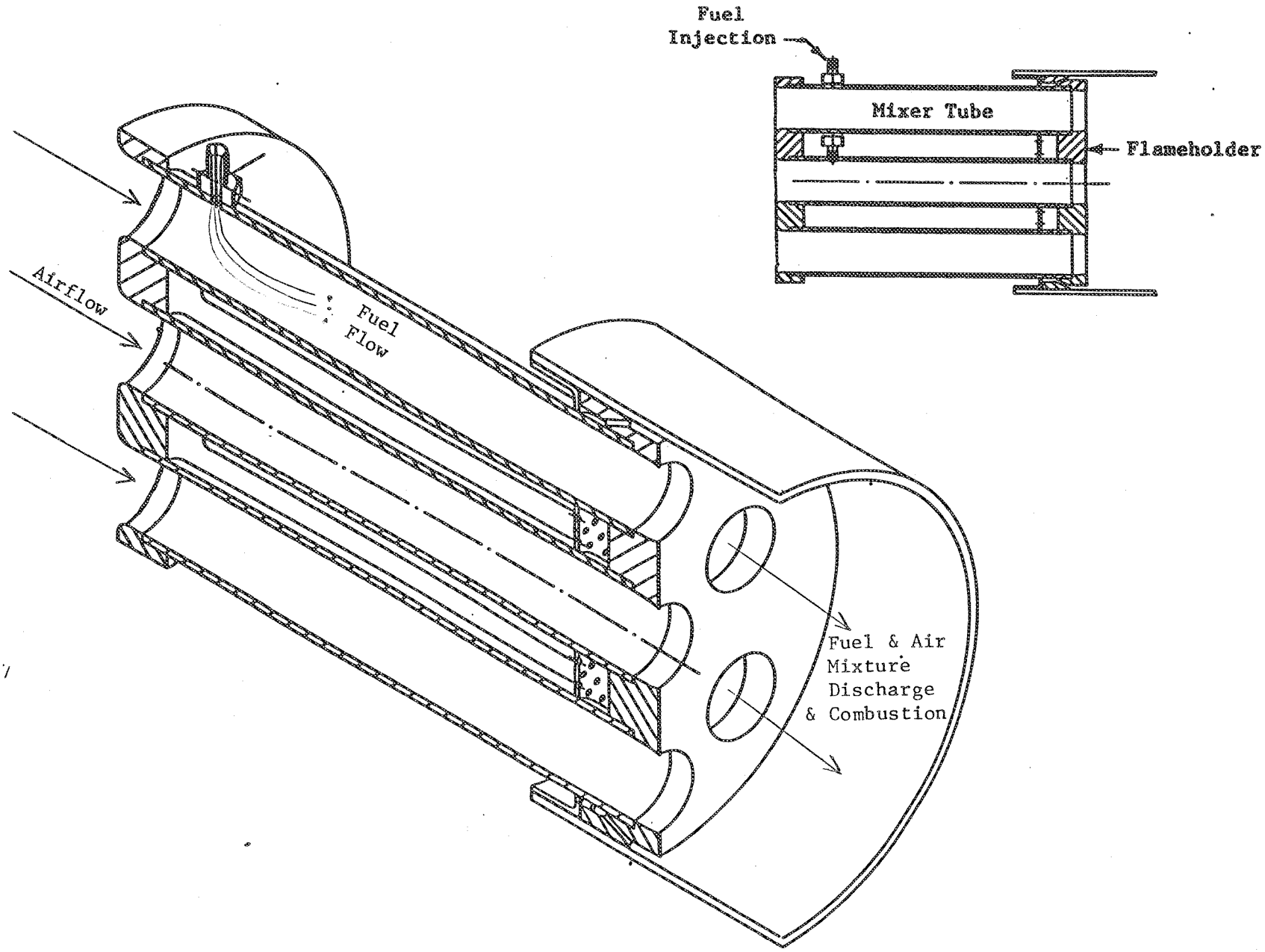

Figure 3-7. Schematic of the Integrated Mixer Flame Holder (IMFH) Premixer.

- Multiple injection points
- Venturis for uniform airflow distribution
- Presuure atomizers for 10 μm droplets
- Swirler for mixing and flame stabilization

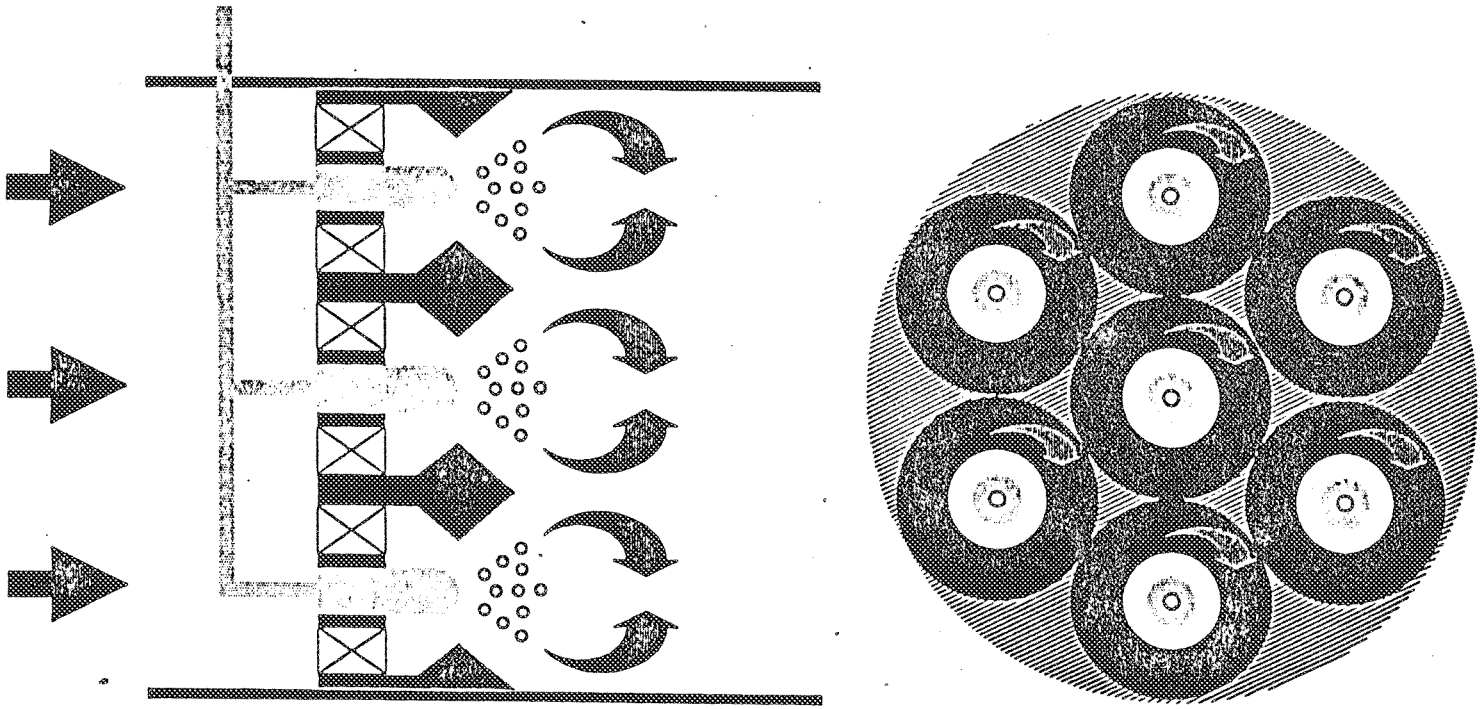

Figure 3-8. Schematic of the Multi-Venturi.

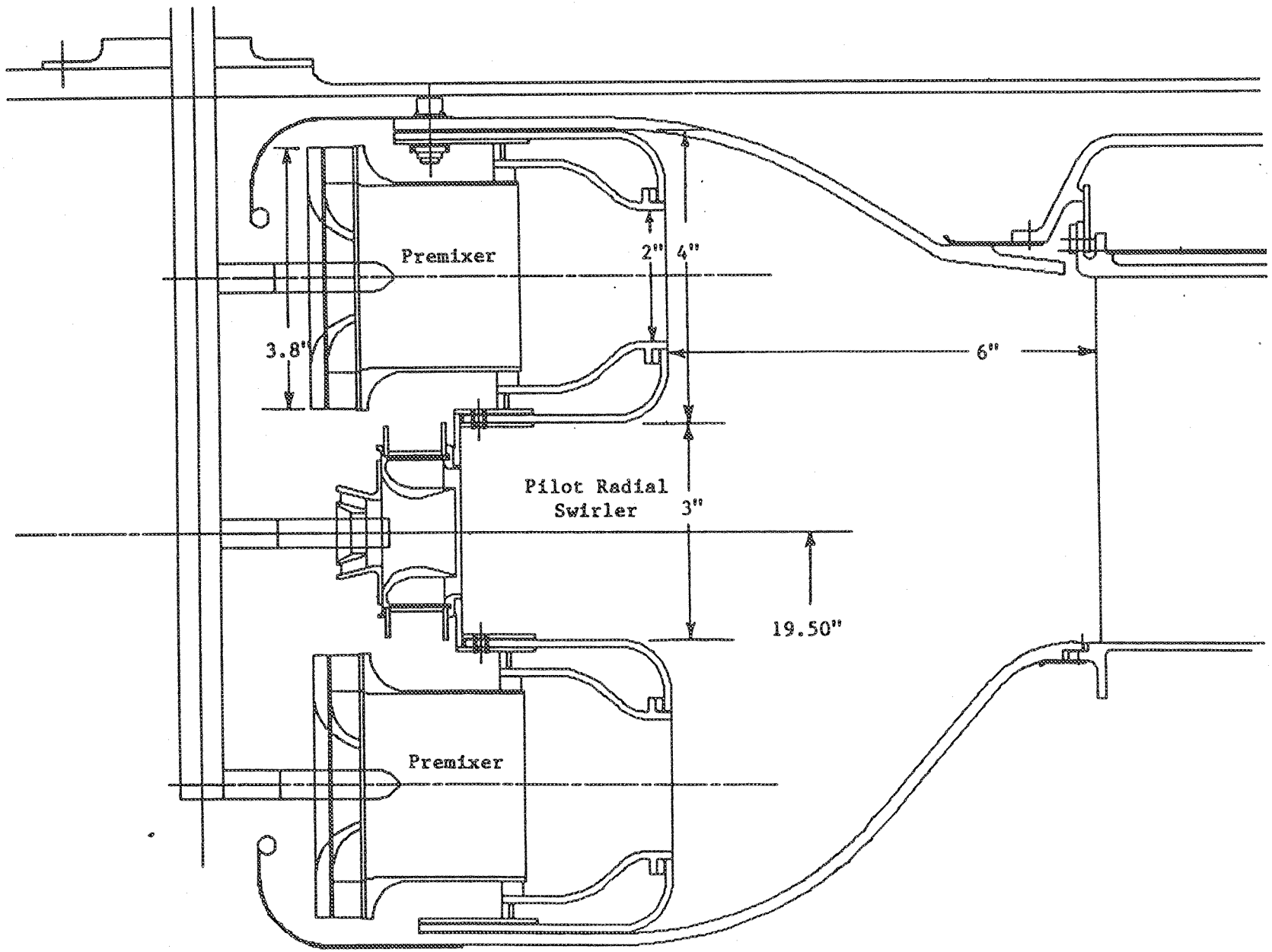

Figure 3-9. Triple Annular Combustor using the Swirl-Jet Premixer (Cross Section).

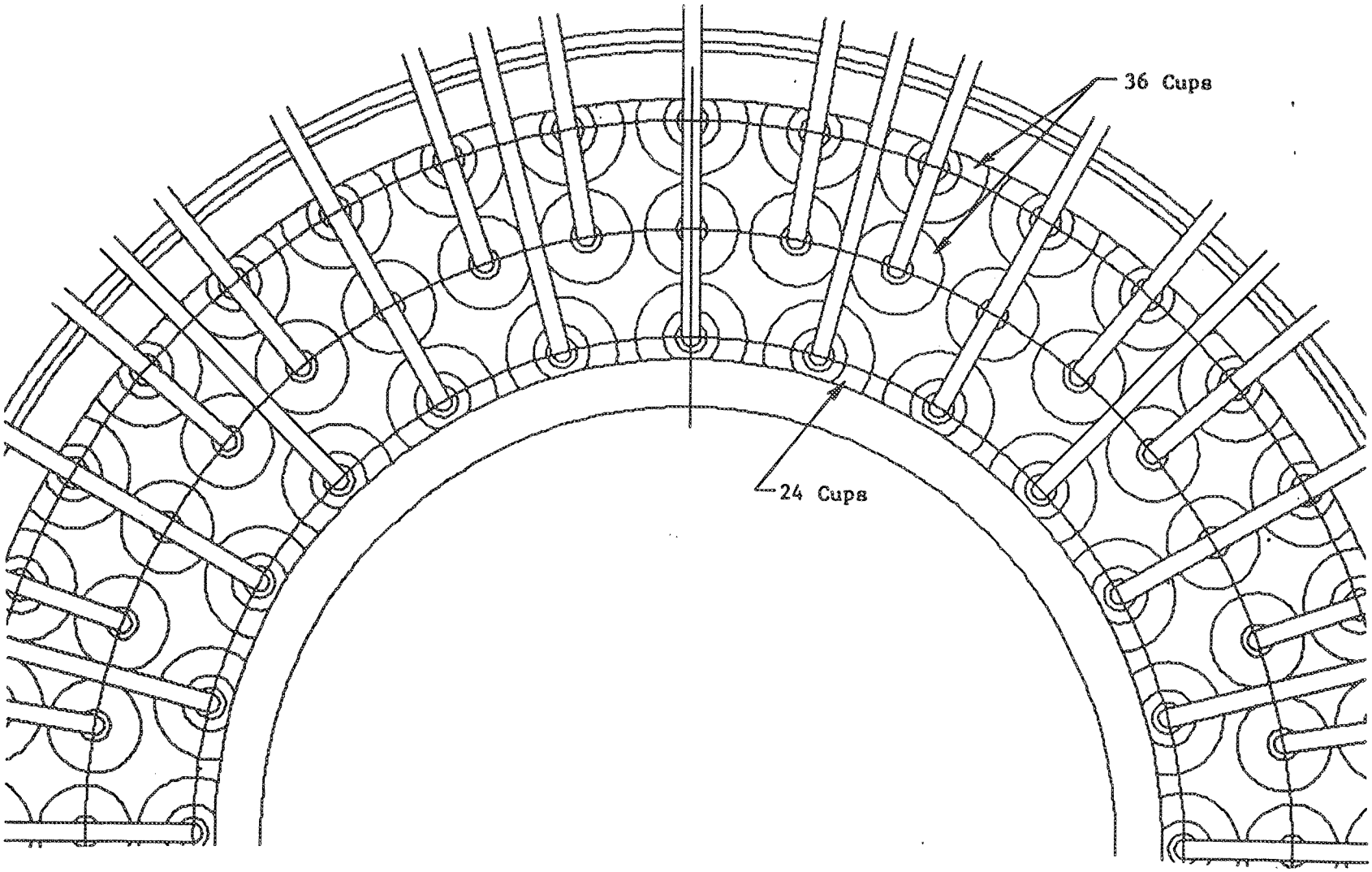

Figure 3-10. Triple Annular Combustor using the Swirl-Jet Premixer (End View FLA).

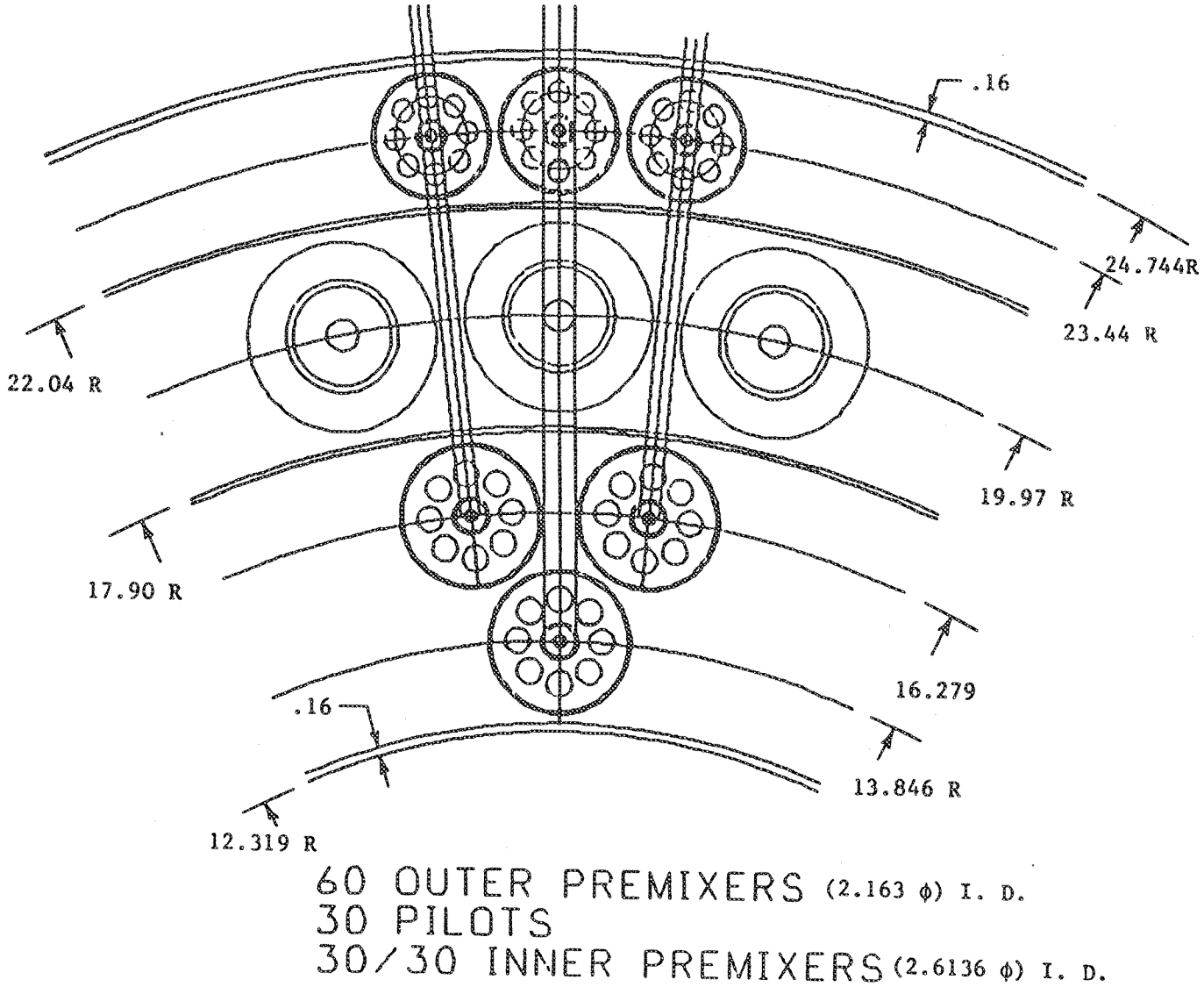

Figure 3-11. End View (ALF) of the Jet-Mix LDI Combustor Preliminary Design.

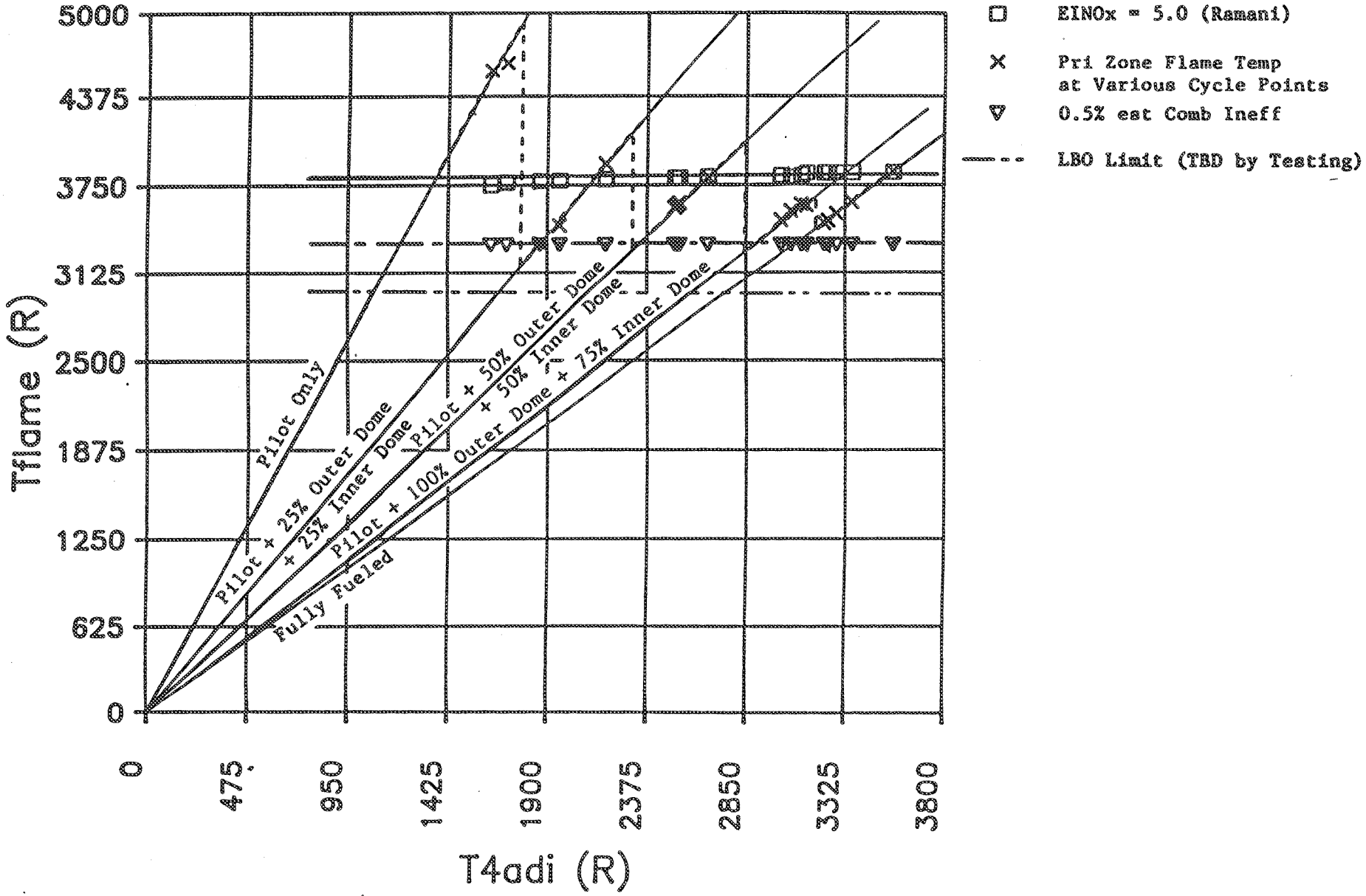

Figure 3-12. Fuel Staging for the Jet-Mix LDI Design.

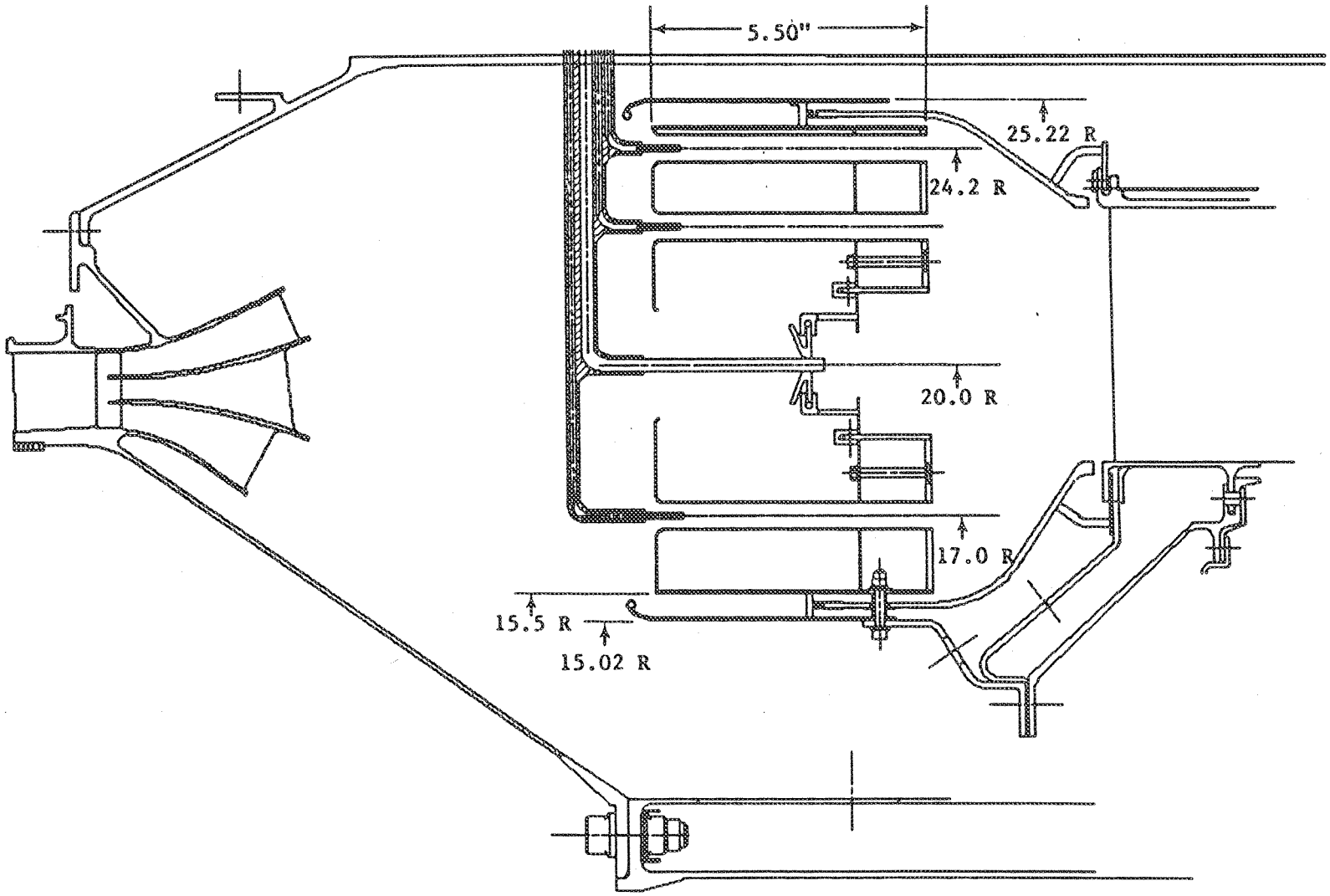

Figure 3-13. Mechanical Design Layout of the IMFH Combustor (Side View).

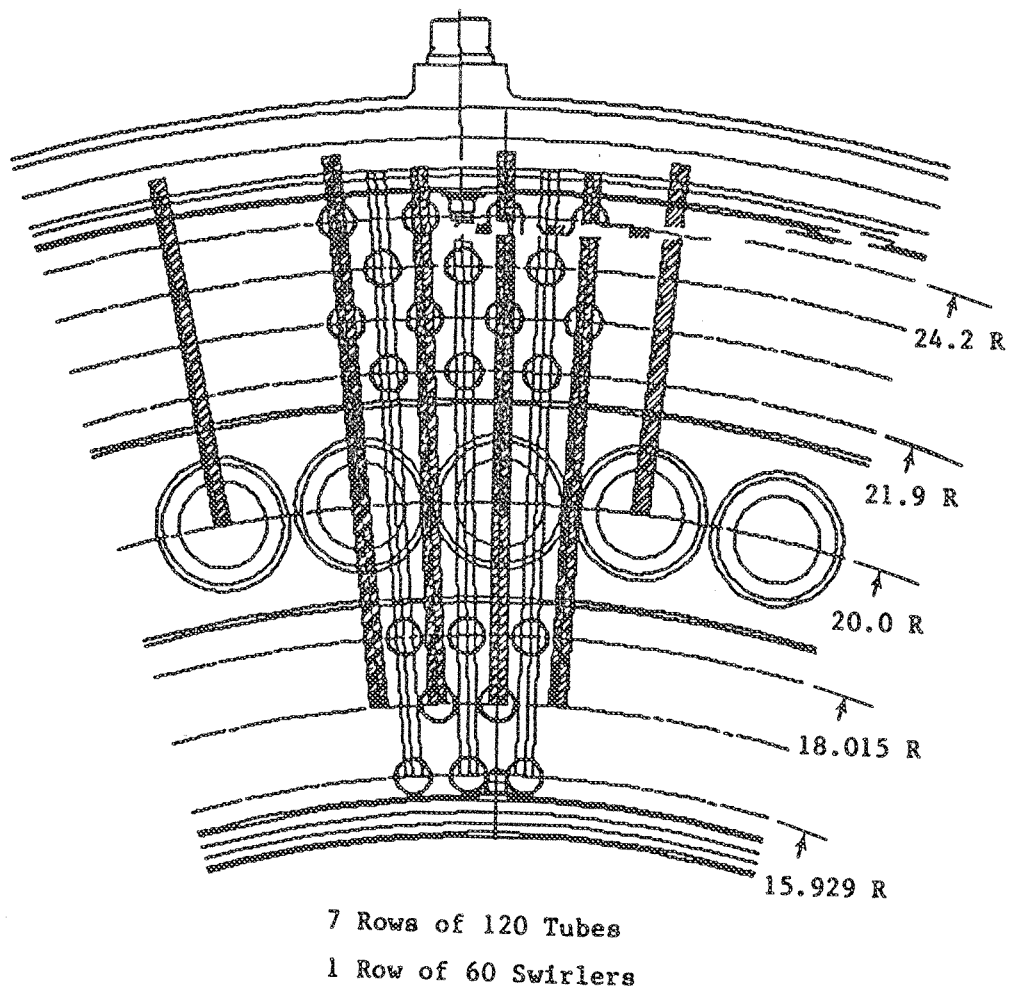

Figure 3-14. Mechanical Design Layout for the IMFH Combustor (End View FLA).

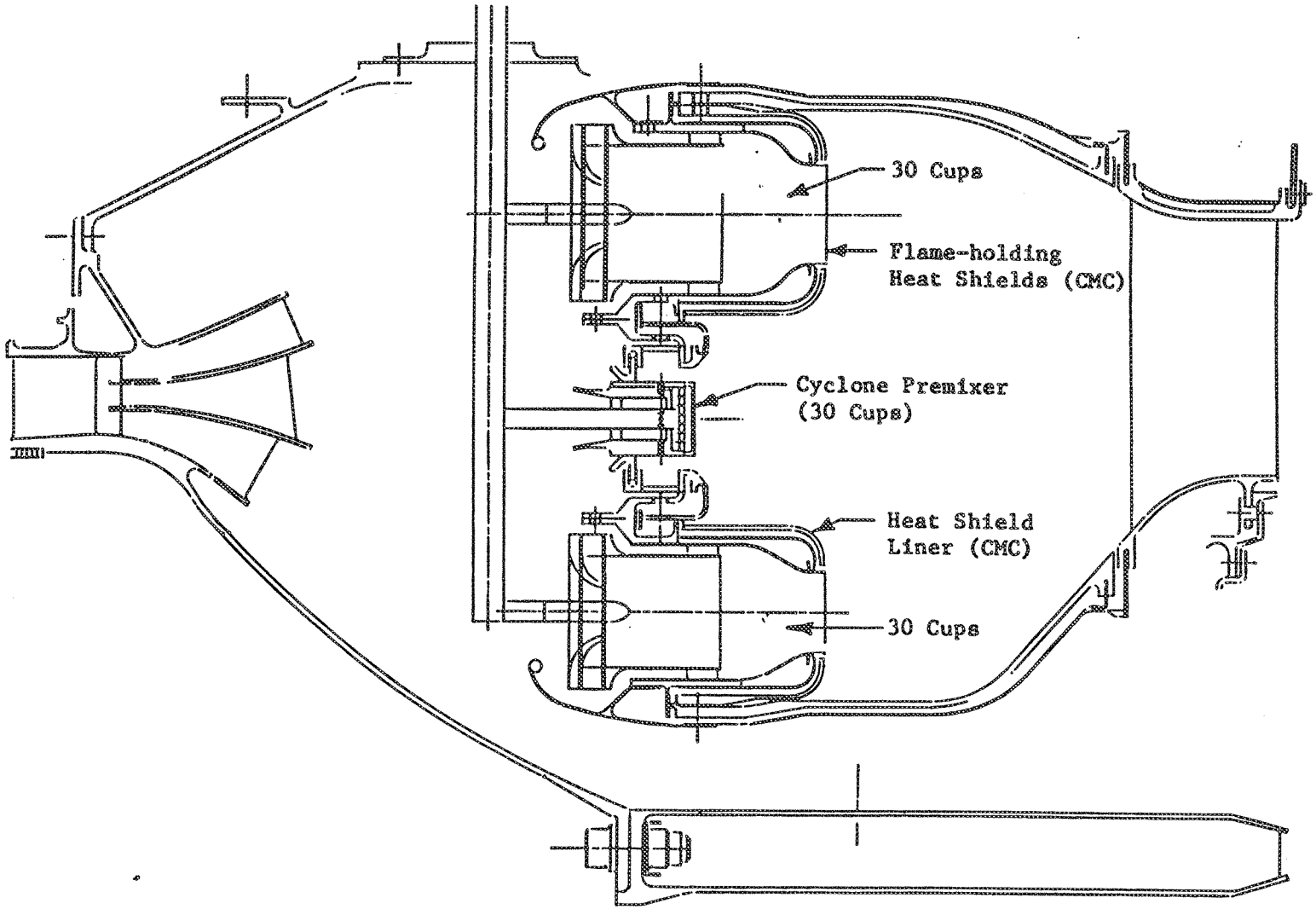

Figure 3-15. The Revised Swirl-Jet Combustor Layout.

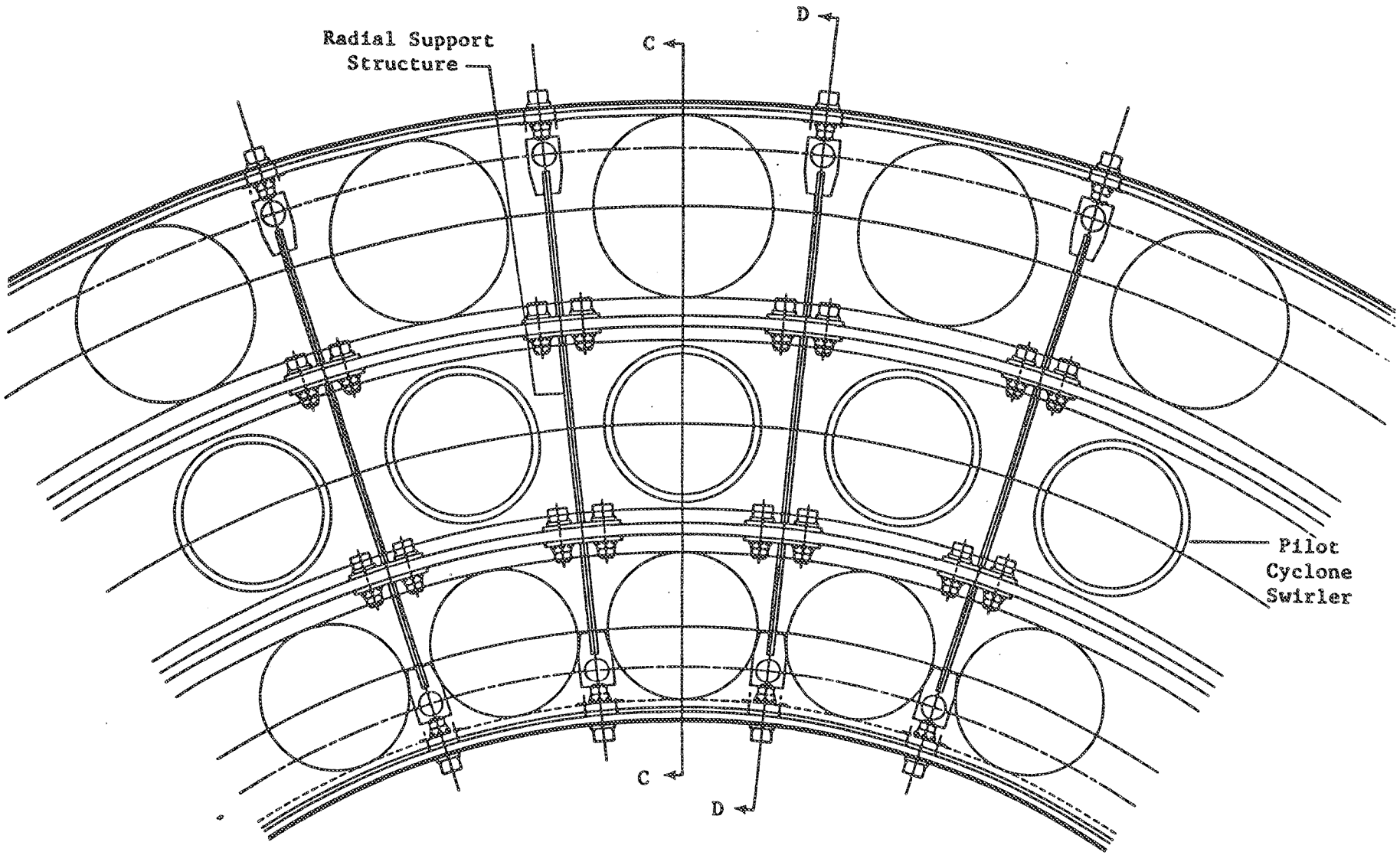

Figure 3-16. Mechanical Design Swirl-Jet Combustor (FLA).

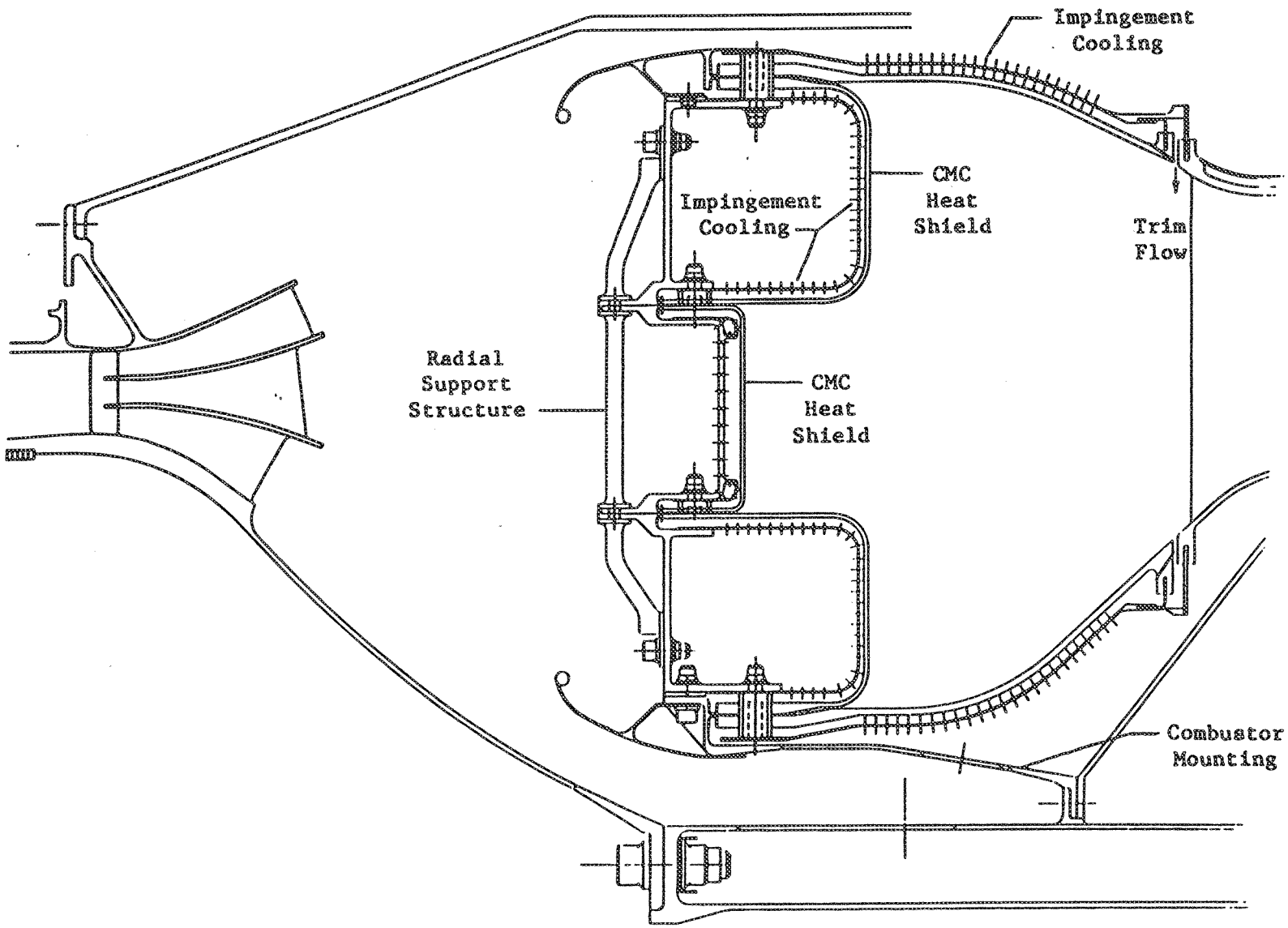

Figure 3-17. Swirl-Jet Combustor Mechanical Design Section D-D.

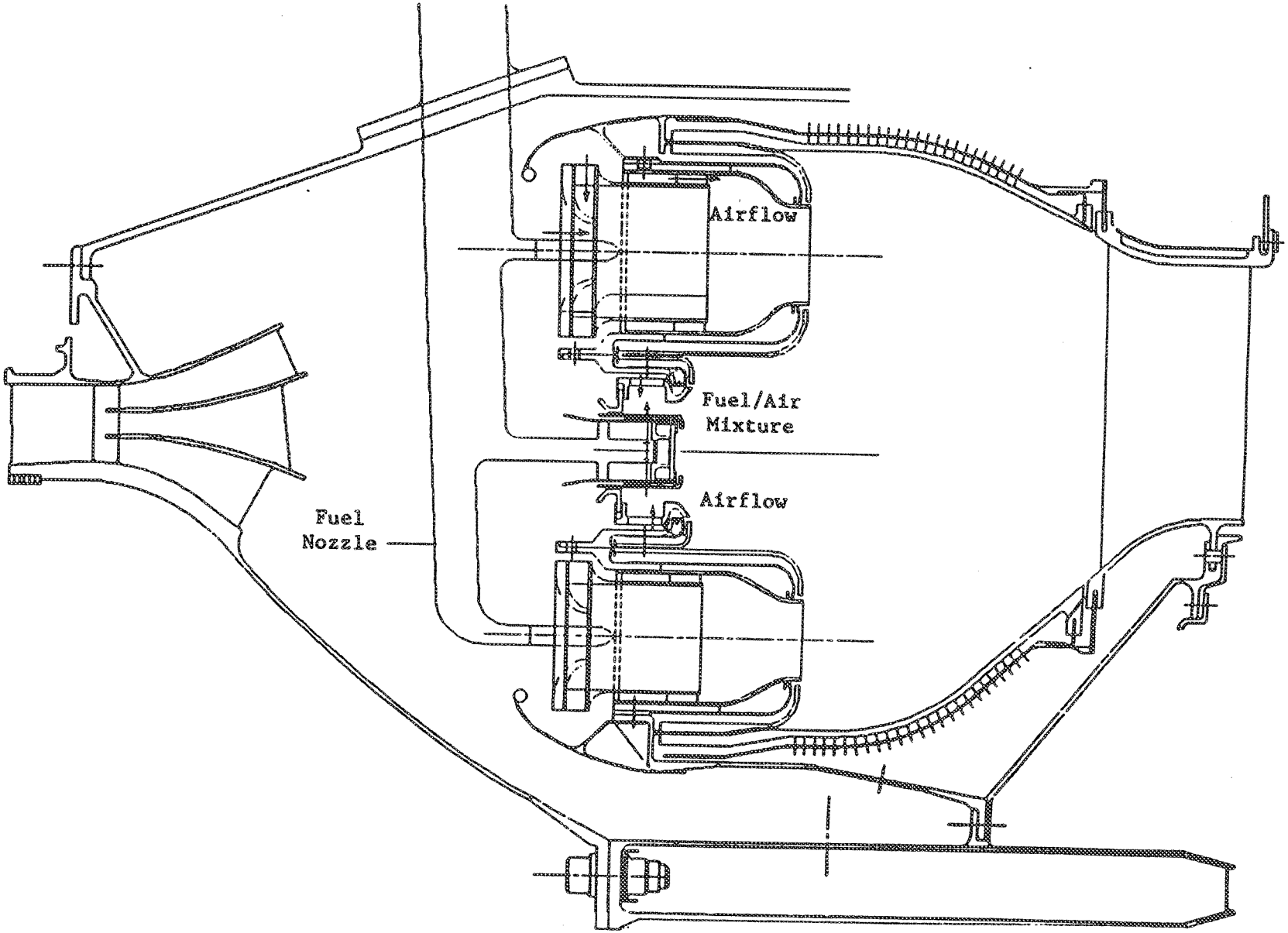

Figure 3-18. Swirl-Jet Combustor Mechanical Design Section C-C.

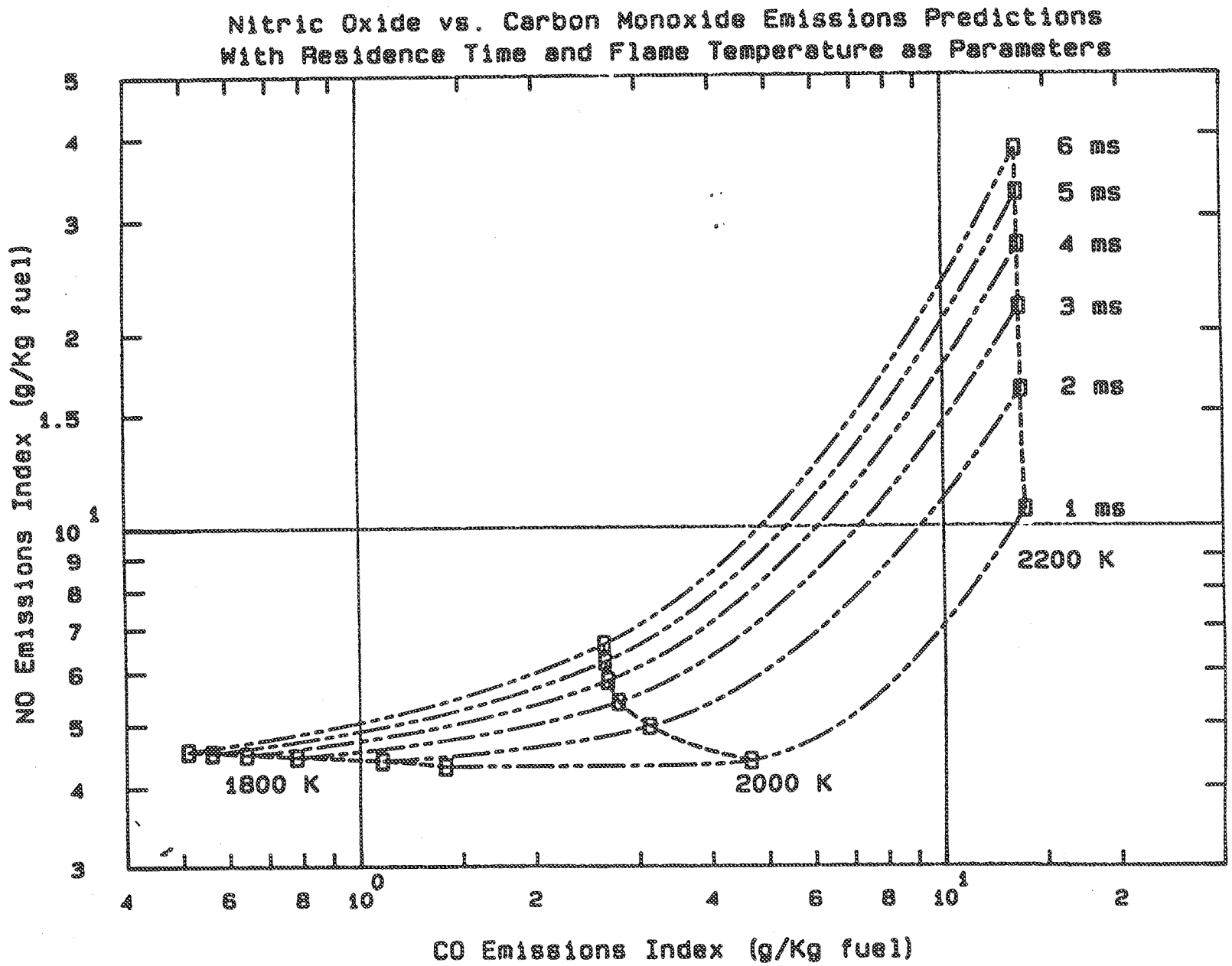

Figure 3-19. Chemical Kinetics Model Computed NOx Emissions as a Function of CO.

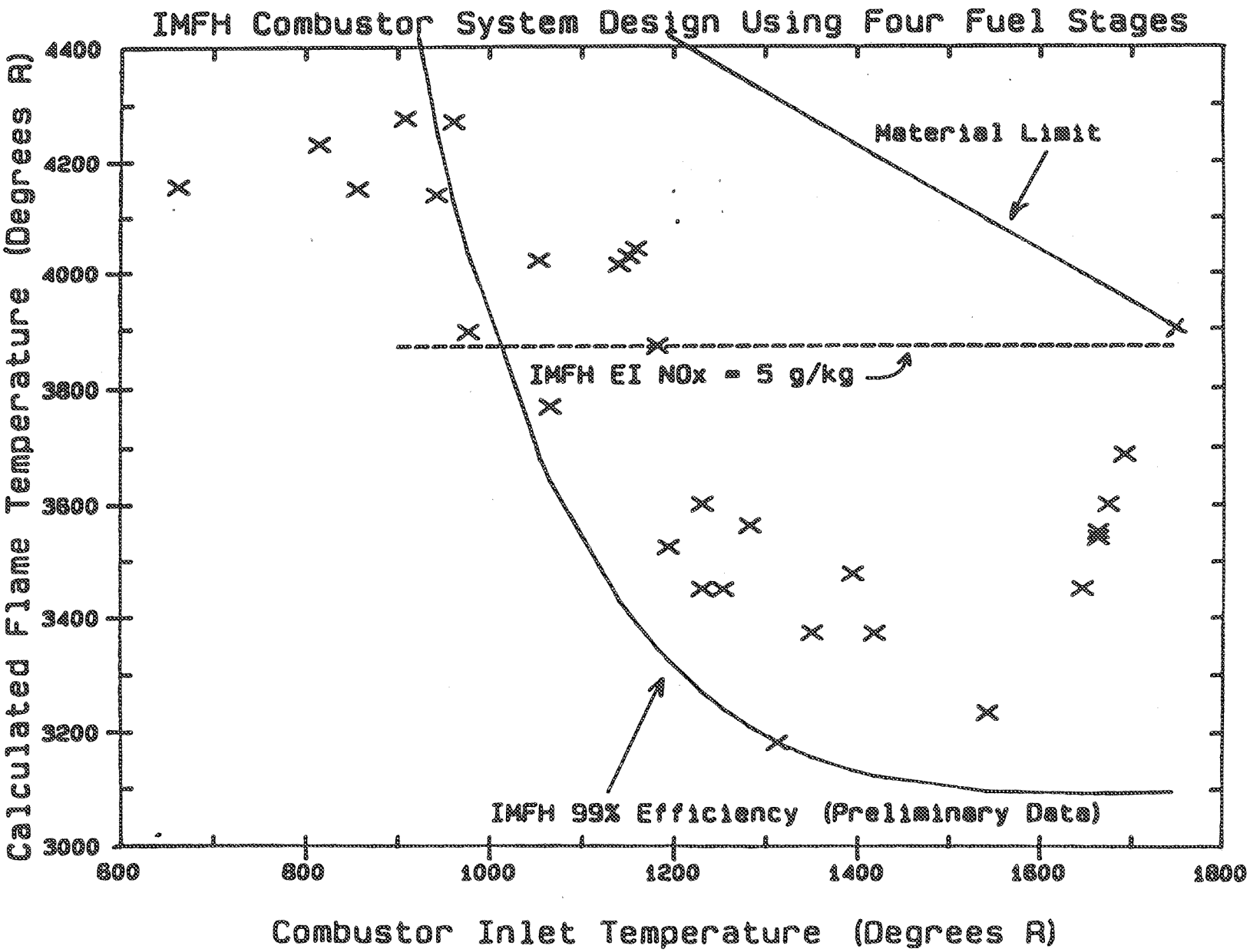

Figure 3-20. Calculated Flame Temperature at 29 Engine Cycle Points for a 4 Fuel Stage IMFH Combustor.

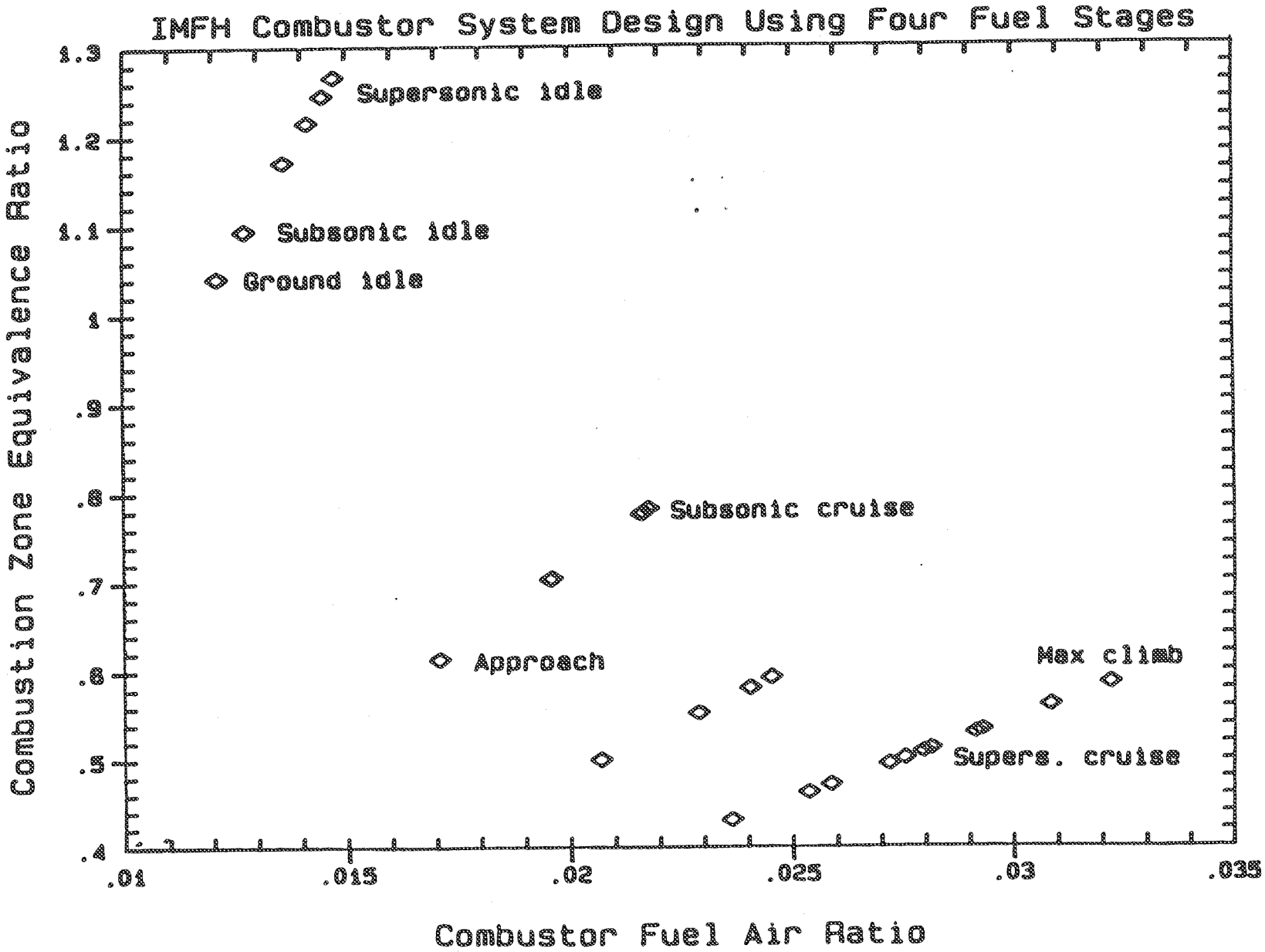

Figure 3-21. IMFH Combustor Fuel Staging Diagram.

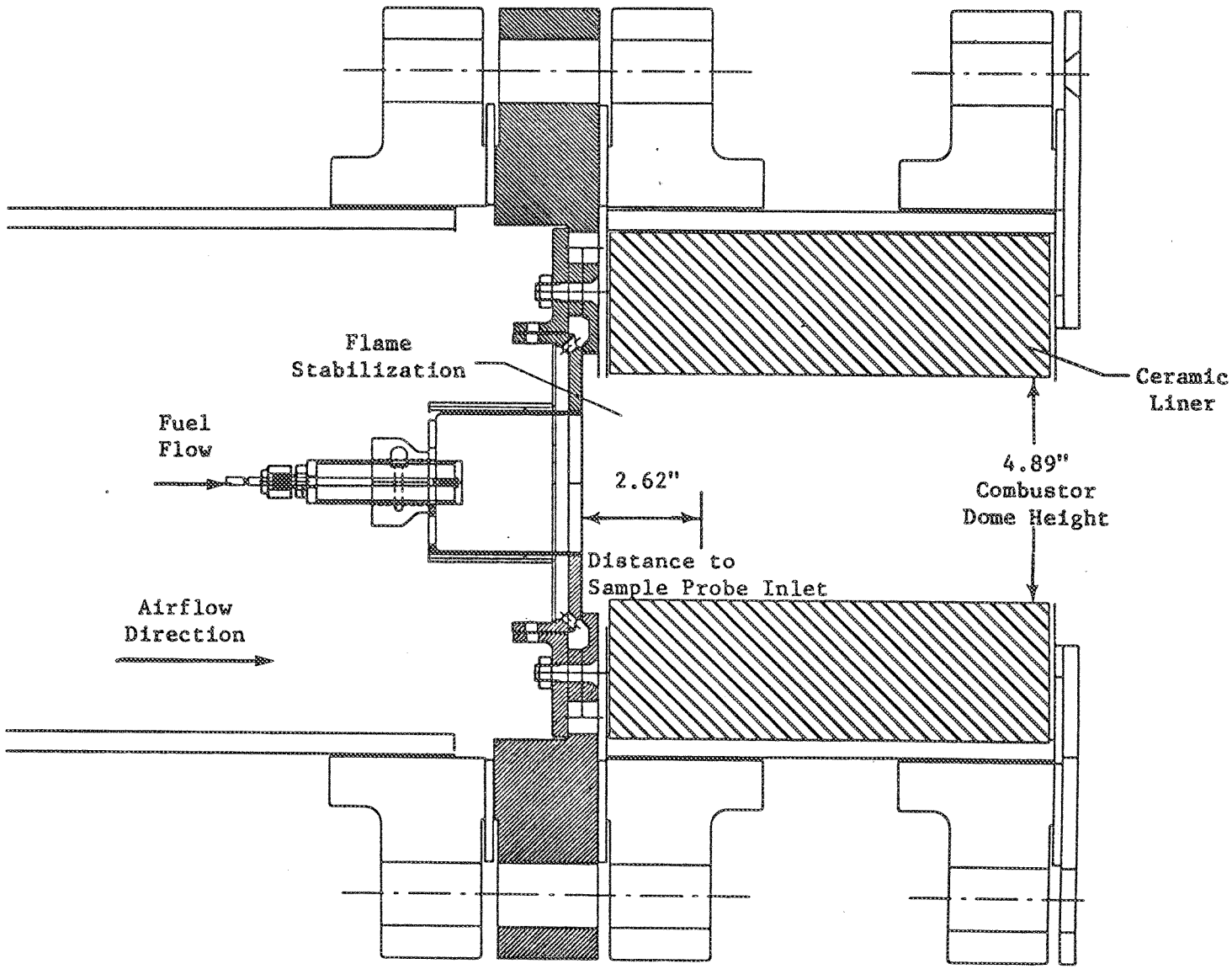

Figure 4-1. A Schematic of the Single Cup Flametube Test Rig.
(Jet-Mix Concept Shown)

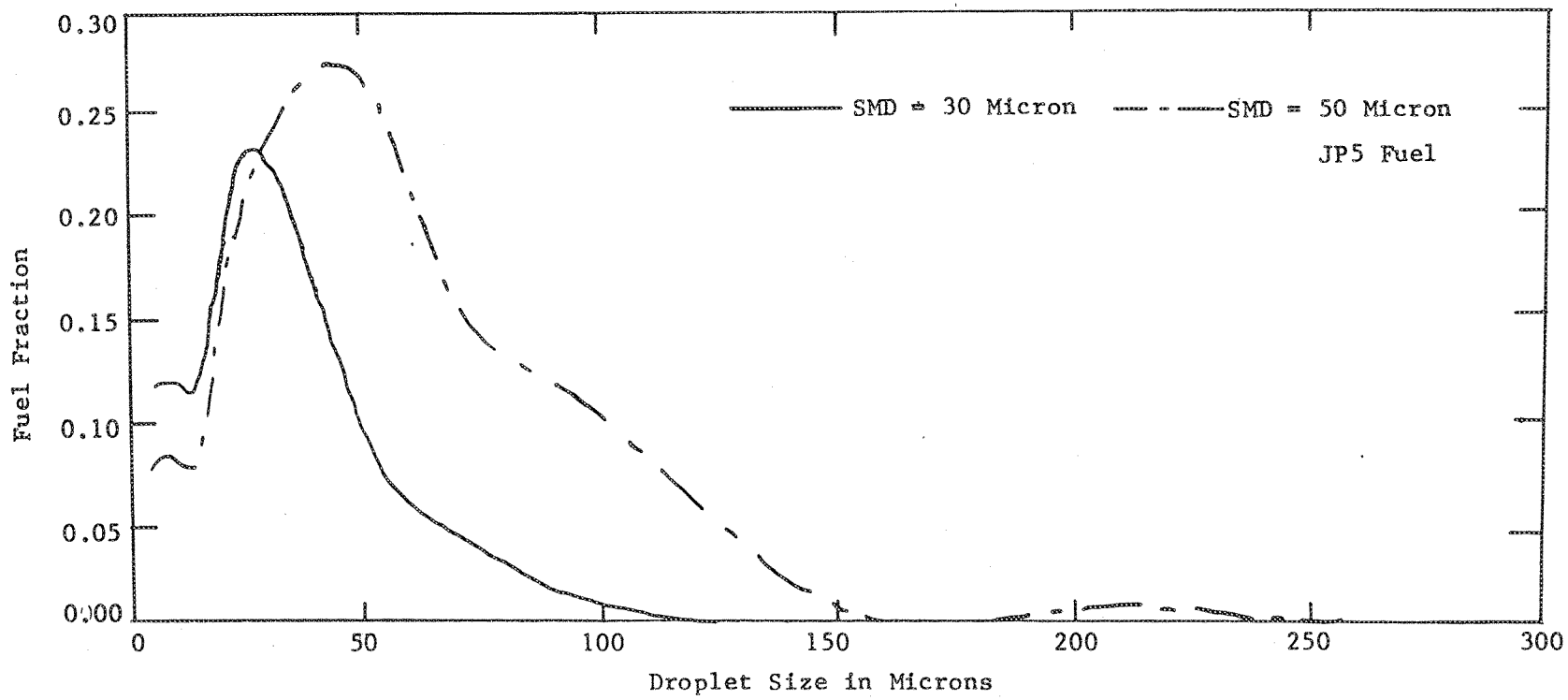

Figure 4-2. Computed Spray Distribution for 30 and 50 Micron Sprays
(Rossin-Rammler Exponent = 1.3)

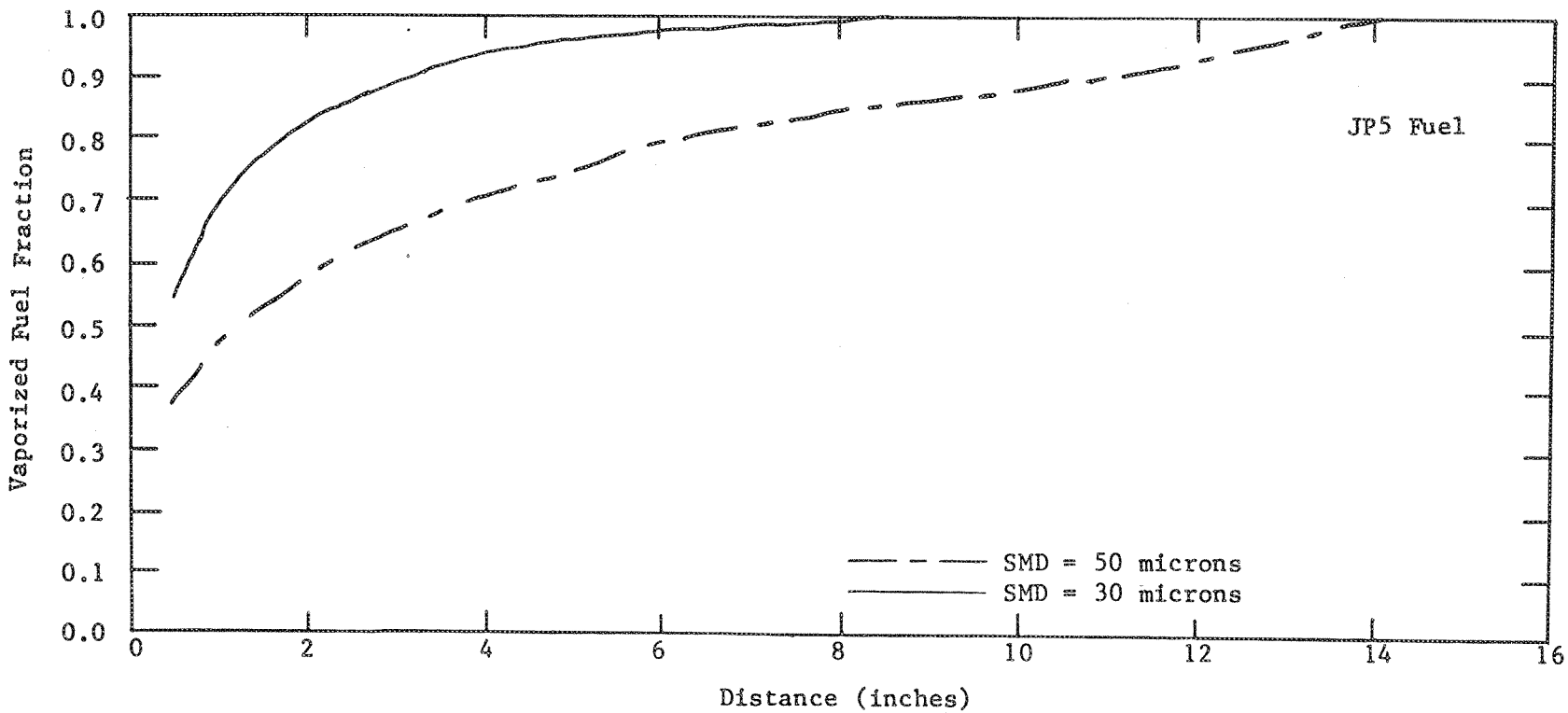

Figure 4-3. Vaporization History of 30 and 50 Micron Sprays.
(Tair = 1660 R, Vair = 500 fps)

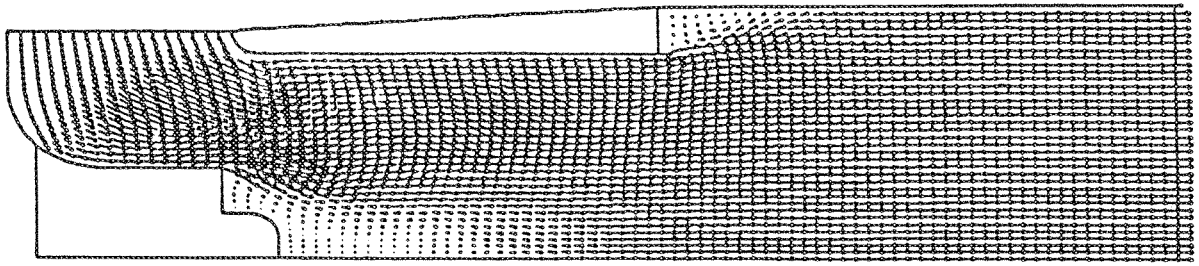

Figure 4-4a. Swirl-Jet Velocity Vectors in the Absence of a Central Jet.

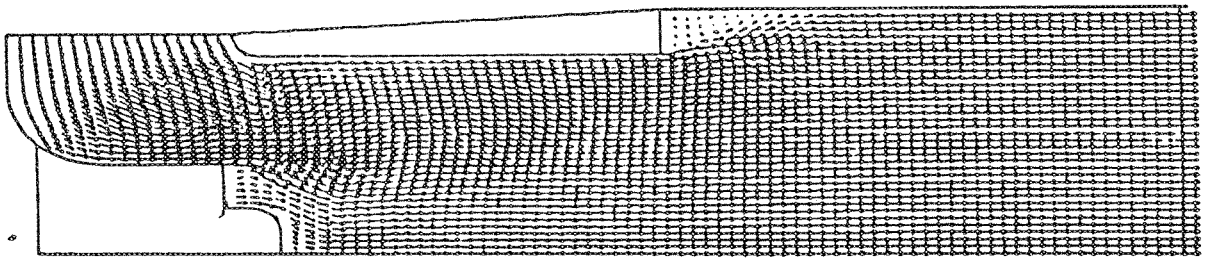

Figure 4-4b. Swirl-Jet Velocity Vectors in the Presence of a Central Jet.

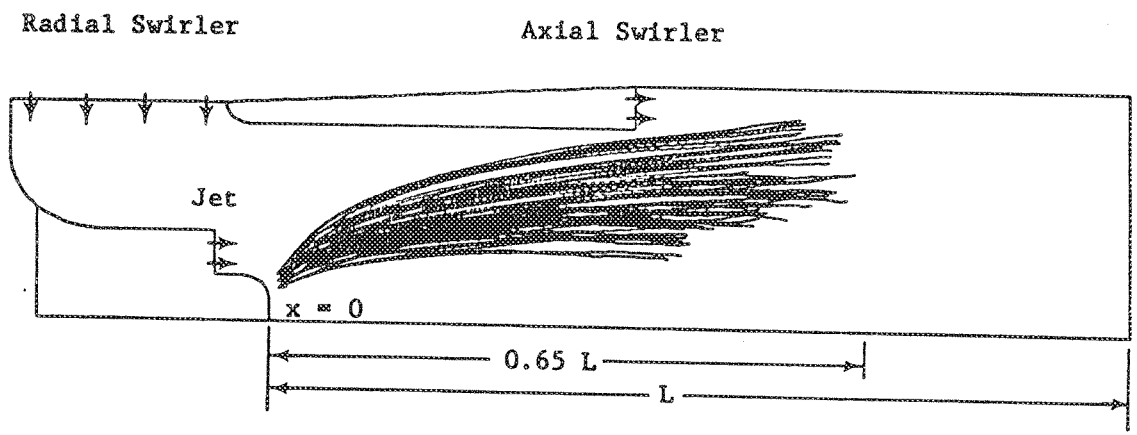

Figure 4-5. Spray Vaporization and Droplet Trajectories in the Swirl-Jet Premixer.

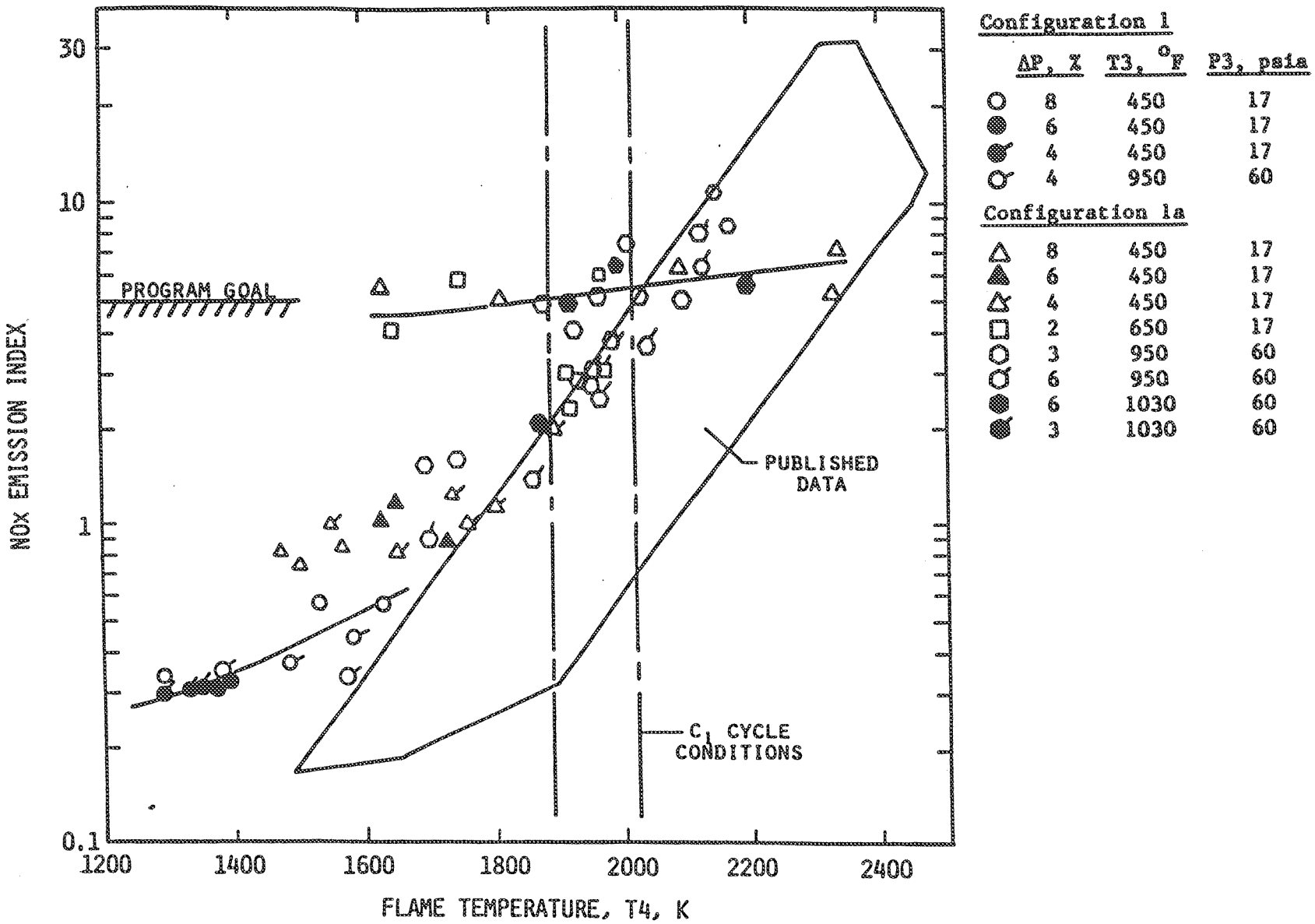

Figure 4-6. Swirl-Jet Configurations 1 and 1A Measured NOx Emission Index.

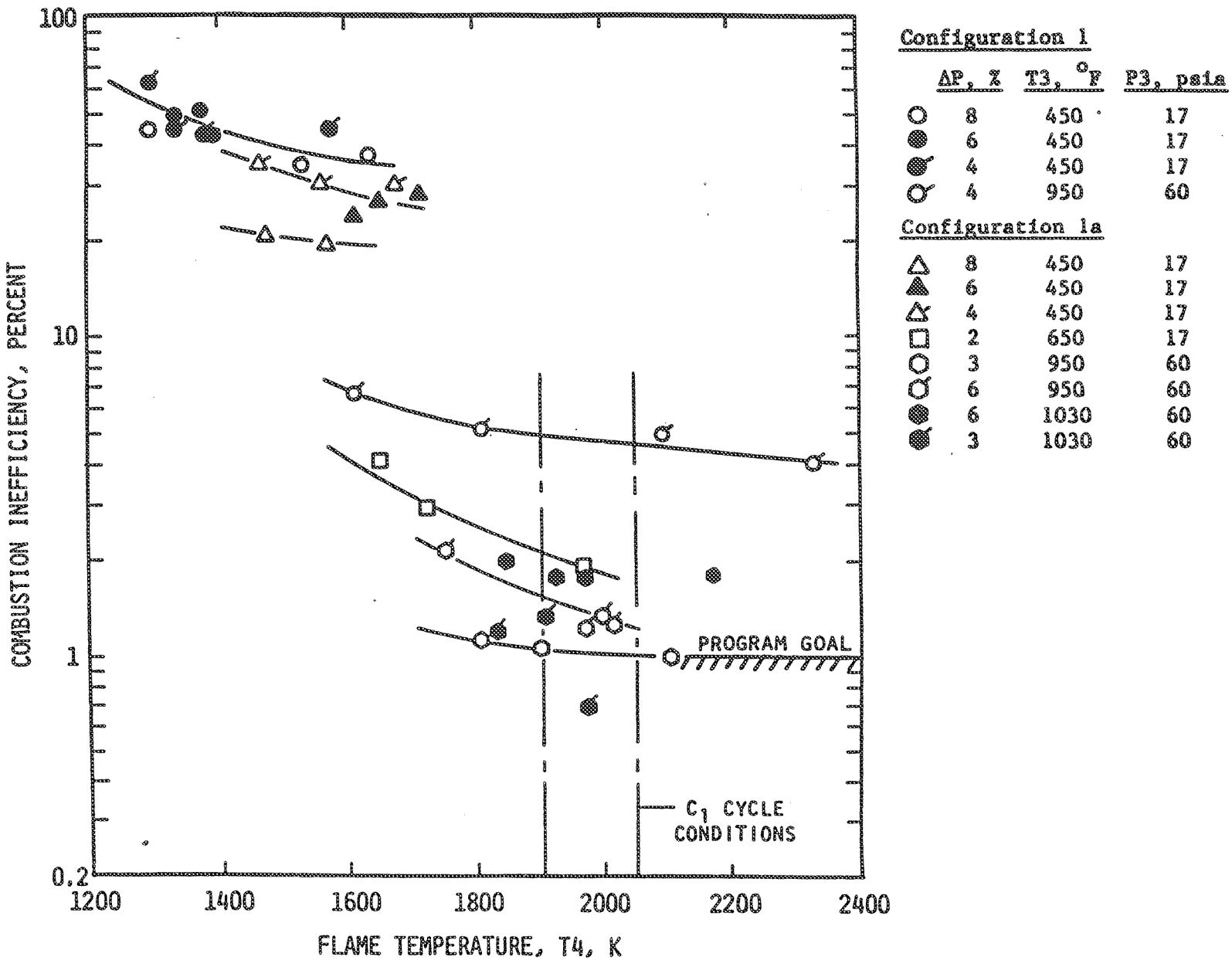

Figure 4-7. Swirl-Jet Configurations 1 and 1A Combustion Inefficiency.

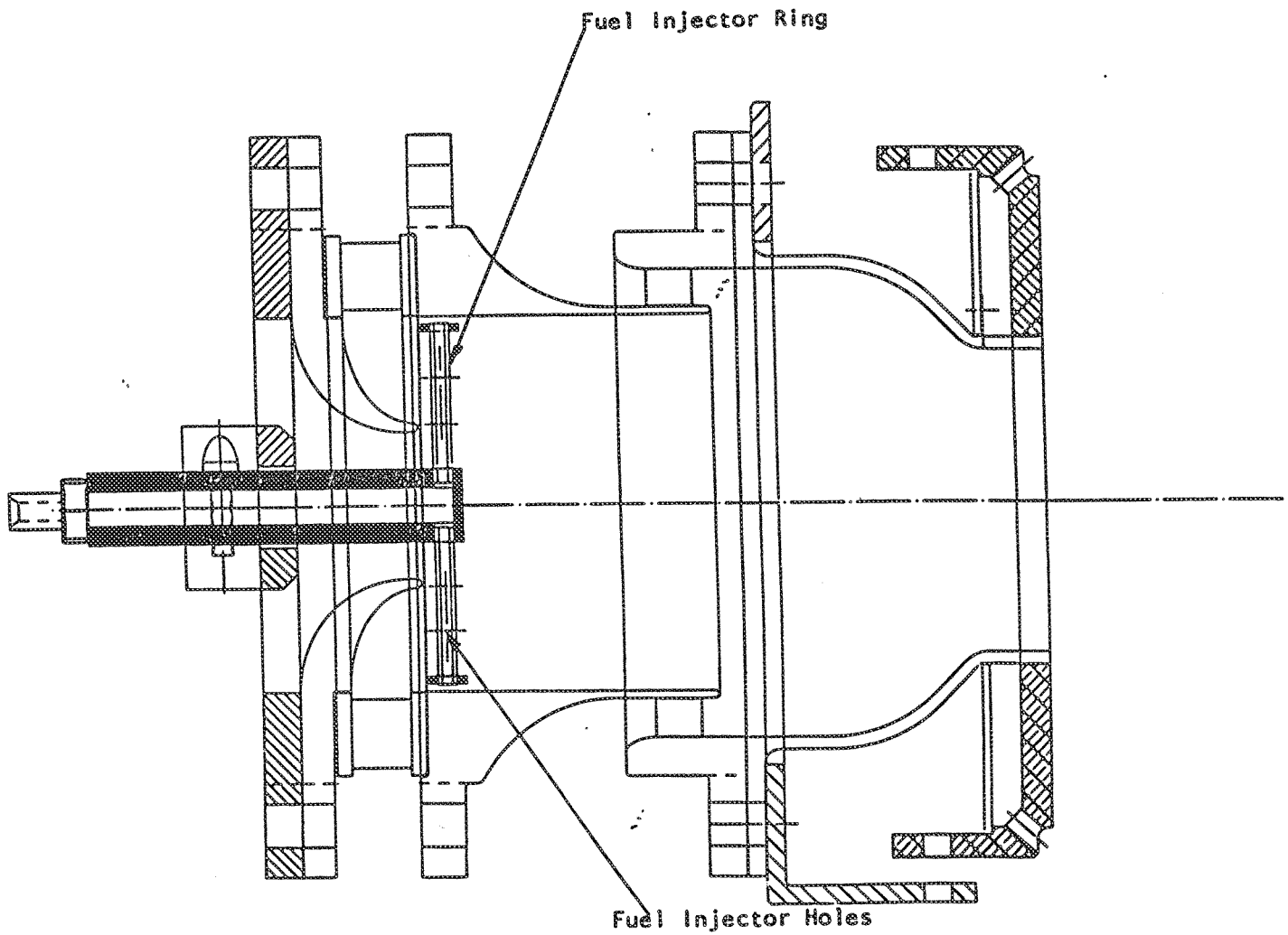

Figure 4-8. Swirl-Jet Premixer with Spray Bar Fuel Injector Ring.

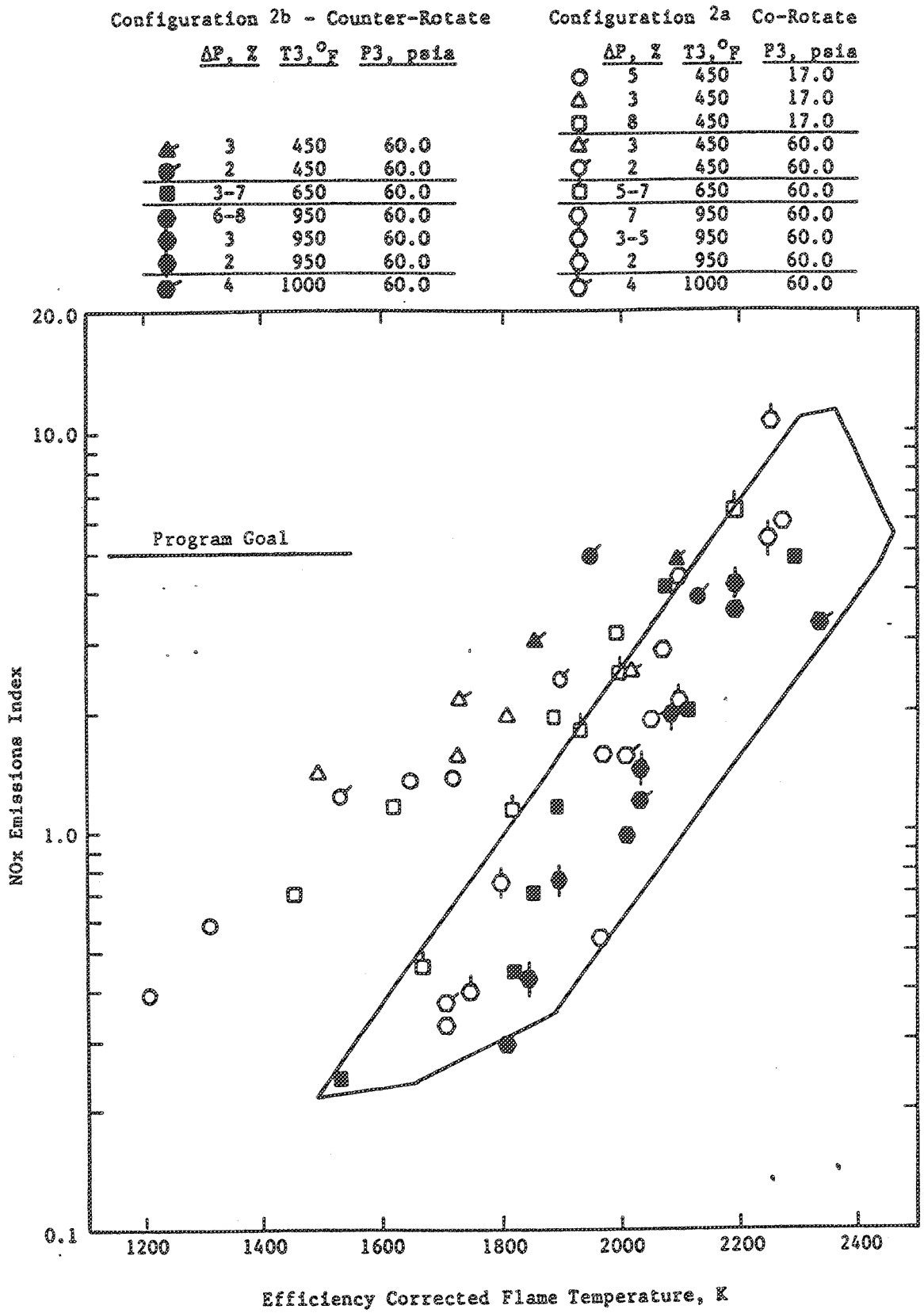

Figure 4-9. Swirl Jet Configurations 2A and 2B NOx Emissions.

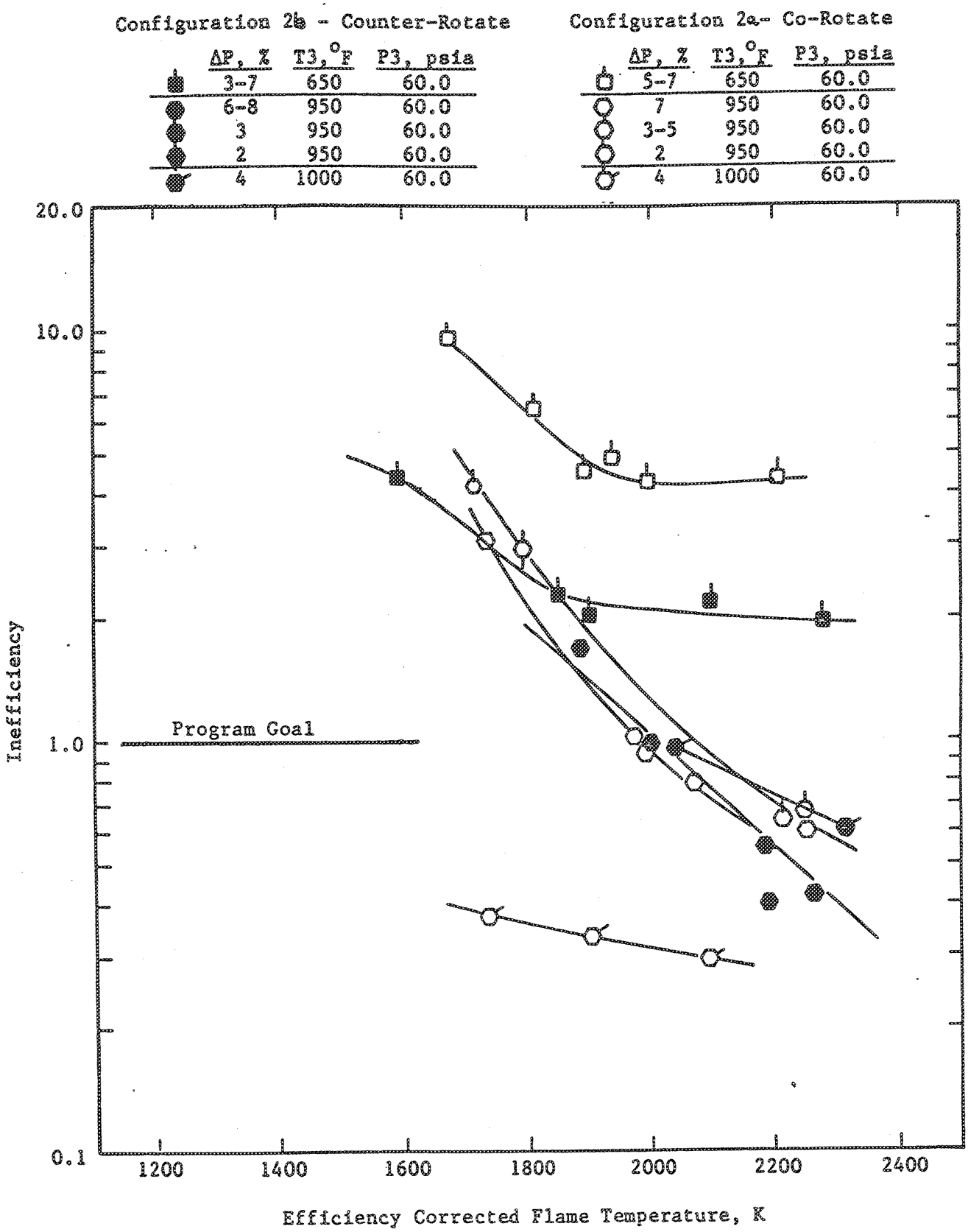

Figure 4-10. Swirl Jet Configurations 2A and 2B Combustion Inefficiency.

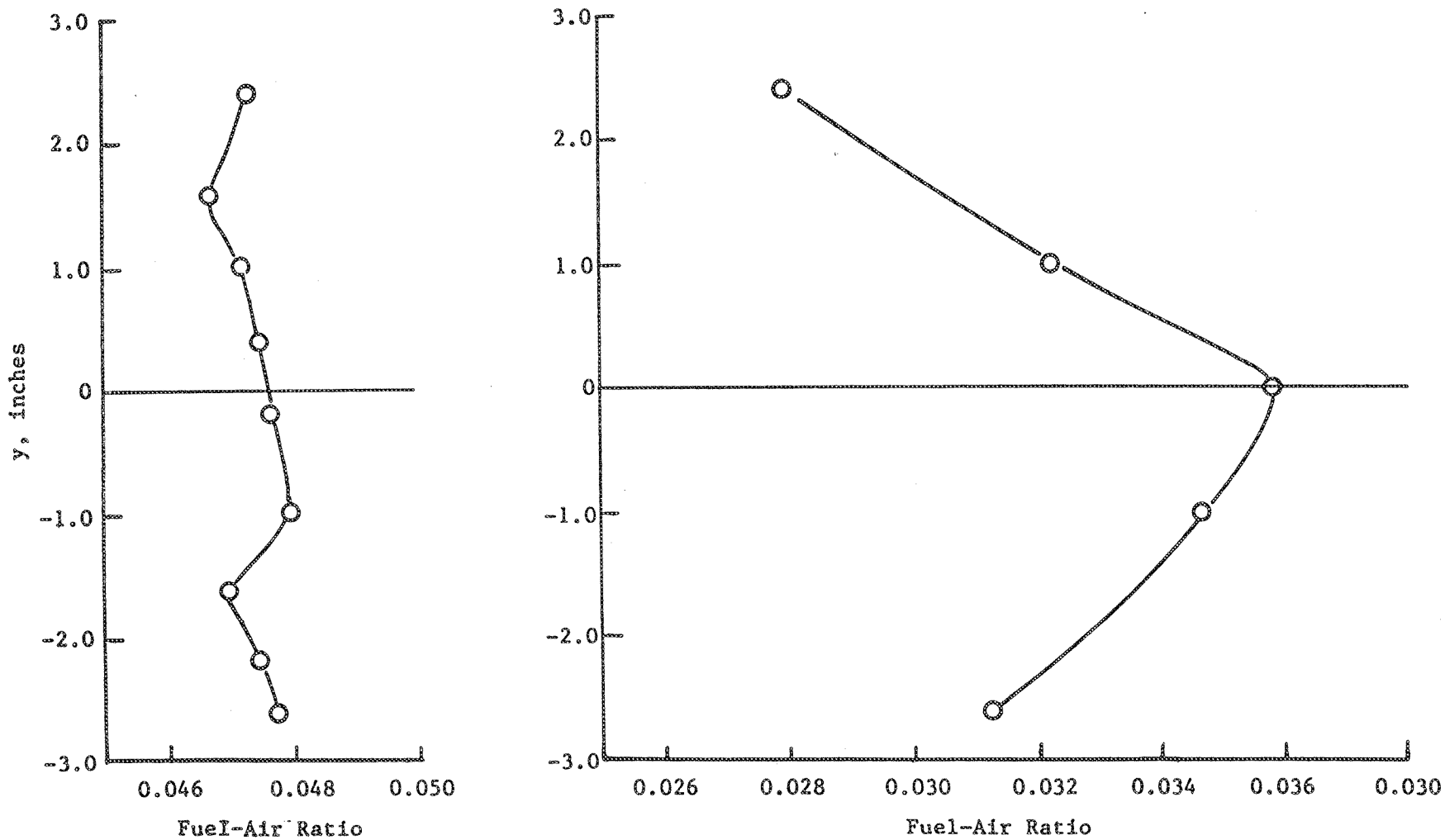

(A) P_3/T_3 = 60 psia/950 °F

(B) P_3/T_3 = 250 psia/1140 °F

Figure 4-11. Pressure and Temperature Impact on Swirl Jet Fuel/Air Ratio Profile.

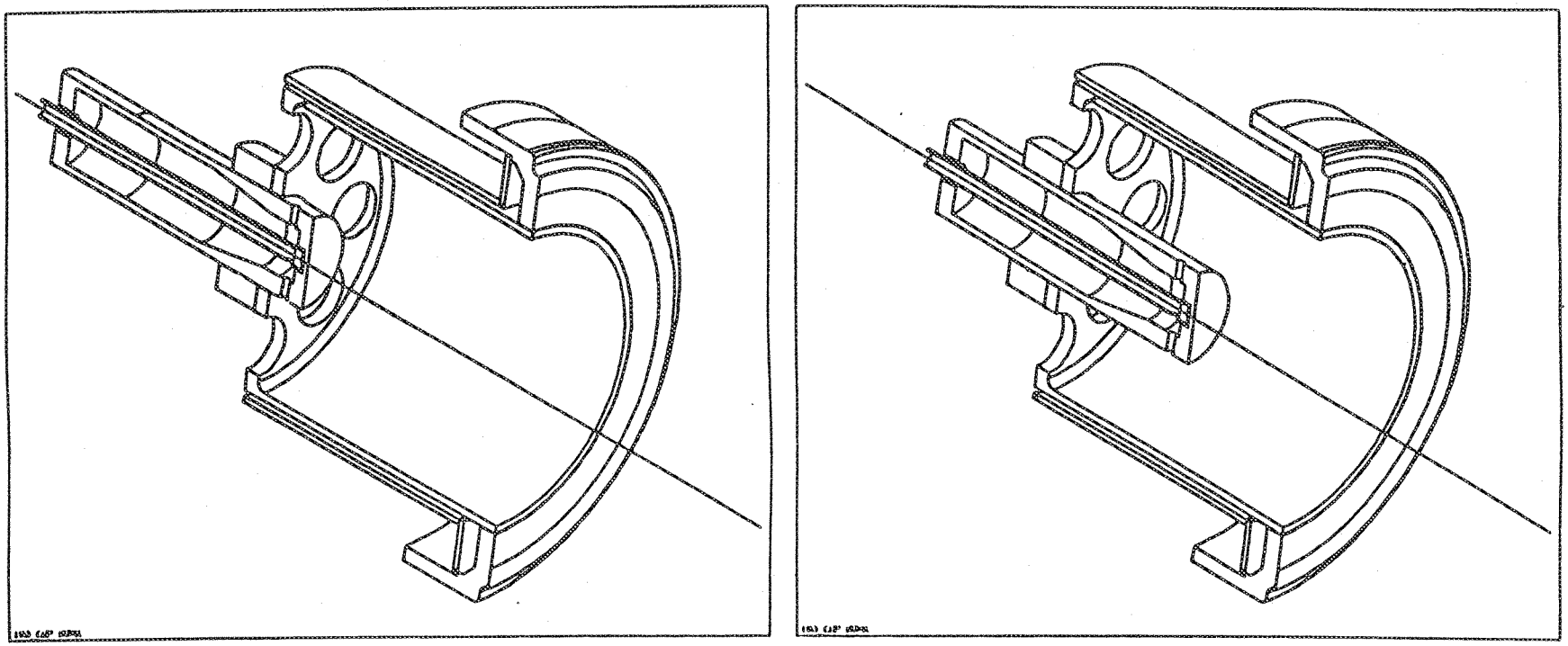

Build #1 Build #2

Build #3 - Same as Build #1 except radial holes are in-between the axial holes

Build #4 - Same as Build #2 except radial holes are in-between the axial holes

Figure 4-12. A Schematic of the Jet Mix Fuel Injection Variations.

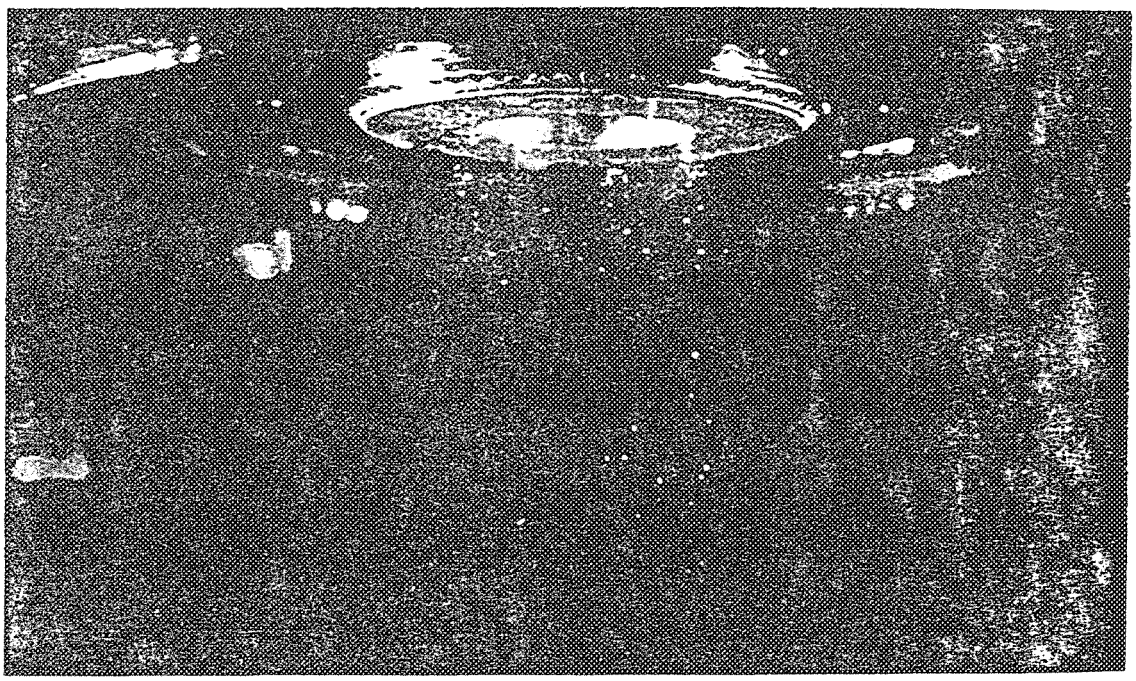

26 pph

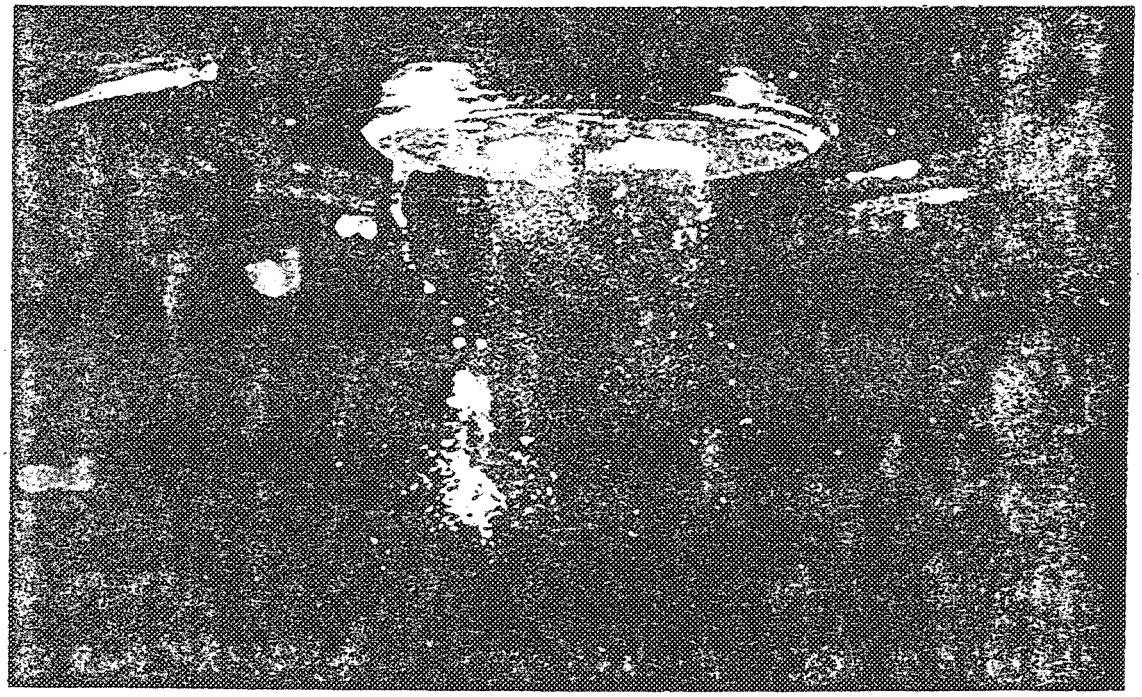

50 pph

Figure 4-13. Jet Mix Spray Visualization at 26 and 50 pph.

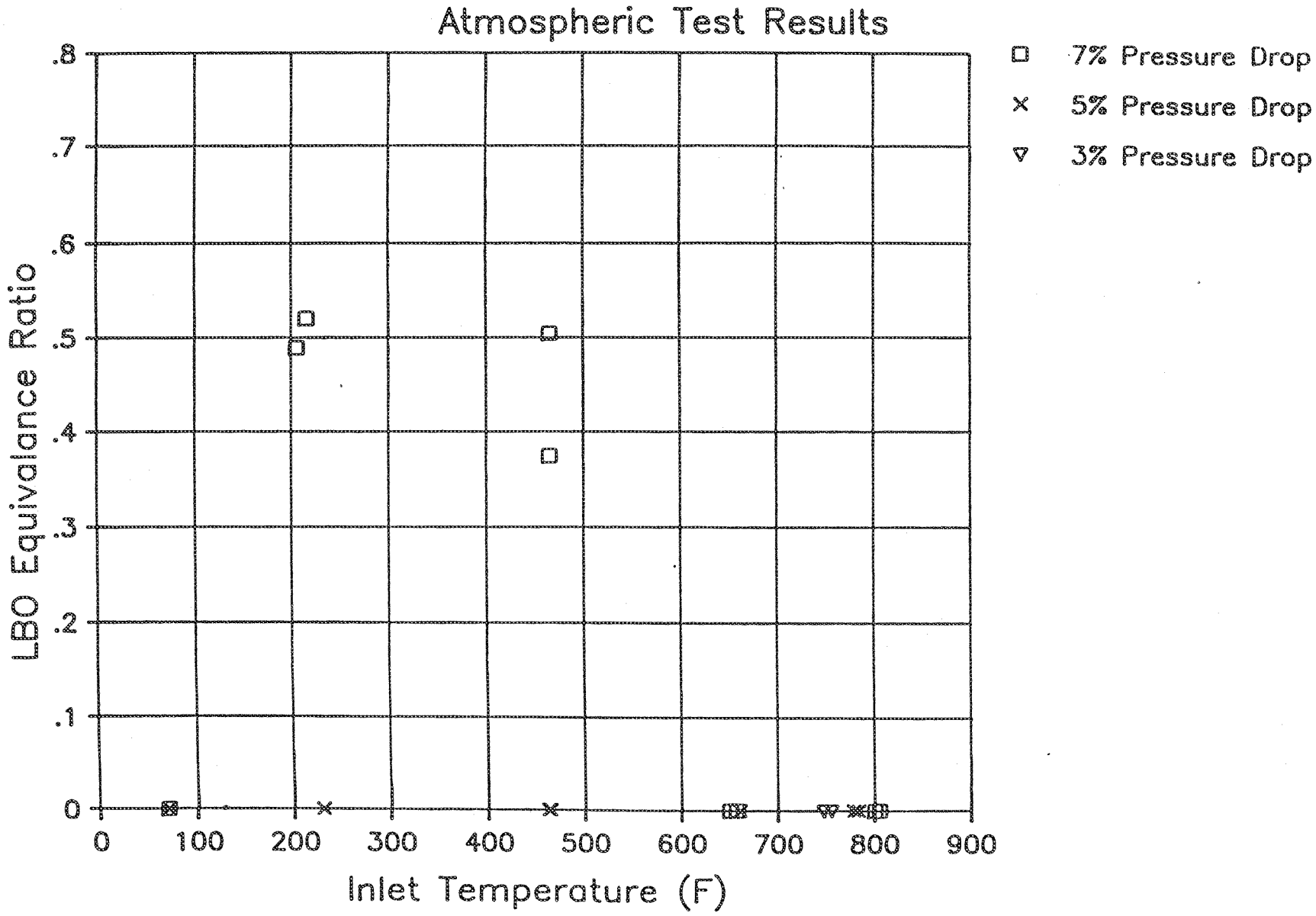

Figure 4-14. Jet Mix Configuration 1 Stability Limits.

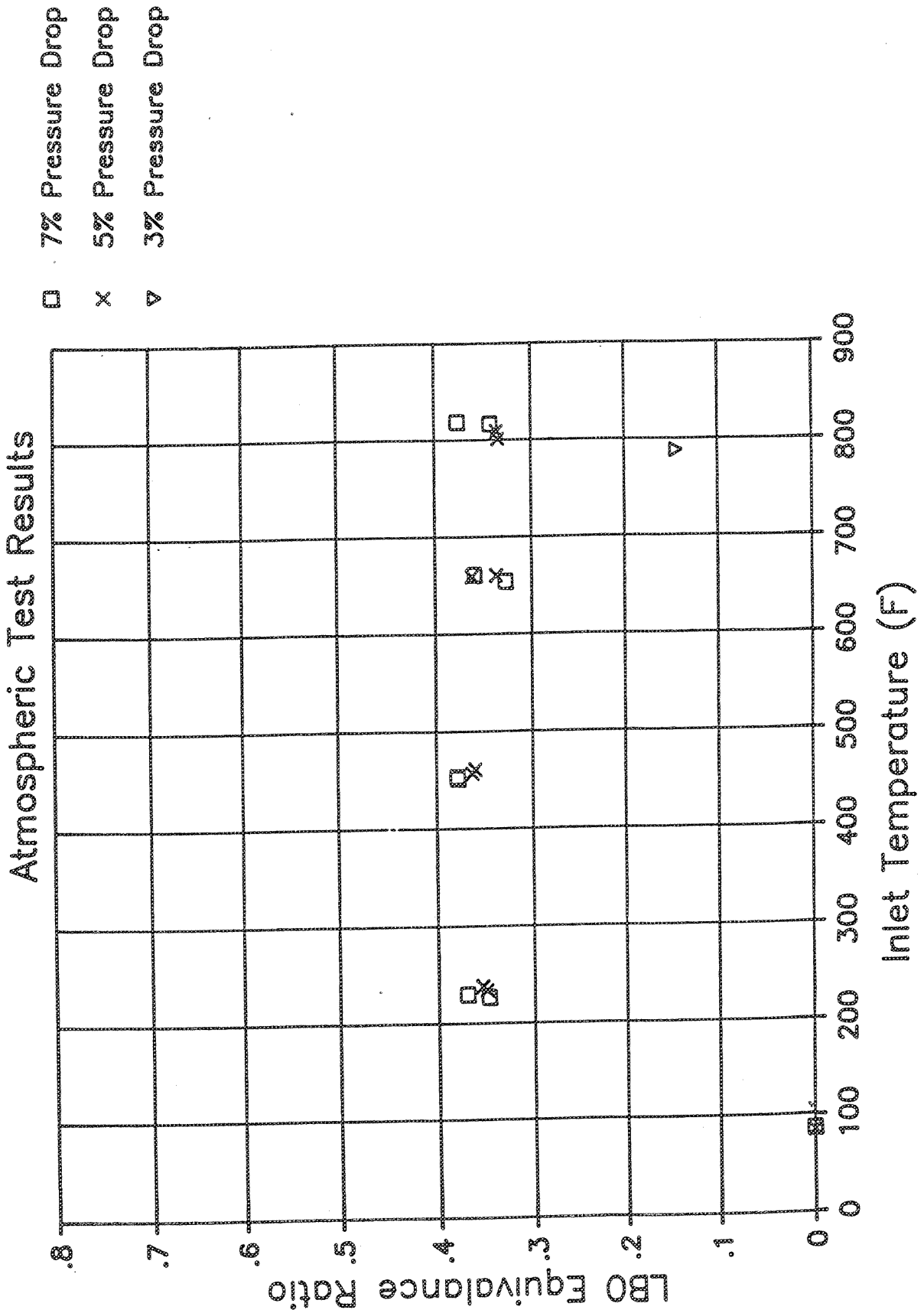

Figure 4-15. Jet Mix Configuration 2 Stability Limits.

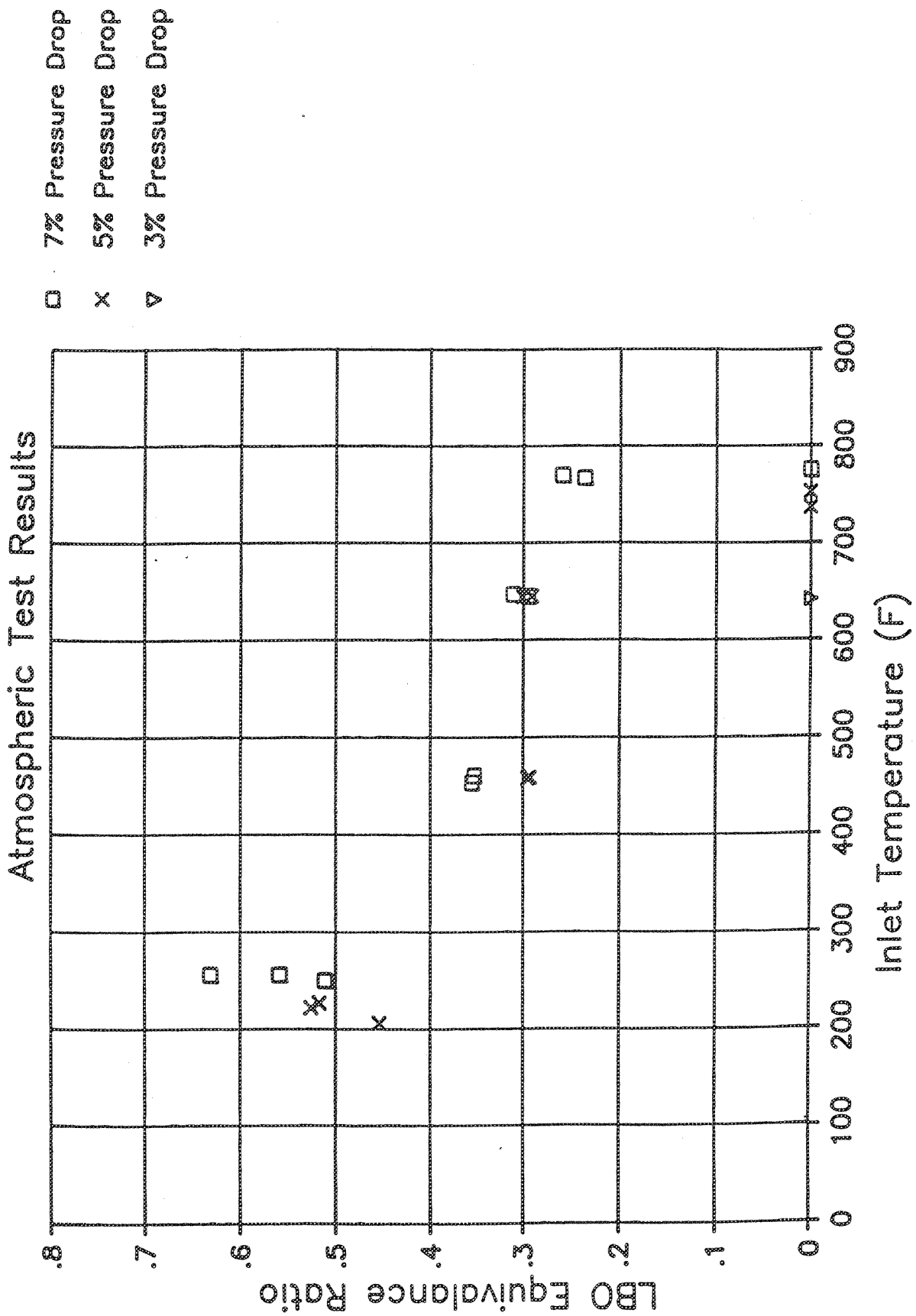

Figure 4-16. Jet Mix Configuration 3 Stability Limits.

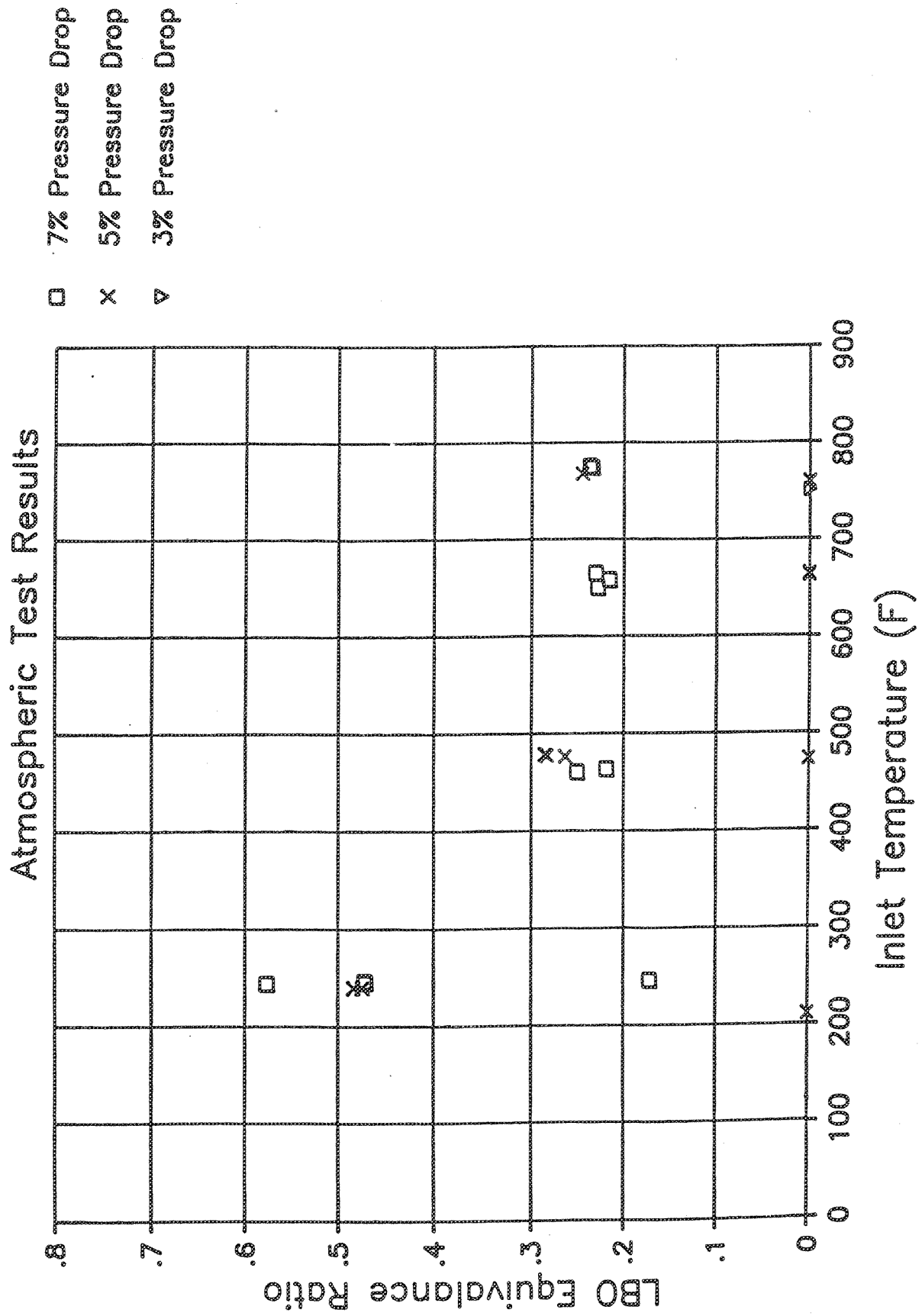

Figure 4-17. Jet Mix Configuration 4 Stability Limits.

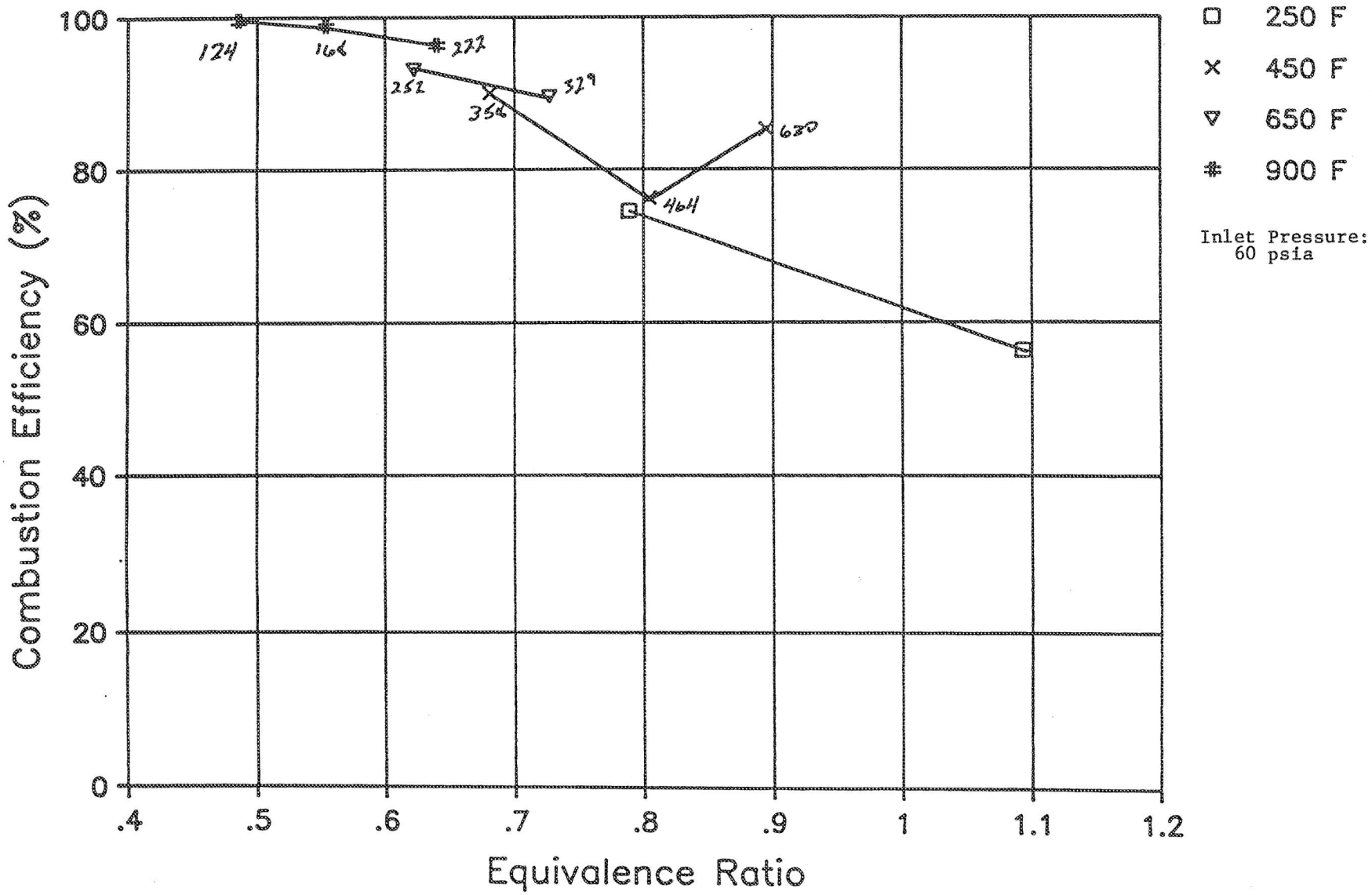

Figure 4-18. Jet Mix Configuration 1 Combustion Efficiency.

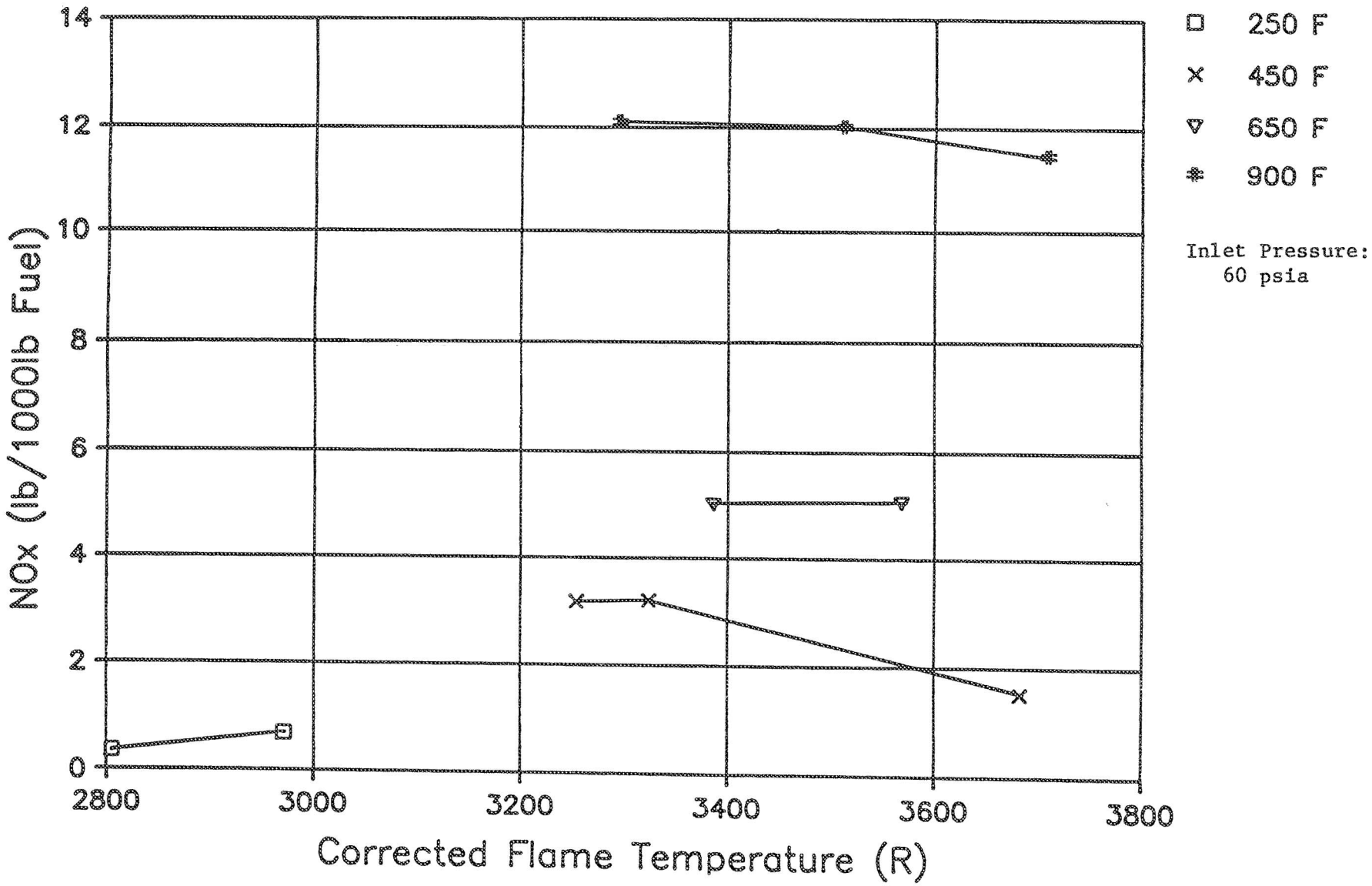

Figure 4-19. Jet Mix Configuration 1 NOx Emissions.

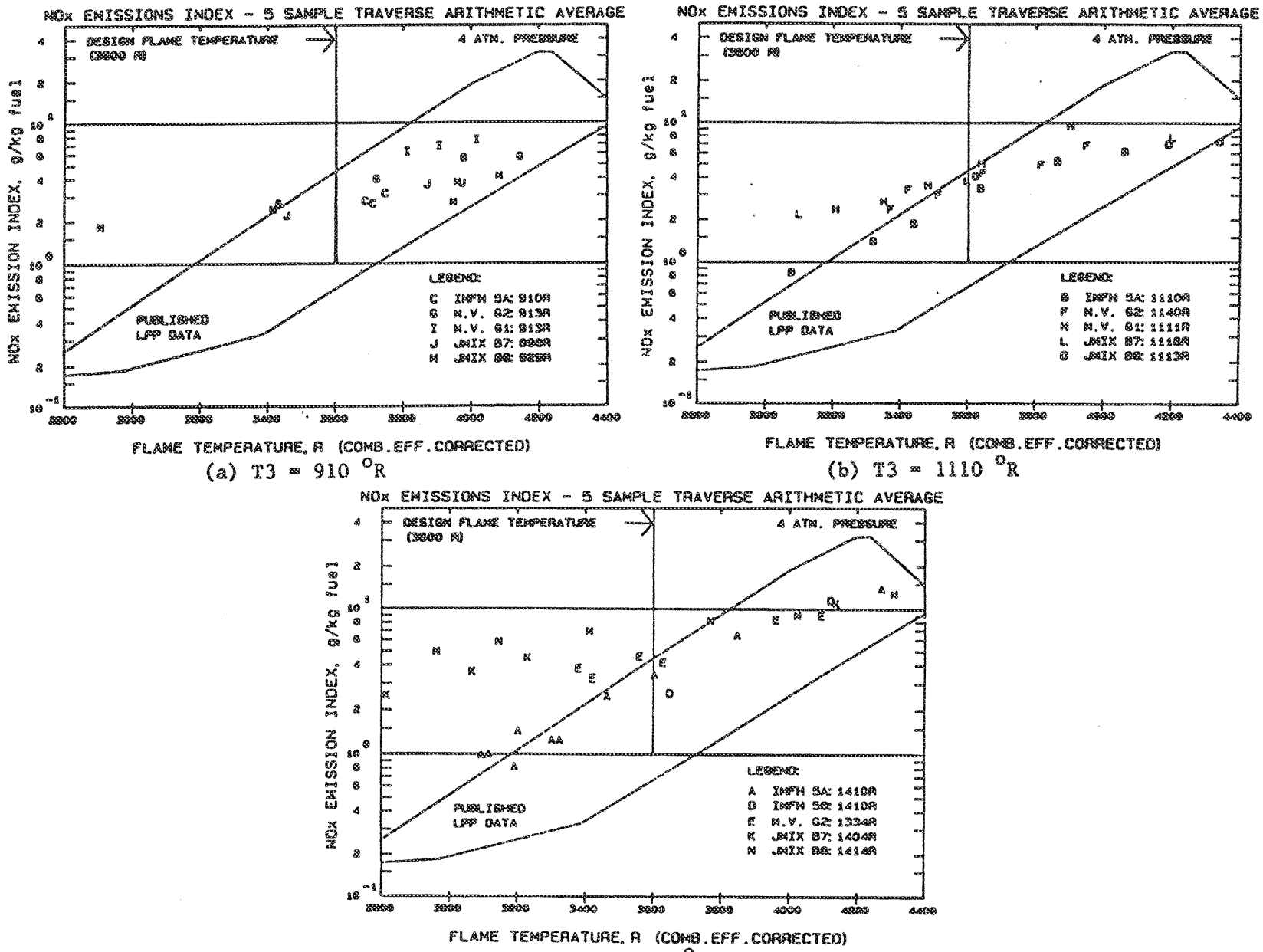

(a) T3 = 910 °R

(b) T3 = 1110 °R

(c) T3 = 1410 °R

Figure 4-20. Comparison of Jet-Mix NOx with the IMFH and Multi-Venturi.

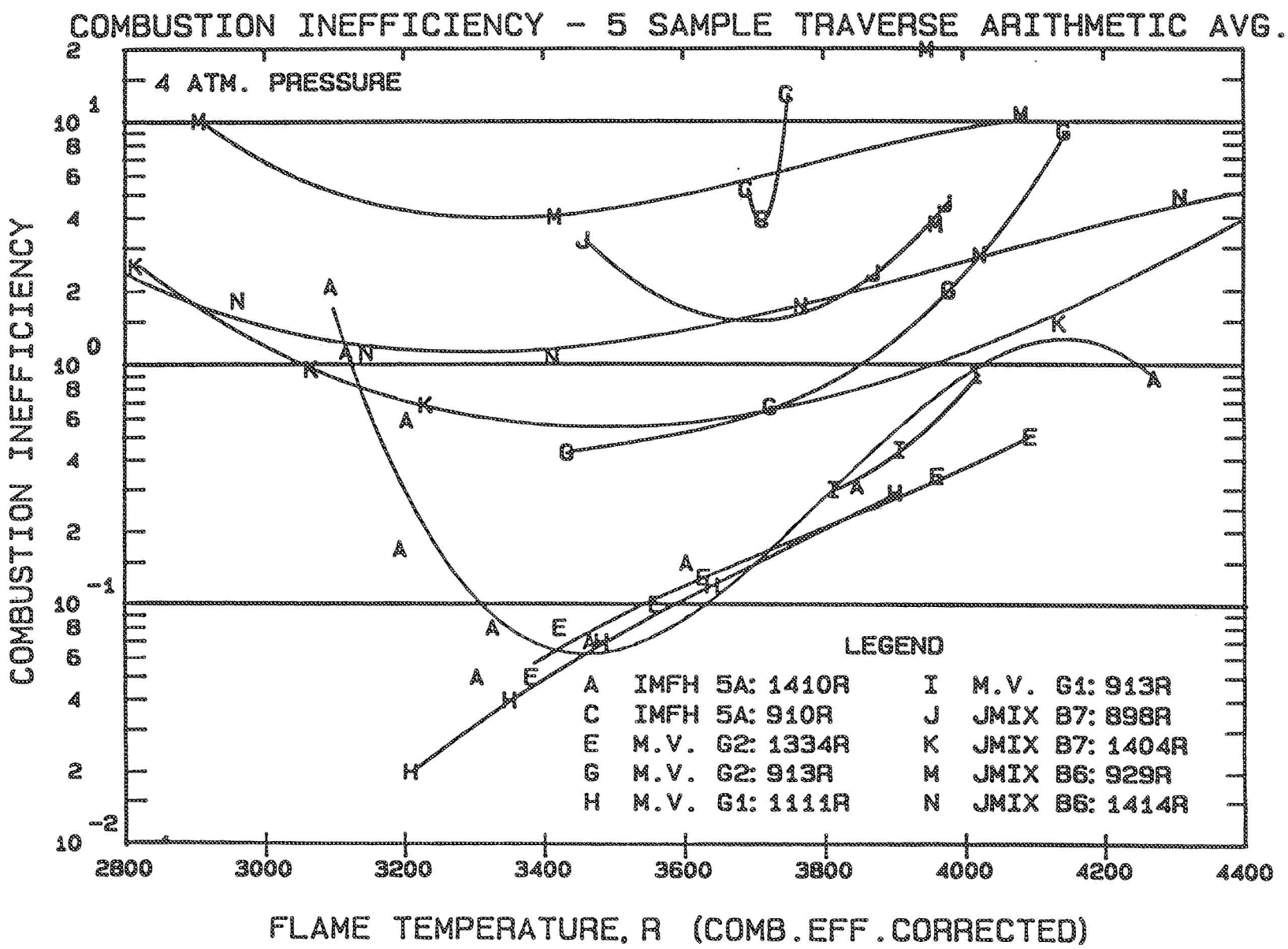

Figure 4-21. Comparison of Jet Mix Combustion Efficiency with the IMFH and Multi-Venturi.

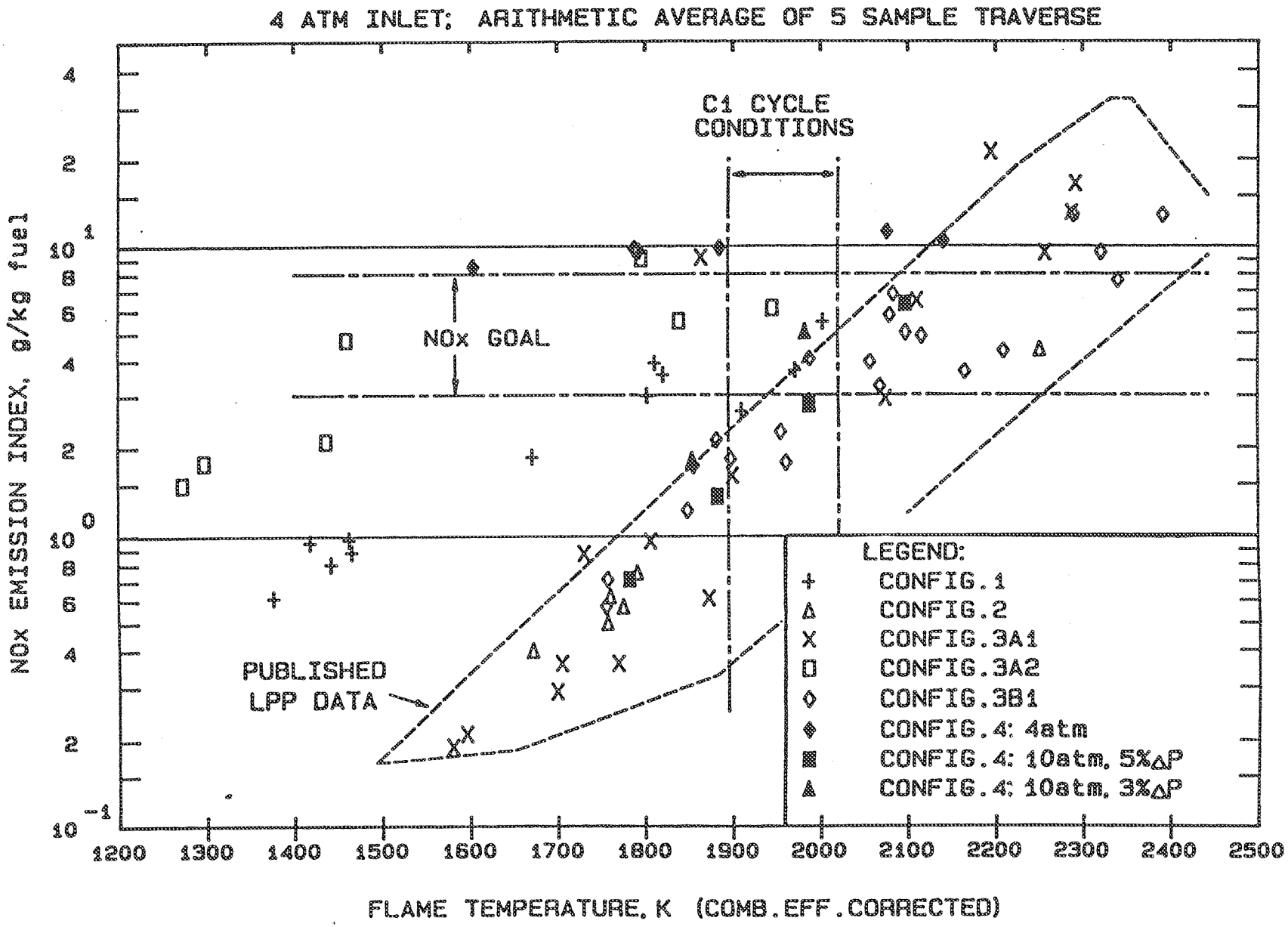

Figure 4-22. IMFH Configurations 1 - 4 NOx Emissions.

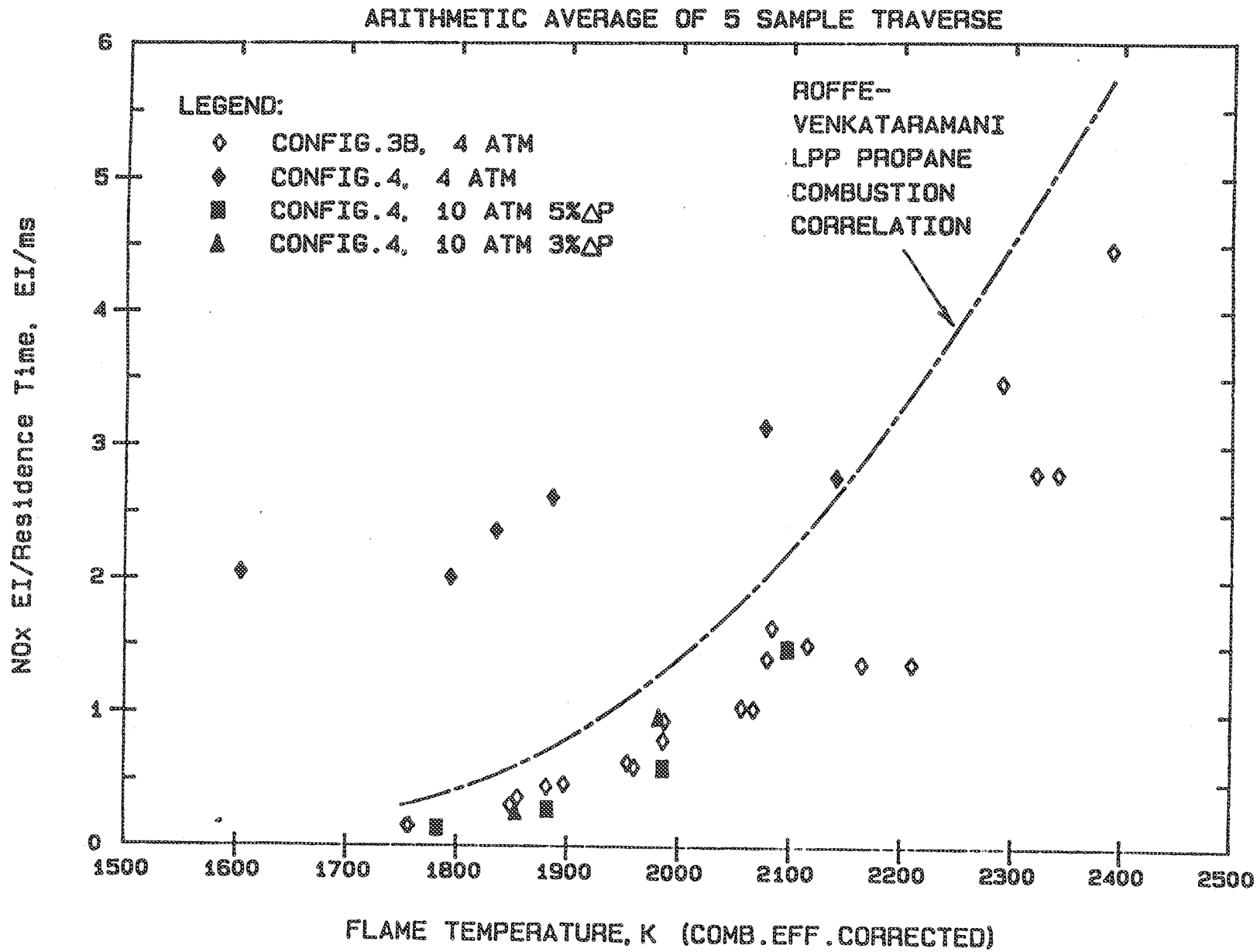

Figure 4-23. IMFH Configurations 3B and 4 NOx Emissions.

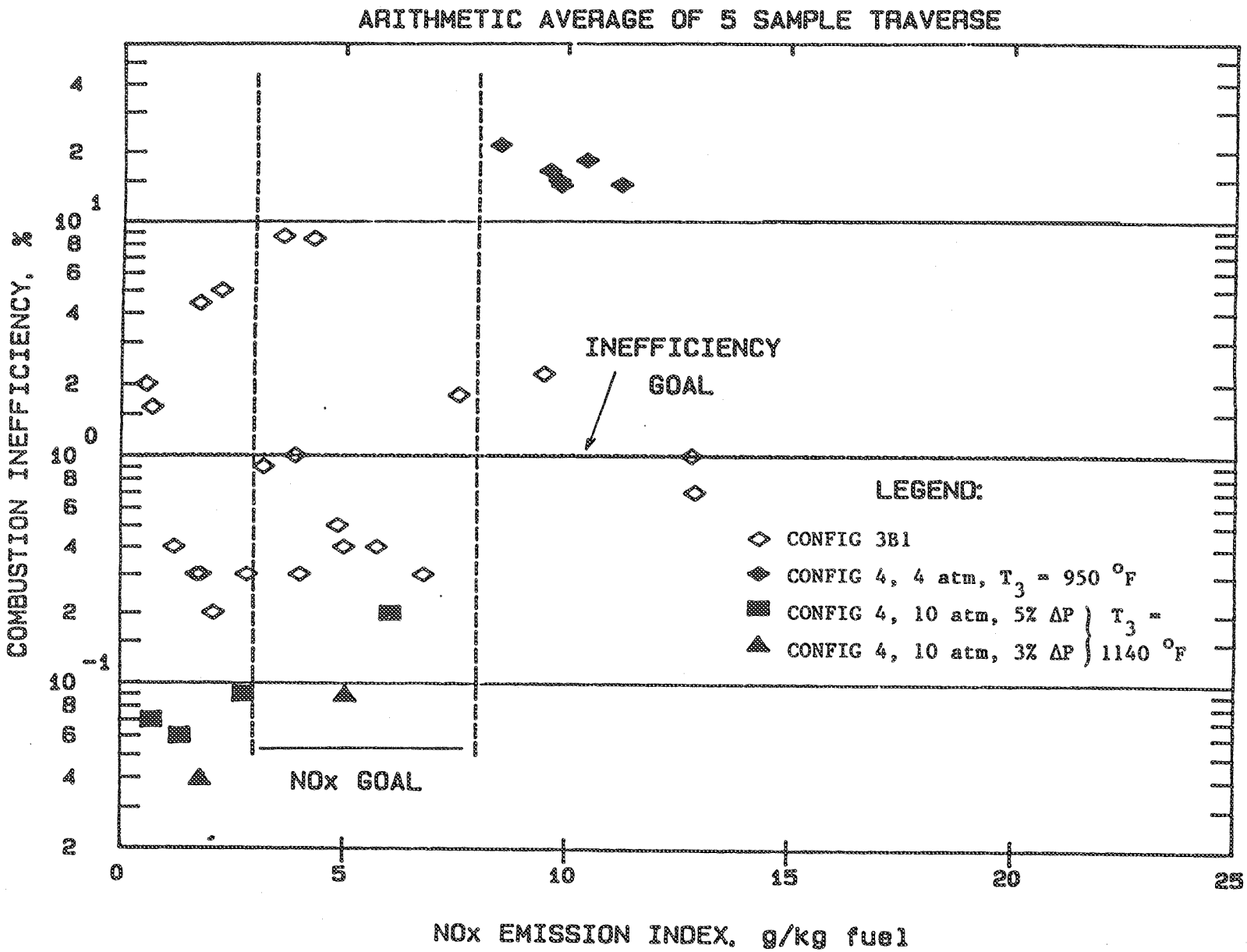

Figure 4-24. IMFH Configurations 3B and 4 Combustion Inefficiency as a Function of NOx EI.

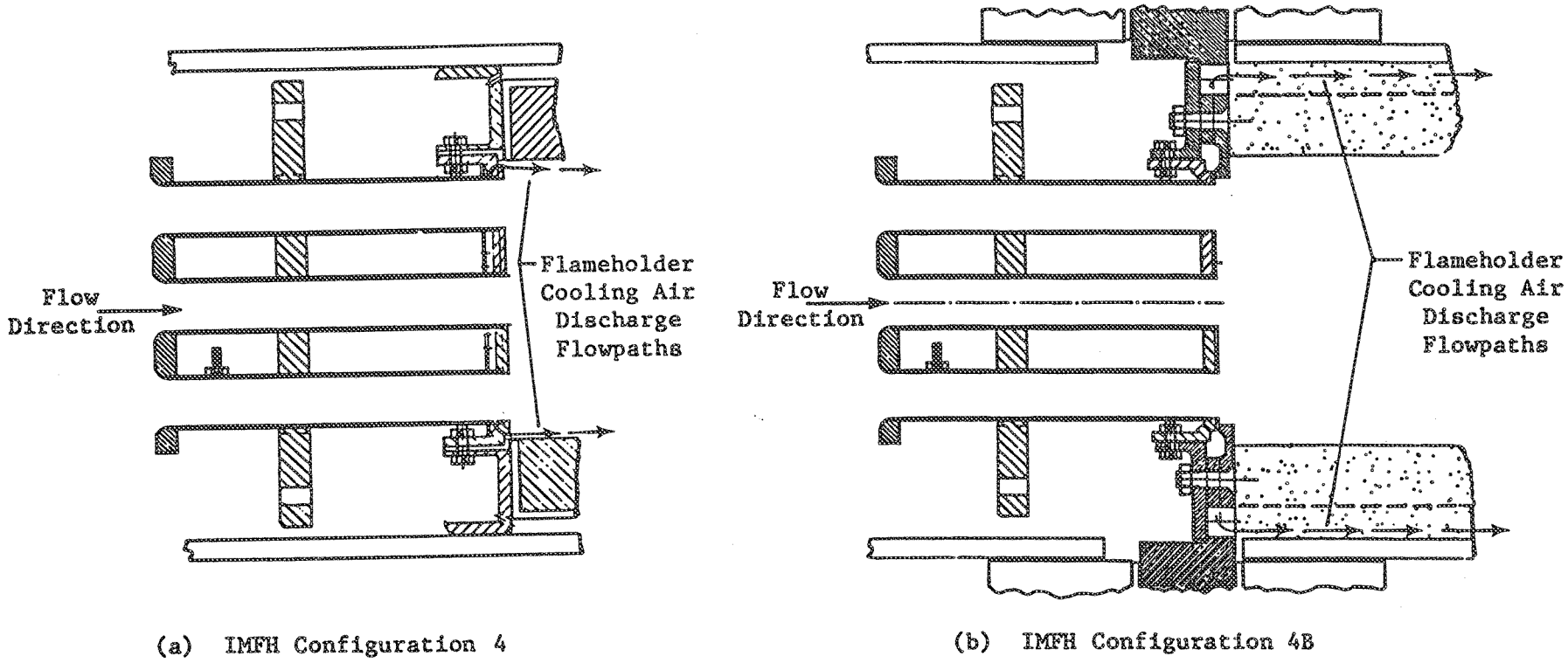

Figure 4-25. IMFH Configurations 4. and 4B Flameholder Cooling Air Discharge Schemes.

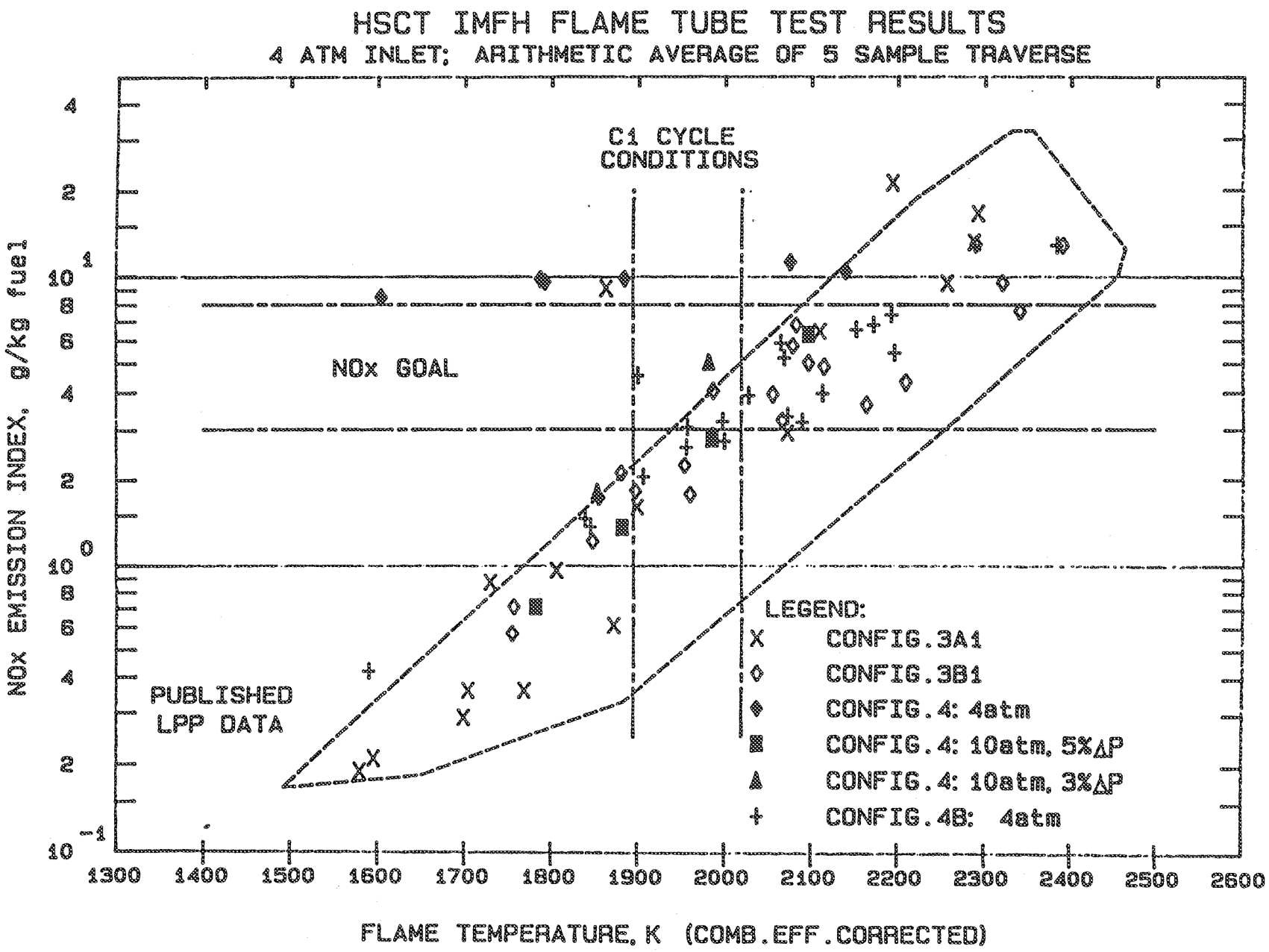

Figure 4-26. IMFH Configuration 4B Flame Tube NOx Emissions.

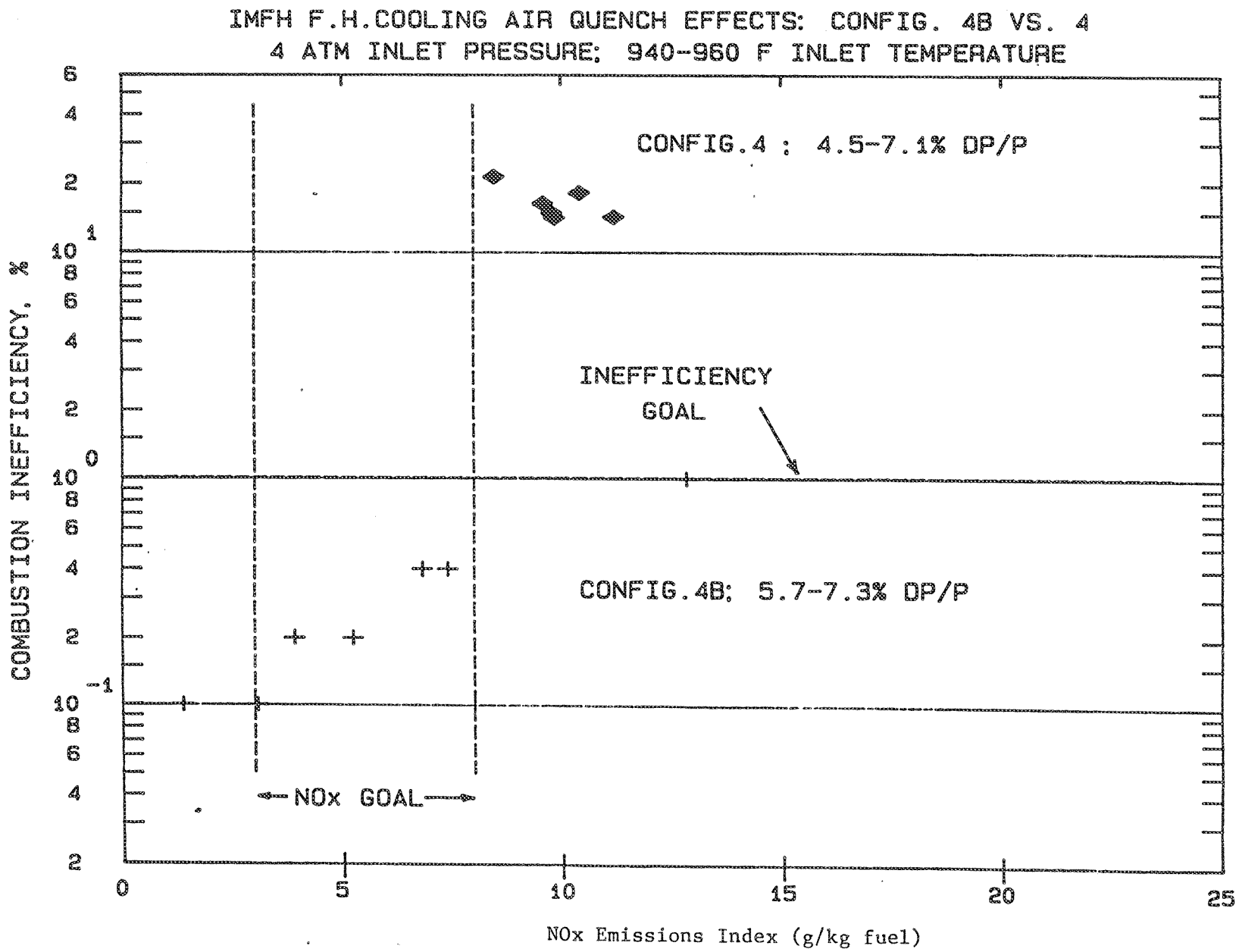

Figure 4-27. IMFH Flameholder Cooling Air Quench Effects.

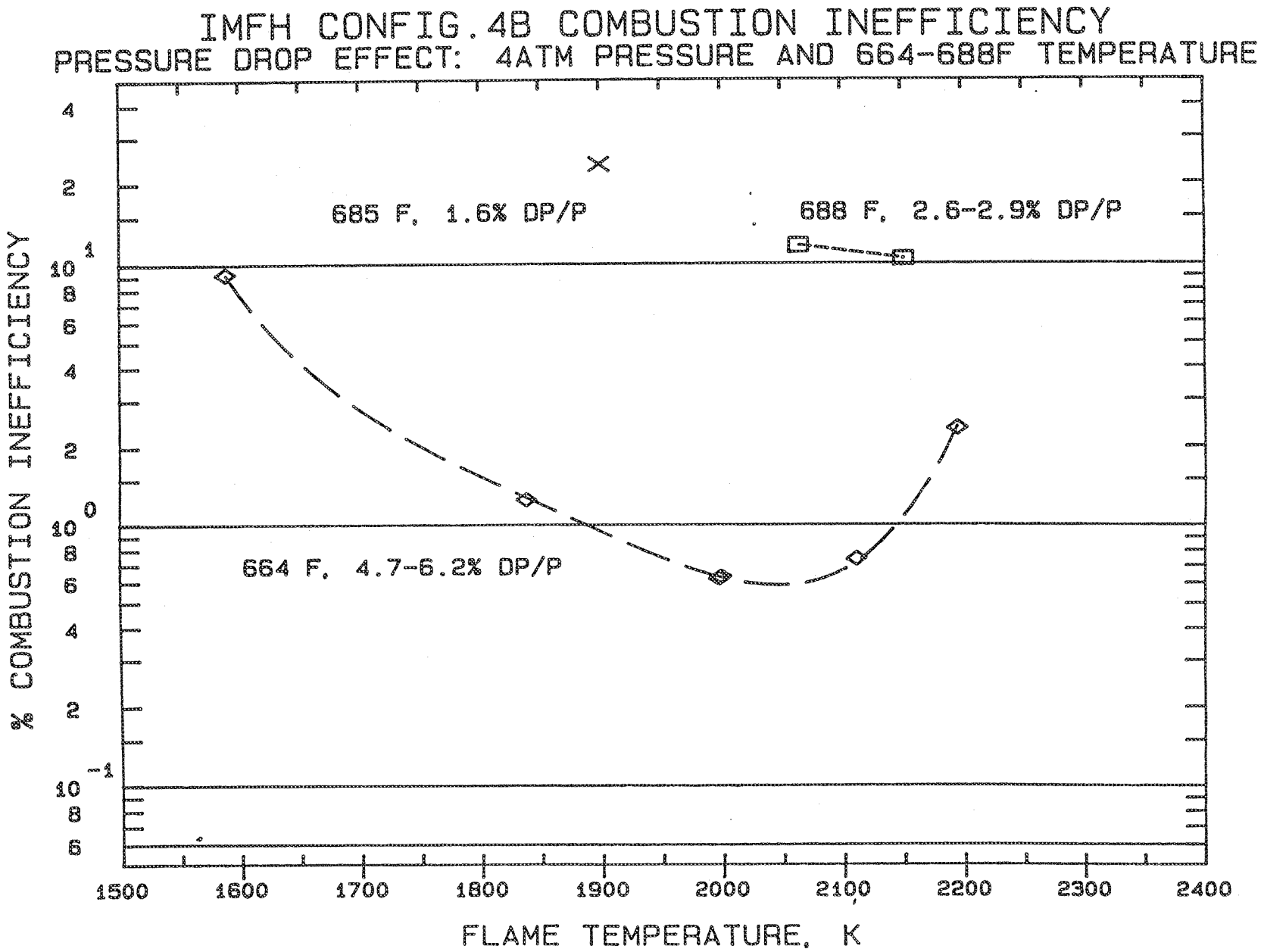

Figure 4-28. Pressure Drop Influence on IMFH Combustion Inefficiency.

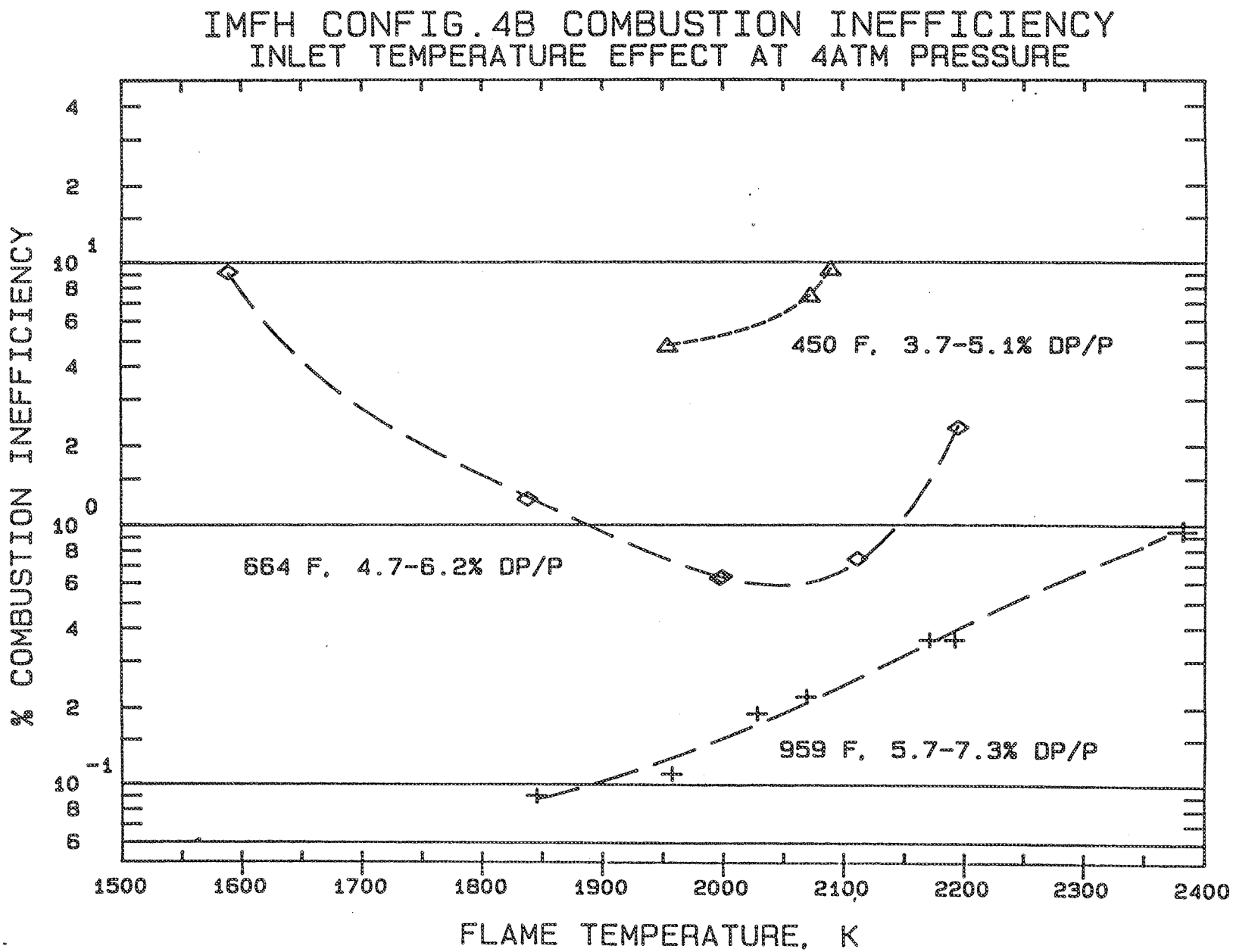

Figure 4-29. Inlet Temperature Effect on IMFH Combustion Inefficiency.

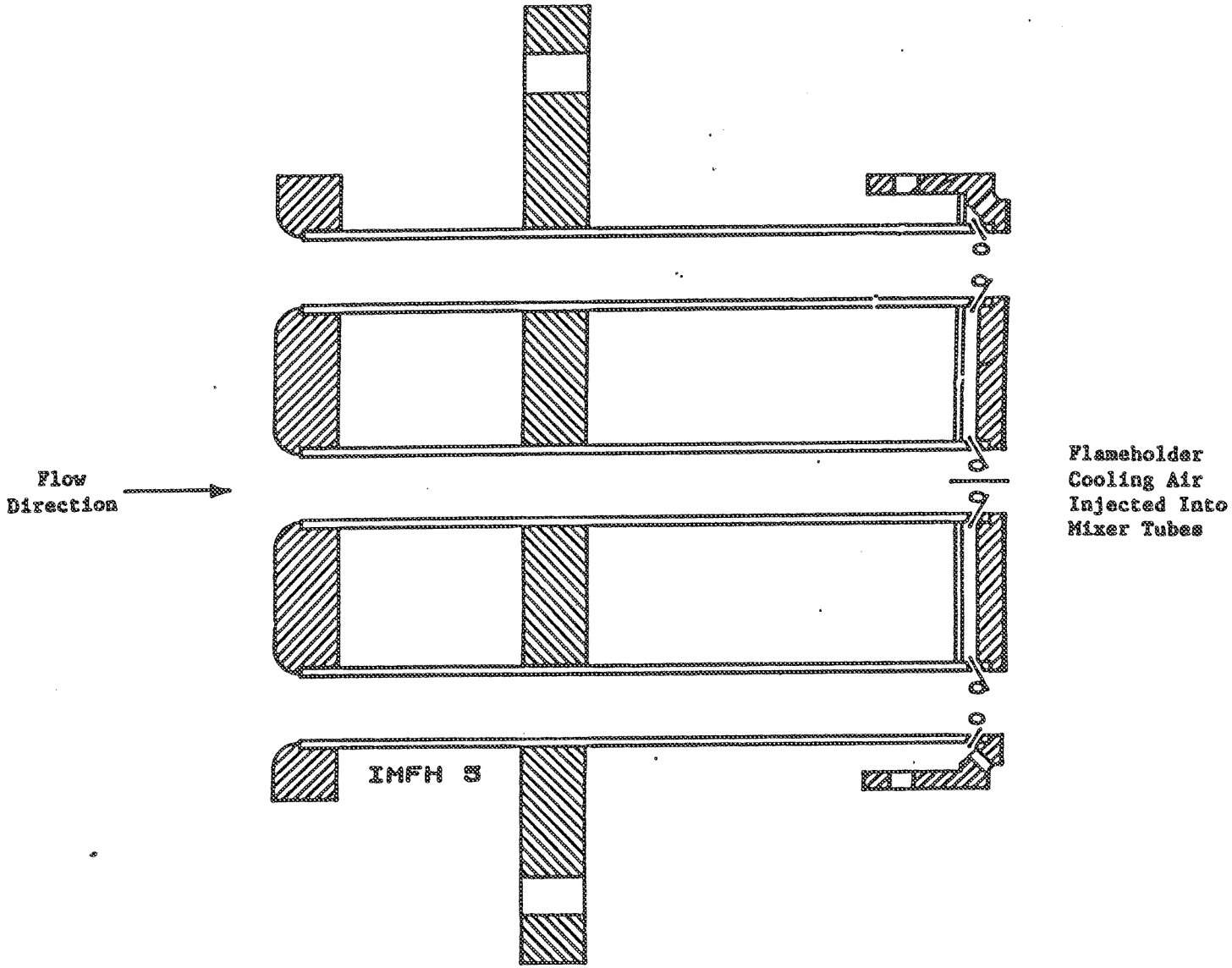

Figure 4-30. IMFH Configuration 5 Flame Holder Cooling Air Injection Scheme.

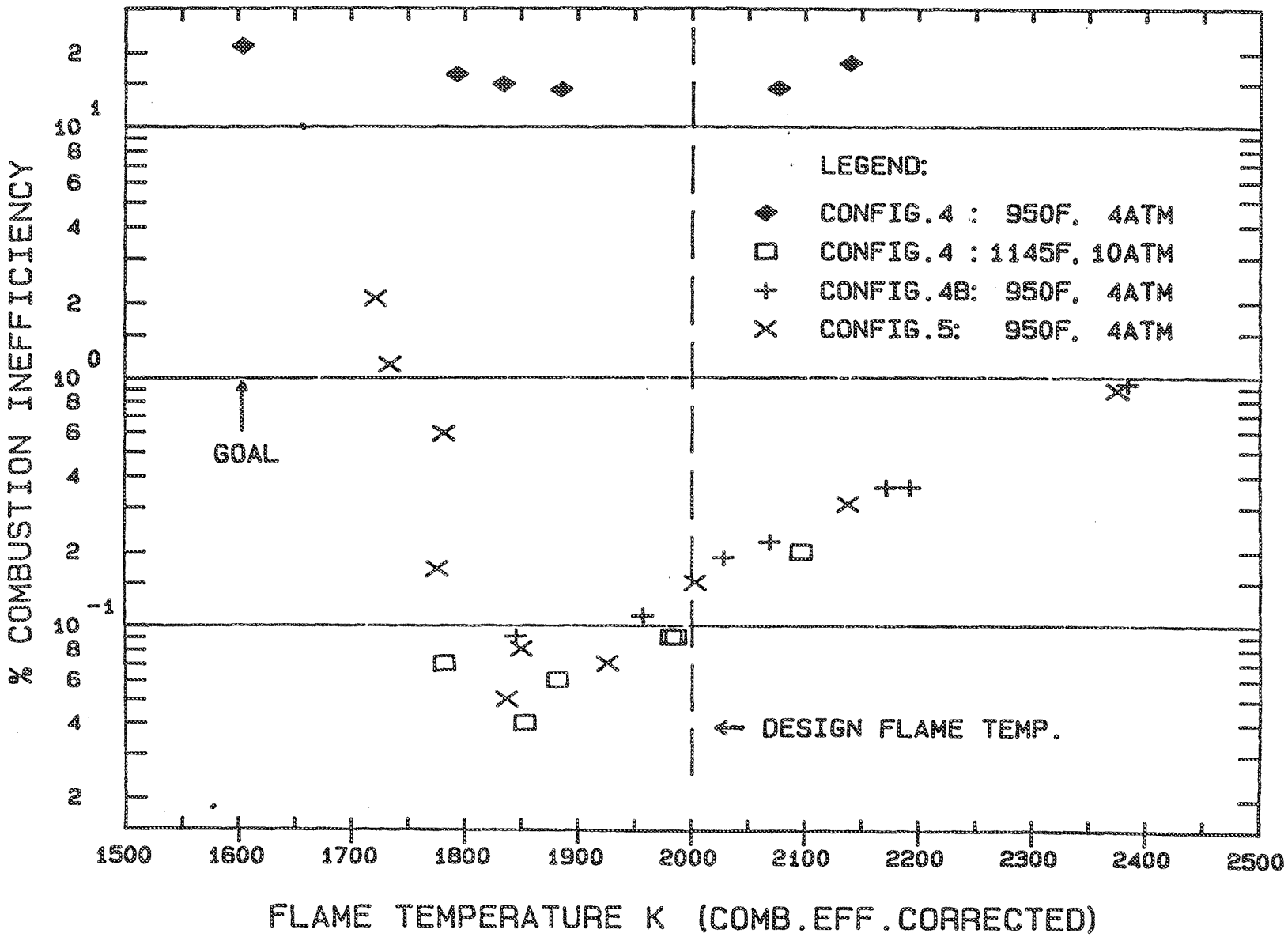

Figure 4-31. IMFH Configurations 4, 4B and 5 Combustion Inefficiency.

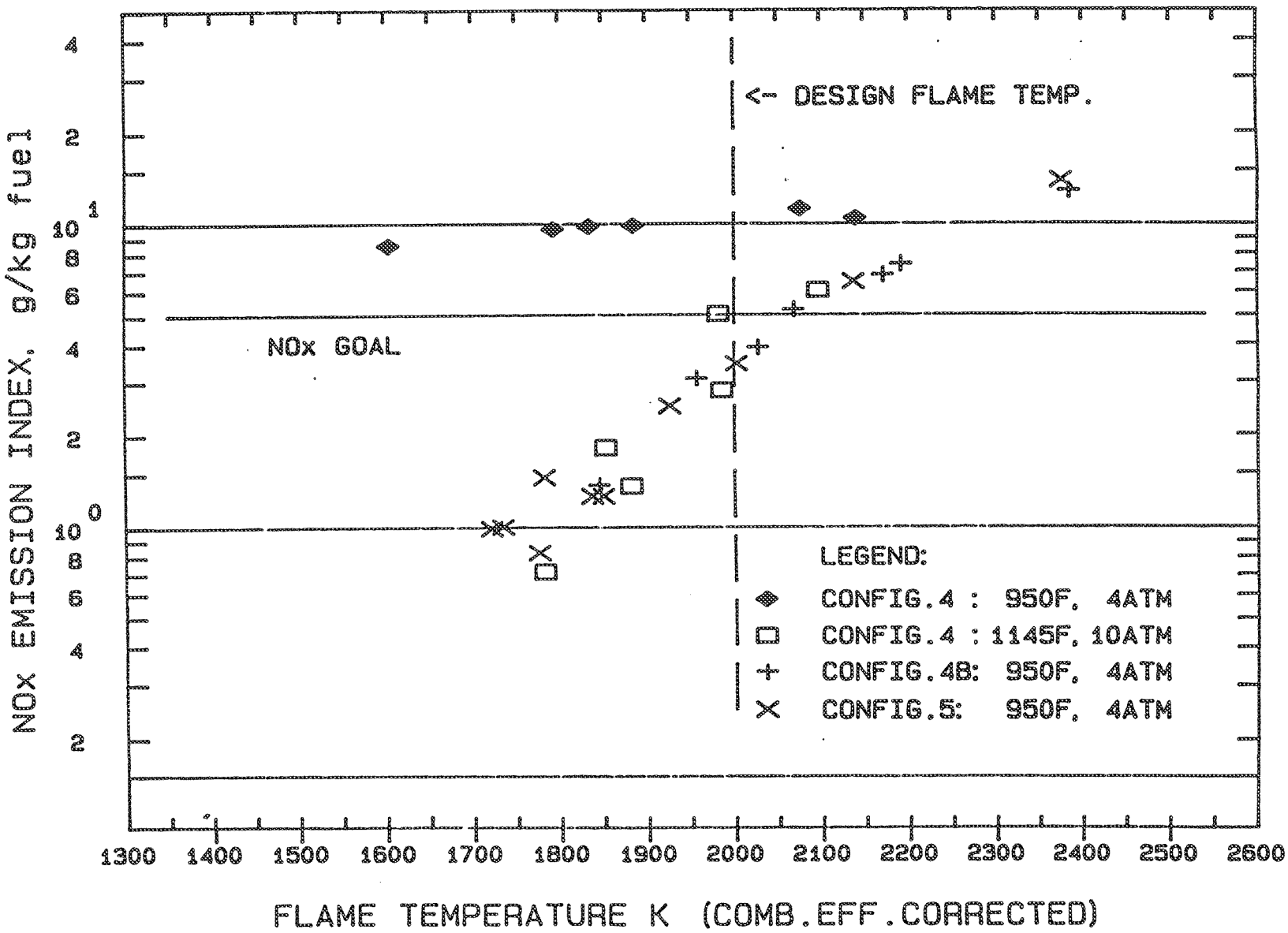

Figure 4-32. IMFH Configurations 4, 4B and 5 NOx Emissions.

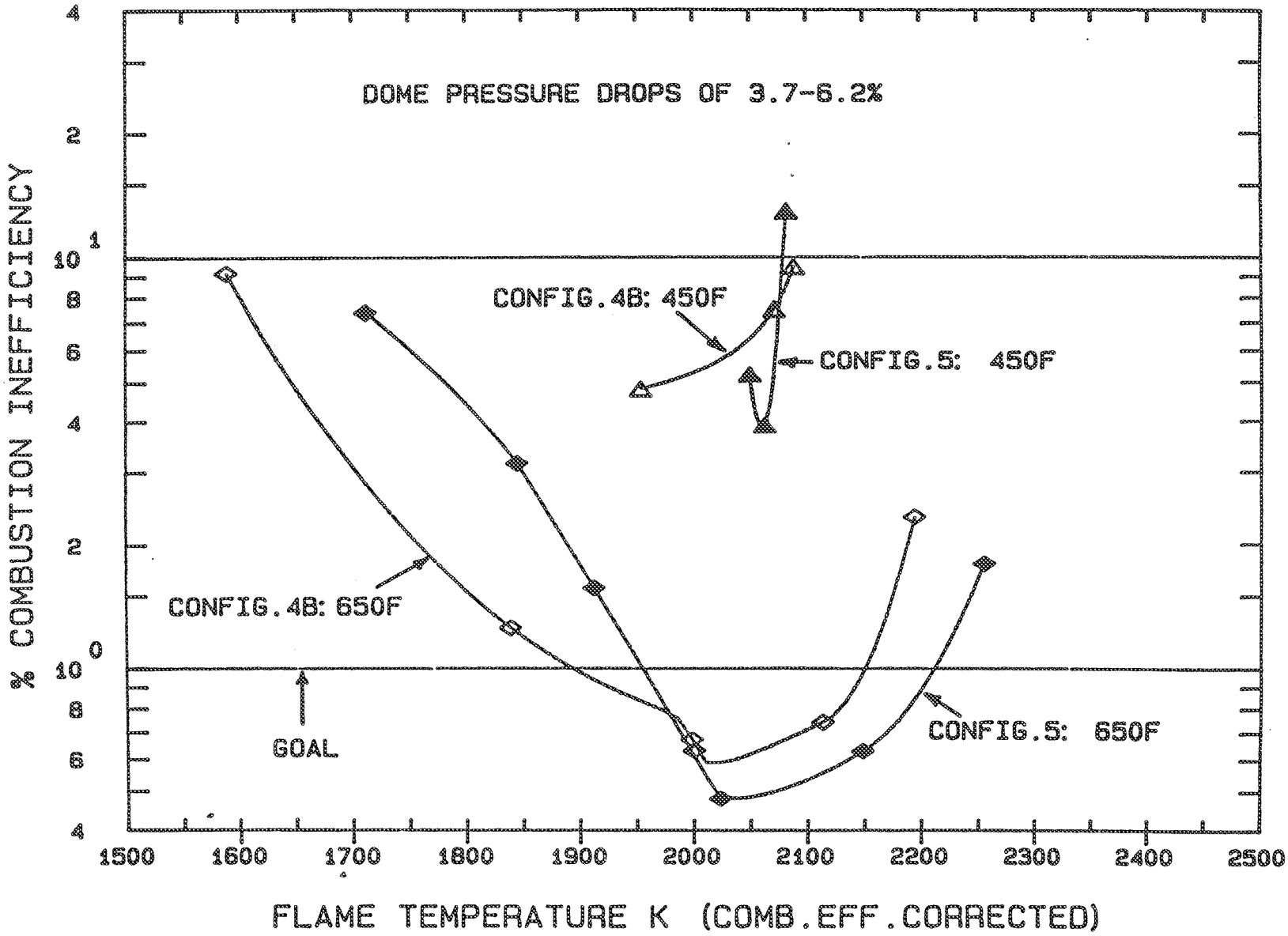

Figure 4-33. IMFH Configurations 4B and 5 Combustion Inefficiency.

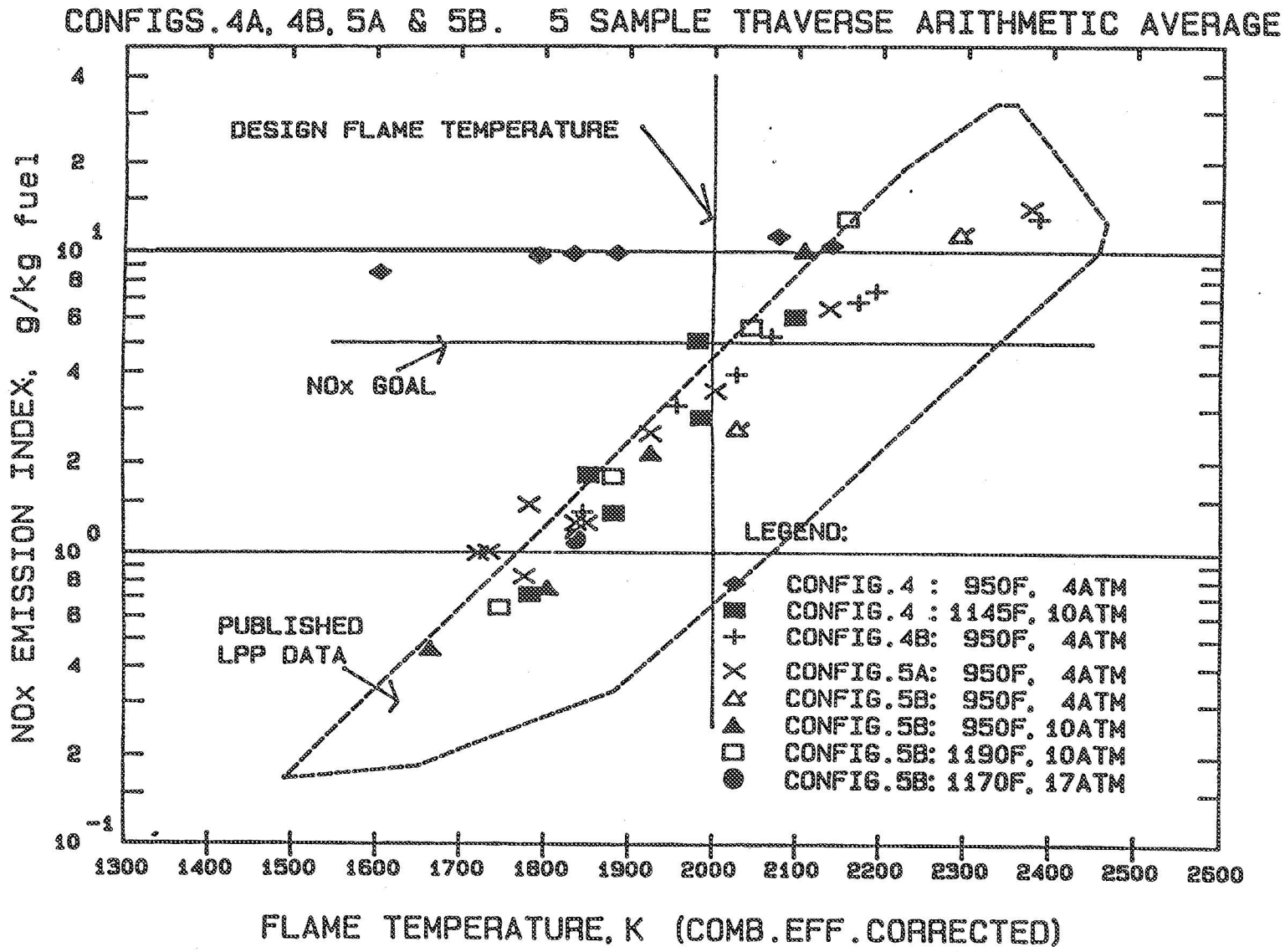

Figure 4-34. IMFH Configurations 4, 4B, 5A and 5B NOx Emissions Results.

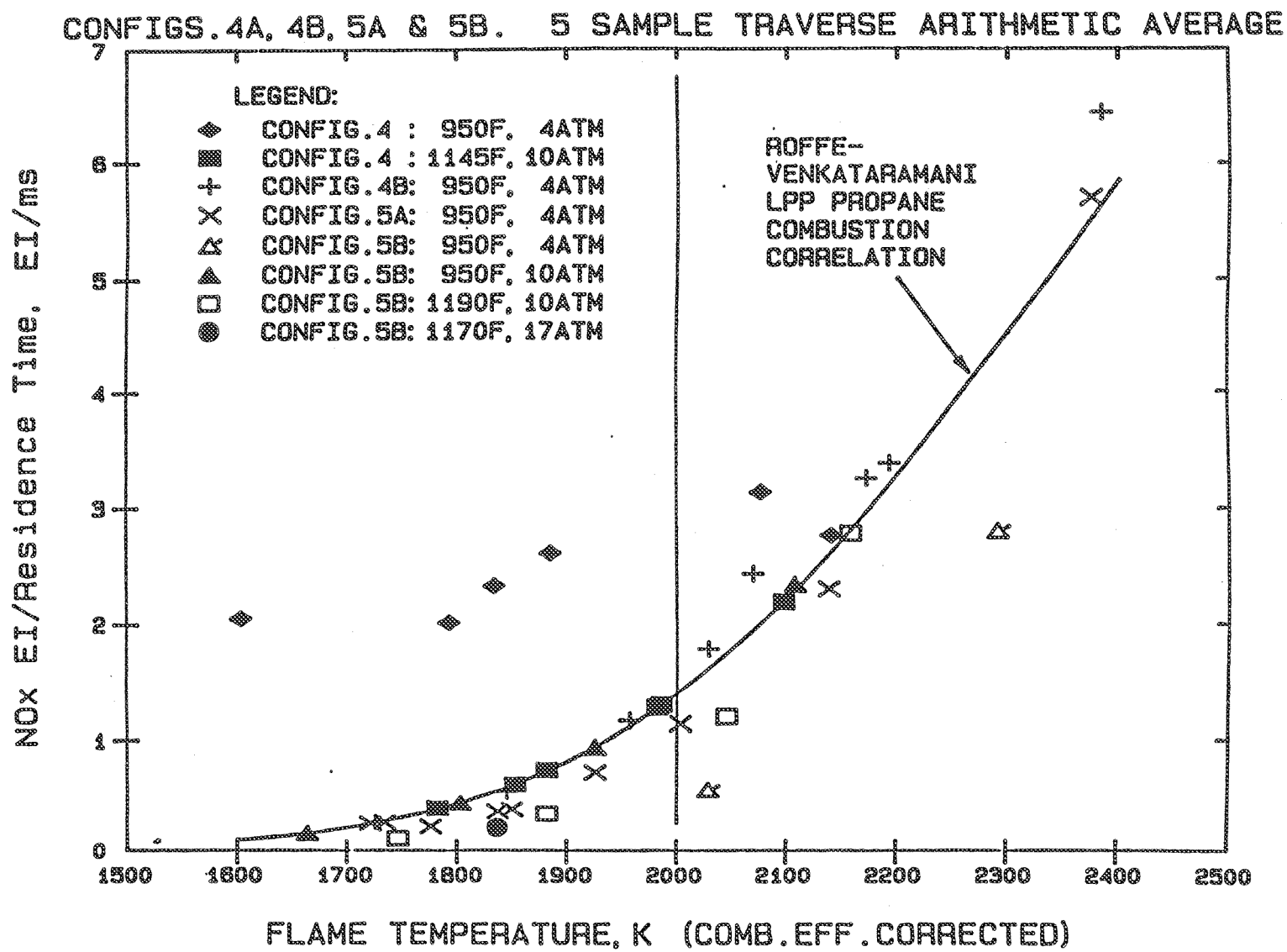

Figure 4-35. IMFH Configurations 4, 4B, 5A, and 5B NOx Emissions per Millisecond Combustor Residence Time.

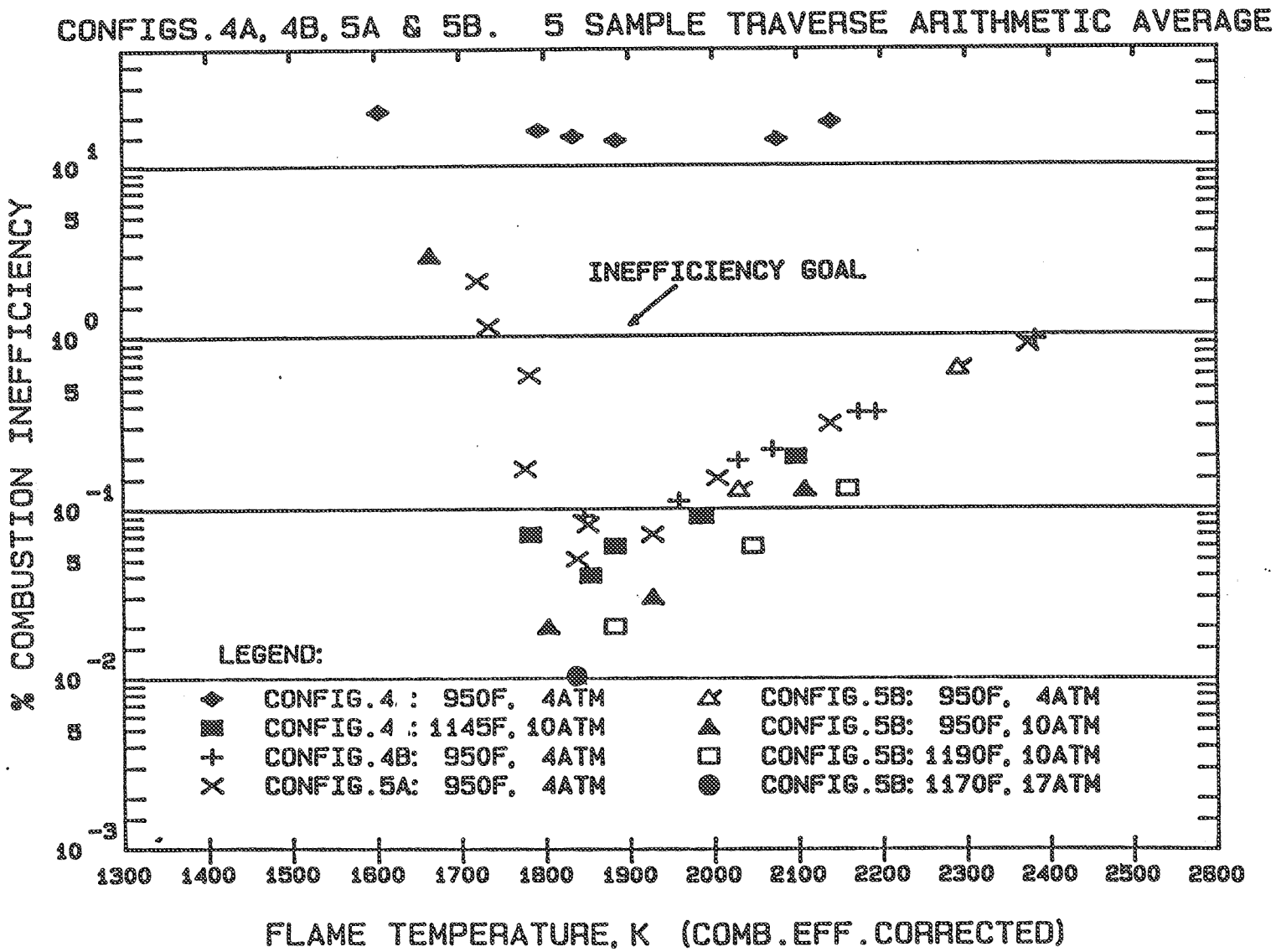

Figure 4-36. IMFH Configurations 4, 4B, 5A, and 5B Combustion Inefficiency.

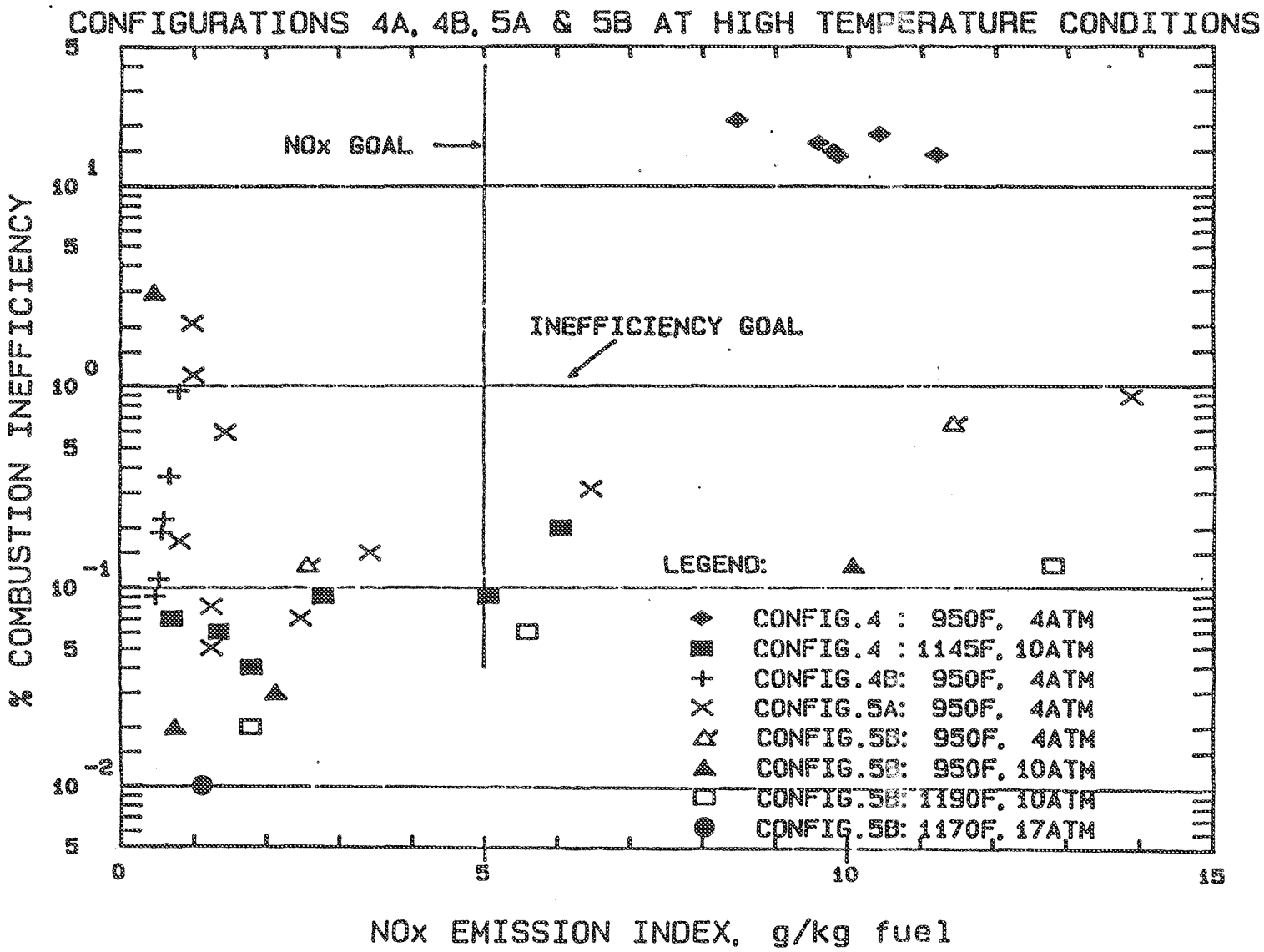

Figure 4-37. IMFH Configurations 4, 4B, 5A, and 5B Combustion Inefficiency versus NOx Emissions.

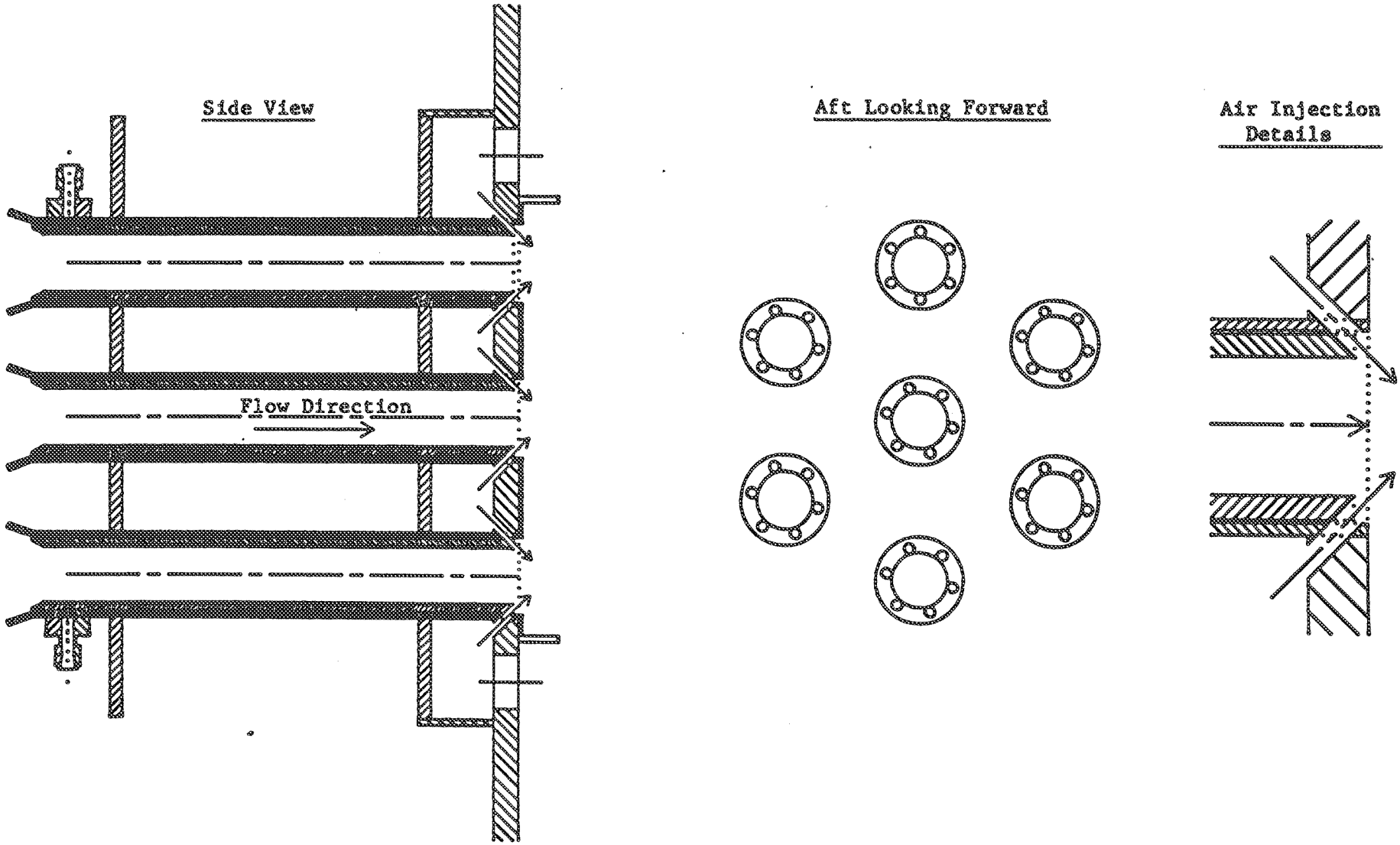

Figure 4-38. IMFH Configuration 6 Flameholder Cooling Air Injection Scheme.

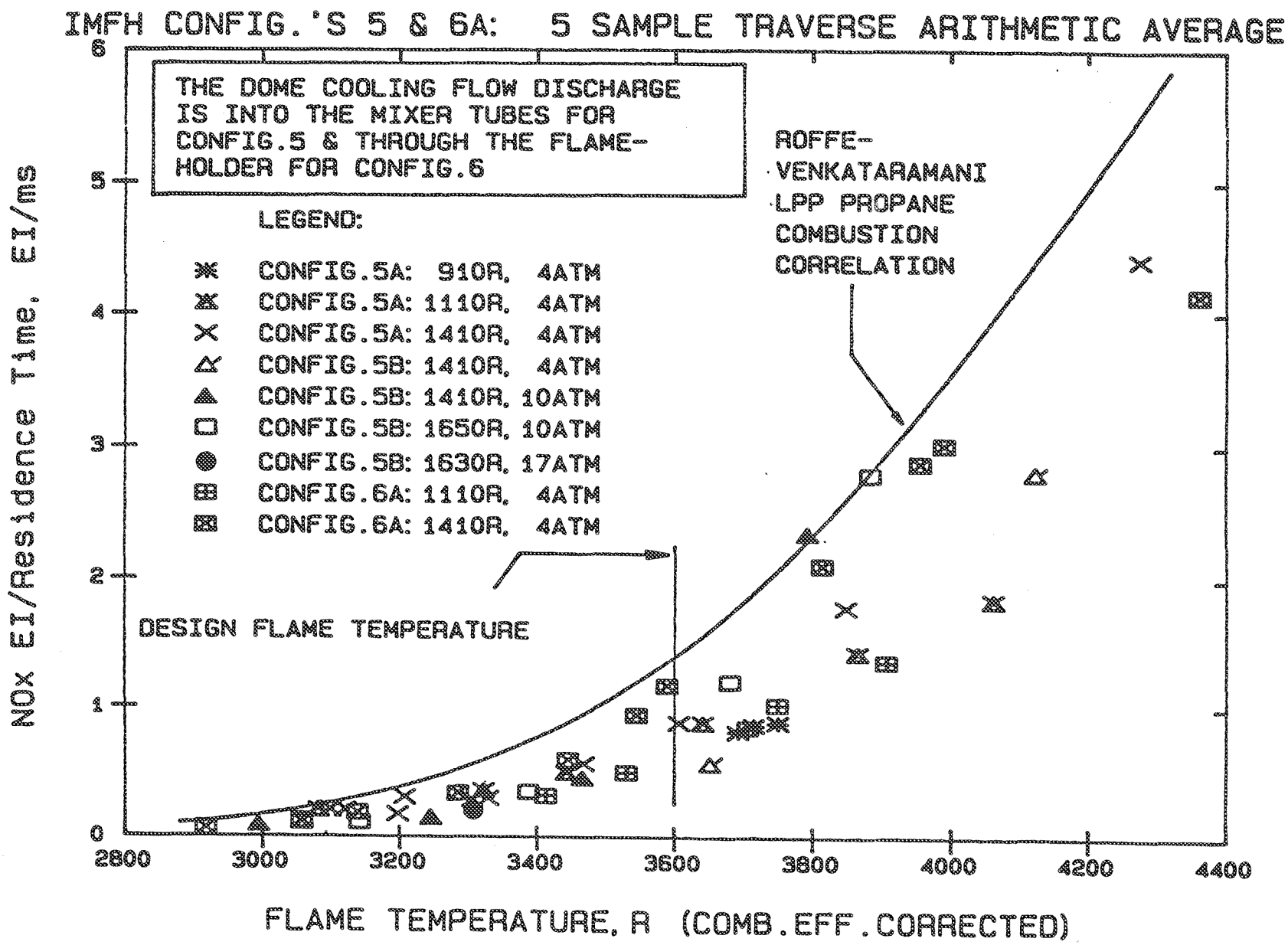

Figure 4-39. Dome Cooling Flow Impact on IMFH Configurations 5A, 5B, and 6A NOx Emissions.

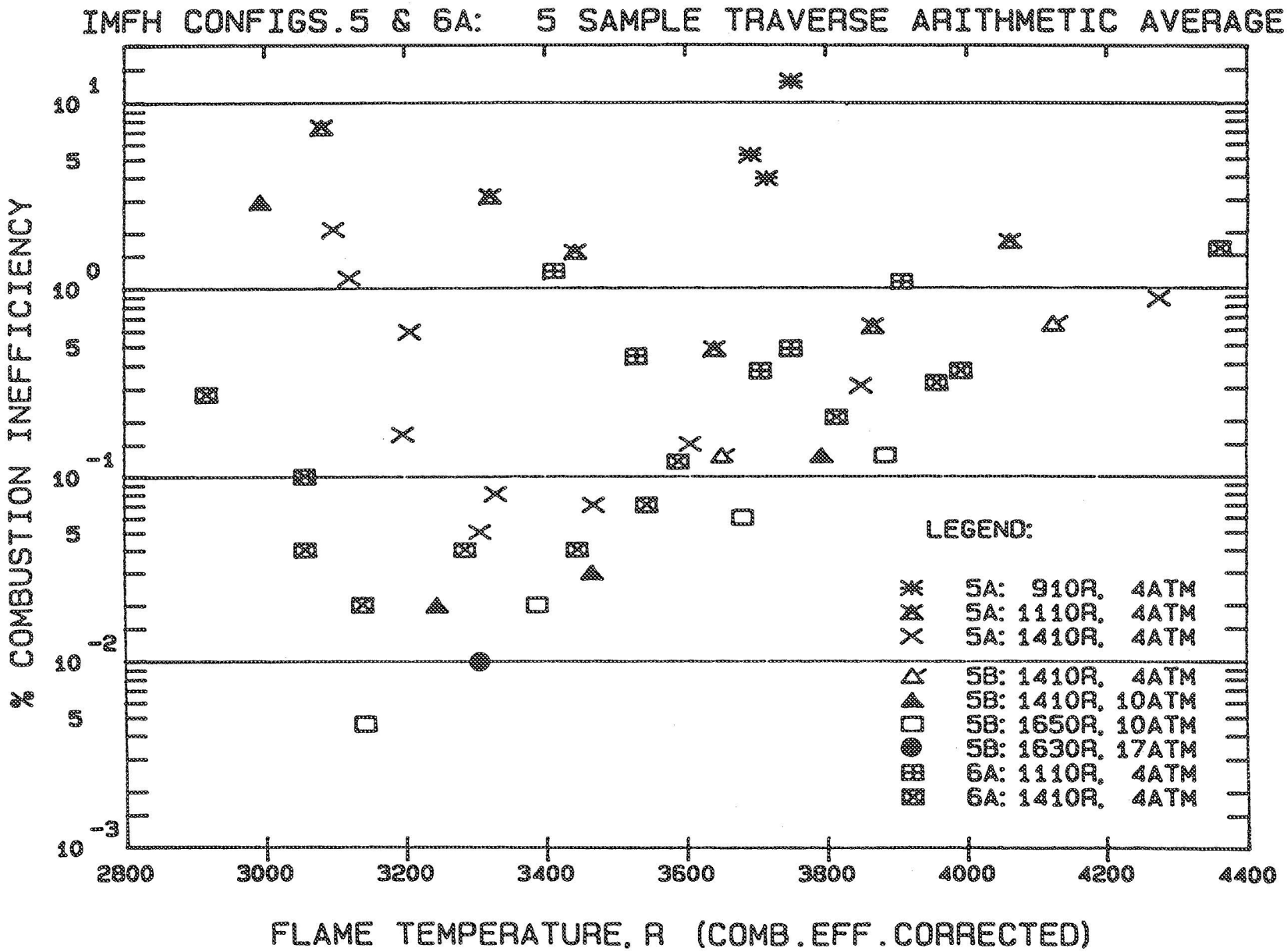

Figure 4-40. Dome Cooling Flow Impact on IMFH Configurations 5A, 5B, and 6A Combustion Inefficiency.

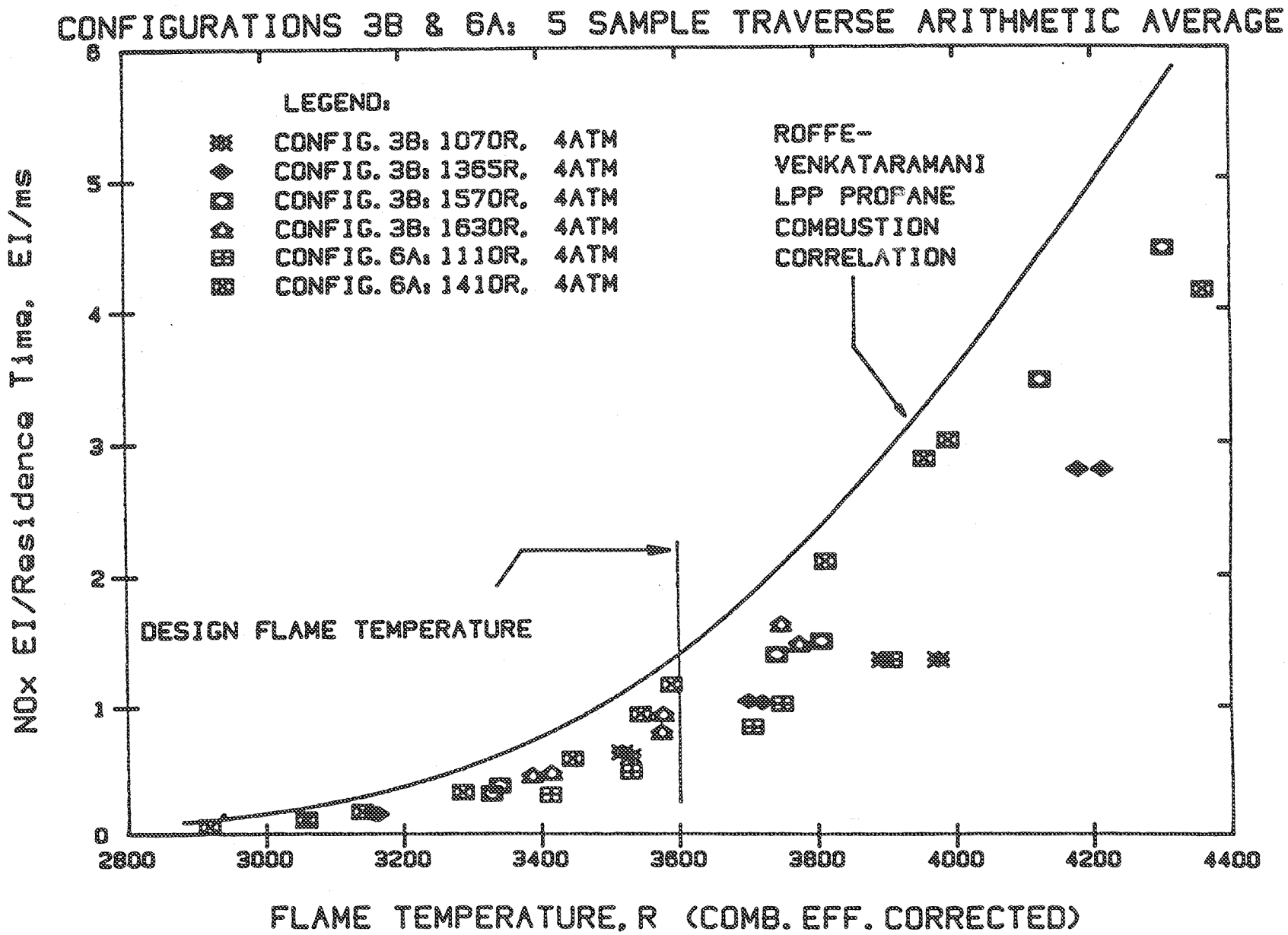

Figure 4-41. Dome Cooling Flow Flameholder Discharge Impact on IMFH Configurations 3B and 6A NOx Emissions.

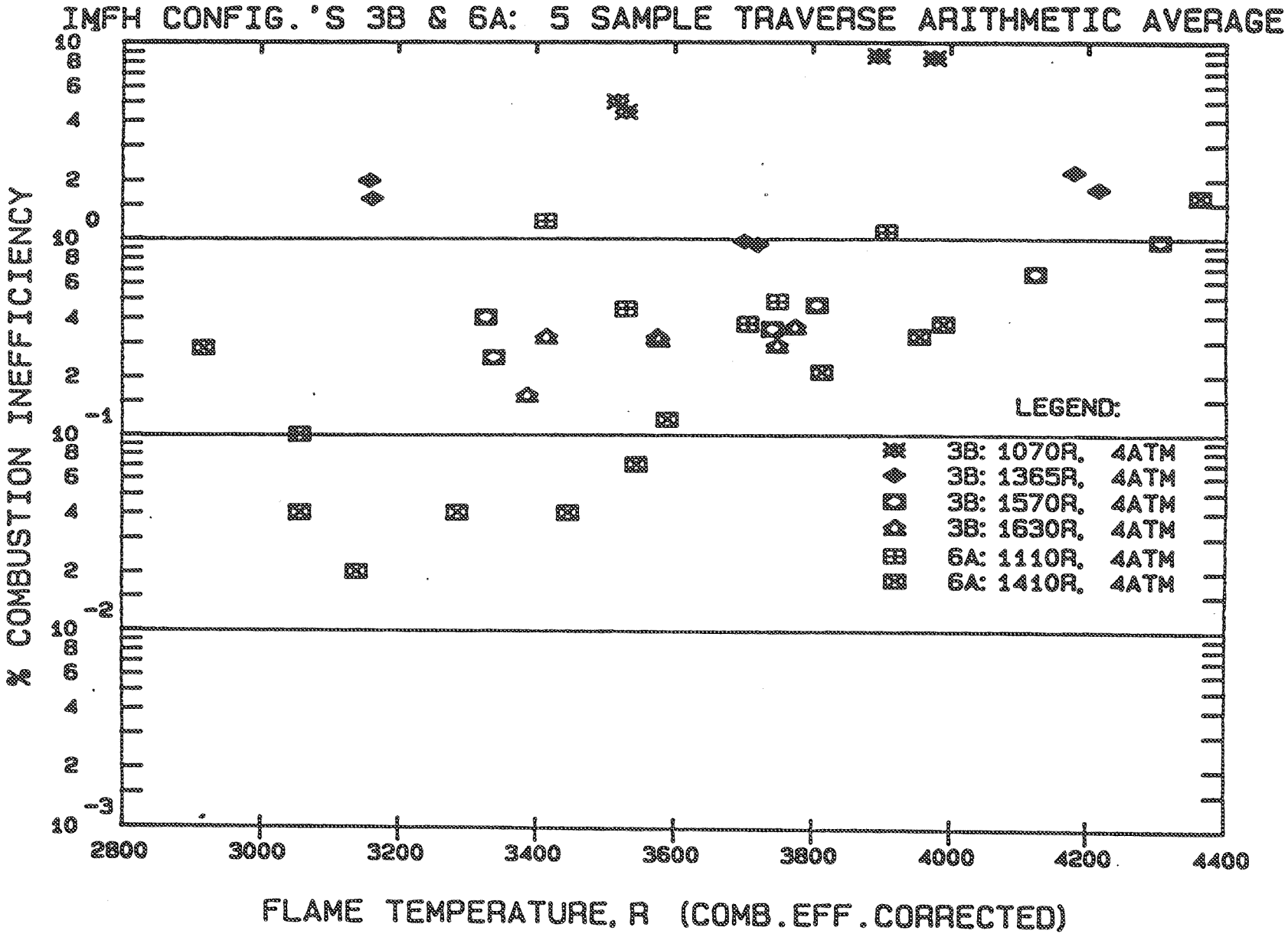

Figure 4-42. Dome Cooling Flow Flameholder Discharge Impact on IMFH Configuration 3B and 6A Combustion Inefficiency.

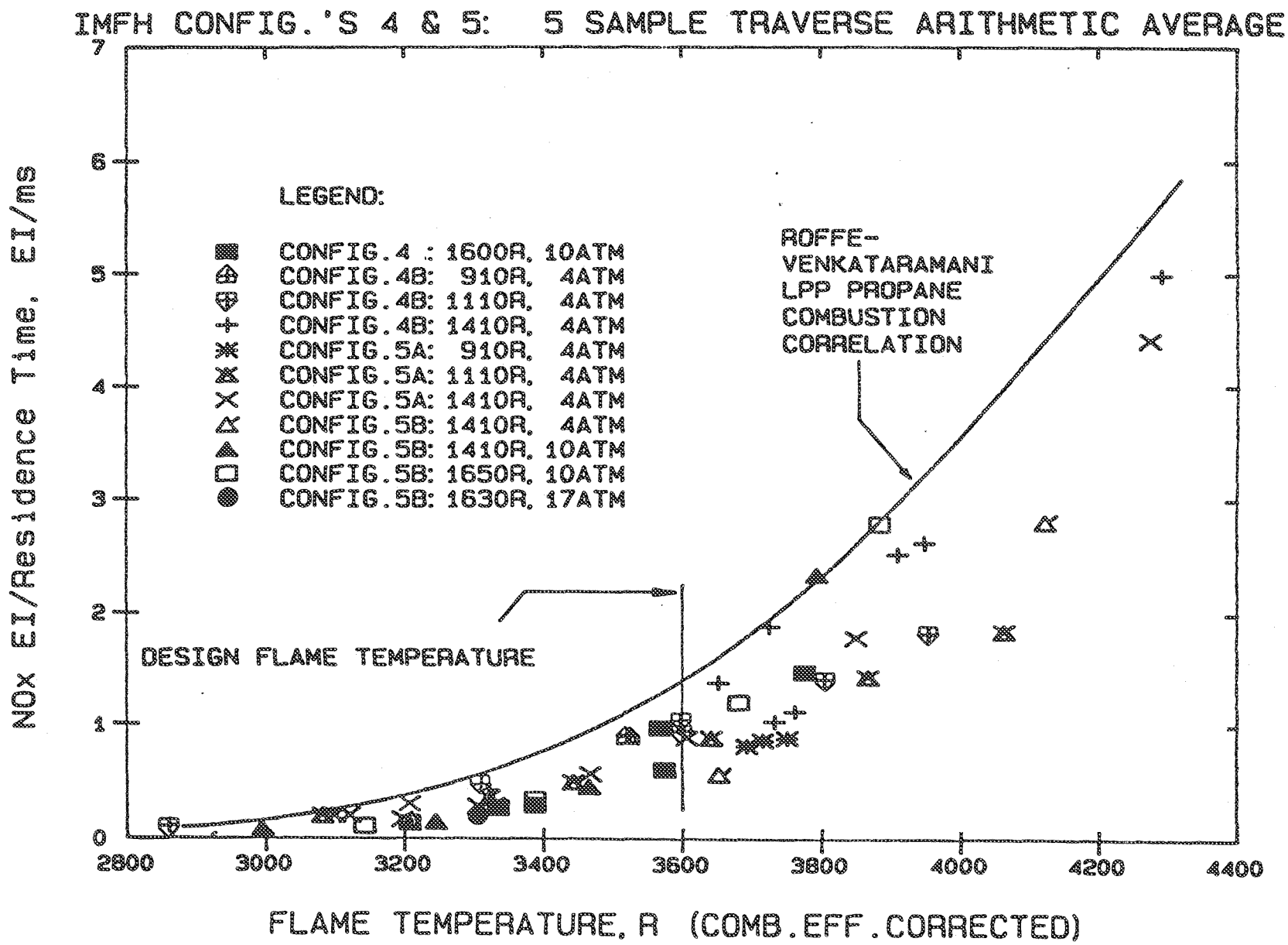

Figure 4-43. Dome Cooling Flow Impact on IMFH Configuration 4 , 4B, 5A, and 5B NOx Emissions.

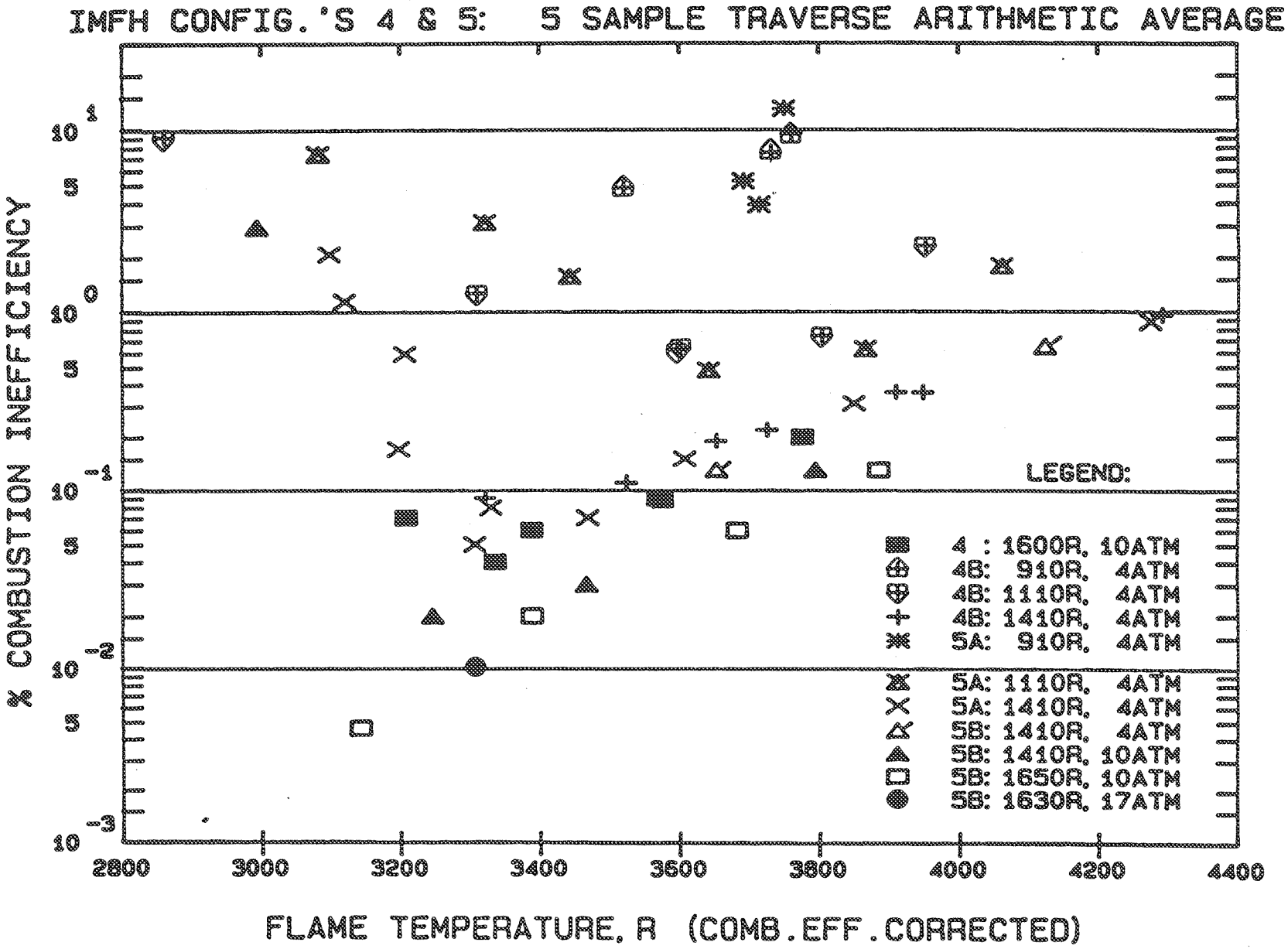

Figure 4-44. Dome Cooling Flow Impact on IMFH Configuration 4, 4B, 5A, and 5B Combustion Inefficiency.

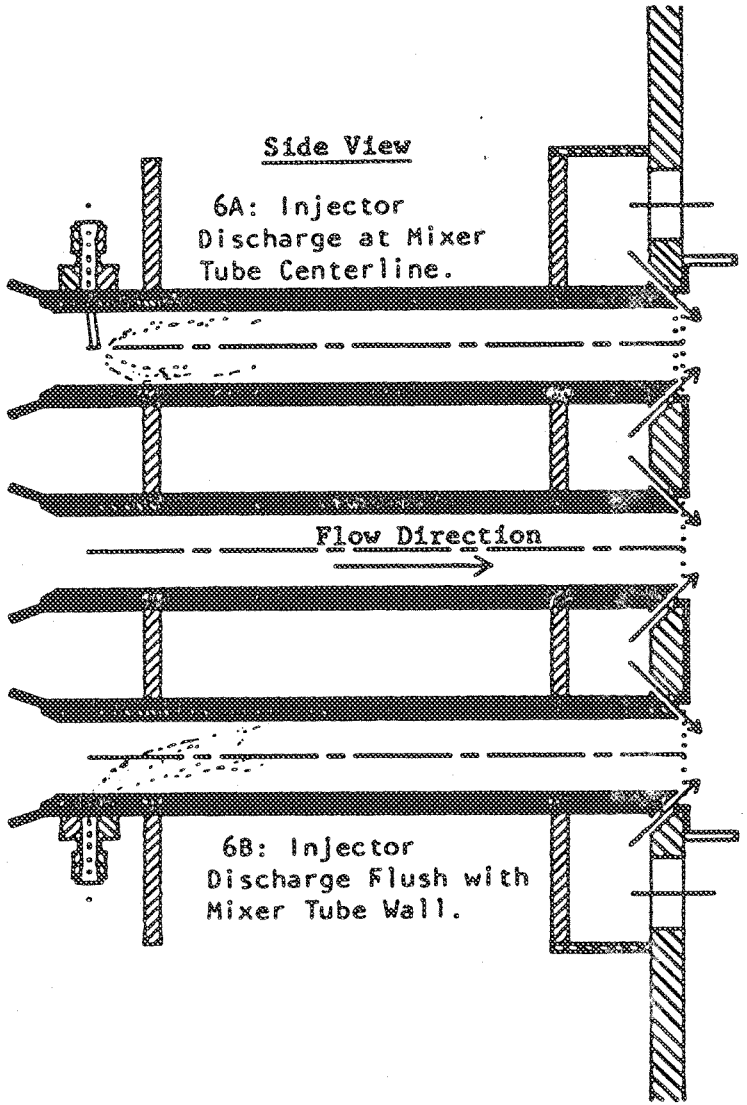

Figure 4-45. Schematic of IMFH Configurations 6A and 6B.

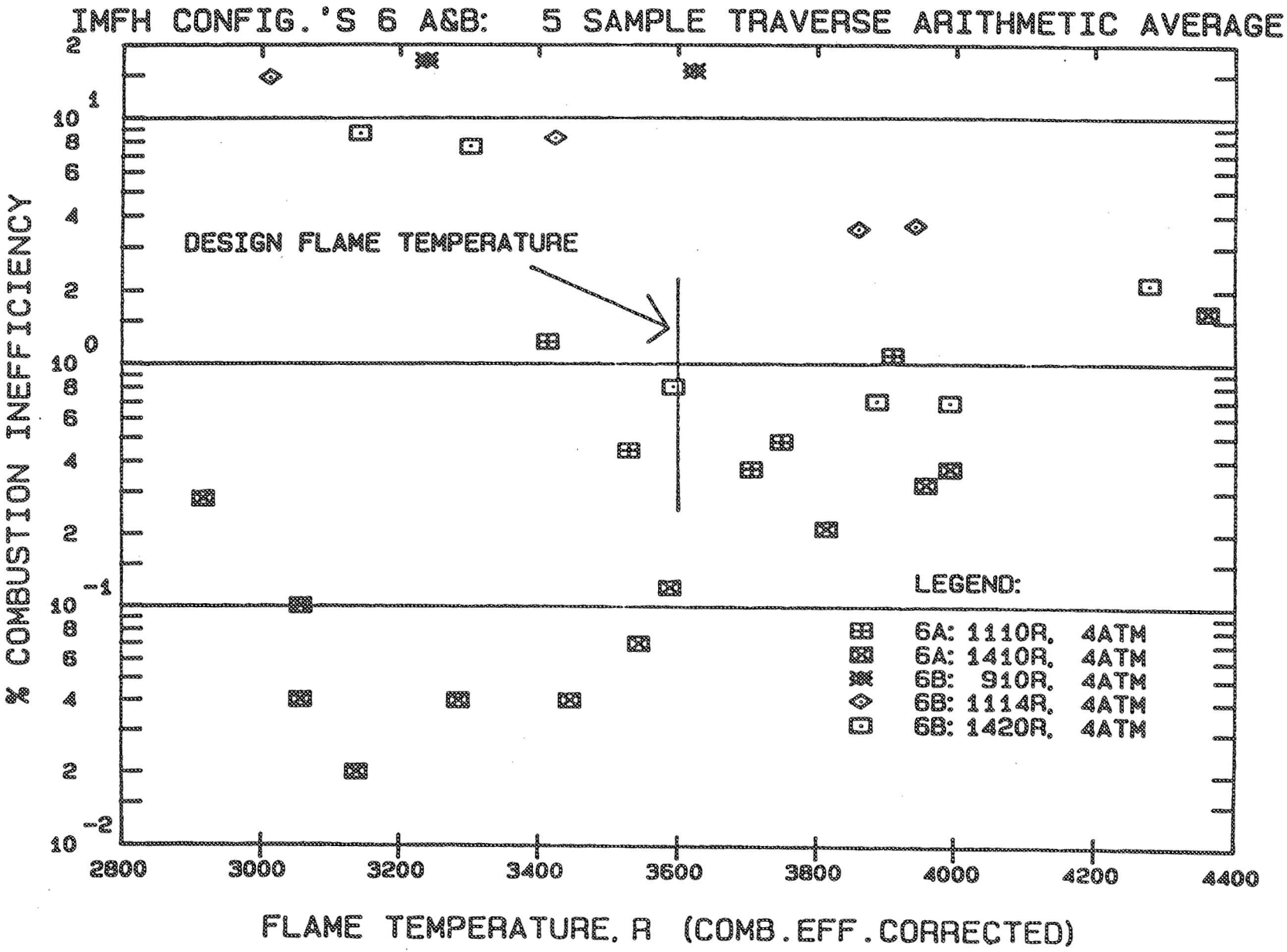

Figure 4-46. Fuel Injector Immersion Impact on IMFH Combustion Inefficiency.

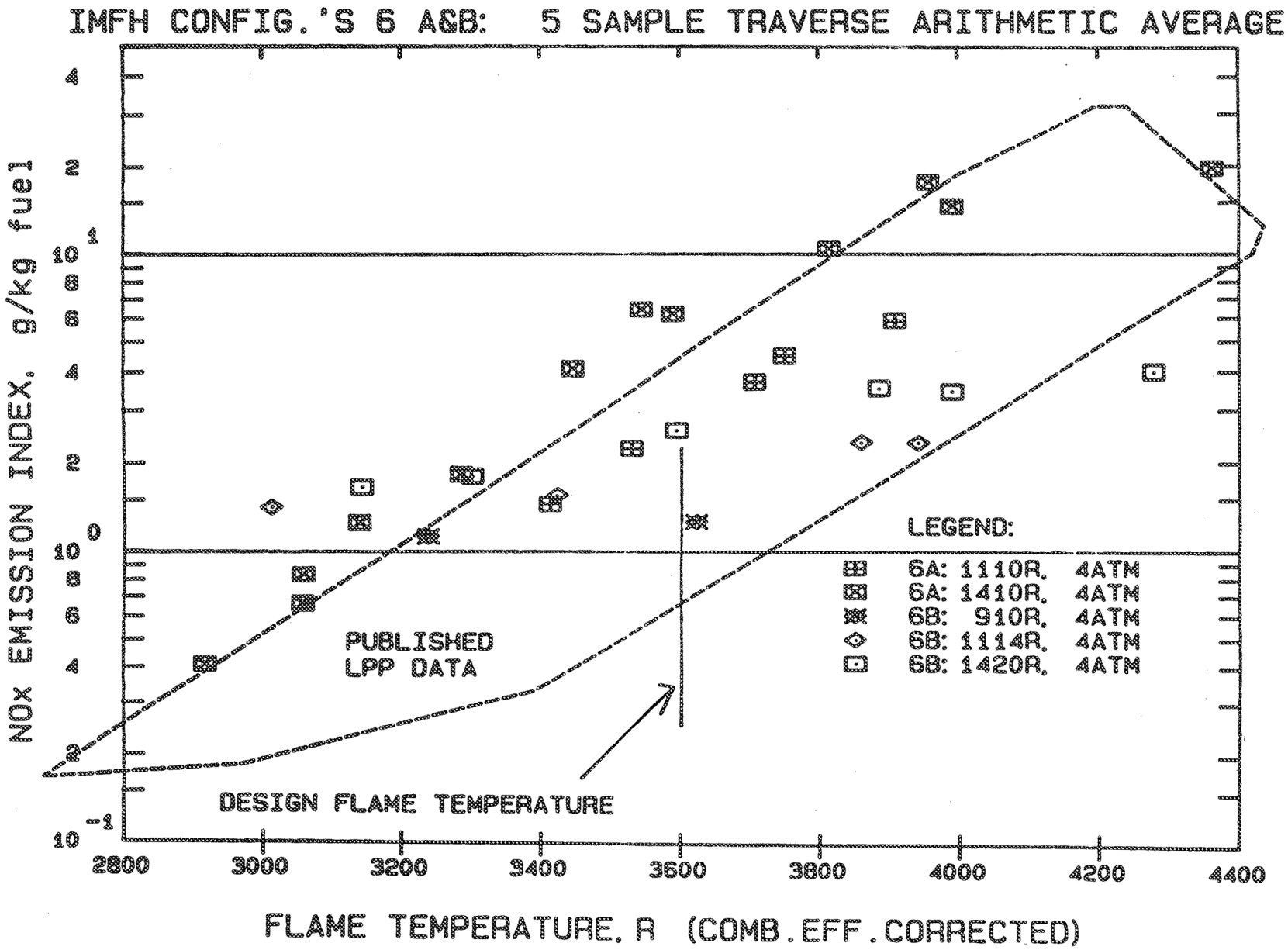

Figure 4-47. Fuel Injector Immersion Impact on IMFH NOx Emissions.

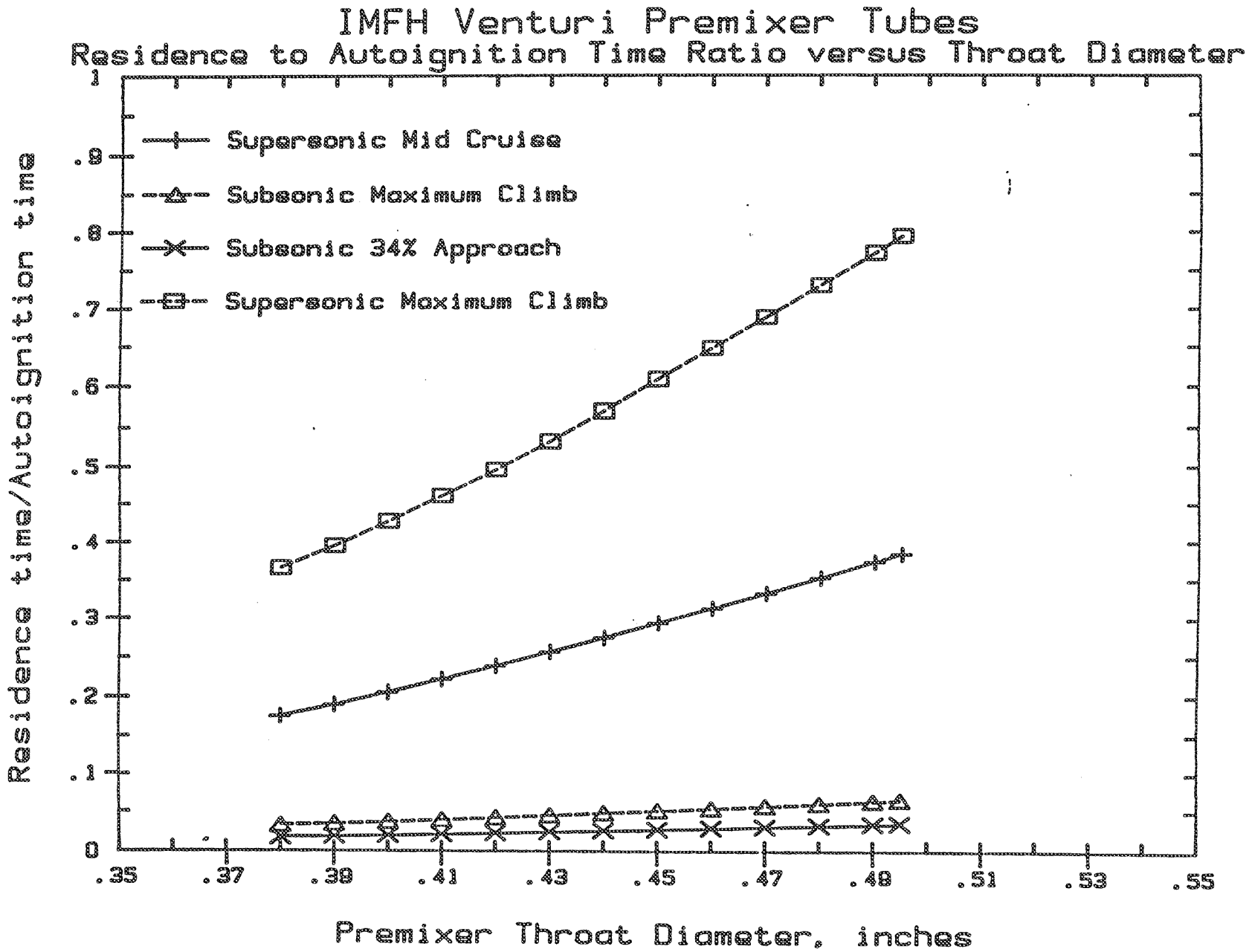

Figure 4-48. IMFH Venturi Mixer Tube Autoignition Margin as a Function of Throat Diameter.

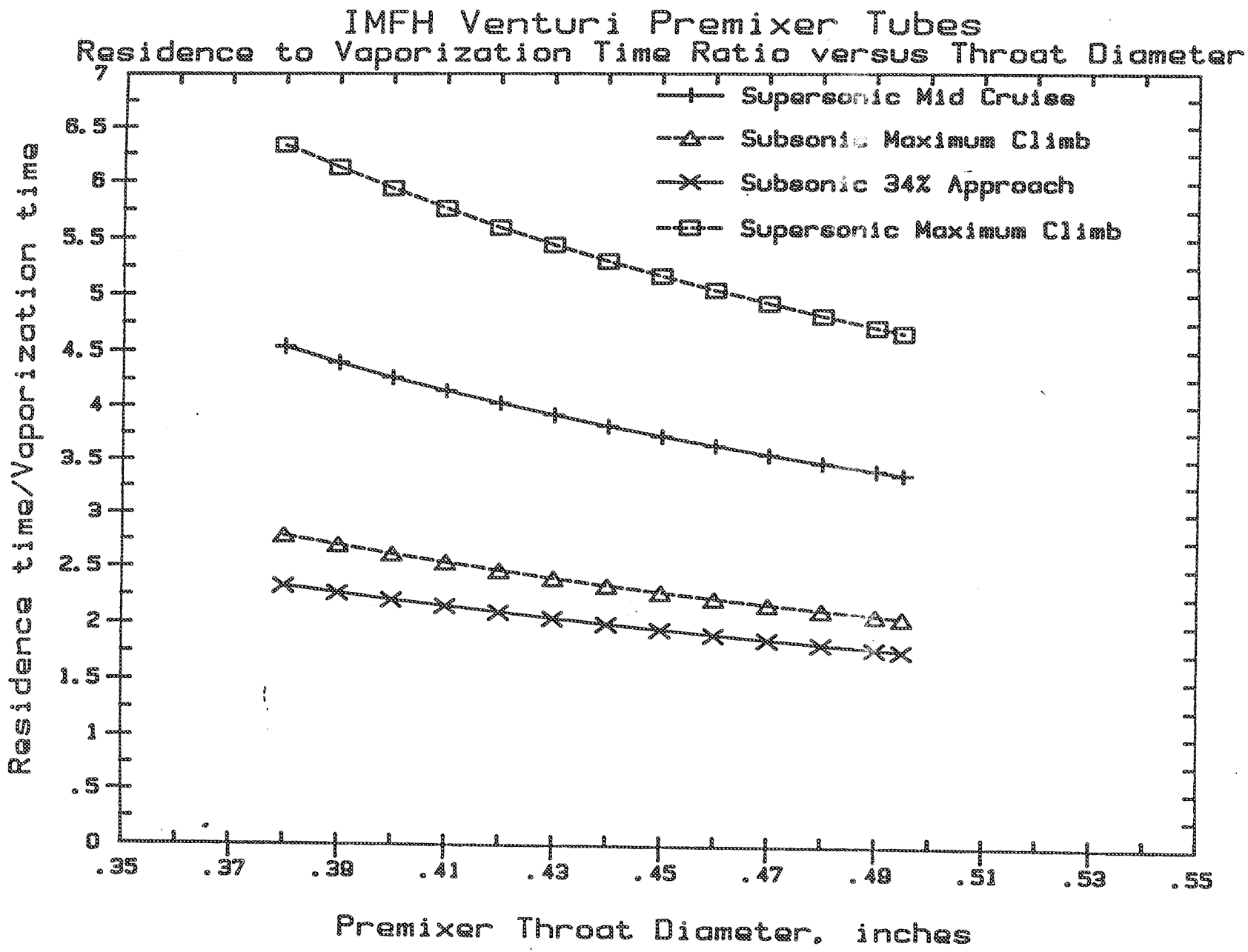

Figure 4-49. IMFH Venturi Mixer Tube Vaporization Time as a Function of Throat Diameter.

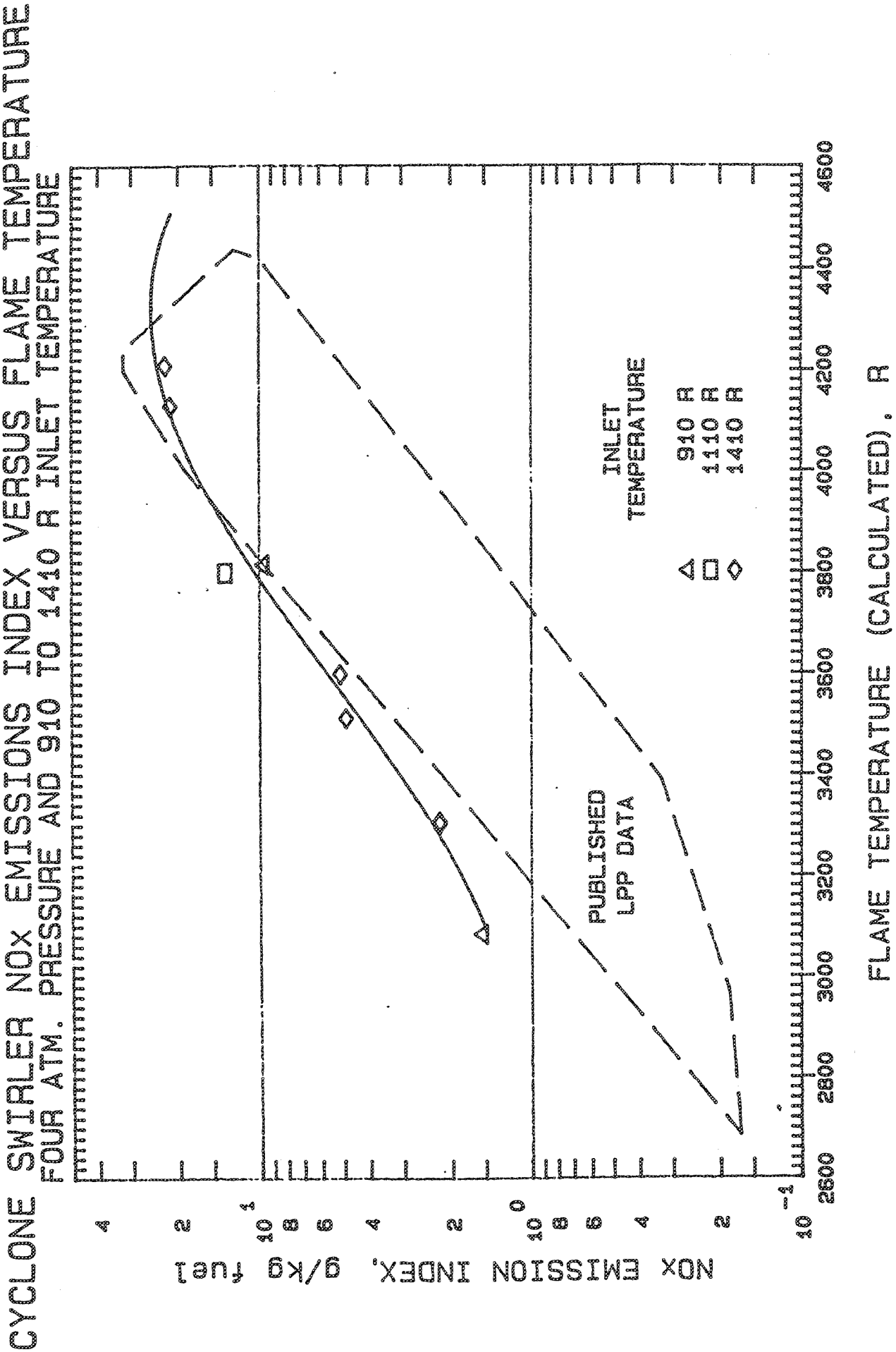

Figure 4-50. Cyclone Swirler Configuration 1 NOx Emissions.

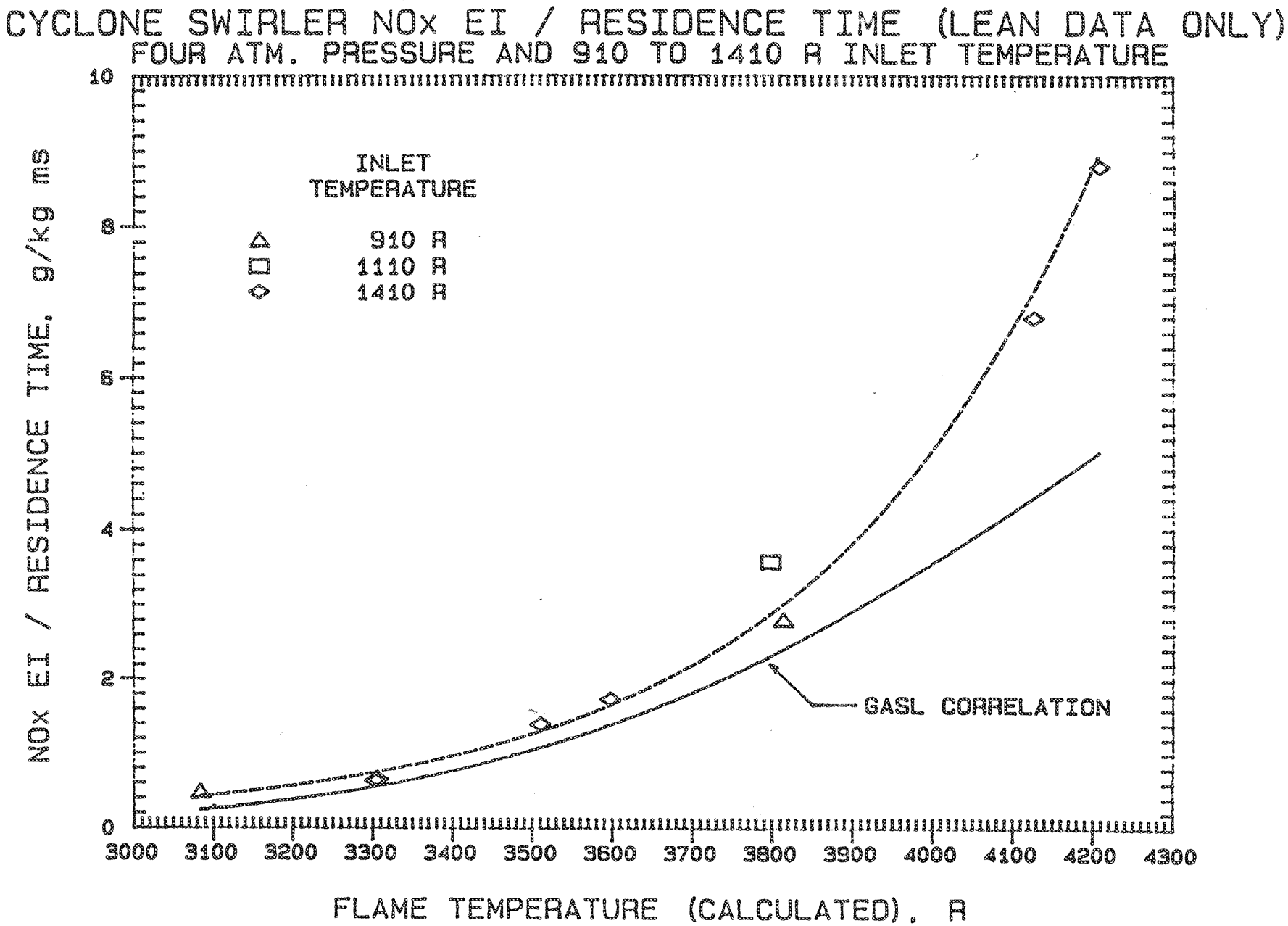

Figure 4-51. Cyclone Swirler Configuration 1 Normalized NOx Emissions.

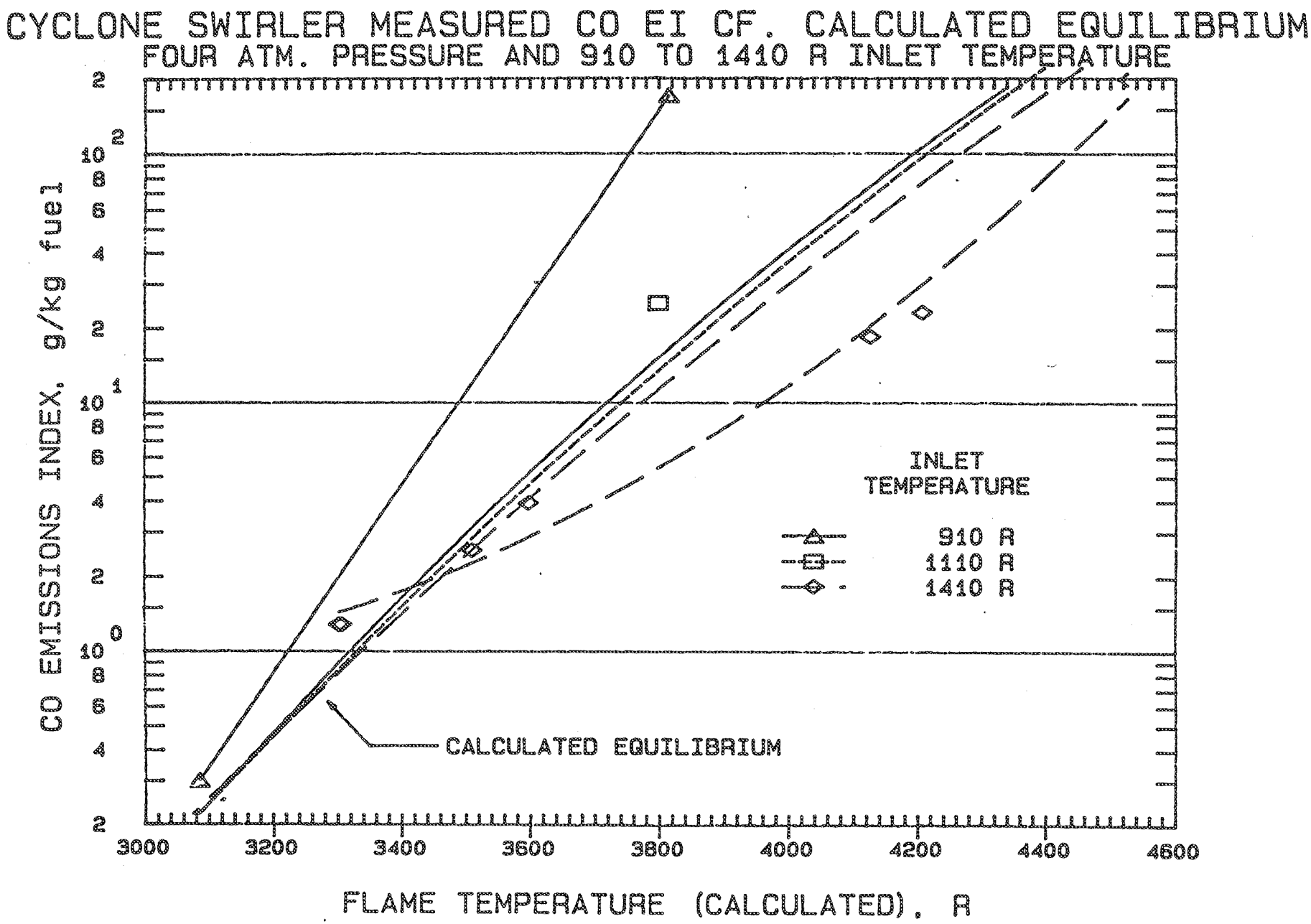

Figure 4-52. Cyclone Swirler Configuration 1 CO Emissions.

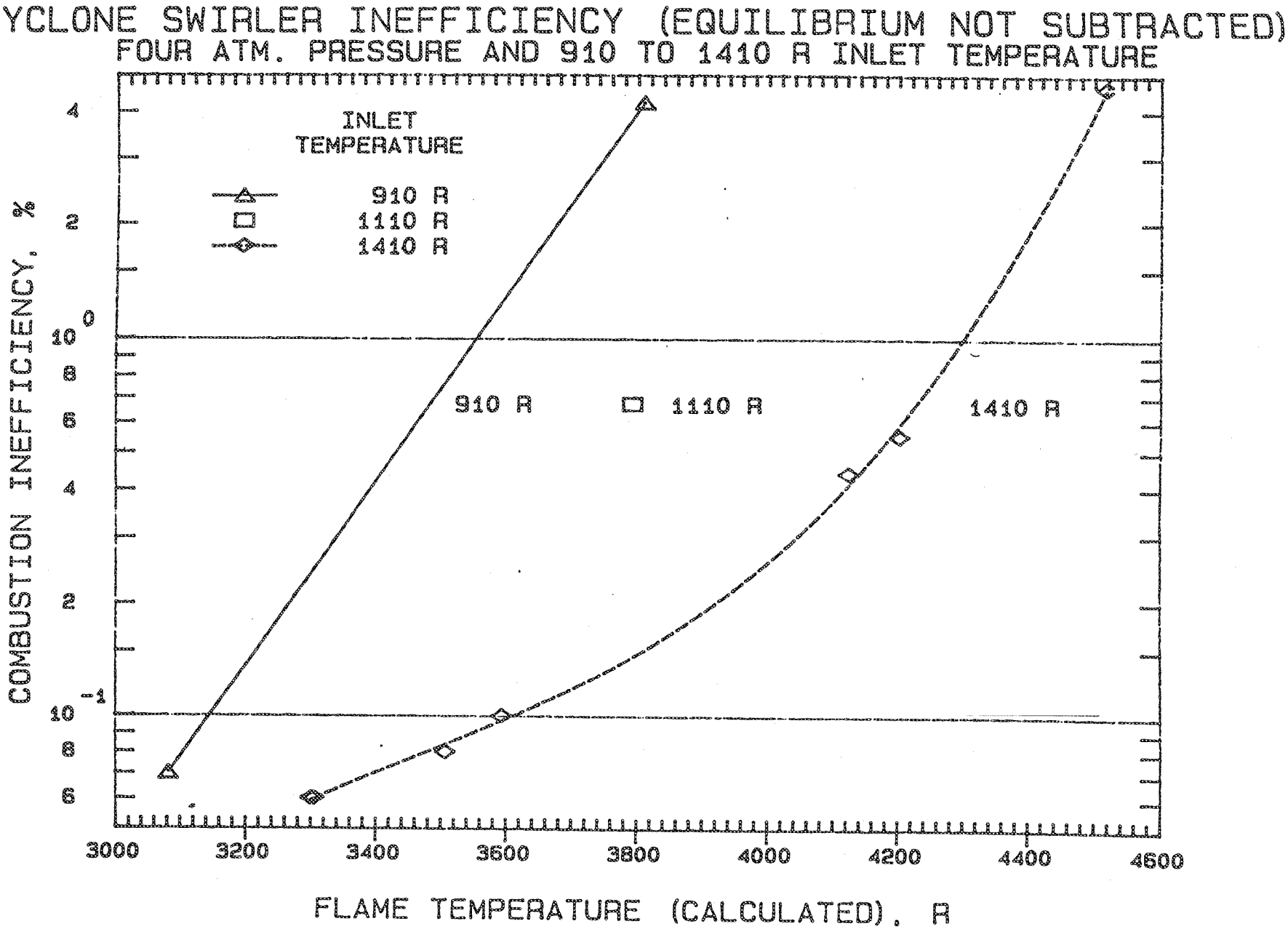

Figure 4-53. Cyclone Swirler Configuration 1 Combustion Inefficiency.

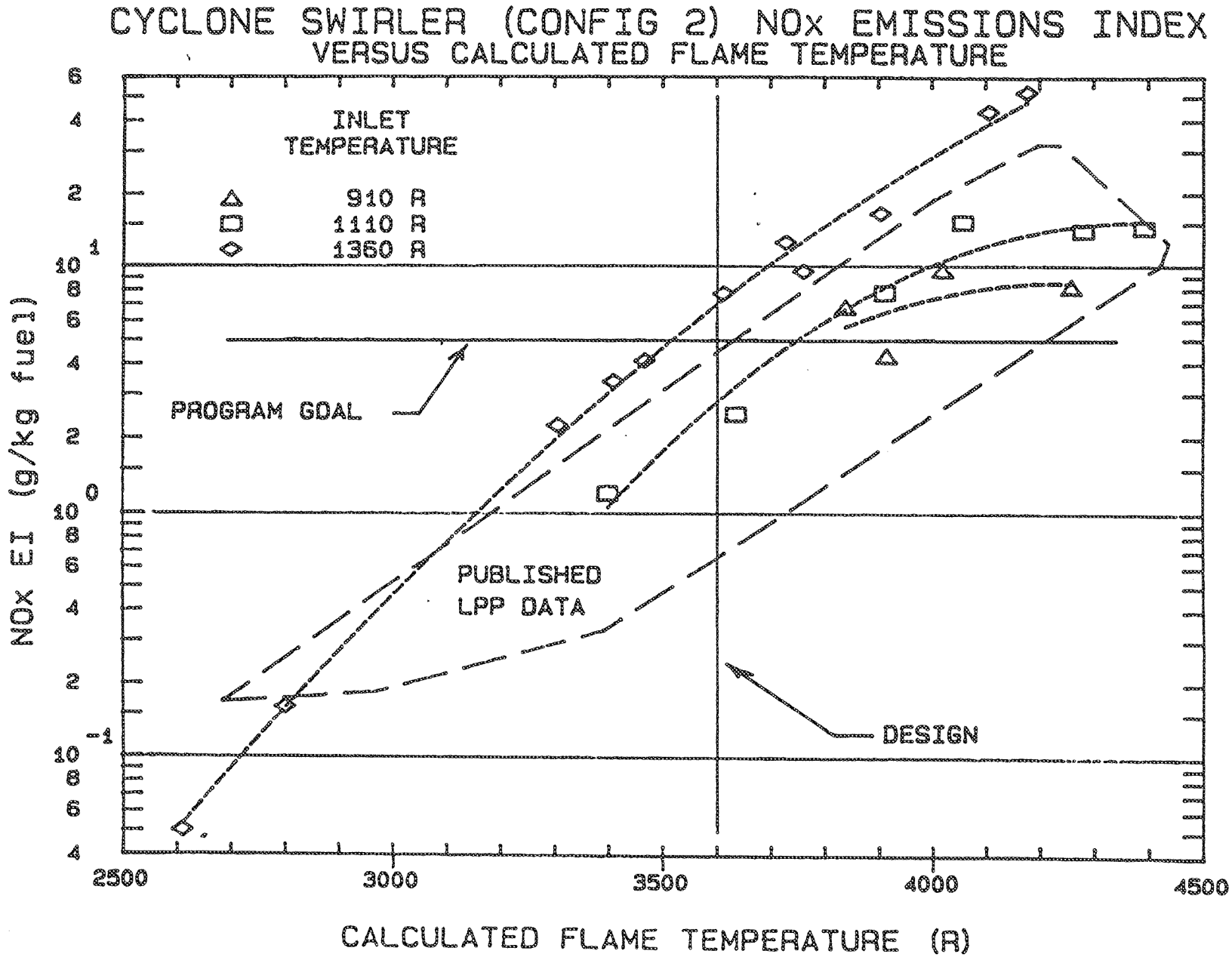

Figure 4-54. Cyclone Swirler Configuration 2 NOx Emissions.

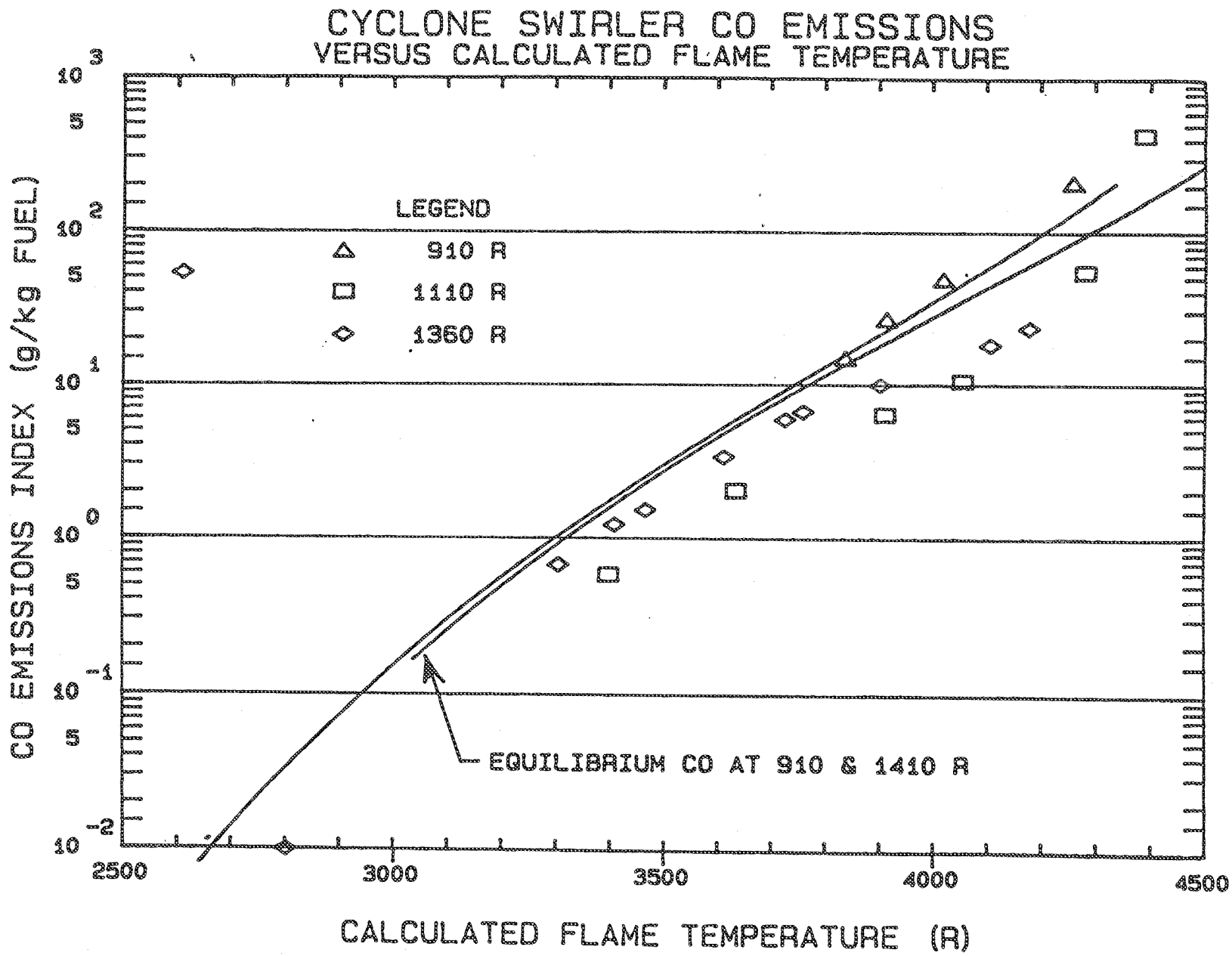

Figure 4-55. Cyclone Swirler Configuration 2 CO Emissions.

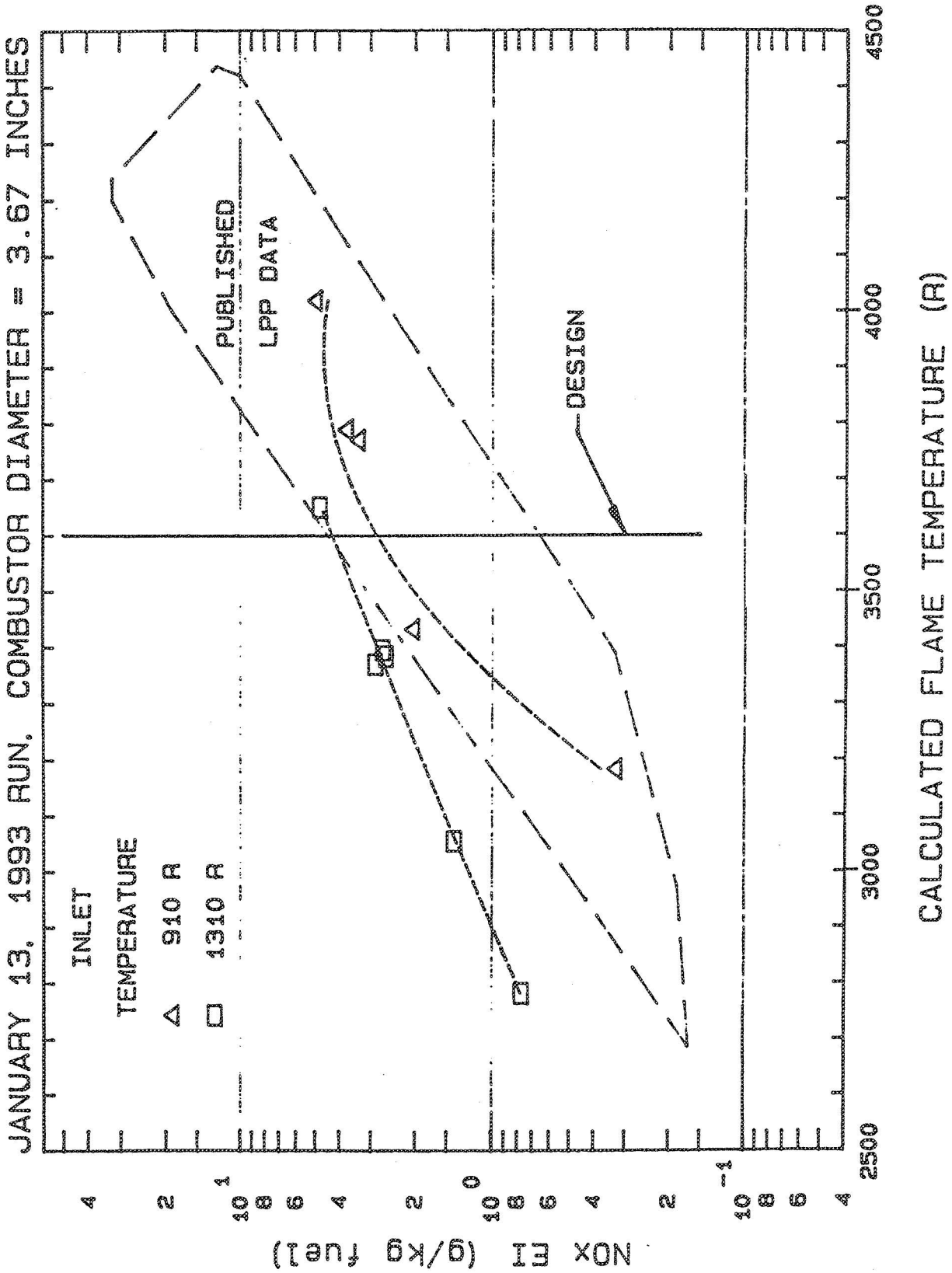

Figure 4-56. Cyclone Swirler Configuration 2A NOx Emissions.

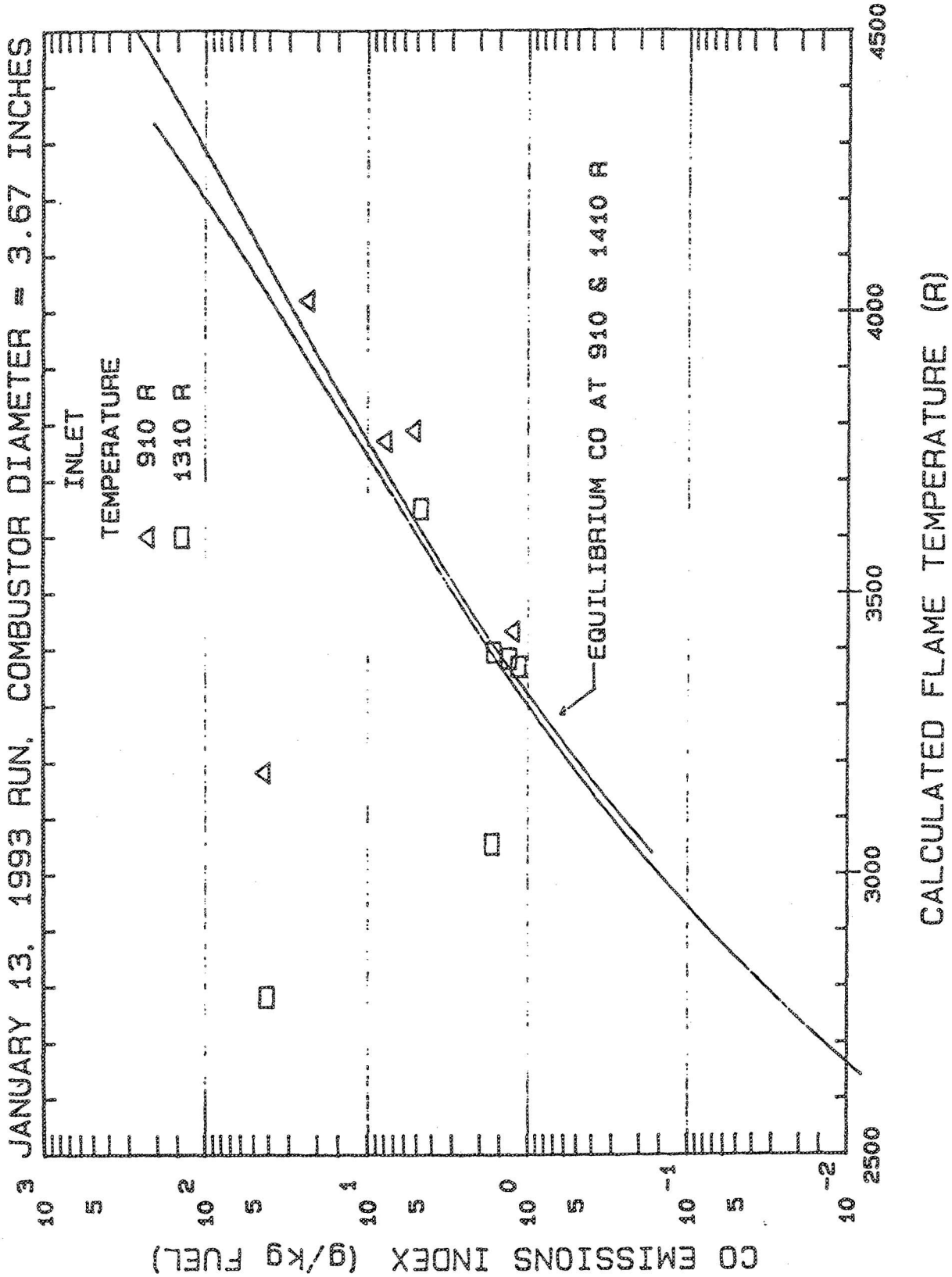

Figure 4-57. Cyclone Swirler Configuration 2A CO Emissions.

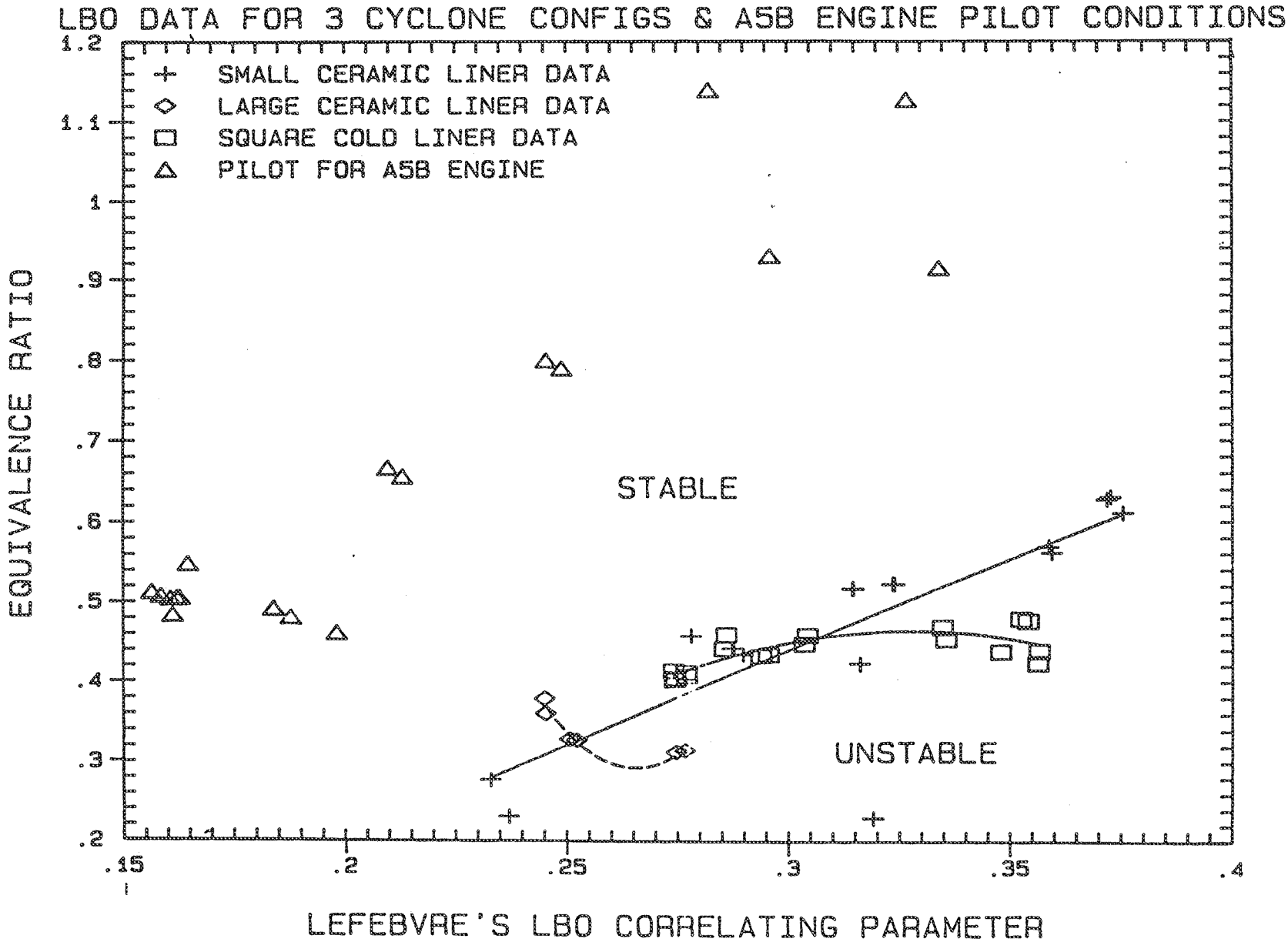

Figure 4-58. Cyclone Measured Lean Blowout Data Compared to Lefebvre's Correlating Parameter.

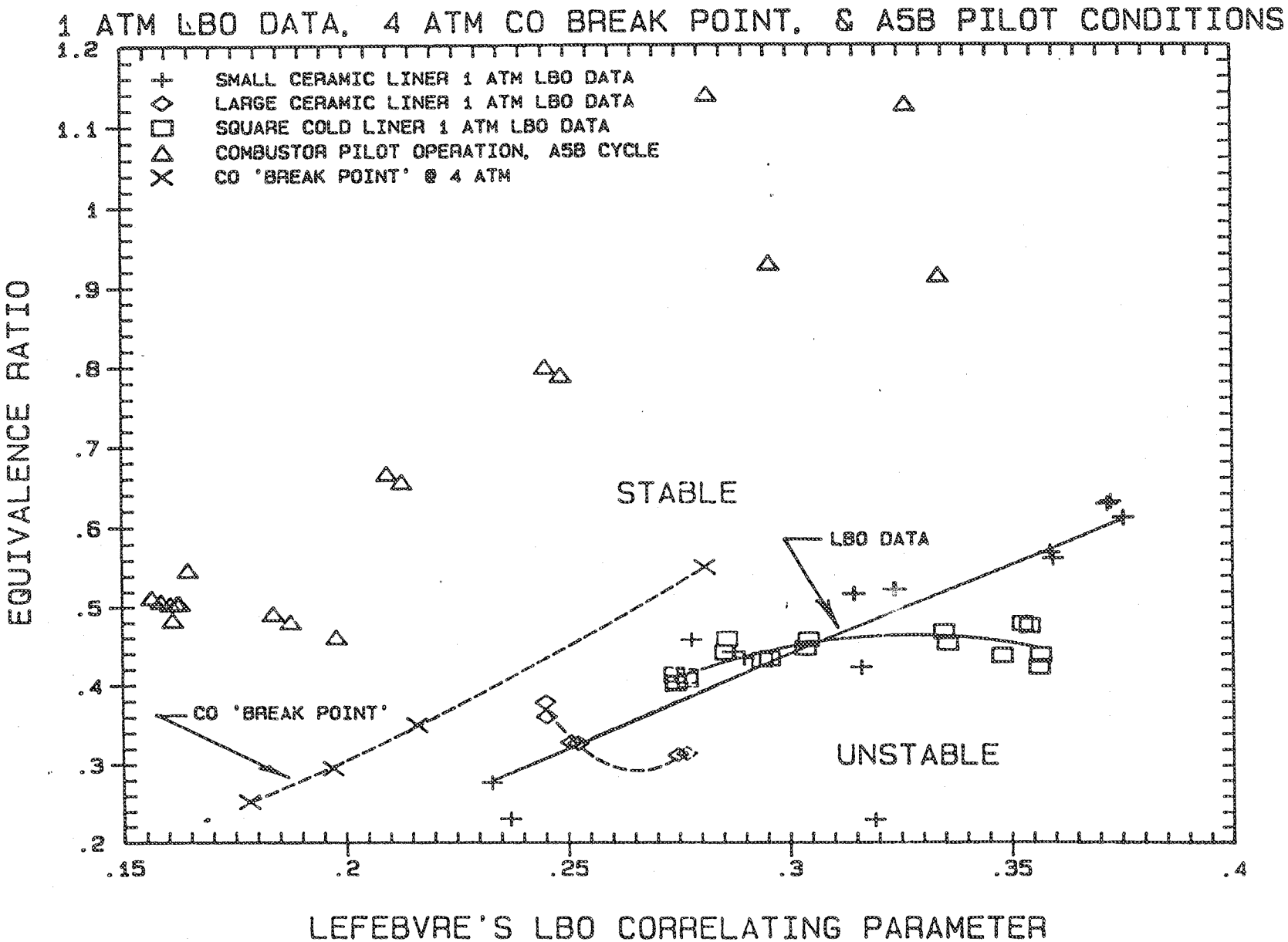

Figure 4-59. Cyclone Measured Lean Blowout Data and 4.0 atm. CO Break Point.

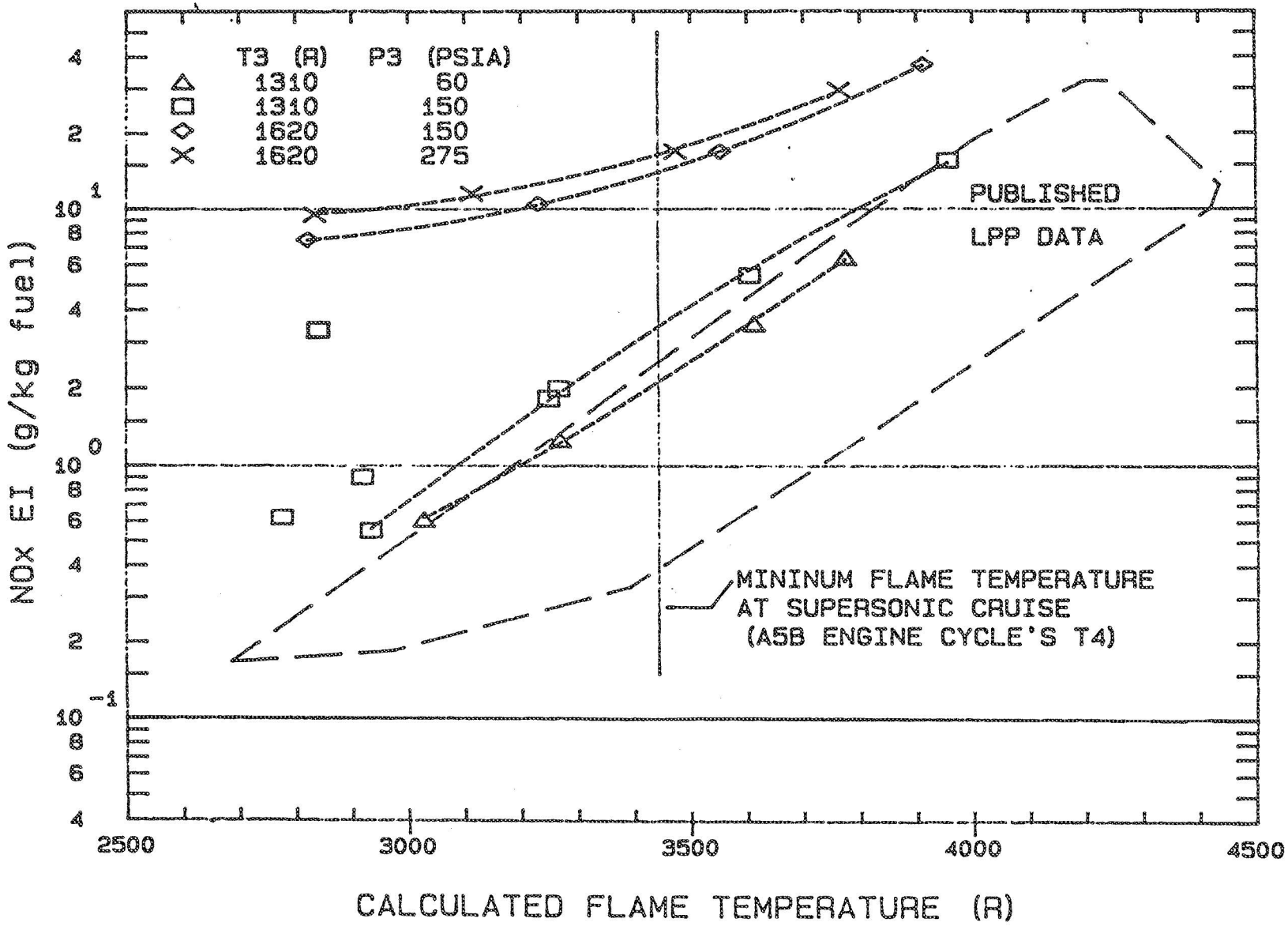

Figure 4-60. Cyclone Swirler Configuration 2 Measured NOx Emissions.

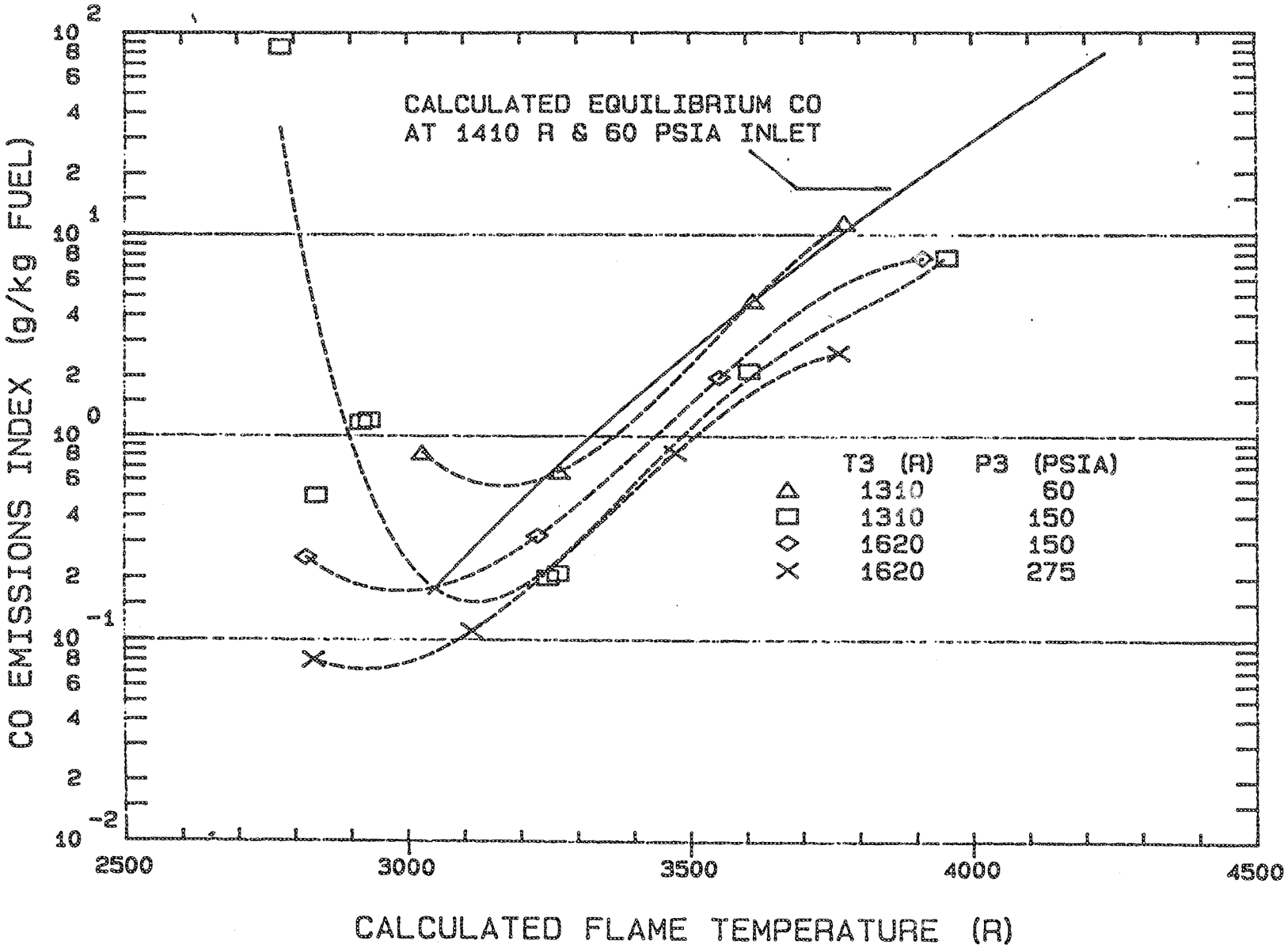

Figure 4-61. Cyclone Swirler Configuration 2 CO Emissions.

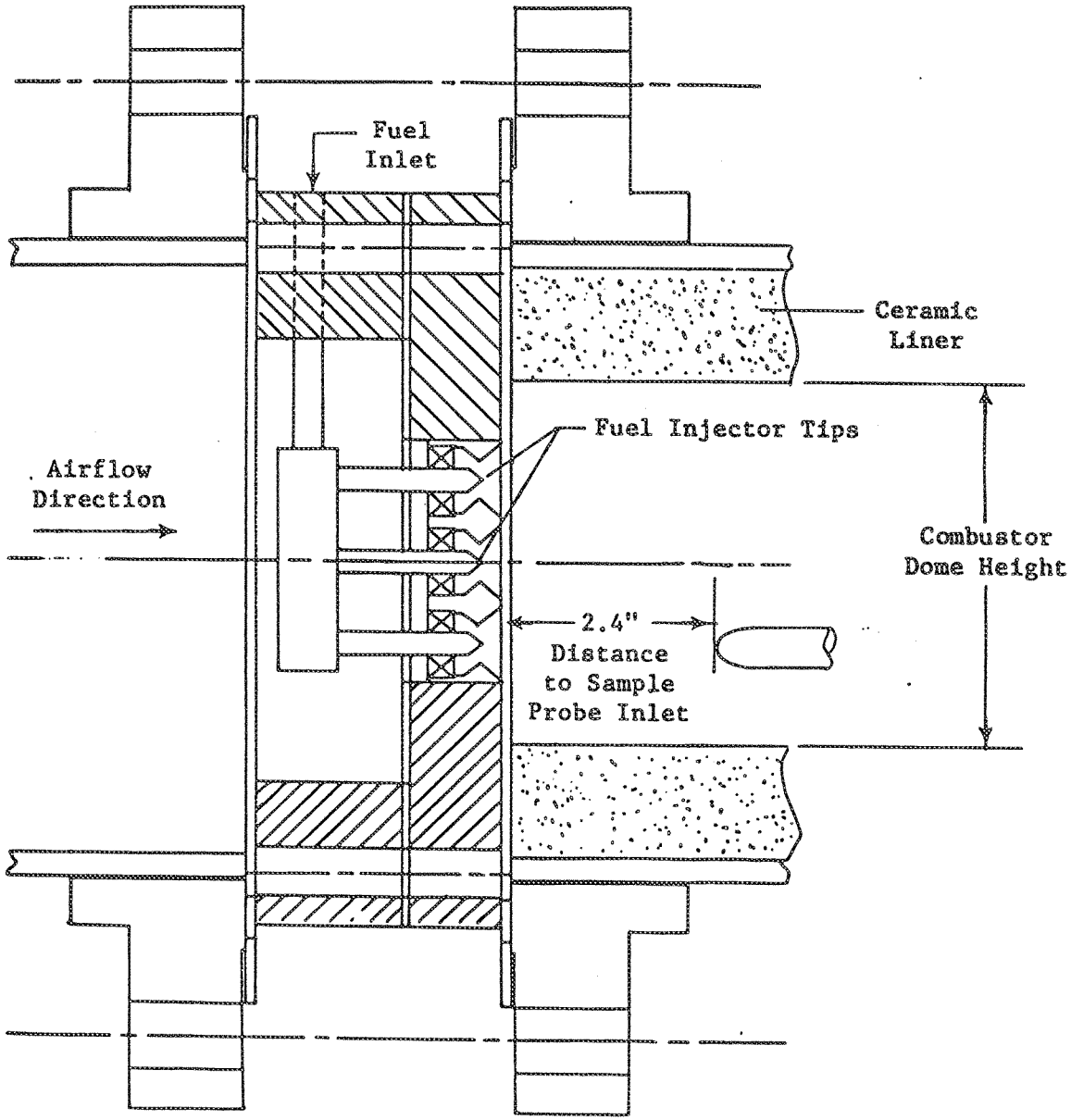

Figure 4-62. Schematic of the Multi-Venturi Mixer.

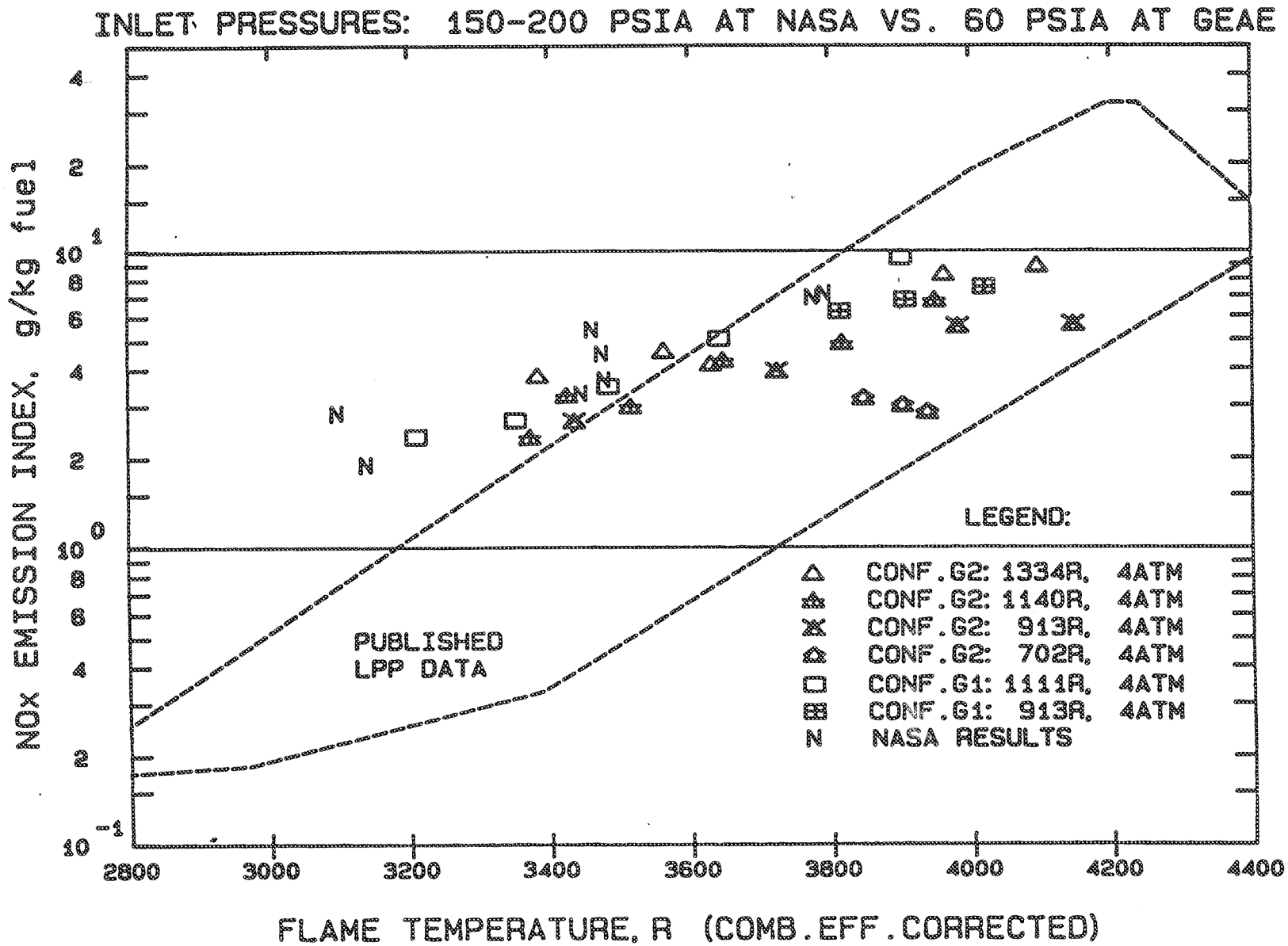

Figure 4-63. Multi-Venturi NOx Emissions (NASA and GEAE Data).

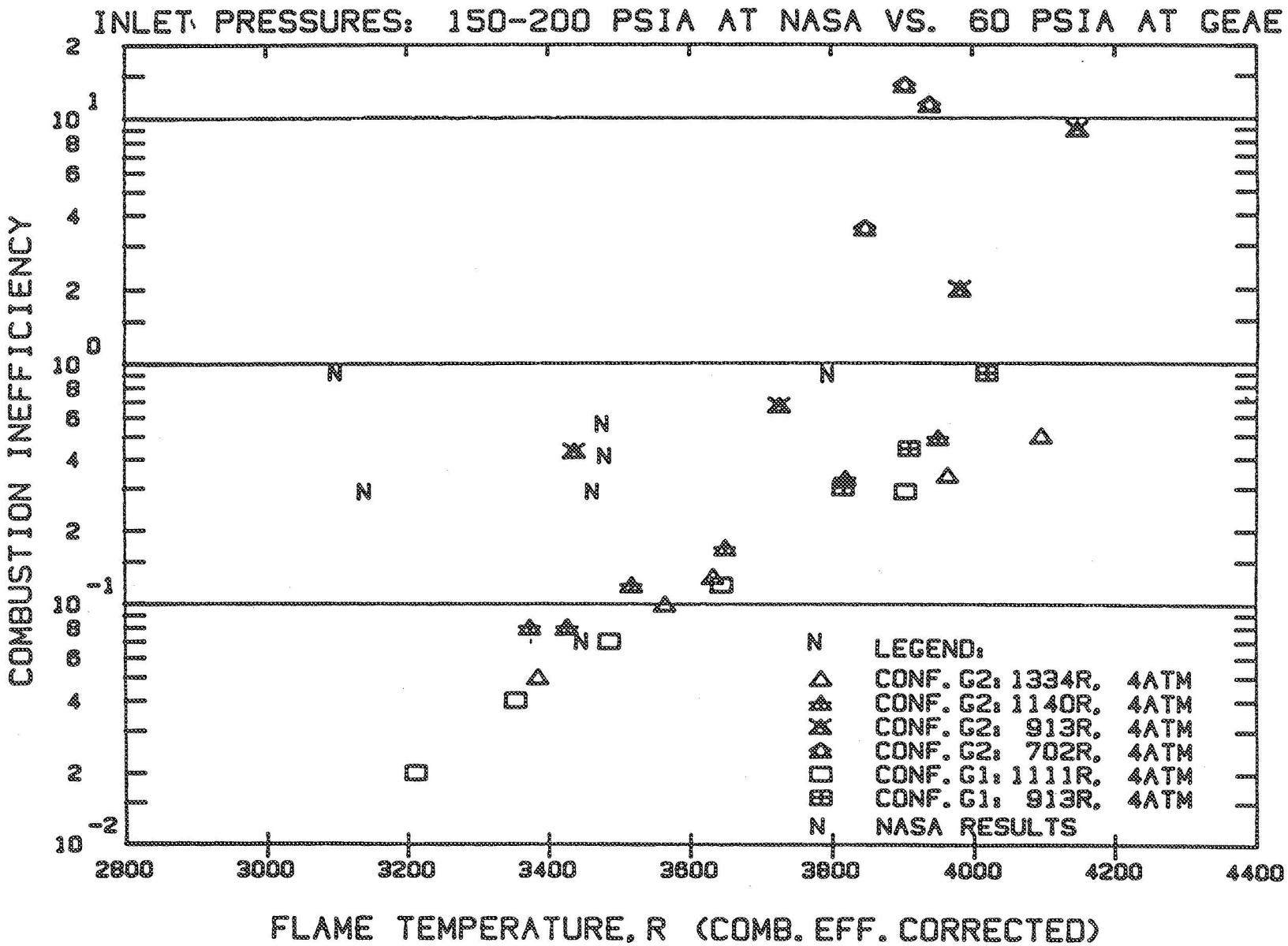

Figure 4-64. Multi-Venturi Combustion Inefficiency (NASA and GEAE Data).

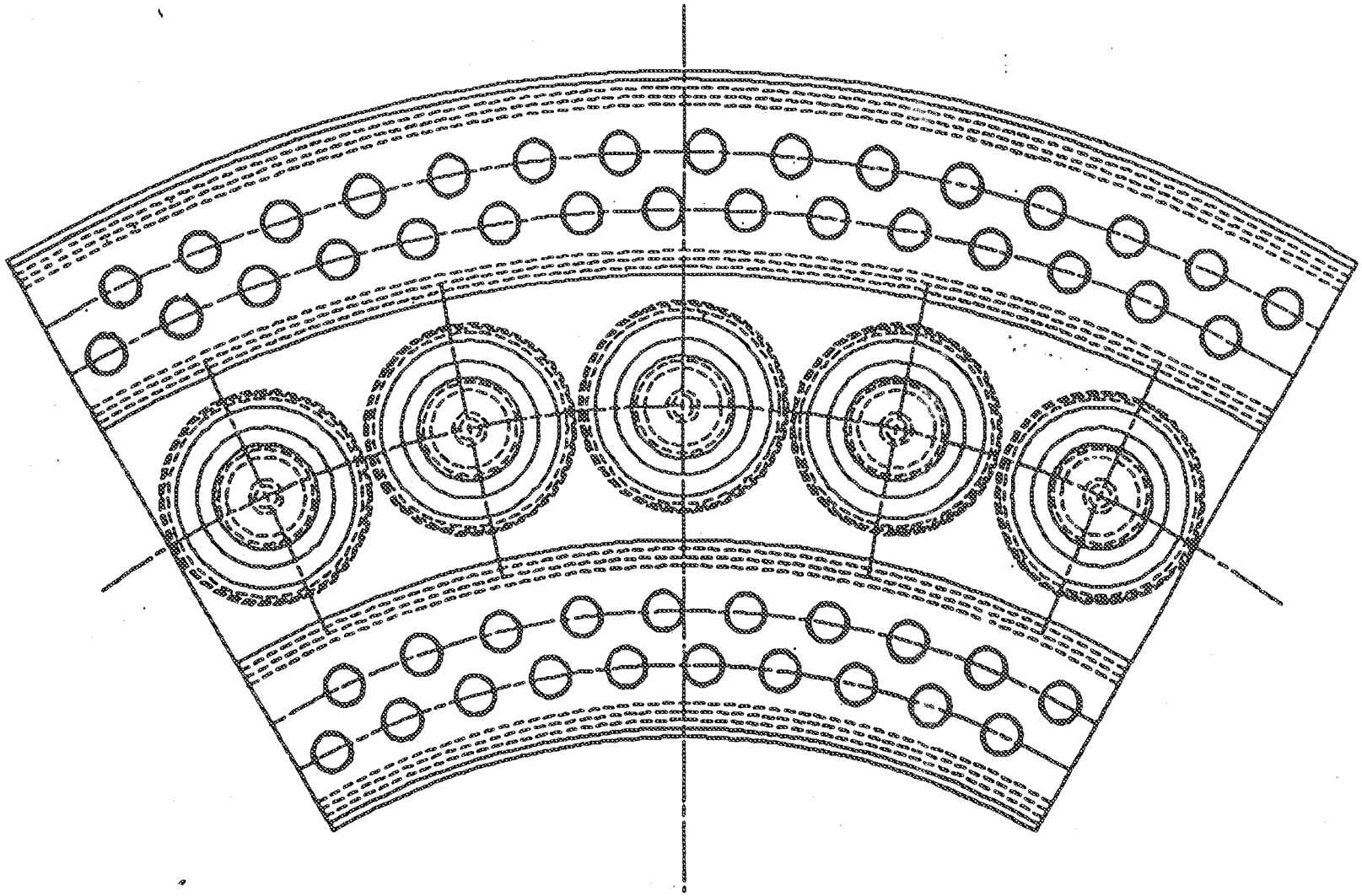

Figure 6-1. Schematic of the IMFH/Cyclone 5 Cup Sector (Initial Configuration).

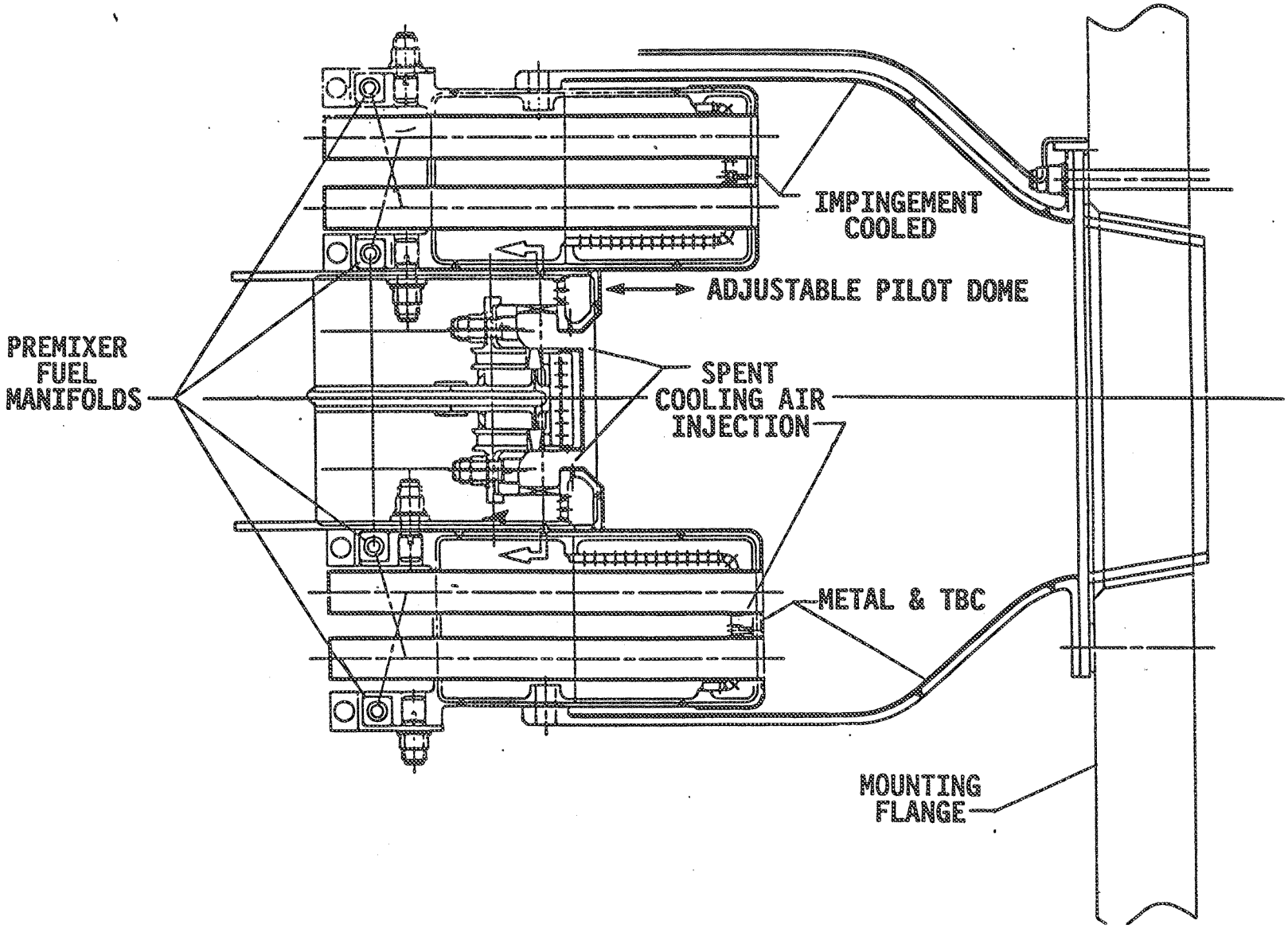

Figure 6-2. Cross Section of the IMFH/Cyclone Sector Combustor.

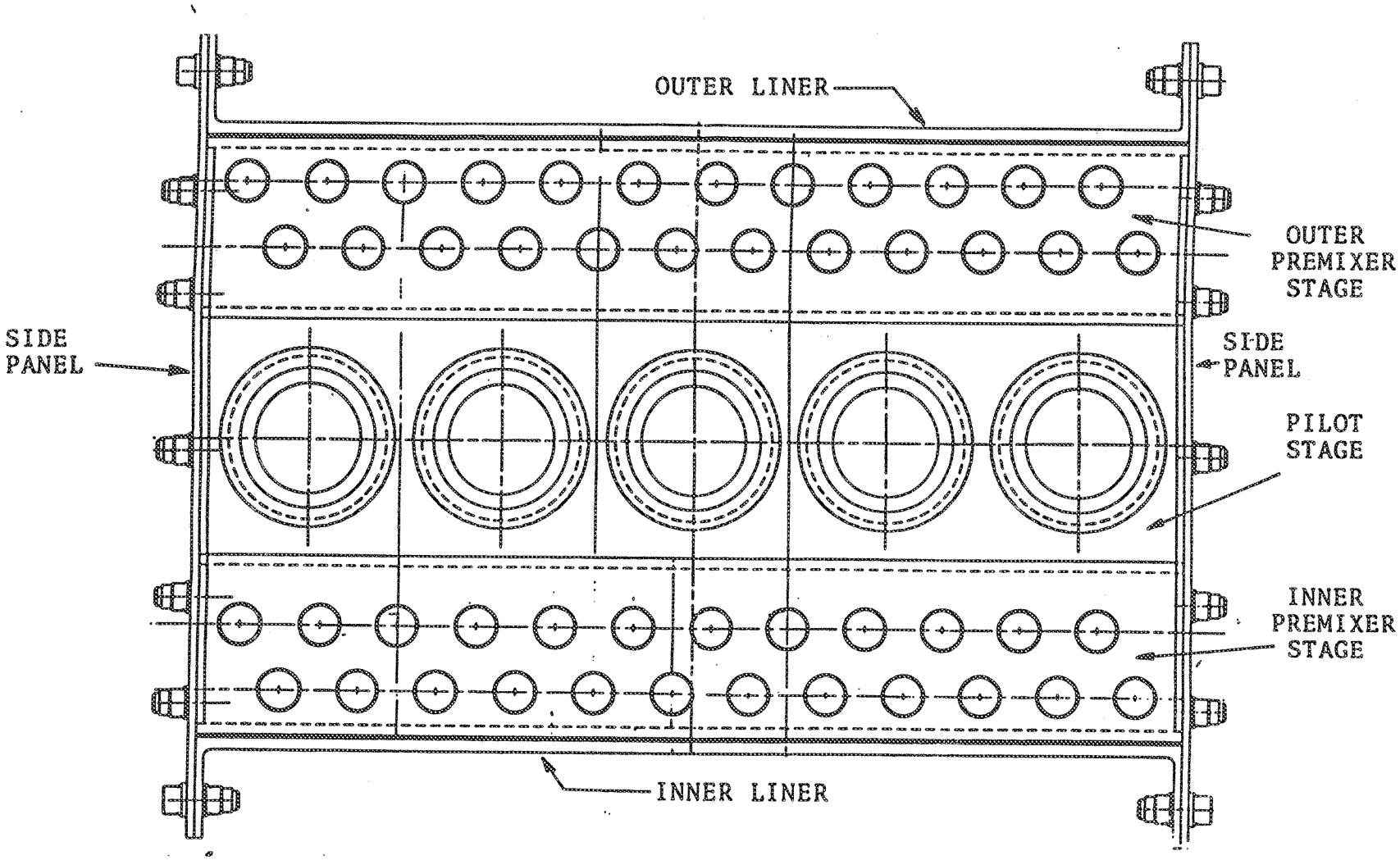

Figure 6-3. End View (ALF) IMFH/Cyclone Sector Combustor.

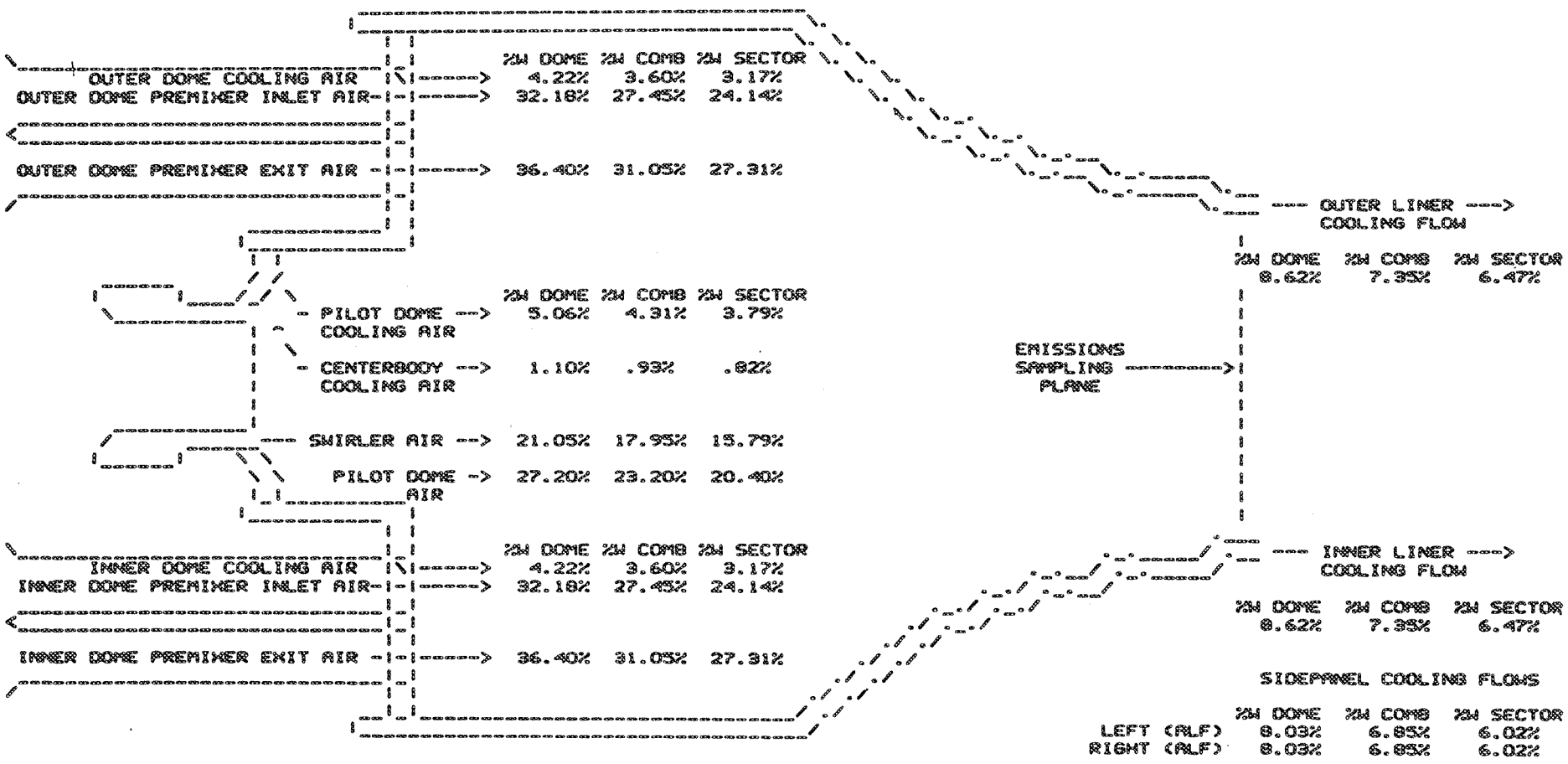

Figure 6-4. IMFH/Cyclone Sector Combustor Air Flow Splits.

HSCT - LDI Jet - Mix Build #1
Atmospheric Test Results

Pbarom = 29.49 in Hg
Ae = 0.8829 in2

Rdg.	T3 (F)	Dome dP (in H2O)	Wf (LBO) (pph)	Wa (pph)	FAR
1	70.0	20.5	0.0	0.13825	0.00000
2	70.0	30.0	0.0	0.16725	0.00000
3	205.0	30.0	18.0	0.14931	0.03349
4	215.0	30.2	19.1	0.14869	0.03568
5	230.0	20.0	0.0	0.11968	0.00000
6	465.0	30.0	11.7	0.12660	0.02567
7	465.0	30.2	15.8	0.12702	0.03455
8	464.0	20.5	0.0	0.10471	0.00000
9	462.0	20.6	0.0	0.10508	0.00000
10	650.0	30.5	0.0	0.11653	0.00000
11	657.0	30.0	0.0	0.11520	0.00000
12	660.0	21.0	0.0	0.09626	0.00000
13	805.0	30.0	0.0	0.10826	0.00000
14	800.0	30.0	0.0	0.10847	0.00000
15	783.0	20.0	0.0	0.08917	0.00000
16	778.0	20.0	0.0	0.08935	0.00000
17	755.0	12.5	0.0	0.07130	0.00000
18	747.0	12.5	0.0	0.07154	0.00000

HSCT - LDI Jet - Mix Build #2
Atmospheric Test Results

Pbarom = 29.43 in Hg
Ae = 0.8829 in2

Rdg. ---	T3 (F)	Dome dP (in H2O)	Wf (LBO) (pph)	Wa (pph)	FAR
1	84.0	20.0	0.0	0.1347	0.00000
2	86.0	30.1	0.0	0.1649	0.00000
3	86.0	30.0	0.0	0.1646	0.00000
4	226.0	30.0	12.6	0.1469	0.02383
5	229.0	30.0	13.4	0.1465	0.02540
6	233.0	20.0	10.3	0.1193	0.02398
7	237.0	20.0	10.4	0.1190	0.02429
8	451.0	30.0	11.9	0.1274	0.02594
9	453.0	30.0	11.9	0.1273	0.02597
10	456.0	20.0	9.3	0.1038	0.02490
11	460.0	20.0	9.2	0.1035	0.02468
12	653.0	30.0	9.3	0.1153	0.02241
13	660.0	30.0	10.2	0.1149	0.02465
14	658.0	20.0	8.4	0.0939	0.02484
15	659.0	20.0	7.8	0.0939	0.02308
16	816.0	30.0	9.1	0.1077	0.02348
17	818.0	30.0	10.0	0.1076	0.02582
18	808.0	20.0	7.3	0.0882	0.02299
19	800.0	20.0	7.3	0.0885	0.02292
20	787.0	12.5	2.5	0.0703	0.00988

HSCT - LDI Jet - Mix Build #3
Atmospheric Test Results

Pbarom = 29.38 in Hg
Ae = 0.8829 in2

Rdg. ---	T3 (F)	Dome dP (in H2O)	Wf (LBO) (pph)	Wa (pph)	FAR
1	205.0	20.0	13.6	0.1217	0.03105
2	221.0	20.5	15.8	0.1217	0.03605
3	226.0	20.3	15.4	0.1207	0.03544
4	249.0	30.0	18.2	0.1443	0.03503
5	255.0	30.0	22.4	0.1437	0.04329
6	255.0	30.0	19.8	0.1437	0.03827
7	453.0	30.3	11.2	0.1278	0.02434
8	460.0	31.0	11.2	0.1288	0.02415
9	458.0	19.7	7.4	0.1028	0.02000
10	457.0	19.8	7.5	0.1031	0.02021
11	644.0	30.0	8.4	0.1157	0.02017
12	646.0	29.6	8.8	0.1148	0.02130
13	643.0	20.0	7.0	0.0945	0.02058
14	644.0	20.2	6.8	0.0949	0.01990
15	641.0	12.5	0.0	0.0748	0.00000
16	775.0	30.0	0.0	0.1094	0.00000
17	766.0	30.0	6.4	0.1098	0.01620
18	769.0	30.0	7.0	0.1096	0.01774
19	752.0	20.0	0.0	0.0901	0.00000
20	736.0	20.0	0.0	0.0907	0.00000

HSCT - LDI Jet - Mix Build #4
Atmospheric Test Results

Pbarom = 29.31 in Hg
Ae = 0.8829 in2

Rdg. ---	T3 (F)	Dome dP (in H2O)	Wf (LBO) (pph)	Wa (pph)	FAR
1	210.0	20.5	---	0.1226	0.00000
2	239.0	20.4	14.0	0.1197	0.03248
3	239.0	20.5	14.3	0.1200	0.03310
4	243.0	30.0	20.6	0.1448	0.03953
5	244.0	30.0	16.8	0.1447	0.03226
6	245.0	30.3	16.9	0.1453	0.03231
7	245.0	30.0	6.1	0.1446	0.01172
8	460.0	30.0	7.8	0.1266	0.01712
9	463.0	30.0	6.8	0.1263	0.01495
10	473.0	20.0	0.0	0.1026	0.00000
11	476.0	21.0	6.8	0.1050	0.01799
12	478.0	20.0	7.2	0.1023	0.01954
13	477.0	20.4	7.2	0.1034	0.01934
14	649.0	30.2	6.5	0.1156	0.01561
15	657.0	30.0	6.1	0.1149	0.01475
16	664.0	30.0	6.5	0.1145	0.01577
17	664.0	20.0	0.0	0.0935	0.00000
18	662.0	20.0	0.0	0.0936	0.00000
19	775.0	30.2	6.4	0.1096	0.01622
20	773.0	30.0	6.3	0.1093	0.01601
21	767.0	20.0	5.4	0.0895	0.01676
22	758.0	20.0	0.0	0.0898	0.00000
23	759.0	20.0	0.0	0.0898	0.00000
24	750.0	12.5	0.0	0.0712	0.00000

HSCT - LDI Jet - Mix Build #1, Test 5
Atmospheric Test Results

Pbarom = 29.5 in Hg
Ae = 0.8829 in2

Rdg. ---	T3 (F)	Dome dP (in H2O)	Wf (LBO) (pph)	Wa (pph)	FAR
1	82.8	19.3	12.5	0.1326	0.02619
2	83.7	19.5	13.3	0.1332	0.02775
3	85.5	29.0	12.5	0.1621	0.02142
4	86.5	29.5	13.1	0.1634	0.02228
5	260.0	20.0	9.1	0.1172	0.02157
6	255.0	20.1	9.0	0.1179	0.02121
7	279.0	30.0	15.9	0.1417	0.03118
8	283.0	29.3	17.3	0.1396	0.03442
9	281.0	29.2	17.7	0.1396	0.03523
10	445.0	30.4	15.5	0.1289	0.03341
11	452.0	30.5	15.9	0.1286	0.03435
12	448.0	20.6	8.8	0.1059	0.02308
13	453.0	20.6	9.1	0.1056	0.02393
14	776.0	30.3	9.5	0.1101	0.02397
15	781.0	30.0	11.7	0.1093	0.02973
16	765.0	20.1	7.1	0.0901	0.02190
17	763.0	20.0	7.2	0.0899	0.02224
18	740.0	12.0	5.0	0.0703	0.01975

HSCT - Jetmix Build #1 Pressure Test #1, Run #6

Pbaro = 29.47 in Hg Ae mix = 0.8829 in^2
Ae tot = 1.3302 in^2

RDG	Point	T3 (F)	Pt3 (psia)	Dome dP (psid)	Wf (pph)	Wa tot (pps)	Wa mixer (pps)	Immersion: 1.0 = Top 0.0 = Bot.	Combustion Efficiency (%) 1.000	0.872	0.747	0.502	0.249	0.125	0.000	Avg
1	2	239.0	15.7	0.88	36.9	0.2060	0.1368		41.92		47.62	50.44	64.73		76.83	56.31
2	1	256.0	15.7	0.93	27.0	0.2089	0.1386		80.65		77.53	73.25	68.82		72.24	74.50
3	10	464.0	60.4	3.09	73.3	0.6572	0.4362		85.44		89.61	90.80	90.81		93.06	89.94
4	11	503.0	61.7	2.95	83.7	0.6348	0.4213		76.16		90.58	91.90	93.43		92.80	76.16
5	12	455.0	61.0	3.09	97.3	0.6634	0.4403			76.53		90.12		88.78		85.14
6	20	647.0	63.0	3.00	61.5	0.6033	0.4004		85.11		87.11	94.98	99.09		99.46	93.15
7	21	635.0	62.5	2.95	71.4	0.5993	0.3978		78.70		80.82	89.67	98.79		99.71	89.54
8	32	900.0	62.0	3.00	43.0	0.5401	0.3585		99.52		99.39	99.45	99.60		99.82	99.56
9	33	908.0	60.5	3.24	50.2	0.5530	0.3671		97.10		98.30	99.01	99.66		99.90	98.79
10	34	895.0	62.9	3.05	57.6	0.5494	0.3646		94.90		92.07	95.59	99.35		99.92	96.27

HSCT - Jetmix Build #1 Pressure Test #1, Run #6 (Continued)

RDG	Point	Tflame	NOx Emissions (lb/1000 lb fuel)								Sample Fuel - Air Ratio							
		(R)	1.000	0.872	0.747	0.502	0.249	0.125	0.000	Avg	1.000	0.872	0.747	0.502	0.249	0.125	0.000	Avg
1	2	2805	0.28		0.28	0.26	0.36		0.57	0.35	0.05651		0.05202	0.04266	0.04558		0.05417	0.05019
2	1	2971	1.20		0.85	0.54	0.44		0.40	0.69	0.06742		0.06312	0.04311	0.03096		0.03155	0.04723
3	10	3323	4.06		4.43	2.64	2.04		2.75	3.18	0.07031		0.06085	0.04362	0.04152		0.04304	0.05187
4	11	3253	1.87		4.03	3.06	2.95		3.86	3.15	0.06796		0.06025	0.04524	0.04628		0.05290	0.05453
5	12	3682		2.03		1.90		0.61		1.51		0.06978		0.04385		0.03954		0.05106
6	20	3385	4.21		5.62	7.17	5.52		2.53	5.01	0.06134		0.07252	0.06046	0.04138		0.03160	0.05346
7	21	3568	2.49		4.34	6.31	7.17		5.01	5.06	0.06016		0.06979	0.06989	0.05143		0.04019	0.05829
8	32	3294	14.34		17.66	14.93	8.76		4.80	12.10	0.03495		0.04821	0.04464	0.03387		0.02716	0.03776
9	33	3511	13.52		16.26	15.76	9.96		4.60	12.02	0.04097		0.05300	0.05175	0.03808		0.02697	0.04215
10	34	3709	11.99		14.12	14.81	11.08		5.32	11.46	0.05083		0.07026	0.06313	0.04376		0.02828	0.05125

HSCT - Jetmix Build #6 Pressure Test #2, Run #1

Lcomb = 2.623 in
Ae mix = 0.8829 in^2
Ae tot = 1.3302 in^2
Pbaro = 29.27 in Hg
Adome = 18.77 in^2

RDG	Point	T3 (F)	Pt3 (psia)	Dome dP (psid)	Wf (pph)	Wa tot (pps)	Wa mix (pps)	Immersion: Top = 1.0 Bot. = 0.0	Combustion Efficiency (%) 0.7371	0.615	0.493	0.3662	0.2441	Avg	Tflame (R)
1	1	47	22.6	0.874	26.0	0.2884	0.1914		55.40	37.65	23.48	39.88	55.24	42.33	1510
2	2	47	21.8	0.884	30.6	0.2849	0.1891		49.19	31.32	19.82	36.53	51.65	48.06	1805
4	10	473	59.3	2.947	72.0	0.6323	0.4197		97.83	95.74	95.66	94.90	97.19	96.26	3539
5	11	456	60.9	3.040	83.3	0.6569	0.4360		94.16	90.35	87.20	86.53	88.53	89.36	3540
6	12	473	59.2	3.045	97.4	0.6422	0.4263		79.14	80.52	73.23	79.56	77.89	80.07	3590
7	10A	469	59.1	2.996	53.0	0.6379	0.4234		91.96	96.75	97.98	97.30	95.90	95.98	2959
8	10B	475	60.7	2.986	43.4	0.6433	0.4270		75.84	87.84	98.32	96.12	91.61	89.94	2535
9	32	942	59.8	2.942	42.9	0.5176	0.3435		99.62	98.99	95.12	97.99	99.60	98.27	3369
10	33	955	60.2	3.011	50.2	0.5229	0.3471		99.70	98.55	91.58	96.71	99.47	97.20	3615
11	34	960	60.6	3.045	57.7	0.5267	0.3496		99.61	98.77	86.19	92.64	98.96	95.17	3817
12	32A	943	60.7	3.001	34.8	0.5264	0.3494		98.72	99.34	97.95	99.11	99.52	98.93	3026
13	32B	953	57.8	3.011	30.4	0.5127	0.3403		97.69	98.90	99.14	99.42	99.22	98.88	2881
14	32C	963	60.8	3.035	26.2	0.5262	0.3492		94.94	98.18	99.45	99.42	98.88	98.18	2661
15	32D	965	59.6	2.947	21.7	0.5129	0.3405		91.70	95.38	99.48	99.06	98.27	96.78	2471
17	35	956	59.7	2.996	68.2	0.5193	0.3447		98.69	95.85	86.68	91.20	97.95	94.08	4140
18	20	654	59.2	3.045	61.0	0.5877	0.3901		99.38	98.05	93.83	93.77	97.58	96.52	3507
19	21	650	60.4	3.045	71.7	0.5947	0.3947		97.78	94.33	86.29	88.14	94.16	92.14	3674
20	20A	655	59.0	3.030	48.0	0.5851	0.3883		98.25	98.82	96.97	98.00	98.67	98.14	3125

HSCT - Jetmix Build #6 Pressure Test #2, Run #1 (Continued)

RDG	Point	NOx Emissions (lb/1000 lb fuel)						Sample Fuel - Air Ratio					
		0.7371	0.615	0.493	0.3662	0.2441	Avg	0.7371	0.615	0.493	0.3662	0.2441	Avg
1	1	1.65	1.73	1.58	1.58	0.99	1.51	0.01815	0.00379	0.00244	0.00976	0.05544	0.01791
2	2	1.25	0.94	0.53	1.14	0.94	0.96	0.02451	0.00485	0.00300	0.01146	0.05715	0.03554
4	10	3.55	3.82	4.60	3.69	3.03	3.74	0.05158	0.06063	0.06649	0.06400	0.05082	0.05870
5	11	6.02	4.01	3.44	3.19	3.97	4.13	0.06717	0.06949	0.07276	0.07297	0.06931	0.07034
6	12	2.81	2.60	3.14	2.55	2.39	2.70	0.07814	0.07851	0.07682	0.07959	0.07794	0.07820
7	10A	1.47	2.24	3.53	2.83	2.02	2.42	0.03436	0.04415	0.05656	0.05202	0.03810	0.04504
8	10B	1.09	1.41	2.83	2.24	1.53	1.82	0.02599	0.03336	0.04891	0.04175	0.03228	0.03646
9	32	6.07	8.04	11.00	8.81	7.08	8.20	0.02875	0.04246	0.06405	0.04971	0.03166	0.04332
10	33	7.65	9.13	10.19	9.11	8.76	8.95	0.03543	0.04776	0.07076	0.05586	0.03898	0.04976
11	34	14.72	11.21	9.16	11.32	14.72	12.73	0.04314	0.05241	0.07603	0.06830	0.05389	0.05875
12	32A	4.83	6.28	10.01	7.68	5.77	6.92	0.02218	0.03193	0.05433	0.03993	0.02839	0.03535
13	32B	3.70	5.11	8.79	6.45	5.12	5.84	0.01946	0.02645	0.04554	0.03429	0.02380	0.02991
14	32C	3.33	4.46	7.13	5.61	4.34	4.97	0.01573	0.02365	0.03979	0.03053	0.02253	0.02645
15	32D	3.04	3.51	5.65	4.40	3.74	4.07	0.01300	0.01898	0.03260	0.02563	0.01883	0.02181
17	35	22.23	13.12	8.39	9.76	16.85	14.27	0.05991	0.06623	0.07823	0.07298	0.06214	0.06790
18	20	7.81	6.22	5.95	5.97	8.82	6.95	0.05083	0.05645	0.06845	0.06744	0.06156	0.06095
19	21	10.67	7.45	4.79	5.14	8.36	7.28	0.06308	0.06793	0.07727	0.07500	0.06949	0.07055
20	20A	2.92	4.01	5.48	4.51	3.42	4.07	0.03388	0.04378	0.06140	0.05113	0.03580	0.04520

HSCT - Jetmix Build #7 Pressure Test #3, Run #1

Lcomb = 2.623 in
Ae mix = 0.8829 in^2
Ae tot = 1.3302 in^2
Pbaro = 29.31 in Hg
Adome = 18.76516 in^2

RDG	Point	T3 (F)	Pt3 (psia)	Dome dP (psid)	Wf (pph)	Wa tot (pps)	Wa mix (pps)	Immersion: 1.0 = Top 0.0 = Bot.	Combustion Efficiency (%) 0.737	0.615	0.493	0.366	0.244	Avg	Tflame (R)
2	10	439	61.1	2.96	73.4	0.6555	0.4351		96.16	95.57	99.11	99.23	98.18	97.65	3518
3	10A	435	59.2	3.06	65.0	0.6568	0.4359		98.21	98.17	99.05	97.60	90.86	96.78	3257
4	11	440	59.8	2.98	82.9	0.6497	0.4313		88.87	92.95	98.63	98.78	98.00	95.45	3718
5	35	929	61.7	2.96	62.3	0.5295	0.3514		86.64	89.01	97.70	98.23	97.20	93.76	3892
6	32A	944	60.1	3.07	35.2	0.5296	0.3515		99.84	99.68	99.67	99.68	97.75	99.32	3041
7	32B	948	56.7	3.00	30.6	0.5075	0.3368		99.67	99.72	99.75	99.42	96.64	99.04	2903
8	32C	955	57.0	3.03	25.8	0.5101	0.3385		97.63	99.51	99.71	97.38	93.16	97.48	2664
9	33	948	59.9	3.06	50.0	0.5267	0.3496		98.71	97.97	97.82	98.53	99.61	98.53	3618
10	34	940	61.0	2.95	57.7	0.5240	0.3478		95.05	93.24	95.33	97.18	98.01	95.76	3825
11	20	651	59.5	3.07	61.2	0.5924	0.3932		96.38	94.90	97.13	98.47	99.32	97.24	3514
12	20A	645	59.2	3.01	48.0	0.5863	0.3892		99.62	99.00	99.21	99.47	99.53	99.36	3139
13	20B	670	58.0	2.98	39.2	0.5715	0.3793		99.65	99.55	99.65	98.30	90.39	97.51	2843
14	20C	660	58.3	3.03	34.2	0.5803	0.3852		98.57	98.07	98.66	94.93	84.69	94.98	2585
15	2	256	22.3	0.86	31.3	0.2397	0.1591		42.83	13.31	9.61	30.51	57.50	30.75	1653
16	1	167	22.2	0.83	27.0	0.2512	0.1667		45.68	11.67	8.08	33.93	60.71	32.01	1482

HSCT - Jetmix Build #7 Pressure Test #3, Run #1 (Continued)

RDG	Point	NOx Emissions (lb/1000 lb fuel)						Sample Fuel - Air Ratio					
		0.737	0.615	0.493	0.366	0.244	Avg	0.737	0.615	0.493	0.366	0.244	Avg
2	10	5.13	3.66	3.24	2.95	3.04	3.61	0.06439	0.06336	0.05165	0.04995	0.04961	0.05579
3	10A	3.16	2.77	2.01	1.59	1.43	2.19	0.05414	0.05186	0.04341	0.04142	0.03972	0.04611
4	11	4.92	3.39	3.44	3.30	3.24	3.66	0.07380	0.06759	0.05459	0.05300	0.05371	0.06054
5	35	17.15	13.53	15.30	13.54	15.60	15.02	0.07400	0.07085	0.06124	0.05635	0.05794	0.06408
6	32A	3.57	4.94	6.27	4.61	3.12	4.50	0.02688	0.03613	0.04077	0.03197	0.02196	0.03154
7	32B	2.85	4.15	4.95	3.56	2.58	3.62	0.02416	0.03309	0.03687	0.02828	0.01971	0.02842
8	32C	2.05	2.73	3.18	2.43	2.11	2.50	0.02106	0.02802	0.03038	0.02402	0.01662	0.02402
9	33	9.99	11.89	13.33	11.15	8.13	10.90	0.05039	0.05528	0.05777	0.05202	0.04368	0.05182
10	34	20.96	17.10	14.15	13.78	17.11	16.62	0.06665	0.06885	0.06671	0.06051	0.05720	0.06398
11	20	11.20	8.38	7.20	6.07	6.51	7.87	0.06608	0.06706	0.06274	0.05614	0.05142	0.06069
12	20A	4.05	4.30	4.33	3.37	2.73	3.76	0.04542	0.04846	0.04700	0.04234	0.03740	0.04412
13	20B	1.98	2.79	2.74	1.85	1.56	2.18	0.03193	0.03990	0.04177	0.03264	0.02332	0.03391
14	20C	1.42	1.46	1.46	1.42	1.36	1.42	0.02846	0.03225	0.03294	0.02897	0.02051	0.02863
15	2	1.42	0.79	0.66	1.27	0.94	1.02	0.03289	0.01605	0.01493	0.02262	0.05735	0.02877
16	1							0.05600	0.02187	0.01369	0.01503	0.03280	0.02788

HSCT IMFH Configuration 4A Tested November 19-20, 1992
13 x 0.495" Diameter Mixer Tubes

Rdg.	Point	Inlet T (F)	Inlet P (psia)	Dome DP (psid)	Wf (pph)	Wa mixer (pps)	CO EI (g/kg)	HC EI (g/kg)	NOx EI (g/kg)	Sample Equiv. Ratio	Comb. Eff., %
5	300	943	60.66	3.00	156.5	0.86	578.80	72.58	10.42	0.838	81.78%
6	100	959	59.70	2.68	107.1	0.80	205.75	132.59	9.59	0.555	83.64%
7	200	956	60.49	3.28	115.3	0.89	260.26	101.49	9.79	0.571	85.06%
8	500	961	60.77	4.33	125.6	1.02	153.89	203.60	8.47	0.466	78.69%
10	600	958	61.77	3.89	136.5	0.98	251.86	94.76	9.85	0.597	85.85%
11	700	957	62.83	3.65	155.1	0.96	406.72	54.54	11.20	0.733	85.70%
15	113	1139	147.30	9.45	269.0	2.22	0.66	0.28	1.02	0.449	99.96%
17A	114	1138	146.40	7.20	326.1	1.93	3.46	0.12	5.19	0.569	99.91%
17B	114	1138	146.40	7.20	326.1	1.93	6.84	0.51	6.06	0.572	99.80%
18	115	1141	149.00	6.60	297.4	1.86	2.49	0.35	2.79	0.510	99.91%
19	116	1142	148.04	6.84	270.8	1.89	1.08	0.35	1.36	0.456	99.94%
20	117	1144	147.50	6.75	244.9	1.87	0.87	0.54	0.71	0.405	99.93%
21	118	1136	146.12	5.16	230.9	1.63	3.04	0.24	5.06	0.509	99.91%
22	119	1136	144.63	3.60	210.3	1.36	0.97	0.22	1.81	0.442	99.96%

HSCT IMFH Configuration 5A Tested March 25-26, 1992
13 x 0.495" Diameter Mixer Tubes

Rdg.	Point	Inlet T (F)	Inlet P (psia)	Dome DP (psid)	Wf (pph)	Wa mixer (pps)	CO EI (g/kg)	HC EI (g/kg)	NOx EI (g/kg)	Sample Equiv. Ratio	Comb. Eff., %
2	31	447	60.51	2.84	187.9	1.00	124.72	26.36	2.75	0.774	94.78%
11	21	453	59.08	2.52	176.5	0.92	284.04	72.00	3.13	0.898	87.07%
12	31	448	58.43	3.32	188.2	1.06	102.56	17.19	2.64	0.767	96.10%
4	43	646	62.67	2.87	174.6	0.92	25.51	0.31	5.22	0.733	99.37%
5	42	646	54.63	2.82	154.1	0.85	14.82	1.47	3.34	0.655	99.52%
6	41	646	59.49	3.24	135.3	0.95	62.70	67.79	0.84	0.525	92.63%
7	411	651	60.57	3.04	145.0	0.93	36.58	26.29	1.40	0.571	96.86%
8	44	643	60.17	2.94	185.7	0.92	73.77	0.60	6.15	0.819	98.21%
9	412	647	59.89	3.16	149.2	0.95	23.07	11.76	1.86	0.599	98.44%
13	53	951	58.98	3.41	144.6	0.86	11.26	0.55	6.47	0.644	99.69%
14	52	951	58.98	3.41	126.7	0.86	5.01	0.41	3.44	0.565	99.85%
15	51	951	58.72	3.25	109.5	0.84	2.17	0.34	1.26	0.482	99.92%
16	501	960	60.11	3.01	99.9	0.82	4.40	0.75	0.82	0.443	99.83%
17	50	947	60.68	2.89	91.7	0.81	26.17	16.89	0.99	0.427	97.92%
18	502	955	60.48	2.91	95.1	0.81	10.31	0.99	1.45	0.449	99.41%
19	503	947	61.25	3.04	93.3	0.83	18.93	7.88	1.00	0.429	98.87%
20	504	955	59.00	3.03	105.6	0.81	1.57	0.20	1.26	0.475	99.95%
21	511	950	59.71	2.91	115.0	0.80	2.79	0.11	2.48	0.523	99.93%
22	54	954	55.10	3.44	172.0	0.84	37.29	0.08	13.87	0.798	99.12%

HSCT IMFH Configuration 5B Tested July 16, 1992
13 x 0.495" Diameter Mixer Tubes

Rdg.	Point	Inlet T (F)	Inlet P (psia)	Dome DP (psid)	Wf (pph)	Wa mixer (pps)	CO EI (g/kg)	HC EI (g/kg)	NOx EI (g/kg)	Sample Equiv. Ratio	Comb. Eff., %
25	1	944	60.65	2.85	153.6	0.8	27.38	0.04	11.43	0.743	99.35%
26	3	958	60.55	2.85	123.5	0.8	4.49	0.27	2.58	0.578	99.87%
27	12	948	145.6	7.3	340.8	1.99	5.42	0.02	10.07	0.625	99.87%
28	13	943	145.99	7.3	281.8	1.99	1.27	0.01	2.14	0.524	99.97%
29	14	952	146.64	7.62	249.4	2.03	0.73	0.05	0.75	0.457	99.98%
30	15	953	146.21	7.64	217.2	2.03	42.42	22.47	0.46	0.401	97.05%
31	31	1187	145.61	7.16	291	1.82	5.44	0.03	12.8	0.594	99.87%
32	32	1197	144.41	7.75	264	1.88	2.48	0.02	5.6	0.528	99.94%
33	33	1188	146.11	7.41	221.8	1.85	0.63	0.01	1.79	0.445	99.98%
34	34	1188	147.32	7.3	189.4	1.85	0.12	0.02	0.64	0.377	100.00%
35	41	1170	248.23	11.38	350.6	3.01	0.21	0.01	1.11	0.426	99.99%

HSCT IMFH Configuration 6A Tested October 21-22, 1992
7 x 0.560" Diameter Mixer Tubes

Rdg.	Point	Inlet T (F)	Inlet P (psia)	Dome DP (psid)	Wf (pph)	Wa mixer (pps)	CO EI (g/kg)	HC EI (g/kg)	NOx EI (g/kg)	Sample Equiv. Ratio	Comb. Eff., %
8	434	649	57.03	3.73	117.7	0.78	17.68	9.42	1.45	0.586	98.77%
9	432	648	57.55	3.49	128.1	0.76	15.00	0.20	3.71	0.675	99.63%
10	431	643	58.34	3.30	137.4	0.75	44.58	0.38	5.88	0.753	98.92%
11	435	649	57.81	3.43	131.6	0.76	19.83	0.15	4.49	0.691	99.52%
12	436	644	57.57	3.60	123.1	0.78	12.28	1.71	2.23	0.619	99.56%
14	54	961	59.85	2.93	120.7	0.63	69.53	0.02	19.62	0.837	98.37%
15	55	960	58.86	3.31	107.1	0.66	15.89	0.01	14.52	0.689	99.63%
16	53	964	58.41	3.41	96.6	0.67	8.90	0.00	10.40	0.628	99.79%
17	52	958	58.67	3.27	87.1	0.66	7.54	0.02	11.97	0.616	99.82%
18	53	950	61.38	2.16	87.1	0.55	13.55	0.03	17.60	0.680	99.68%
19	52	948	60.86	2.20	69.8	0.55	1.54	0.02	4.09	0.517	99.96%
20	52	952	60.81	2.15	73.6	0.55	3.06	0.01	6.42	0.546	99.93%
21	51	957	59.62	2.54	59.8	0.59	1.38	0.05	0.83	0.405	99.96%
22	50	956	58.97	2.69	55.1	0.60	8.49	0.93	0.41	0.368	99.72%
23	500	958	56.58	3.62	78.9	0.68	1.51	0.02	1.83	0.468	99.96%
24	502	952	57.29	3.27	89.9	0.65	4.97	0.01	6.20	0.560	99.88%
25	499	954	55.73	3.84	71.2	0.70	3.63	0.20	0.66	0.406	99.90%
26	510	954	58.75	2.57	65.1	0.59	0.92	0.01	1.25	0.427	99.98%

HSCT IMFH Configuration 6B Tested January 5, 1993
7 x 0.560" Diameter Mixer Tubes

Rdg.	Point	Inlet T (F)	Inlet P (psia)	Dome DP (psid)	Wf (pph)	Wa mixer (pps)	CO EI (g/kg)	HC EI (g/kg)	NOx EI (g/kg)	Sample Equiv. Ratio	Comb. Eff., %
5	310	441	49.44	2.60	133.2	0.68	204.07	142.79	1.12	0.731	82.80%
6	320	459	49.23	2.27	146.3	0.62	277.33	104.85	1.26	0.876	84.37%
7	43	656	59.48	3.00	130.7	0.72	75.49	20.18	2.34	0.758	96.47%
8	42	650	58.98	3.07	114.8	0.72	67.72	78.17	1.55	0.646	91.75%
9	41	656	58.94	3.01	100.7	0.71	80.12	148.10	1.41	0.553	85.24%
10	44	654	59.58	3.08	140.0	0.73	91.84	17.24	2.33	0.790	96.35%
11	53	962	60.11	2.99	101.8	0.64	15.45	3.93	3.54	0.656	99.30%
12	54	961	60.23	3.14	115.0	0.65	20.08	2.48	3.45	0.692	99.31%
13	52	964	60.64	2.97	89.1	0.64	13.99	5.37	2.57	0.563	99.20%
14	51	958	60.08	3.15	77.1	0.65	59.66	106.43	1.65	0.473	91.35%
15	55	959	60.93	3.02	130.3	0.64	61.87	1.10	4.00	0.811	97.87%
16	515	957	59.94	3.10	82.5	0.65	47.98	74.50	1.80	0.518	92.40%

Test Type	Lean Blow Out
Test Date	May 29, 1992
Test Location	Evendale ACL (Bldg 306)
Fuel-Air Mixer Type	Cyclone Swirler
Configuration	1
Mixer Effective Flow Area	0.646
Cooling Effective Flow Area	0.216 in^2
Dome Diameter	2.70 in
Combustor Pressure	14.47 psia

Rdg #	T in (R)	Dome Pres. Drop (%)	Fuel Flow (pph)	Mixer Air Flow (lb/sec)	F/A (Ratio)
$pt1_{i1}$	$t3r1_{i1}$	$dp\%1_{i1}$	$wf1_{i1}$	$wac1_{i1}$	$far1_{i1}$
1	721	7.07	14.9	0.0994	0.0416
2	732	7.09	15.3	0.0988	0.0430
3	735	7.09	15.2	0.0986	0.0428
4	735	4.87	11.0	0.0798	0.0383
5	735	4.75	11.0	0.0787	0.0388
6	918	4.75	9.1	0.0705	0.0359
7	925	4.75	10.4	0.0702	0.0412
8	926	4.75	10.4	0.0701	0.0412
9	935	6.97	12.0	0.0865	0.0385
10	933	6.97	12.0	0.0866	0.0385
11	1099	6.97	10.0	0.0798	0.0348
12	1112	6.97	10.2	0.0793	0.0357
13	1110	4.75	9.1	0.0641	0.0395
14	1110	4.75	9.1	0.0641	0.0395
15	1405	6.97	7.0	0.0706	0.0276
16	1385	4.98	7.0	0.0588	0.0330
17	1251	6.71	11.1	0.0732	0.0421

Test Type	Lean Blow Out
Test Date	September 22, 1992
Test Location	Evendale ACL (Bldg 306)
Fuel-Air Mixer Type	Cyclone Swirler
Configuration	2
Dome Effective Flow Area	0.73 in^2
Dome Diameter	4.84 in
Combustor Pressure	14.37 psia

Rdg #	T in (R)	Dome Pres. Drop (%)	Fuel Flow (pph)	Air Flow (lb/sec)	F/A (Ratio)
$pt2_{i2}$	$t3r2_{i2}$	$dp\%2_{i2}$	$wf2_{i2}$	$wac2_{i2}$	$far2_{i2}$
1	905	4.78	11.2	0.0894	0.0348
2	918	4.90	11.5	0.0899	0.0355
3	1082	4.74	12.1	0.0813	0.0413
4	1082	4.67	11.6	0.0807	0.0399
5	1093	7.01	12.2	0.1008	0.0336
6	1102	7.01	11.7	0.1004	0.0324

Test Type	Lean Blow Out
Test Date	January 19, 1993
Test Location	Evendale ACL (Bldg 306)
Fuel-Air Mixer Type	Cyclone Swirler
Configuration	2
Dome Effective Flow Area	0.73 in^2
Square Dome Side Length	3.505 in
Combustor Pressure	14.7 psia

Rdg #	T in (R)	Dome Pres. Drop (%)	Fuel Flow (pph)	Air Flow (lb/sec)	F/A (Ratio)
$pt3_{i3}$	$t3r3_{i3}$	$dp\%3_{i3}$	$wf3_{i3}$	$wac3_{i3}$	$far3_{i3}$
1	655	5.70	12.3	0.1185	0.0288
2	663	6.13	13.2	0.1227	0.0299
3	668	4.84	11.5	0.1071	0.0298
4	666	3.05	9.6	0.0836	0.0319
5	668	3.19	9.5	0.0854	0.0309
6	691	7.05	15.2	0.1302	0.0324
7	697	7.03	15.2	0.1294	0.0326
8	906	6.88	12.6	0.1121	0.0312
9	910	6.90	12.3	0.1121	0.0305
10	903	4.84	9.8	0.0921	0.0295
11	905	4.61	9.5	0.0897	0.0294
12	898	3.19	8.3	0.0737	0.0313
13	901	3.21	8.0	0.0739	0.0301
14	1045	6.86	10.4	0.1042	0.0277
15	1046	6.84	10.5	0.1040	0.0281
16	1032	5.59	9.2	0.0934	0.0274
17	1032	5.63	9.3	0.0938	0.0276
18	1032	5.52	9.4	0.0927	0.0282

Test Date	June 25, 1992
Test Location	Evendale ACL (Bldg 306E)
Fuel-Air Mixer Type	Cyclone Swirler
Configuration	1
Dome Effective Area	0.646 in^2
Cooling Effective Area	0.216 in^2
Dome Diameter	2.70 in
Length to Sample	7.0 in
Injector Flow Number	10
Traverse Points	4 to 9
Sample Average Type	Area-weighted

Rdg #	T in (R)	P in (psia)	P Comb. (psia)	Dome Pres. Drop (%)	Fuel Man. P (psia)	Fuel Flow (pph)	CO EI (g/kg)	HC EI (g/kg)	NOx EI (g/kg)	F/A Sample (Ratio)	Comb Eff. (%)
i	$t3r_i$	$p3_i$	$p4_i$	$dph\%_i$	pf_i	wf_i	$coei_i$	$hcei_i$	nox_i	far_i	$ce\%_i$
0	915.2	60.4	57.3	4.92	78.2	47.3	170.79	2.47	9.78	0.0514	95.77
1	916.7	59.5	56.5	4.91	71.6	43.7	0.3	0.72	1.56	0.0356	99.93
2	1113.0	61.1	58.0	4.90	72.2	42.0	25.12	0.96	13.41	0.0480	99.33
3	1424.0	59.5	56.5	4.87	67.4	37.3	2.54	0.2	4.83	0.0371	99.92
4	1410.3	59.1	55.9	5.07	74.2	47.9	18.55	0.08	21.32	0.0517	99.56
5	1416.3	60.1	55.9	6.87	70.7	44.7	3.91	0.05	5.08	0.0390	99.9
6	1418.0	60.0	55.8	6.79	82.3	60.5	23.16	0.04	22.24	0.0540	99.45
7	1416.9	60.7	56.6	6.80	98.4	76.0	197.91	0.03	20.97	0.0703	95.35
8	1413.1	59.2	54.8	7.64	64.2	34.6	1.28	0.29	2.2	0.0330	99.94
9	1406.1	60.5	55.9	7.47	65.9	34.6	1.28	0.29	2.2	0.0330	99.94

Test Date	March 4, 1993
Test Location	Evendale Cell A5
Fuel-Air Mixer Type	Cyclone Swirler
Configuration	2
Dome Effective Area	0.73 in^2
Dome Diameter	3.67 in
Length to Sample	4.5 in
Injector Flow Number	7.1
Traverse Points	4
Sample Average Type	Area-weighted

Rdg # i	T in (R) $t3r_i$	P in (psia) $pt3_i$	P Comb. (psia) $p4_i$	Dome Pres. Drop (%) $dp\%_i$	Fuel Man. P (psia) pf_i	Fuel Flow (pph) wf_i	CO EI (g/kg) $coei_i$	HC EI (g/kg) $hcei_i$	NOx EI (g/kg) nox_i	F/A Sample (Ratio) far_i	Comb Eff. (%) $ce\%_i$
6	1296	59.8	56.7	5.12	112.3	52.0	11.43	0.23	6.41	0.0446	99.71
7	1316	60.1	57.1	4.99	101.4	46.1	4.73	0.14	3.55	0.0407	99.88
8	1319	60.2	57.2	5.00	88.5	37.7	0.66	0.13	1.27	0.0335	99.97
9	1318	59.4	56.4	5.00	81.0	24.7	0.82	0.14	0.61	0.0287	99.97
10	1325	151.1	143.3	5.13	461.4	128.3	7.72	0.05	15.55	0.0479	99.81
11	1308	150.6	143.1	4.95	382.4	110.8	2.12	0.03	5.45	0.0403	99.95
12	1308	149.8	142.2	5.05	329.5	97.5	0.2	0.04	1.83	0.0330	99.99
13	1308	151.3	143.9	4.92	324.5	95.6	0.21	0.04	1.99	0.0334	99.99
14	1308	150.5	143.1	4.93	254.1	73.8	1.2	0.06	0.55	0.0268	99.97
15	1309	150.1	142.1	5.31	240.3	68.6	0.18	0.02	3.35	0.0250	99.99
16	1307	150.5	142.5	5.30	242.6	69.2	0.5	0.02	3.34	0.0250	99.99
17	1618	149.5	141.8	5.14	331.9	98.1	7.66	0.04	37.05	0.0425	99.82
18	1622	149.8	142.0	5.23	282.1	83.3	1.97	0.03	16.88	0.0346	99.95
19	1621	150.8	143.1	5.11	234.1	65.9	0.32	0.03	10.45	0.0280	99.99
20	1622	151.0	143.3	5.13	196.0	48.6	0.25	0.03	7.5	0.0197	99.99
21	1608	274.9	261.3	4.97	775.0	164.2	2.6	0.04	29.39	0.0390	99.94
22	1607	275.9	261.3	5.28	634.9	138.3	0.82	0.03	16.92	0.0330	99.98
23	1604	276.3	261.9	5.20	511.3	111.6	0.11	0.05	11.53	0.0257	99.99
24	1602	270.1	256.6	4.99	402.9	83.7	0.08	0.06	9.48	0.0202	99.99
25	1311	152.2	144.5	5.08	257.6	74.3	1.17	0.06	0.9	0.0265	99.97
26	1309	149.2	141.4	5.25	243.4	70.0	84.9	16.43	0.62	0.0238	96.58

Test Date	March 13, 1993
Test Location	Evendale ACL (Bldg 306W)
Fuel-Air Mixer Type	Cyclone Swirler
Configuration	2
Dome Effective Area	0.73 in^2
Dome Diameter	3.67 in
Length to Sample	7.0 in
Injector Flow Number	7.1
Traverse Points	4
Sample Average Type	Area-weighted

Rdg #	T in (R)	P in (psia)	P Comb. (psia)	Dome Pres. Drop (%)	Fuel Man. P (psia)	Fuel Flow (pph)	CO EI (g/kg)	HC EI (g/kg)	NOx EI (g/kg)	F/A Sample (Ratio)	Comb Eff. (%)
p_i	$t3r_i$	$pt3_i$	$p4_i$	$dp\%_i$	pf_i	wf_i	$coei_i$	$hcei_i$	nox_i	far_i	$ce\%_i$
1	910.5	61.5	58.7	4.68	99.5	53.5	1.25	0.15	2.06	0.0426	99.96
2	921.2	59.9	57.0	4.77	132.1	62.8	7.94	0.06	3.39	0.0501	99.81
3	912.3	60.7	57.7	4.96	150.8	70.3	43.64	57.43	5.01	0.0572	99.45
4	911.6	60.0	56.8	5.27	103.2	46.7	23.2	0.05	0.33	0.0376	93.98
5	911.0	59.3	57.4	3.15	106.3	48.3	5.27	1.51	3.78	0.0507	99.74
6	1319.5	60.9	56.7	6.91	102.0	46.0	1.62	0.39	2.69	0.0361	99.93
7	1331.9	60.5	57.4	5.11	100.7	45.7	4.68	0.2	4.78	0.0413	99.87
8	1305.1	60.3	57.2	5.12	91.3	39.0	1.3	0.14	2.61	0.0361	99.96
9	1324.5	60.4	57.2	5.31	82.8	32.5	1.66	0.16	1.4	0.0292	99.95
10	1322.5	60.5	57.5	5.06	76.0	26.5	40.91	14.37	0.77	0.0239	97.79
11	1299.5	59.9	58.0	3.12	79.5	30.3	1.14	0.25	2.88	0.0359	99.95

Test Date	November 12, 1992
Test Location	Evendale ACL (Bldg 306E)
Fuel-Air Mixer Type	Cyclone Swirler
Configuration	2
Dome Effective Area	0.73 in^2
Dome Diameter	4.84 in
Length to Sample	7.0 in
Injector Flow Number	9
Traverse Points	4
Sample Average Type	Area-weighted

Rdg #	T in (R)	P in (psia)	P Comb. (psia)	Dome Pres. Drop (%)	Fuel Man. P (psia)	Fuel Flow (pph)	CO EI (g/kg)	HC EI (g/kg)	NOx EI (g/kg)	F/A Sample (Ratio)	Comb Eff. (%)
i	$t3r_i$	$p3_i$	$p4_i$	$dpw\%_i$	pf_i	wf_i	$coei_i$	$hcei_i$	nox_i	far_i	$ce\%_i$
0	1358.7	60.1	56.7	5.22	86.9	53.4	9.91	0.49	16.52	0.0467	99.72
1	1359.1	60.0	56.7	5.13	82.4	48.9	6.57	0.29	9.47	0.0434	99.82
2	1347.1	60.1	56.7	5.34	79.8	45.8	18.15	0.21	43.56	0.0522	99.55
3	1356.0	60.8	57.4	4.99	80.0	45.6	23.49	0.17	52.23	0.0541	99.43
4	1357.1	60.2	56.8	5.28	74.6	39.2	5.84	0.17	12.54	0.0427	99.85
5	1370.6	60.8	57.6	5.17	72.3	35.4	3.33	0.2	7.74	0.0400	99.9
6	1361.0	60.4	57.2	4.91	69.7	32.0	1.22	0.15	3.39	0.0358	99.96
7	1353.9	60.6	57.2	5.17	69.8	31.8	1.52	0.11	4.12	0.0371	99.95
8	1364.2	60.6	57.5	4.91	68.1	29.6	0.67	0.08	2.24	0.0337	99.98
9	1356.2	60.0	57.0	4.87	65.9	27.4	0.01	0.09	0.16	0.0238	99.99
10	1353.0	60.3	57.0	4.94	64.3	23.9	52.91	14.06	0.05	0.0201	97.53

HSCT Multiple Venturi Configuration G1 with 4.89" Dome Height
7 Mixer Array with Injector Discharge 1/16 inch downstream of venturi throat
Tested November 25, 1992

Rdg.	Point	Inlet T (F)	Inlet P (psia)	Dome DP (psid)	Wf (pph)	Wa mixer (pps)	CO EI (g/kg)	HC EI (g/kg)	NOx EI (g/kg)	Sample Equiv. Ratio	Comb. Eff., %
3	15	52	60.72	3.87	79.6	0.49	17.25	1.75	1.51	0.711	99.44%
4	16	54	62.26	4.03	90.4	0.50	26.25	0.30	2.42	0.824	99.36%
5	13	55	60.30	3.10	94.3	0.43	203.32	2.46	3.13	0.988	95.01%
6	31	454	61.06	3.33	49.9	0.34	12.63	0.08	6.21	0.764	99.70%
7	32	448	59.99	3.18	55.1	0.33	18.51	0.06	6.79	0.802	99.56%
8	36	456	60.47	4.26	66.3	0.38	38.55	0.06	7.50	0.848	99.09%
9	40	654	59.93	3.28	36.1	0.30	1.36	0.06	2.67	0.558	99.96%
10	41	647	60.30	3.10	41.6	0.30	5.05	0.04	5.04	0.652	99.88%
11	42	653	60.57	2.94	46.9	0.29	12.20	0.05	9.45	0.741	99.71%
12	400	655	59.67	3.25	37.1	0.30	2.87	0.04	3.48	0.599	99.93%
13	401	644	59.58	3.23	33.2	0.30	0.71	0.05	2.35	0.517	99.98%
3A	15	52	60.72	3.87	79.6	0.49	18.15	1.43	1.92	0.746	99.45%
3B	15	52	60.72	3.87	79.6	0.49	13.79	1.41	1.45	0.698	99.55%
3B	15	52	60.72	3.87	79.6	0.49	23.40	2.37	1.58	0.728	99.24%
4	16	54	62.26	4.03	90.4	0.50	33.56	0.38	2.46	0.840	99.18%
5	13	55	60.30	3.10	94.3	0.43	259.88	3.43	2.95	1.017	93.60%
6	31	454	61.06	3.33	49.9	0.34	16.73	0.08	6.57	0.787	99.60%
7	32	448	59.99	3.18	55.1	0.33	22.96	0.05	6.77	0.817	99.37%
8	36	456	60.47	4.26	66.3	0.38	51.11	0.06	7.57	0.872	98.79%
9	40	654	59.93	3.28	36.1	0.30	1.73	0.06	2.69	0.568	99.95%
10	41	647	60.30	3.10	41.6	0.30	6.39	0.04	5.22	0.667	99.85%
11	42	653	60.57	2.94	46.9	0.29	14.55	0.04	9.69	0.756	99.66%
12	400	655	59.67	3.25	37.1	0.30	3.20	0.04	3.49	0.610	99.92%
13	401	644	59.58	3.23	33.2	0.30	0.94	0.04	2.35	0.524	99.97%

HSCT Multiple Venturi Configuration G2 with 3.67" Dome Height
7 Mixer Array with Injector Discharge 1/16 inch downstream of venturi throat
Tested December 8, 1992

Rdg.	Point	Inlet T (F)	Inlet P (psia)	Dome DP (psid)	Wf (pph)	Wa mixer (pps)	CO EI (g/kg)	HC EI (g/kg)	NOx EI (g/kg)	Sample Equiv. Ratio	Comb. Eff., %
1	150	39	60.78	4.43	73.2	0.53	156.33	85.13	1.57	0.605	88.93%
7	25	220	60.45	4.27	67.6	0.44	145.28	1.09	3.18	0.884	96.49%
8	26	245	60.84	4.32	77.3	0.44	466.77	4.37	2.85	1.048	88.66%
11	21	260	60.41	2.97	64.6	0.36	546.76	9.36	3.01	1.069	86.34%
12	35	454	60.26	4.40	50.1	0.39	28.29	0.08	3.93	0.735	99.33%
13	36	453	60.85	4.20	59.2	0.38	84.49	0.13	5.55	0.847	98.00%
15	352	453	58.90	4.63	45.8	0.39	16.14	0.59	2.66	0.635	99.57%
17	32	450	59.71	3.09	58.3	0.32	381.01	0.96	5.64	1.030	90.97%
18	46	684	60.78	4.01	52.3	0.33	13.84	0.04	4.90	0.703	99.67%
19	45	680	60.65	4.35	41.7	0.35	3.24	0.04	2.35	0.558	99.92%
20	451	671	60.53	4.14	45.2	0.34	5.14	0.04	2.98	0.605	99.88%
21	42	671	61.46	2.85	48.2	0.28	20.96	0.03	6.79	0.755	99.51%
22	41	681	60.22	2.97	41.7	0.29	7.18	0.02	4.27	0.646	99.83%
23	40	697	60.72	3.03	36.2	0.29	3.25	0.02	3.25	0.570	99.92%
24	52	856	60.29	3.14	35.2	0.27	4.34	0.04	4.60	0.575	99.90%
25	53	861	60.22	2.97	42.3	0.26	14.38	0.03	8.34	0.706	99.66%
26	51	863	59.98	3.25	31.9	0.28	2.18	0.03	3.79	0.518	99.95%
27	55	885	60.13	4.15	41.7	0.31	5.32	0.03	4.16	0.589	99.87%
28	56	888	60.26	4.26	51.5	0.31	21.31	0.03	8.92	0.747	99.50%
30	57	892	60.26	4.26	51.5	0.31	2.94	0.18	3.25	0.524	99.92%
1	150	39	60.78	4.43	73.2	0.53	197.17	112.04	1.61	0.587	85.63%
2	16	40	60.66	4.35	90.4	0.52	320.16	62.82	1.71	0.888	87.02%
3	11	41	60.55	2.90	76.2	0.43	131.73	9.32	2.30	0.874	96.10%
5	12	41	60.43	2.87	84.9	0.42	456.80	25.12	2.11	1.043	87.08%
6	111	41	60.47	3.03	79.7	0.44	185.83	10.81	2.35	0.927	94.69%
7	25	220	60.45	4.27	67.6	0.44	158.52	1.03	3.21	0.900	96.19%
8	26	245	60.84	4.32	77.3	0.44	489.57	4.56	2.79	1.057	88.10%
11	21	260	60.41	2.97	64.6	0.36	559.64	10.23	3.02	1.080	85.97%
12	35	454	60.26	4.40	50.1	0.39	34.16	0.08	4.17	0.760	99.19%
13	36	453	60.85	4.20	59.2	0.38	100.83	0.14	4.68	0.871	98.62%
15	352	453	58.90	4.63	45.8	0.39	17.59	0.61	2.79	0.649	99.53%
17	32	450	59.71	3.09	58.3	0.32	406.20	0.91	5.64	1.046	90.38%
18	46	684	60.78	4.01	52.3	0.33	15.23	0.04	4.93	0.713	99.64%
19	45	680	60.65	4.35	41.7	0.35	3.67	0.03	2.45	0.569	99.91%
20	451	671	60.53	4.14	45.2	0.34	5.64	0.03	3.06	0.616	99.87%
21	42	671	61.46	2.85	48.2	0.28	20.59	0.02	6.55	0.759	99.51%
22	41	681	60.22	2.97	41.7	0.29	8.02	0.02	4.30	0.654	99.81%
23	40	697	60.72	3.03	36.2	0.29	3.53	0.02	3.31	0.578	99.91%
24	52	856	60.29	3.14	35.2	0.27	5.14	0.02	4.66	0.585	99.80%
25	53	861	60.22	2.97	42.3	0.26	15.73	0.02	8.31	0.716	99.63%
26	51	863	59.98	3.25	31.9	0.28	2.46	0.02	3.91	0.529	99.94%
27	55	885	60.13	4.15	41.7	0.31	5.84	0.02	4.17	0.596	99.86%
28	56	888	60.26	4.26	51.5	0.31	23.09	0.02	8.86	0.753	99.55%
30	57	892	60.91	4.17	36.4	0.31	3.36	0.18	3.29	0.532	99.91%

10.0 APPENDIX B: GE CR&D FINAL REPORT

FINAL REPORT

Laser Diagnostics at CR&DC

Sub Task II
Task No. 5
Contract NAS3-25951
Advanced Engineering Technologies

Aero-Propulsion Technology (APT) Program

Prepared
by

Anil Gulati

at

GE - Corporate Research & Development Center
Schenectady, N.Y.

SUMMARY

The non-intrusive laser-based diagnostic technique of Spontaneous Raman/Rayleigh scattering has been successfully extended to elevated pressures to measure the scalar flowfield downstream of a single IMFH (Integrated Mixer Flame Holder) tube at elevated pressures of upto 150 psig (10 atm.). This study represents the first practical application of Raman\Rayleigh scattering at elevated pressures. A single IMFH tube is mounted in a 8" combustion tunnel with large optical access built specifically for this purpose. Detailed measurements of mean and rms of temperature and major species are made at three axial locations downstream of the burner exit in a premixed flame region with liquid fuel (both kerosene and Jet-A) to demonstrate the enhanced capabilities of the technique. Provision is made to account for laser-induced fluorescence and flame generated luminescence anticipated in this application. Measured data, however, shows that under the conditions examined in this study i.e. of lean premixed combustion with significant pre-heat of upto 750 F; the interferences from laser-induced fluorescence and flame generated luminescence are minimal and are easily accounted for. The study is conducted in a simple jet-shaped flame downstream of a modified single IMFH arrangement. The results show the measured temperature and scalar profiles to be representative of flowfield established by premixed fuel\air jet issuing into recirculating product field downstream of the exit. The expertise and experience gained from this unique application is expected to be applicable to all such applications at elevated pressures. The major goal of the program to demonstrate the feasibility of such measurements has been successfully met.

Introduction

As the performance demands on current and planned advanced combustors (such as required for HSCT) increase in terms of the requirement for increased efficiency and reduced emissions new technology is needed both to meet the required goals and to verify\diagnose the actual performance of these devices. The problem is two-fold: (a) increased temperature limits of the combustion technique render physical probes such as thermocouples suspect and vulnerable to hardware damage. (b) the goal of reducing emissions such as NOx and CO places increased emphasis on minimizing fluctuations in fuel\air mixture fraction ratios and providing a means to measure such unsteadiness in the flowfield. It is believed that rms fluctuations in fuel-air mixture ratios in lean premixed combustion (such as being developed for HSCT) can result in huge increases in NOx formation even with a lean fuel\air mixture on the average. The reason for this is the exponential (non-linear) dependence of NOx formation rate on the local mixture ratio. Physical probes such as thermocouples and gas sampling probes can only measure mean quantities and are unsuitable for the task at hand. New advanced diagnostics are, therefore, needed to provide measurement capabilities for mean and rms scalar field in the combusting region. The advanced diagnostic technique of Spontaneous Raman\Rayleigh used in this study meets all these requirements and in addition possesses excellent spatial and temporal resolution capabilities.

Thus far the applications of advanced diagnostics to practical combustion systems have been far and few. At GE-CR&DC the diagnostic technique of Raman\Rayleigh has been developed over a number of years to measure temperature and major species in laboratory scale flames of H_2 and $CO\backslash H_2\backslash N_2$ mixtures. Current emphasis has been to extend the Raman\Rayleigh technique to full scale hardware with practical fuel (i.e. liquid) at elevated pressures for direct applications to combustion hardware such as in this application. Some of the recent advances and applications include extension of Raman scattering to sooty fuel-rich regions of bluff-body stabilized hydrocarbon flames, F-120 combustor sector exit with both natural gas and liquid fuel (kerosene) and most recently to elevated pressures for this application. In this report the technique of spontaneous Raman\Rayleigh is described in brief and its extension to elevated pressures discussed. Further details about the experimental setup or the physics of the technique are available in Refs. 1-3.

Raman Set-Up

The joint Raman-Rayleigh diagnostic system used in this study is similar to that used in the past [2, 3] except for the modifications made to allow measurements in the harsh environment of a test cell where the sector assembly is located. The original Raman system consists of a Candela LFDL-20 flashlamp pumped dye laser that provides pulses of ~ 1 J in ~ 2 μs, within a 0.2-nm bandpass at 488.0 nm at 10 Hz. The laser has two 20-gallon dye circulating systems to allow continuous operation. The laser beam is approximately 1 cm in diameter and is focused by a 200-mm lens forming the probe volume. The Raman scattered light is collected at right angles by a specially designed achromatic 250-mm f/2 lens, collimated, and refocused onto the entrance slit of a 3/4-m Spex polychromator following a x3 magnification. The probe volume dimensions are approximately 0.3 mm x 0.3 mm x 0.6 mm. The collected light is then dispersed for detection at the exit plane by numerous RCA 4526 photomultiplier tubes located at appropriate locations (Fig. 1) for detecting anti-Stokes Raman scattering from N_2, Stokes vibrational Raman scattering from N_2, O_2, H_2, H_2O, CO, CO_2, and unburnt hydrocarbons (C-H bond) and Rayleigh scattering. The data from the photomultiplier tubes is collected by custom-designed sample and hold circuitry, which integrates the signal over a 2 μs window before and after the firing of the laser with an 8 μs interval. The differential voltages corresponding to the Raman signal minus the background are recorded for all the channels simultaneously using a Data

Translation 12-bit A/D board, Dell 333 based IBM-AT compatible system, and Global Lab data acquisition software. The signals are then corrected for electrical and other background errors corresponding to each channel, and after normalization, are corrected for the relative sensitivities of the photomultiplier tubes using custom written software. Typically, 200 measurements are made at every location although 2000 data points are also collected at some locations for statistical purposes. A schematic of the overall Raman system is shown in Fig. 2.

The Raman system described above has the inherent advantage of filtering any low-frequency (< 125 kHz), low intensity flame background emissions. This is due to the method of subtracting the background signal before the firing of the laser for every shot and subsequently recording only the differential signal as opposed to other integration methods. This system, however, is unable to correct for the high values of laser-induced fluorescence interference observed in the recirculation zone of a turbulent pure CH_4 flame stabilized by a bluff body in a low-speed combustion tunnel [4] because the fluorescence accompanies the Raman signal. It is believed to be due to soot precursors in the flame [5]. An extensive calibration procedure has been developed to account for this laser-induced fluorescence using a procedure similar to that described by Masri et al. [5] for diluted CH_4 flames. Initial studies of this fluorescence had showed that it is fairly broadband and correlates well throughout the measured spectra. The method used to correct for this fluorescence, in brief, is as follows: Two additional photomultiplier tubes termed ``$F_1$" and ``F_2" are added to the exit plane of the polychrometer at Raman free regions of the spectra at 535 and 578 nm between the O_2 and CO_2 and CH_4, and H_2O vibrational bands, respectively, as shown in Fig. 1 to account for and monitor this fluorescence. The system is then applied to a laminar CH_4 flame diluted with CO in a well-defined laminar flame combustor to obtain correction factors corresponding to all the major species. The combustor exit is a 38-mm-diameter tube with thin walls and has a 300-mm-long upstream section filled with screens followed by a honeycomb section for the last 75 mm of the exit. The combustor is installed in the low turbulence tunnel with large optical access. This facility has been used extensively in the past to study turbulent jet and bluffbody flames and is well described [2]. The visual flamefront is conical in shape and consists of a thin (2 to 3 mm) axisymmetric reaction zone, which initially appears blue in the vicinity of the burner exit and progressively becomes yellowish and sooty as it merges downstream. The total flame length is approximately 150 mm. The burner exit velocity is matched to the co-flowing air velocity. The modified Raman system with monitoring channels F_1 and F_2 is traversed through the flamefront 38 mm downstream of the burner exit in the blue region of the flame in steps of 1 mm. The resulting profiles represent the extent of fluorescence interference in all the channels.

Accounting for the laser-induced fluorescence discussed above is somewhat of an art because all of the species are affected to a different extent. Furthermore, the data reduction process is interactive rendering the process of obtaining correction factors for all the species iterative. In the process used here the correction factors for all the species are initially guessed; the data is then reduced after subtracting from the Raman signal for each species a value equal to the F_1 value multiplied by the correction factor for the species on a shot-to- shot basis. Depending on the shapes of the new profiles (obtained based on the corrected Raman signals), new correction factors are guessed to minimize the total error, in some gross manner, in the profiles for all the species and temperature. Temperature being obtained by the sum of mole fractions method is most affected by the choice of correction factors for the various species. More sophisticated methods to minimize total errors such as the least square method recommended by Dibble et al. [6] should yield similar results, albeit in a more rigorous manner. This procedure has been validated by taking extensive data in well known laminar flames where the actual profile can be predicted accurately. In the rest of the Raman data presented here these correction factors have been applied on a shot-to-shot basis to all the data. With kerosene fuel some minimal activity was observed in the F_1 and F_2 channels and the required corrections were found to be minimal.

The maximum value of F_1 recorded are less than one-tenth of those measured in the laminar CH_4/CO calibration flame discussed above.

Extension to Elevated Pressures

All of the above data for calibration and other purposes was obtained at atmospheric pressure. Most practical combustors such as the candidate combustor for HSCT operate at elevated pressures and therefore Raman measurements need to be extended to this regime. As a first step, a room temperature cell capable of withstanding pressures of upto 225 psia (15 atm.) with quartz windows for optical access was built. As the pressure increases the Raman signal is expected to increase linearly with pressure since it is proportional to the number density of the molecules of the species probed all else held constant. Figure 3 shows the measured Spontaneous Raman signal from both N_2 and O_2 present in room air to indeed increase linearly with pressure at upto 200 psig examined in this test. This confirms the linear dependence of Raman signal on pressure and also suggests improved S\N ratios at elevated pressures since the signal levels are much higher. Anticipated increase in the amount of soot at elevated pressures could adversely affect this signal-to-noise ratio. In this application no such adverse effect was observed, probably because it is a lean premixed flame.

High Pressure HSCT Combustor Rig

Figure 4 shows a schematic of the HSCT combustor rig built specifically for this task. The overall combustor assembly consists of an inlet section to uniformly distribute preheated air, a flange assembly to allow rapid mounting of the swirler\premixer hardware and hold the quartz liner separating the cooling air from the main combustion air, a test-section with three large optical quality fused quartz windows to allow optical access and a downstream end with a back pressure valve and cooling assembly. The combustor test-section is a specially designed 8" SS pipe with two 7" diameter (open area) quartz windows across from each other and a third 5.5" diameter window in the same plane. The quartz windows allow optical access in three directions for the Raman system and for any potential applications such as LV, PDPA, flow visualization etc.. The combustor rig can accommodate upto 4.7" diameter swirler\premixer assemblies. The rig is capable of operating at pressures of upto 225 psia (15 atm.) with pre-heated air of upto 1000 F. Provision has been provided for cooling air to enter the rig from both upstream and downstream ends to keep the test-section walls and the optical windows cool. The cooling-air is separated from the main combustion air by a quartz liner (not shown in the schematic). Water-cooling is also provided in the downstream end to keep the high temperature back pressure valve operational. The combustor is capable of operation with both gaseous (natural gas) and liquid (kerosene/Jet-A) fuels. Maximum flowrates are 1.5 lb/s for the main combustion air and 1.0 lb/s for the cooling air. A number of taps are provided along the combustor for mounting of pressure taps, thermocouples, ignitor etc. The plane of the windows is 9" from one end of the 24" combustor. This allows monitoring of the flame conditions over its complete length by switching the combustor side-to-side (symmetrical). Figure 5 shows photographs of the overall combustor, the Raman system and the details of the test-section.

The Raman system (schematic shown in Fig. 2) is mounted on a 3-D traversing table which is remotely operated. In addition to the modifications described earlier, for this application the Raman system had to be redesigned to result in the pulsed dye laser beam traversing the test-section in a horizontal manner through the two large windows. Due to the relatively small diameter of the traversing beam in the 7" diameter windows a large section of the combusting region can be probed with this arrangement. The scattered signal is collected by an air-cooled lens from the third window mounted on

top of the test-section. The light is then folded and passed into the entrance slit of the polychromator for further processing.

Application to IMFH Tube Exit

The IMFH tube used in this study consists of a single premixer tube based on the concept of a cluster of such tubes studied at GEAE. The tube is of 0.5" diameter, is approximately 5" long and is located symmetrically exiting in a dump plane consisting of a TBC coated SS plate of 4.72" diameter to fit into the combustor rig described above. The IMFH tube and dump plate etc. are provided by GEAE. To allow flame stabilization at the conditions of interest here the tube exit was modified by attaching a step to provide recirculation zone at the face plate as shown in Fig. 6. A small amount of H_2 was also provided in the recirculation zone to help better anchor the flame. A Delavan peanut nozzle aligned symmetrically with the axis of the tube facing downstream approximately 0.25" upstream of the tube inlet was used to supply Jet-A fuel. The operating conditions are a pressure drop across the tube of 6.5%, static pressure in the combustor of 158 psig, inlet preheat air temperature of 650 F and an estimated equivalence ratio of 0.34. There is cooling flow provided for the face plate which is taken from the main combustion flow (which is measured to be 0.65 lb/s) and therefore the equivalence ratio is an approximate value based on the fuel flow rate (21.2 pph) and estimated airflow through the premixer tube. At these conditions the flame appears jet like, extends approximately 5" downstream of the burner exit and is fairly steady. The flame, however, has some yellow streaks (is not completely blue) in the vicinity of the tube exit and is somewhat asymmetric to the eye with the bottom half of the jet flame visually appearing to be more stable and better anchored. Downstream of the exit the flame appears symmetric with a 2" wide turbulent flame brush of bluish-white color. Raman traverses are obtained in the vertical plane at three axial locations at 1", 3" and 6" downstream of the original tube exit.

Figure 7 (a, b) shows profiles of the mean normalized raw Raman data obtained at X = 1" for the major species i.e. H_2, H_2O, CO, CO_2, O_2, N_2, and CH containing species such as CH_4, C_2H_2, C_2H_6 and other higher hydrocarbons which are all lumped together. Figure 7c is the tabulated series of all the raw Raman data at various radial locations at this axial plane for all the species. These are average data based on 200 shots at every location. The interference from laser-induced fluorescence discussed above is maximum at this location (i.e. X = 1") compared to the downstream axial locations (X = 3", 6") and is shown in Fig. 7c in terms of measured voltage at F_1 and F_2 background monitoring channels. As can be seen, however, these interferences are minimal even at this location e.g. the peak value of F_1 of 0.132 Volts (data is shown x1000) is much less than the corresponding Raman signals of all species. At further downstream locations of X = 3" and 6" these values are much lower since the soot precursors probably burn up by then. This is confirmed by the fact that visually the yellow streaks in the flame are confined to the initial anchoring region. This does suggest, however, that the fuel\air mixture is not perfectly premixed which certainly cannot be ruled out at these operating conditions. The Raman signals at these conditions are much higher than those obtained in atmospheric jet flames. This is due to the elevated pressure of 158 psig. The noise represented by background scattered light and photomultiplier dark current is independent of pressure and remains low. The Raman signal/noise ratios are therefore considerably higher in this flame.

The raw Raman data shown in Fig. 7 is then reduced using standard correction procedures and 100% calibration gases to result in mean and rms quantities of temperature, mole fraction of major species and mixture fraction from the mole fractions. Instantaneous temperature is obtained from the Raman\Rayleigh data using two independent methods. The first method is an iterative scheme in which an initial temperature is guessed, based upon which the mole fractions of all major species are calculated

using their measured vibrational intensities. The mole fractions are then corrected using high temperature correction factors to account for changes in the fraction of the Raman band falling in the fixed exit slits of the respective photomultiplier tubes. The process is repeated until the sum of the mole fractions is unity. This iterative procedure converges in two or three iterations since the correction factors are relatively weak functions of temperature. An independent measurement of temperature is also obtained via Rayleigh scattering. In premixed flames the Rayleigh signal is directly proportional to density and therefore inversely proportional to the temperature via the equation of state. Data obtained showed reasonable agreement between the two procedures. All the temperature data presented here is based on the first method.

Figs. 8 through 10 show the data worksheets and the mean temperature and major species profiles for the three axial locations. As can be seen initially the jet of premixed fuel/air mixture close to the exit has a diffusion jet like structure with a valley in the temperature field at the centerline. The peak temperature is lower than the final equilibrium temperature. The major species show the expected trends. Since it is a lean premixed flame the concentration of Nitrogen does not vary much anywhere as expected. Oxygen deficit occurs in typical jet like fashion representing completion of combustion as the flame progresses downstream of the exit. The combustion products are more interesting. The profile of water (vapor) track the temperature field and is double peaked close to the exit but exhibits a typical well developed jet profile at x = 6" with a peak value of 7%. The temperature profile is also representative of a typical jet flame at this location. The peak temperature value is 2400 F. At x=6" the visible flame zone has already ended and the flow has equilibrated. The other major product species of CO_2 also shows similar trend. The maximum centerline value of CO_2 is 5%. The intermediate species in any hydrocarbon flame are CO and H_2 since that is the route by which most higher hydrocarbons burn. Figs. 8 - 10 again show the expected trends with there being measurable amounts of CO and H_2 in the initial regions of the flame as evidenced by the visible structure of the flame at x=1" and x=3". The blue color of the flame is in fact believed to be due to chemiluminescence arising from CO -> CO_2 reaction. By the furthest downstream location of x = 6" both CO and H_2 and unburnt hydrocarbons represented by the C-H species are less than 1% and are below the detection limits of the Raman system. This suggests very high combustion efficiency of the combustor of upto 99% at this location. The Raman system can measure major species accurately only for greater than 1% on an average basis. This data, however, clearly shows that the flame is representative of typical turbulent jet flame with an initial lean premixed fuel/air mixture representing the fuel. There is no evidence of any significant unburnt fuel downstream of this last measurement location. The data can be also expressed in terms of the mixture fraction depending on the element chosen. Based on 200 or more shots taken at every location statistics such as mean, rms, pdf etc. for all species can be obtained. The data (shown in part here) clearly shows that the Raman system has good S/N ratio at these operating conditions and there are no surprise interferences from any combustion intermediates, soot etc. in this lean premixed situation. Raman diagnostics are thus not only practical but represent a useful tool in diagnosing the flame structure and the temperature field.

One final Figure of interest is the rms temperature field at x= 1" measured using this system shown in Fig. 8e. This data cannot be obtained by any conventional means. The data again clearly shows the jet like structure of the flame with a double peaked profile for the normalized rms temperature field. The peaks represent the fluctuating edges of the flame front which are strained by the shear layer between the jet fuel/air mixture and the low velocity hot recirculating products. The rms temperature fluctuations diminish to low values at the edges of the turbulent jet as expected. Such data including rms profiles of major species can be readily obtained from the Raman shot-to-shot statistical data obtained at every location. Spectral data, however, cannot be obtained due to the limiting firing rate of the pulsed dye laser of 5 Hz used in this study. These results represent the first application of Spontaneous Raman scattering to high pressure combusting system.

References

1. Eckbreth, A.C., "Laser Diagnostics for Combustion, Temperature and Species", Energy and Engineering Science Series, Ed. by A.K. Gupta and D.G. Lilley, The Abacus Press, 1988.

2. Gulati, A., "Measurements of Scalar Flowfield at Exit of Combustor Sector Using Raman Diagnostics", AIAA Paper No. 92-3350, presented at the AIAA/SAE/ASME/ASEE 28th Joint Propulsion Conference, July 6-8, Nashville, TN, 1992.

3. Correa, S.M. and Gulati, A., "Measurements and Modeling of a Bluff Body Stabilized Flame", Combustion and Flame, Vol. 89, No. 2, 1992.

4. Gulati, A. and Dibble, R.W., "Raman Measurements in a Bluff Body Stabilized Pure CH_4 Flame", in Preparation.

5. Masri, A.R., Bilger, R.W. and Dibble, R.W., Combustion and Flame, 73, 261, 1988.

6. Dibble, R.W., Starner, S.H., Masri, A.R. and Barlow, R.S., "An Improved Method of Data Acquisition and Reduction of Laser Raman-Rayleigh Scattering from Multispecies", Appld. Physics B Special Issue on Combustion Diagnostics, pp. 1727-1731, 1990.

Figure Captions

1. Location of Raman vibrational bands and polychromator exit slit maskings for all major species with respect to each other and C_2 bands. Location of fluorescence monitoring channels F_1 and F_2 is also shown in the Figure.

2. Schematic of the Raman system.

3. Raw Raman signals from N_2 and O_2 in room air as a function of pressure at room temperature.

4. Schematic of the HSCT combustor rig.

5. Photographs of the HSCT rig showing the laser beam and details of the test-section.

6. Schematic of the modified IMFH single tube mounted in the HSCT combustor rig.

7. Tabulated series and profile of raw Raman data at X= 1" from IMFH tube exit.

8. Reduced Raman data showing the mean temperature and major species profiles at X = 1"

9. Reduced Raman data showing the mean temperature and major species profiles at X = 3"

10. Reduced Raman data showing the mean temperature and major species profiles at X = 6"

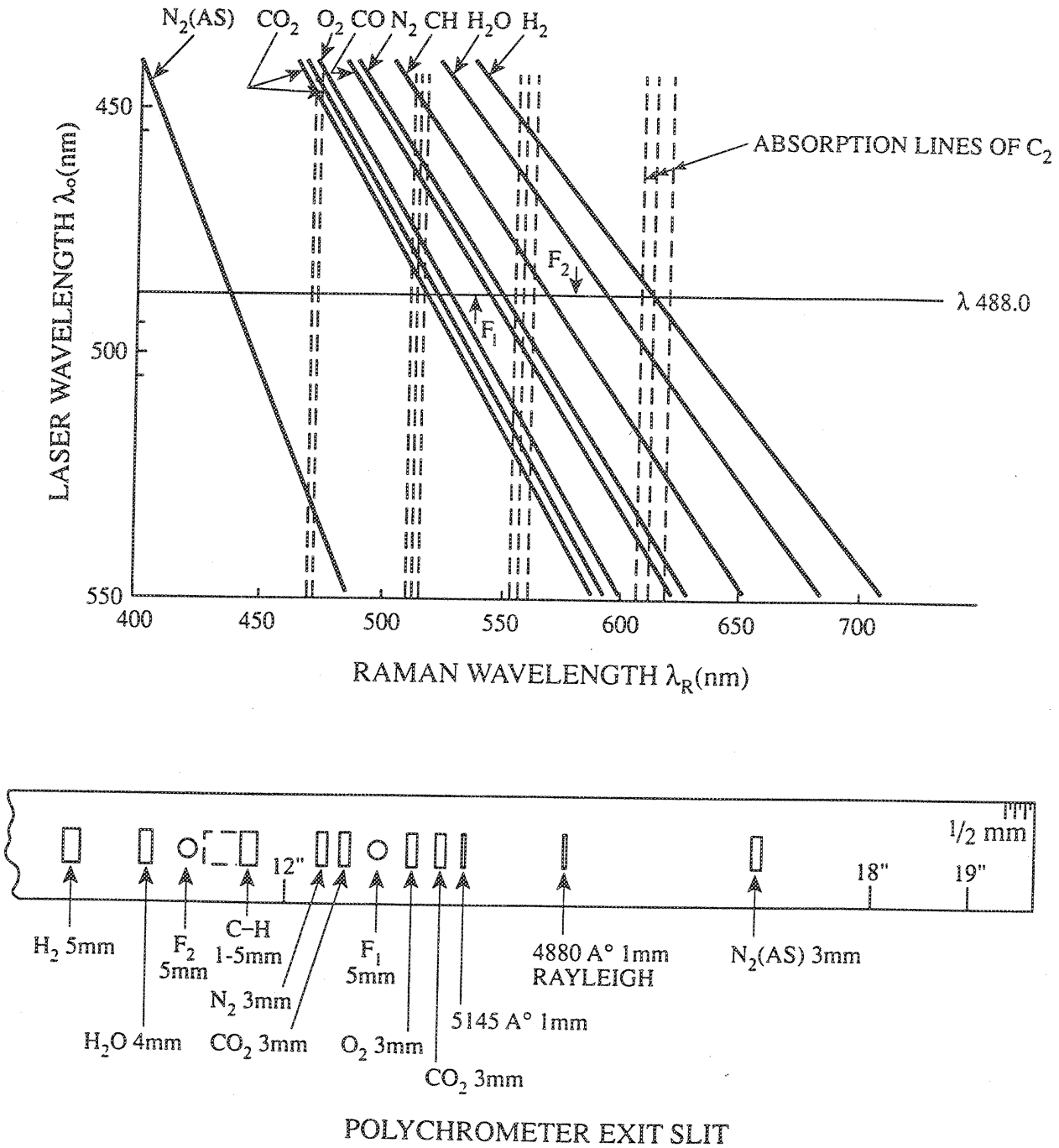
N2(AS)
CO2
O2 CO N2 CH H2O H2
ABSORPTION LINES OF C2
F2
F1
λ 488.0
LASER WAVELENGTH λo(nm)
450
500
550
400
450
500
550
600
650
700
RAMAN WAVELENGTH λR(nm)
1/2 mm
12"
18"
19"
H2 5mm
F2 5mm
C–H 1-5mm
N2 3mm
F1 5mm
4880 A° 1mm RAYLEIGH
N2(AS) 3mm
H2O 4mm
CO2 3mm
O2 3mm
5145 A° 1mm
CO2 3mm
POLYCHROMETER EXIT SLIT

Figure 1

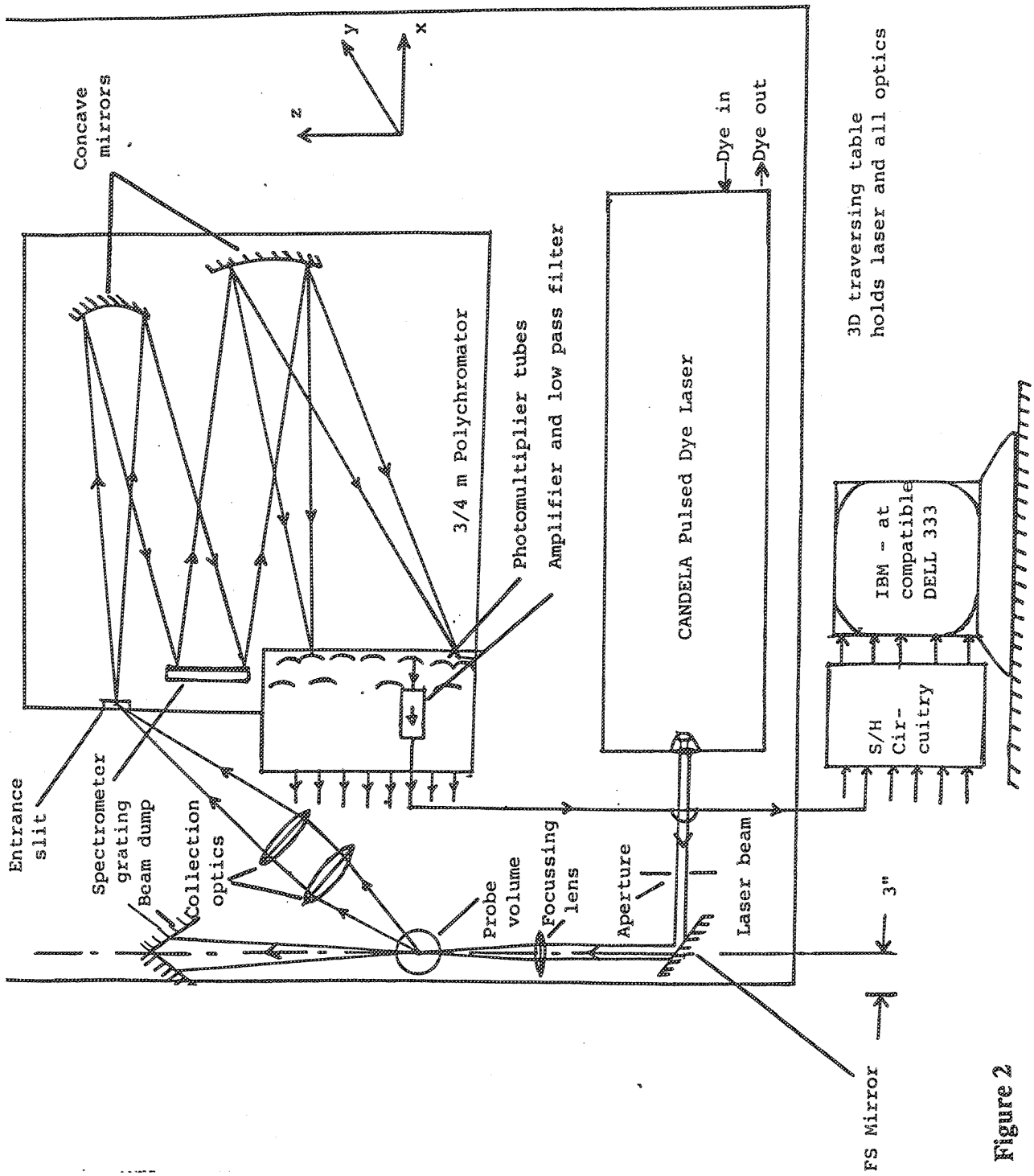
Concave mirrors
y
x
z
Dye in
Dye out
3D traversing table holds laser and all optics
3/4 m Polychromator
Photomultiplier tubes
Amplifier and low pass filter
CANDELA Pulsed Dye Laser
IBM - at compatible DELL 333
S/H Cir-cuitry
Entrance slit
Spectrometer grating
Beam dump
Collection optics
Probe volume
Focussing lens
Aperture
Laser beam
3"
FS Mirror

Figure 2

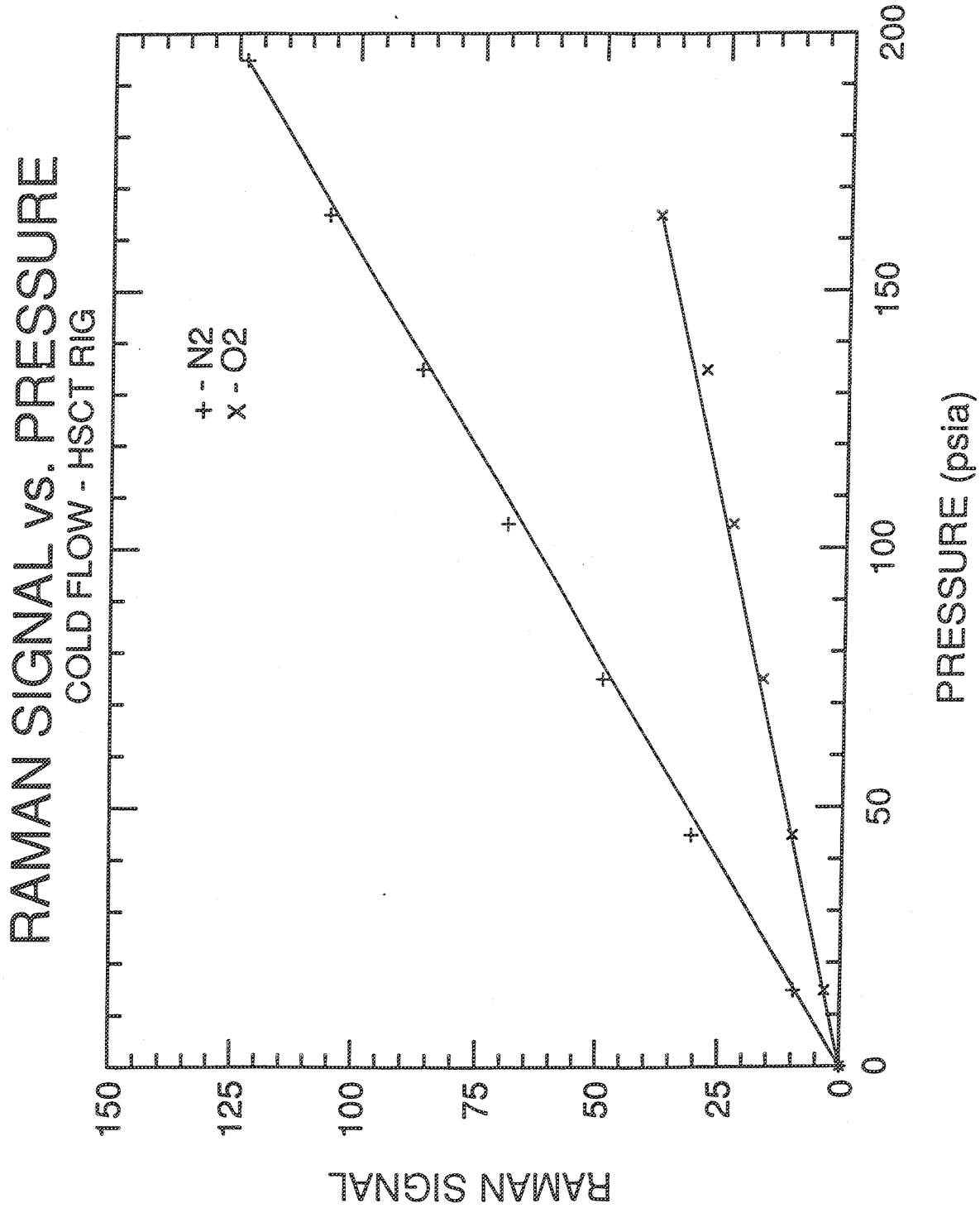
RAMAN SIGNAL vs. PRESSURE
COLD FLOW - HSCT RIG
+ - N2
x - O2
RAMAN SIGNAL
150
125
100
75
50
25
0
0
50
100
150
200
PRESSURE (psia)

Figure 3

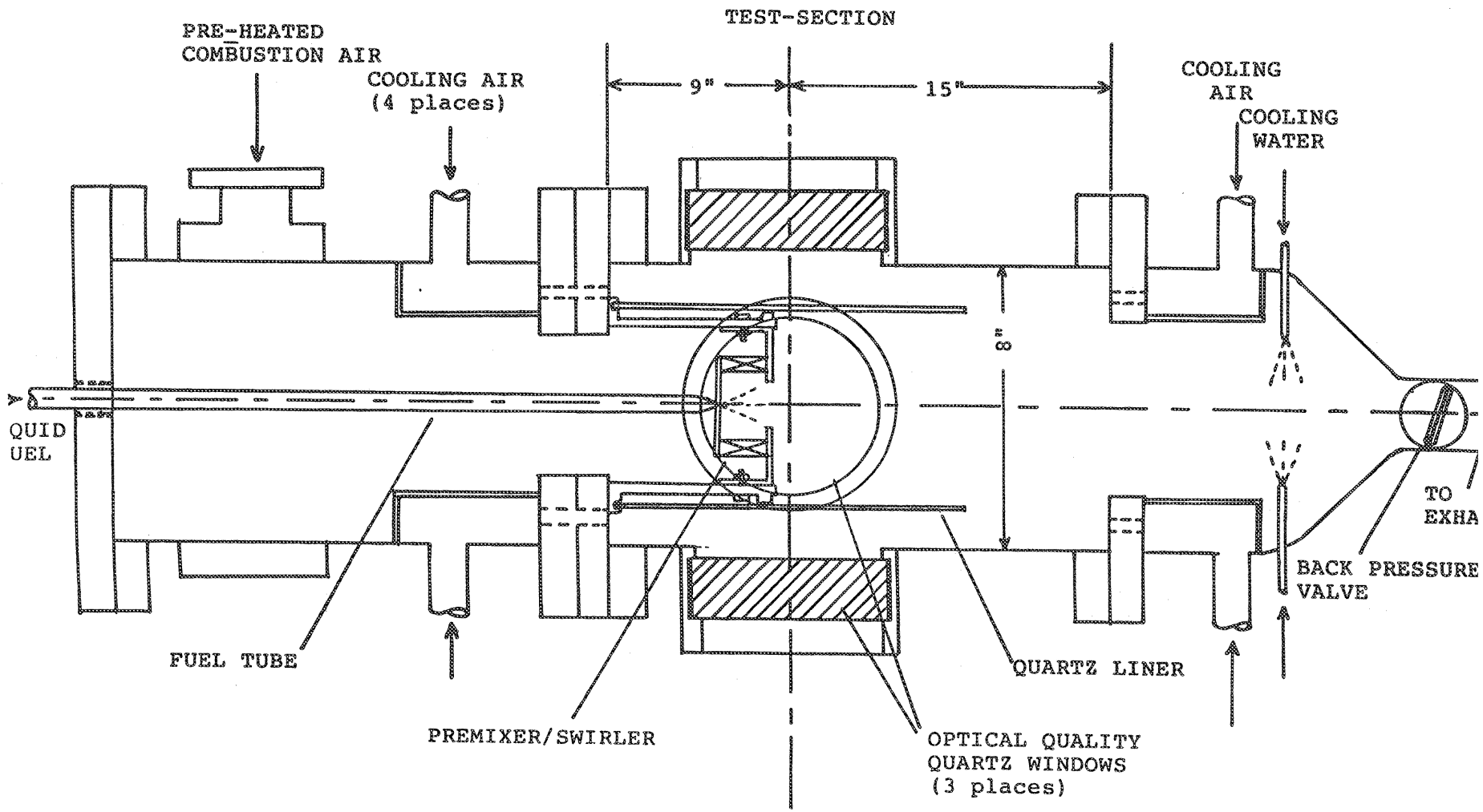
TEST-SECTION
PRE-HEATED
COMBUSTION AIR
COOLING AIR
(4 places)
9"
15"
COOLING
AIR
COOLING
WATER
8"
QUID
UEL
TO
EXHA
BACK PRESSURE
VALVE
FUEL TUBE
QUARTZ LINER
PREMIXER/SWIRLER
OPTICAL QUALITY
QUARTZ WINDOWS
(3 places)

Figure 4

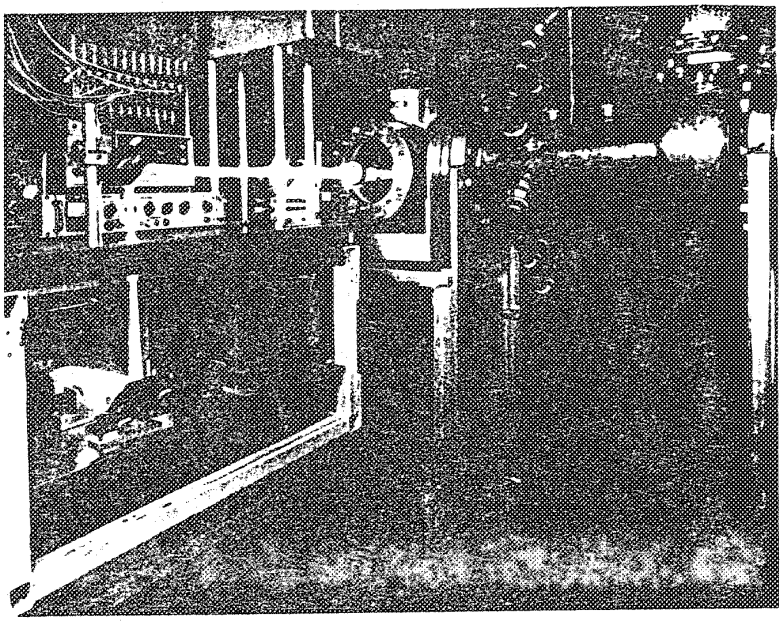

(a)

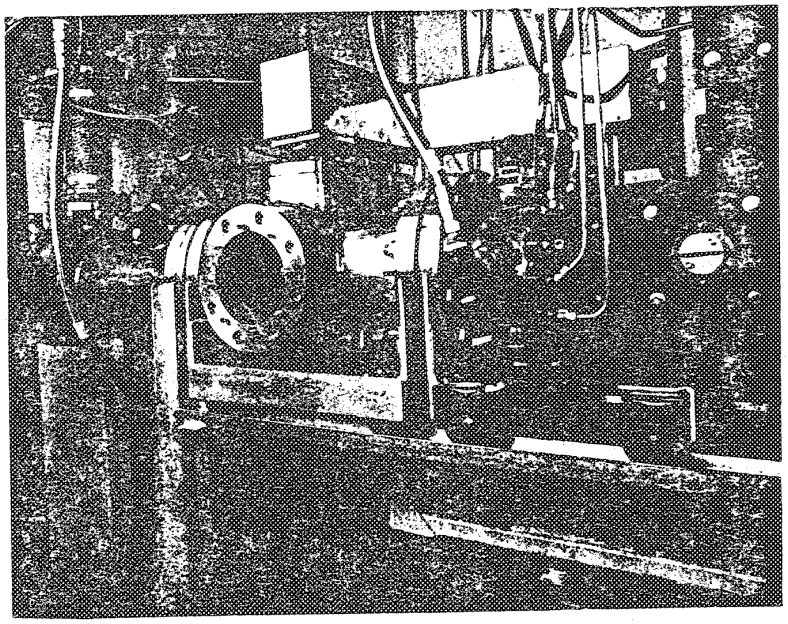

(b)

Figure 5

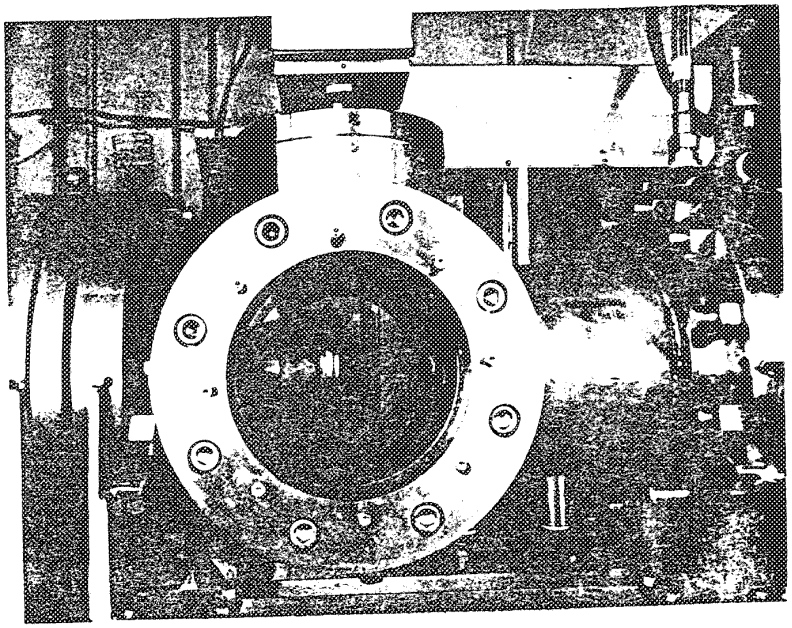

(c)

Figure 5

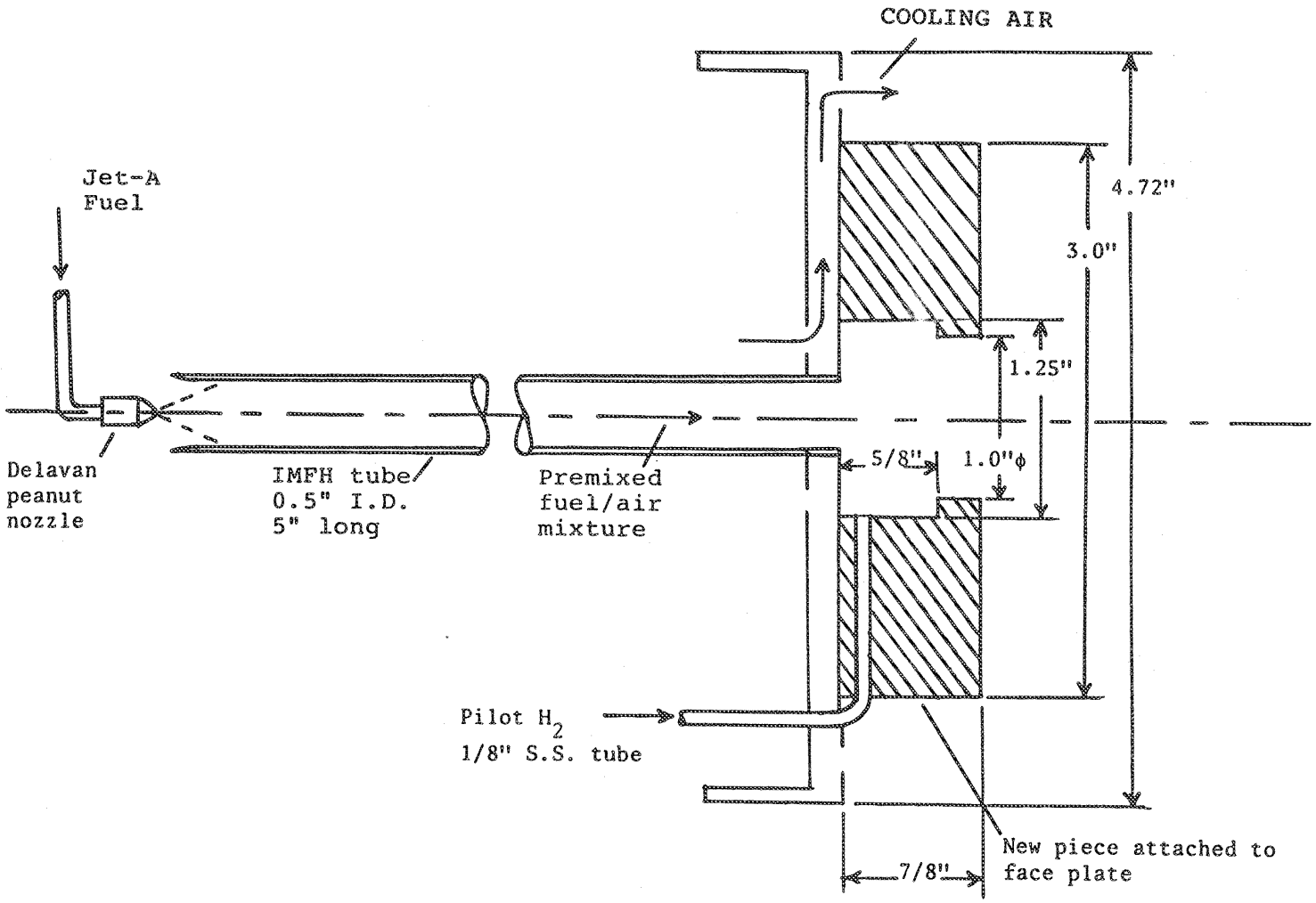
COOLING AIR
Jet-A
Fuel
4.72"
3.0"
1.25"
5/8"
1.0"ϕ
Delavan
peanut
nozzle
IMFH tube
0.5" I.D.
5" long
Premixed
fuel/air
mixture
Pilot H_2
1/8" S.S. tube
New piece attached to
face plate
7/8"

Figure 6

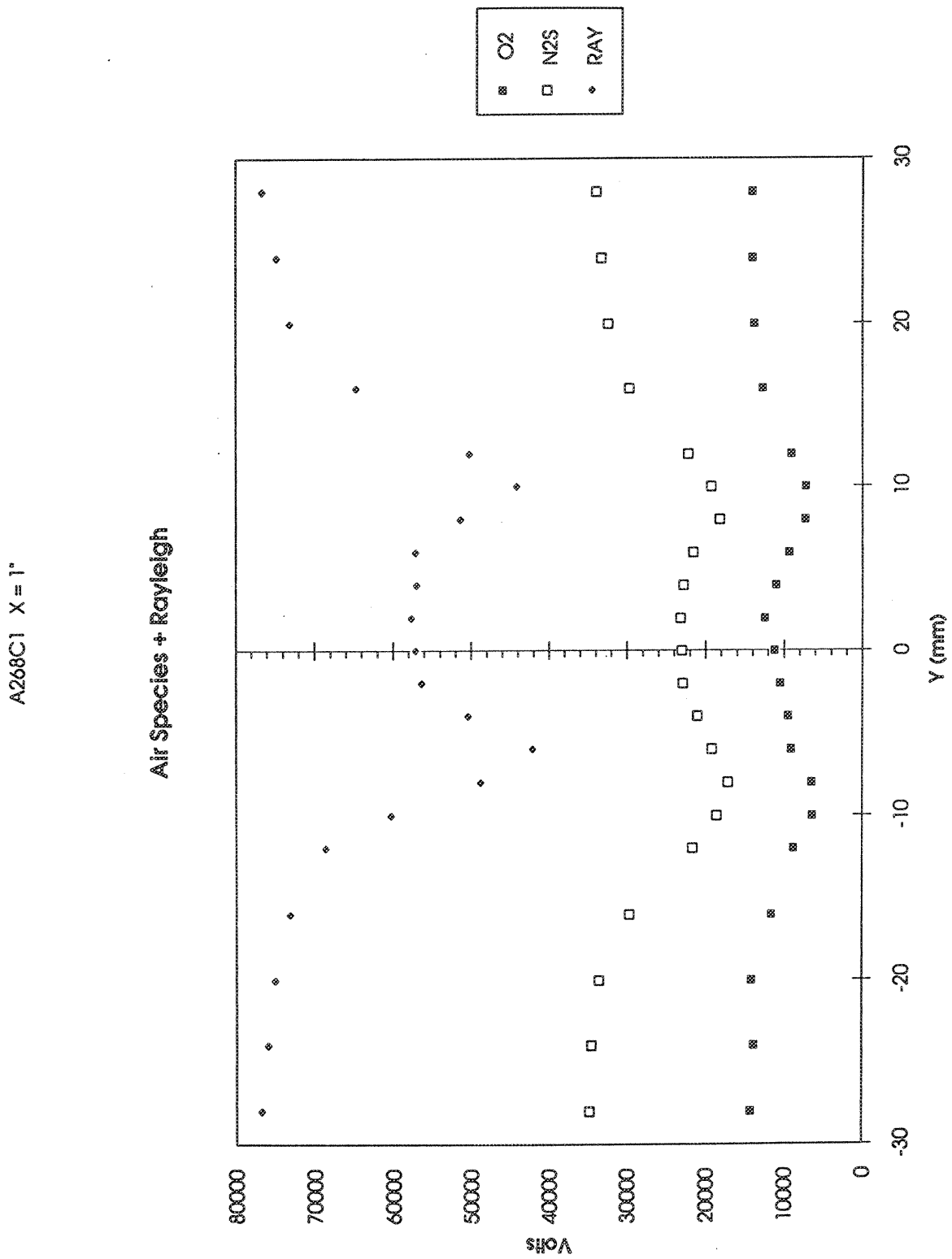
A268C1 X = 1"
Air Species + Rayleigh
O2
N2S
RAY
Volts
80000
70000
60000
50000
40000
30000
20000
10000
0
-30
-20
-10
0
10
20
30
Y (mm)

Figure 7(a)

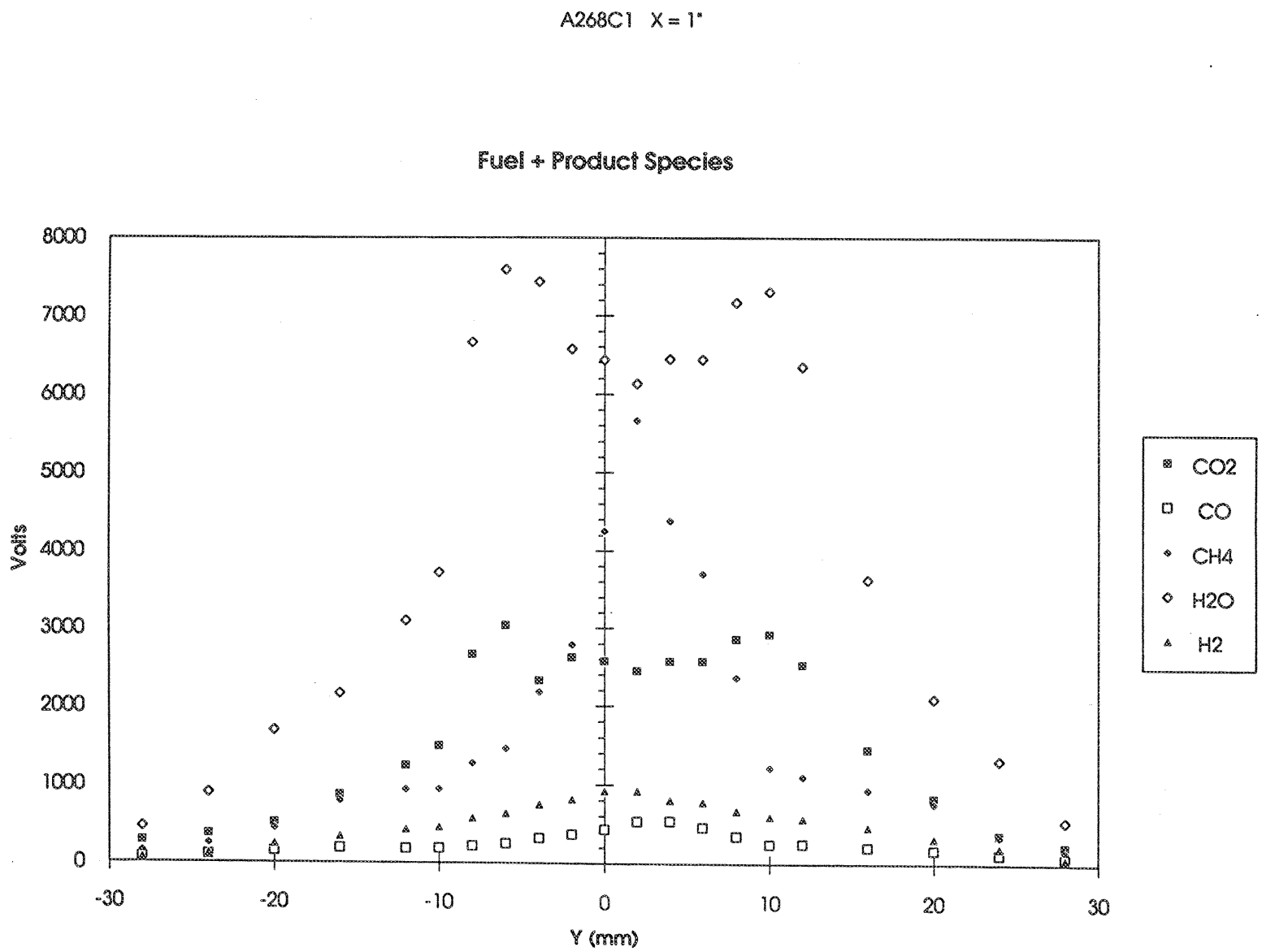
A268C1 X = 1"
Fuel + Product Species
Volts
8000
7000
6000
5000
4000
3000
2000
1000
0
-30
-20
-10
0
10
20
30
Y (mm)
CO2
CO
CH4
H2O
H2

Figure 7(b)

A268C1.WKS

NORMALIZED RAW RAMAN DATA X = 1°

FILE	Y(mm)	LE	CO2	O2	CO	N2S	CH4	H2O	H2	RAY	F1BG	F2BG
R268C3	-28	2554	280	14214	69	34761	143	457	69	76740	45	60
C4	-24	2513	368	13825	101	34500	246	887	121	75873	55	72
C5	-20	2451	512	14100	148	33569	439	1688	249	74987	76	97
C6	-16	2493	863	11561	186	29645	785	2158	342	73065	66	79
C7	-12	2496	1236	8800	182	21599	929	3090	434	68567	71	91
C8	-10	2434	1488	6400	186	18540	938	3719	466	60235	78	106
C9	-8	2439	2662	6454	217	17098	1265	6654	578	48778	102	128
CA	-6	2370	3036	9100	249	19139	1452	7589	637	42111	114	143
CB	-4	2535	2326	9431	317	21000	2175	7432	754	50399	89	113
CC	-2	2501	2627	10462	364	22860	2785	6567	817	56342	67	86
CD	0	2459	2573	11153	432	23015	4253	6433	926	57123	76	97
CE	2	2441	2452	12452	533	23165	5664	6131	923	57654	85	109
CF	4	2286	2576	10986	539	22810	4383	6441	810	56978	109	137
CG	6	2663	2574	9300	462	21558	3704	6436	788	57085	132	164
CH	8	2548	2866	7252	351	18189	2363	7166	679	51395	121	151
CI	10	2526	2922	7239	249	19250	1220	7305	609	44210	89	113
CJ	12	2455	2538	9044	252	22246	1108	6344	586	50236	49	65
CK	16	2475	1452	12726	210	29699	935	3631	476	64685	44	59
CL	20	2570	837	13819	172	32440	764	2093	328	73085	65	84
CM	24	2489	367	14025	123	33345	347	1315	212	74732	52	68
CN	28	2559	226	14100	76	33990	154	540	75	76628	49	65

Figure 7(c)

D268C1 - X = 1"

					REDUCED RAMAN DATA X = 1"					
	FILE	Y(mm)	T(F)	CO2	O2	CO	N2S	CH	H2O	H2
	R268C3	-28	734.2	0.001	0.210	0.000	0.780	0.000	0.005	0.000
	C4	-24	735.0	0.011	0.210	0.001	0.772	0.000	0.008	0.001
	C5	-20	879.0	0.002	0.220	0.002	0.775	0.002	0.010	0.002
	C6	-16	1009.0	0.004	0.205	0.003	0.765	0.003	0.025	0.003
	C7	-12	1218.0	0.006	0.186	0.004	0.772	0.001	0.032	0.004
	C8	-10	1424.0	0.010	0.167	0.005	0.774	0.002	0.041	0.004
	C9	-8	1654.0	0.014	0.129	0.006	0.770	0.005	0.045	0.005
	CA	-6	1865.0	0.020	0.130	0.007	0.760	0.010	0.060	0.007
	CB	-4	1765.0	0.017	0.144	0.008	0.765	0.012	0.050	0.007
	CC	-2	1476.0	0.014	0.160	0.009	0.770	0.012	0.040	0.008
	CD	0	1355.0	0.010	0.171	0.010	0.775	0.015	0.030	0.009
	CE	2	1209.0	0.008	0.167	0.010	0.770	0.018	0.035	0.011
	CF	4	1288.0	0.010	0.160	0.009	0.760	0.019	0.045	0.010
	CG	6	1401.0	0.015	0.140	0.006	0.760	0.015	0.050	0.007
	CH	8	1568.0	0.016	0.125	0.004	0.765	0.012	0.055	0.005
	CI	10	1744.0	0.014	0.132	0.003	0.773	0.010	0.053	0.004
	CJ	12	1665.0	0.010	0.142	0.002	0.780	0.006	0.040	0.004
	CK	16	1424.0	0.006	0.163	0.001	0.780	0.003	0.032	0.003
	CL	20	1119.0	0.002	0.190	0.000	0.790	0.002	0.026	0.002
	CM	24	865.0	0.001	0.200	0.000	0.790	0.000	0.009	0.001
	CN	28	755.0	0.001	0.210	0.000	0.790	0.000	0.005	0.000

Figure 8(a)

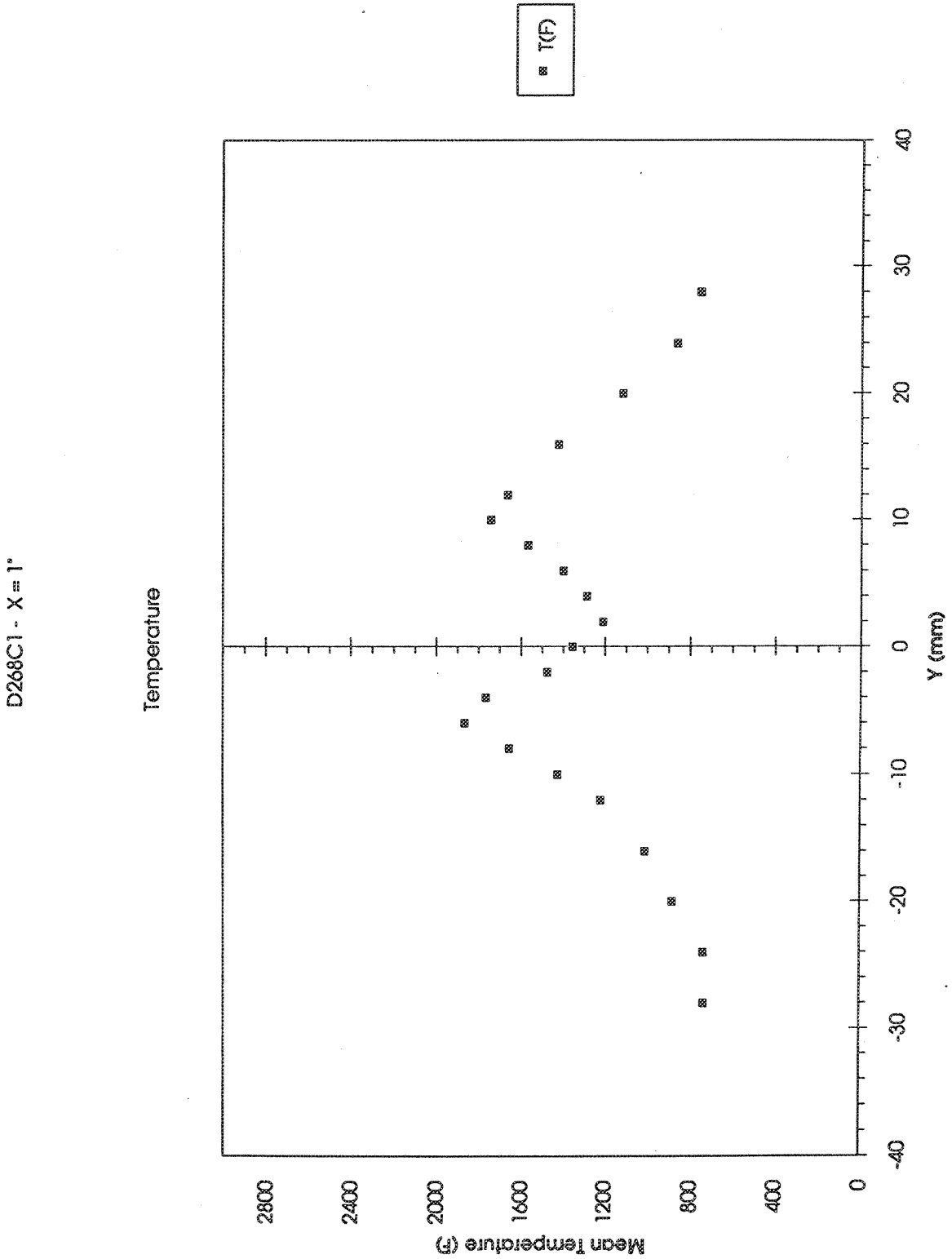
D268C1 - X = 1"
Temperature
T(F)
Mean Temperature (F)
2800
2400
2000
1600
1200
800
400
0
-40
-30
-20
-10
0
10
20
30
40
Y (mm)

Figure 8(b)

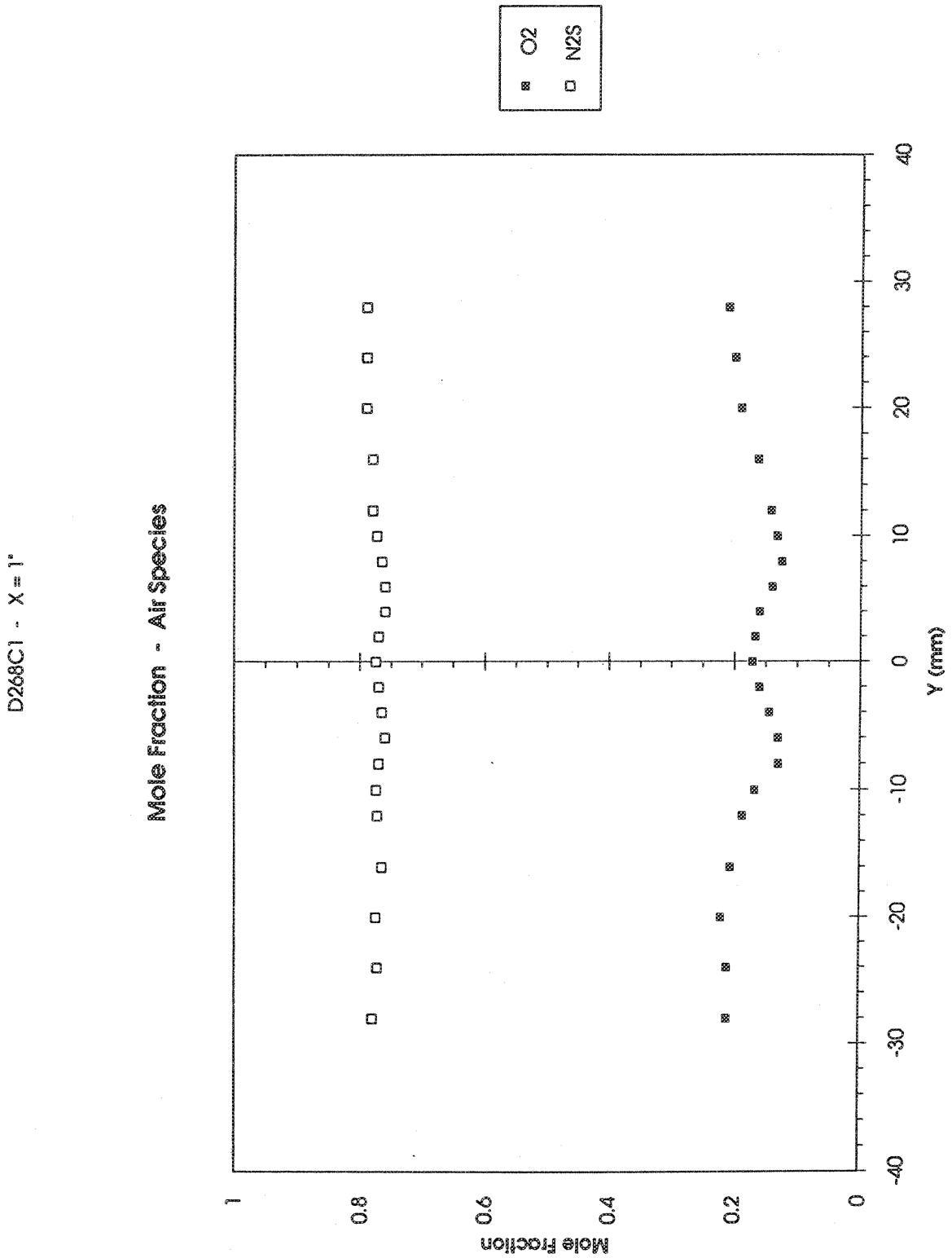
D268C1 - X = 1"
Mole Fraction - Air Species
O2
N2S
Mole Fraction
1
0.8
0.6
0.4
0.2
0
-40
-30
-20
-10
0
10
20
30
40
Y (mm)

Figure 8(c)

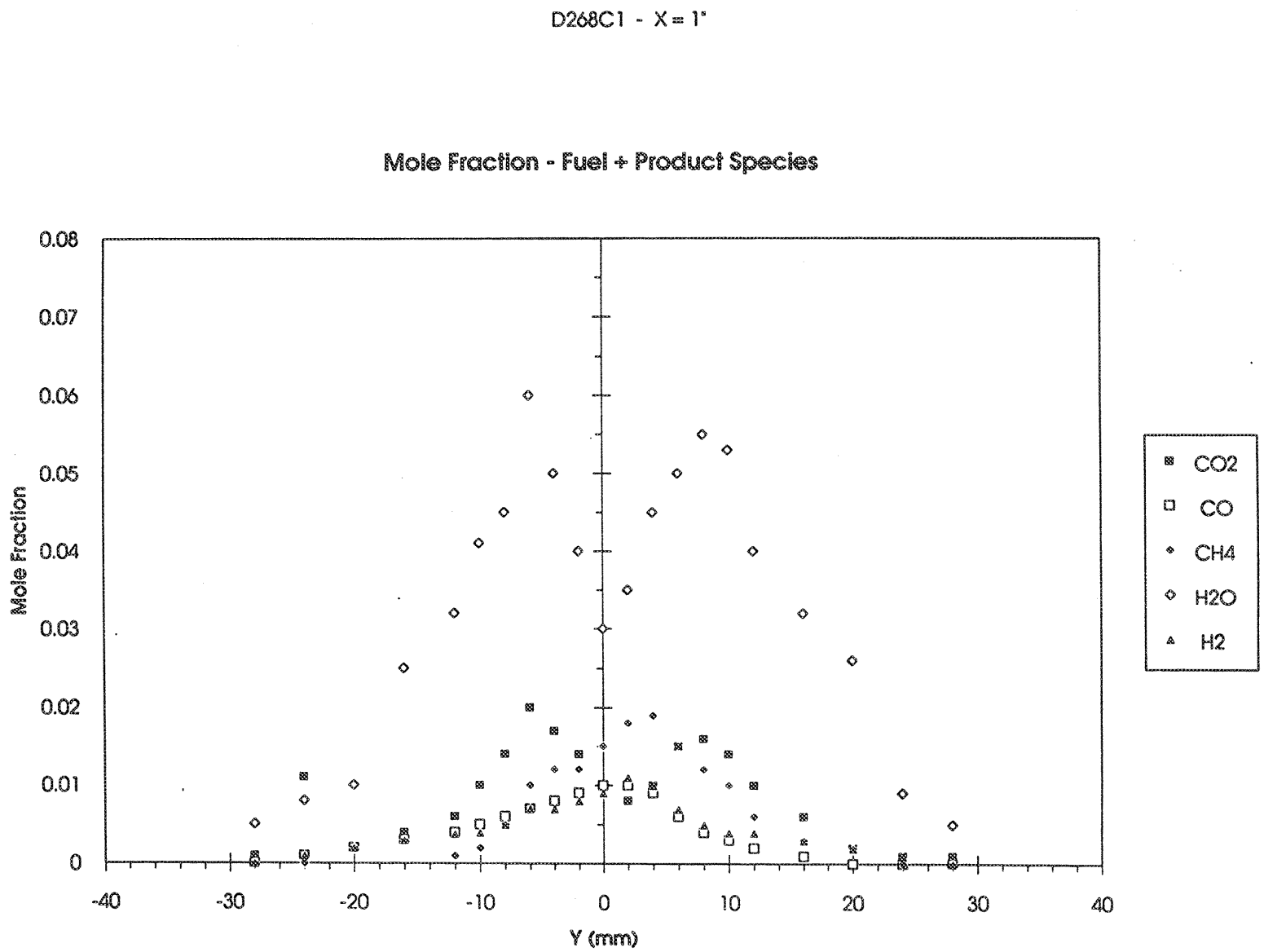
D268C1 - X = 1"
Mole Fraction - Fuel + Product Species
Mole Fraction
0.08
0.07
0.06
0.05
0.04
0.03
0.02
0.01
0
-40
-30
-20
-10
0
10
20
30
40
Y (mm)
CO2
CO
CH4
H2O
H2

Figure 8(d)

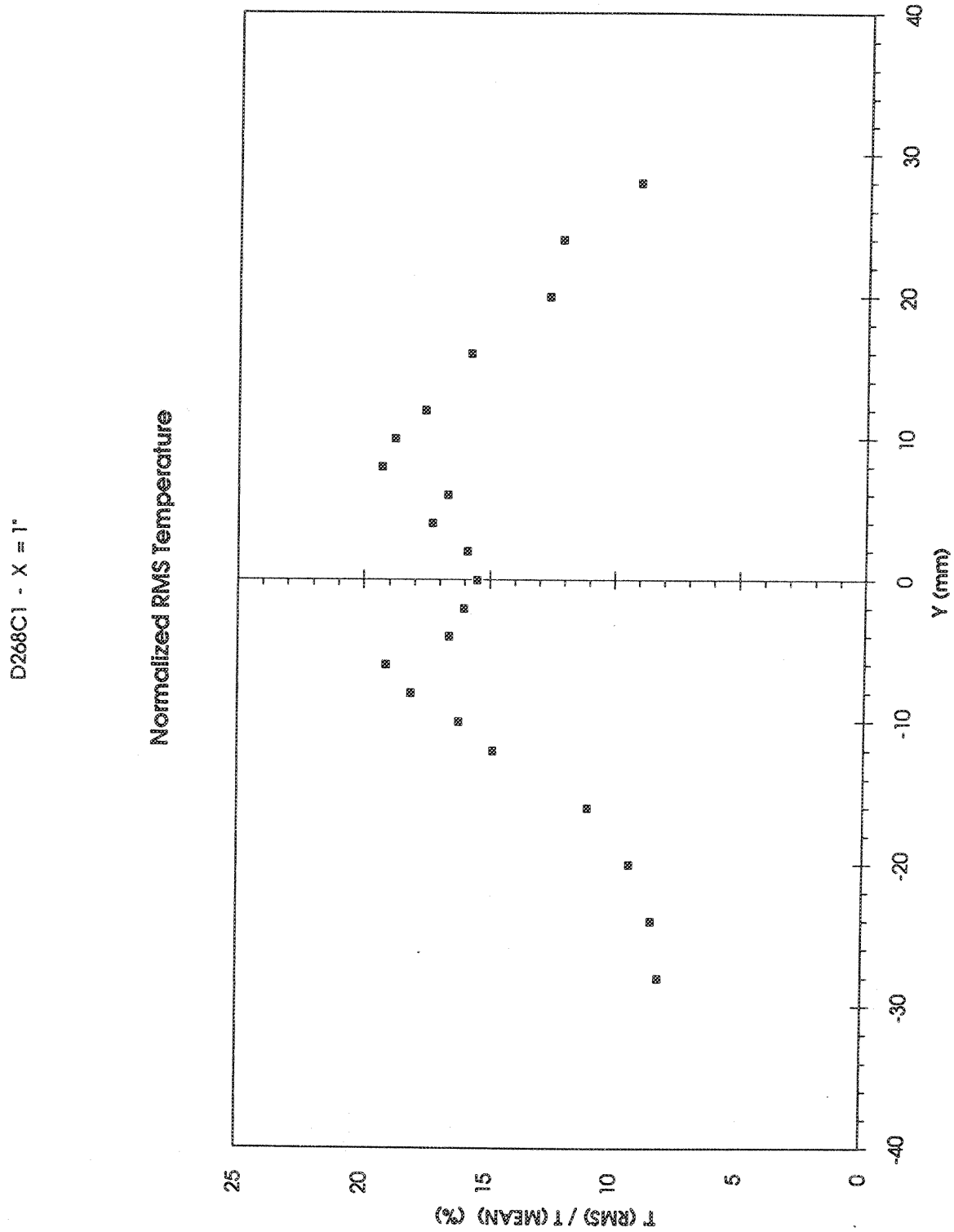
D268C1 - X = 1"
Normalized RMS Temperature
T (RMS) / T (MEAN) (%)
25
20
15
10
5
0
-40
-30
-20
-10
0
10
20
30
40
Y (mm)

Figure 8(e)

D268B1 - X = 3"

				REDUCED RAMAN DATA X = 3"					
FILE	Y(mm)	T(F)	CO2	O2	CO	N2S	CH	H2O	H2
R268B2	-30	745.0	0.001	0.210	0.000	0.780	0.000	0.005	0.000
B3	-28	777.0	0.002	0.216	0.001	0.772	0.000	0.006	0.000
B4	-26	987.0	0.001	0.218	0.001	0.770	0.001	0.003	0.000
B5	-24	1112.0	0.003	0.223	0.003	0.780	0.002	0.005	0.000
B6	-22	1234.0	0.002	0.210	0.001	0.790	0.004	0.005	0.000
B7	-20	1450.0	0.004	0.194	0.001	0.780	0.004	0.004	0.000
B8	-18	1550.0	0.008	0.182	0.000	0.775	0.005	0.005	0.001
B9	-16	1654.0	0.010	0.169	0.002	0.780	0.007	0.010	0.002
BA	-14	1854.0	0.012	0.145	0.004	0.790	0.009	0.015	0.003
BB	-12	2119.0	0.013	0.143	0.006	0.790	0.010	0.020	0.002
BC	-10	2219.0	0.014	0.133	0.006	0.795	0.012	0.024	0.004
BD	-8	2314.0	0.016	0.145	0.010	0.800	0.014	0.032	0.005
BE	-6	2178.0	0.016	0.135	0.012	0.790	0.016	0.044	0.006
BG	-4	1954.0	0.017	0.130	0.014	0.790	0.018	0.047	0.008
BH	-2	2007.0	0.018	0.137	0.010	0.785	0.017	0.053	0.008
BI	0	1758.0	0.021	0.136	0.012	0.780	0.019	0.050	0.010
BJ	4	1879.0	0.018	0.145	0.016	0.778	0.018	0.051	0.009
BK	8	2101.0	0.021	0.128	0.010	0.790	0.014	0.055	0.011
BL	12	2221.0	0.014	0.140	0.008	0.789	0.010	0.044	0.008
BM	16	1845.0	0.018	0.166	0.003	0.780	0.004	0.024	0.006
BN	20	1453.0	0.004	0.189	0.001	0.778	0.001	0.010	0.002
BO	24	912.0	0.001	0.200	0.000	0.775	0.002	0.005	0.000

Figure 9(a)

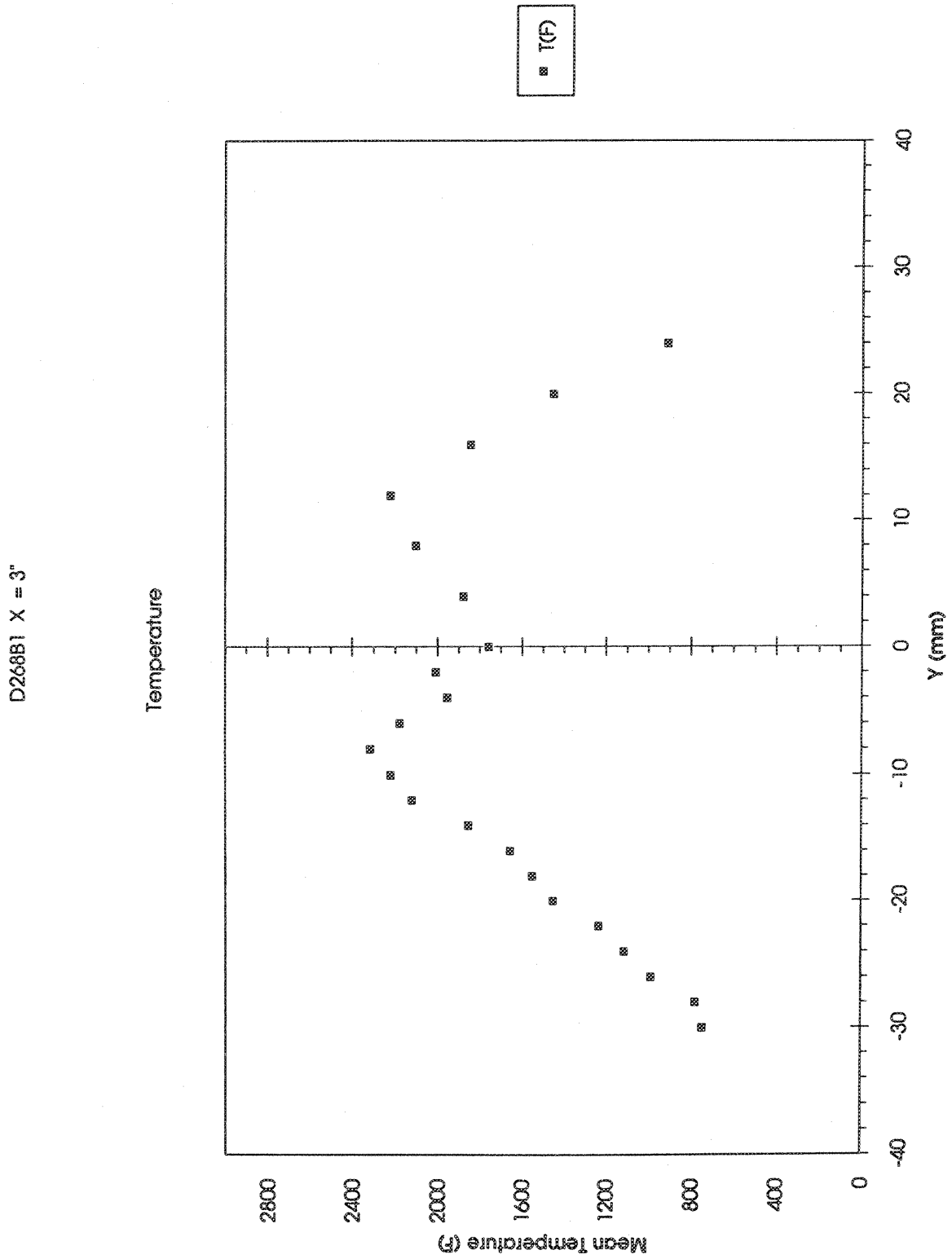
D268B1 X = 3"
Temperature
T(F)
Mean temperature (F)
2800
2400
2000
1600
1200
800
400
0
-40
-30
-20
-10
0
10
20
30
40
Y (mm)

Figure 9(b)

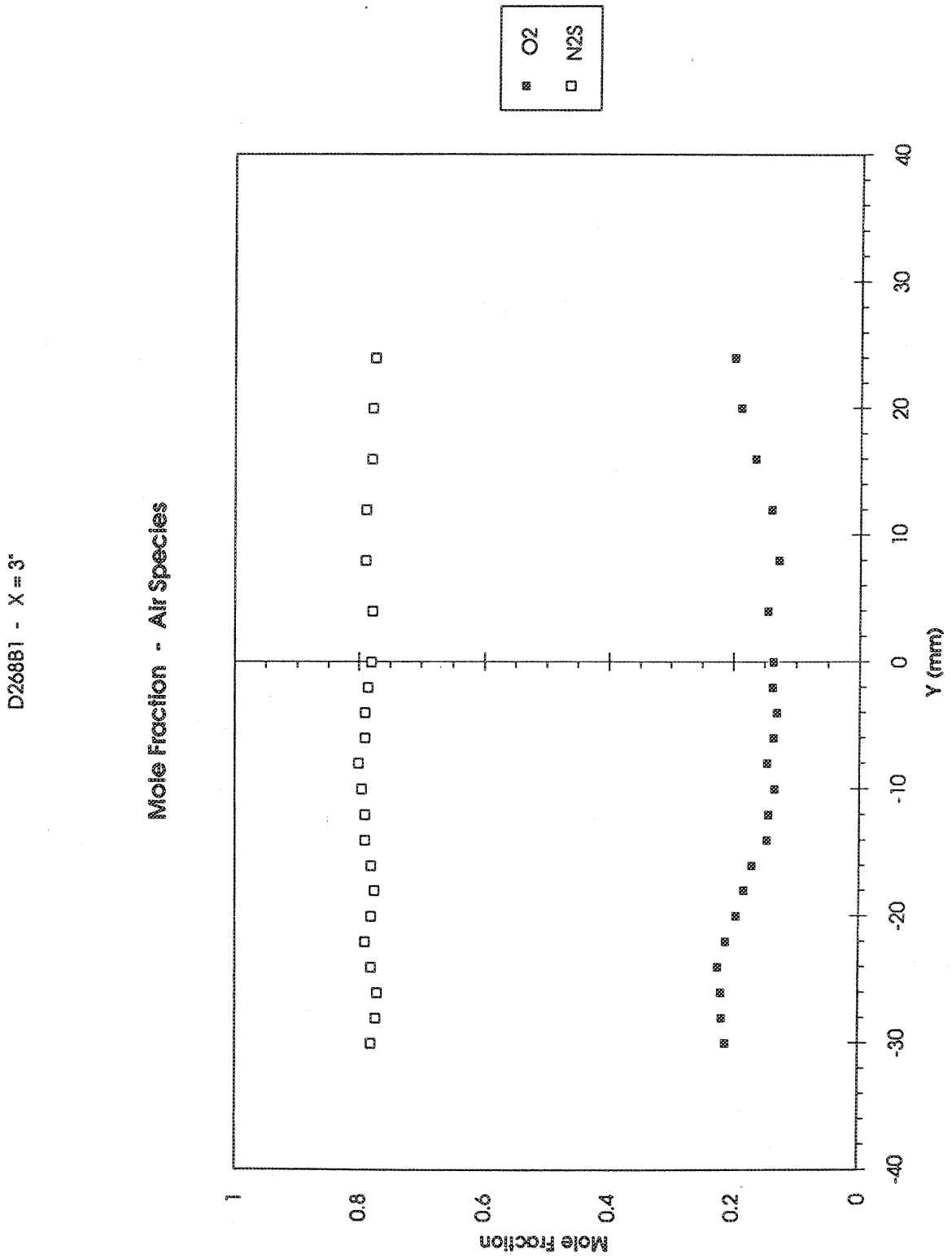
D268B1 - X = 3"
Mole Fraction - Air Species
O2
N2S
Mole Fraction
1
0.8
0.6
0.4
0.2
0
-40
-30
-20
-10
0
10
20
30
40
Y (mm)

Figure 9(c)

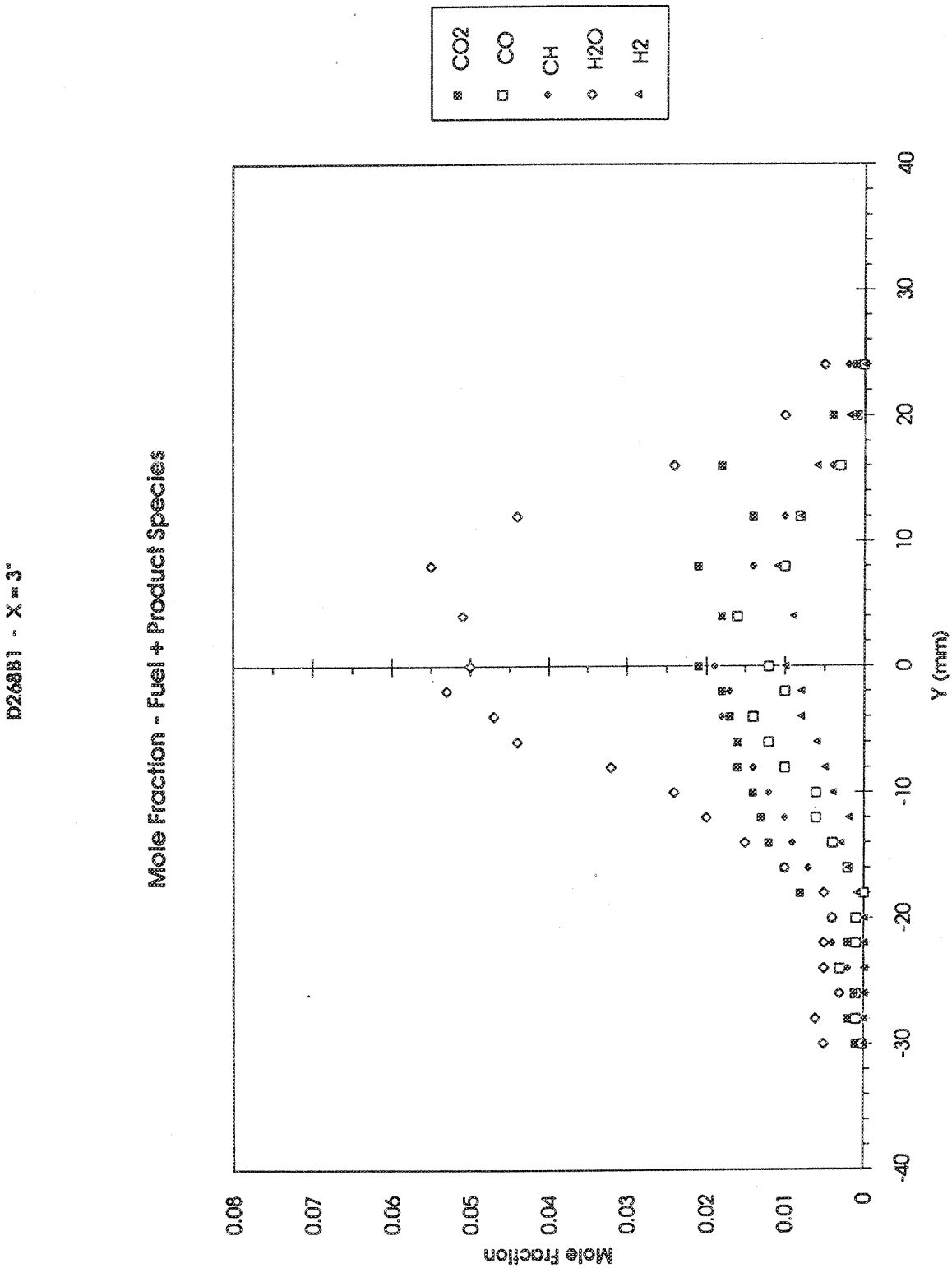
D268B1 - X = 3"
Mole Fraction - Fuel + Product Species
CO2
CO
CH
H2O
H2
Mole Fraction
0.08
0.07
0.06
0.05
0.04
0.03
0.02
0.01
0
-40
-30
-20
-10
0
10
20
30
40
Y (mm)

Figure 9(d)

D269B1 - X = 6"

REDUCED RAMAN DATA X = 6"

FILE	Y(mm)	T(F)	CO2	O2	CO	N2S	CH	H2O	H2
R269B3	-30	910.0	0.012	0.200	0.000	0.770	0.000	0.030	0.000
B4	-26	1118.0	0.016	0.185	0.001	0.769	0.001	0.037	0.000
B5	-22	1367.0	0.022	0.170	0.002	0.770	0.002	0.040	0.002
B6	-18	1670.0	0.029	0.162	0.000	0.771	0.000	0.054	0.003
B7	-14	1774.0	0.034	0.139	0.002	0.777	0.003	0.060	0.000
B8	-10	1928.0	0.037	0.131	0.004	0.781	0.004	0.066	0.001
B9	-6	2198.0	0.039	0.118	0.002	0.791	0.003	0.069	0.002
BA	-2	2240.0	0.044	0.115	0.002	0.789	0.002	0.070	0.003
BB	0	2416.0	0.046	0.104	0.005	0.782	0.003	0.071	0.002
BC	2	2389.0	0.048	0.102	0.003	0.790	0.004	0.071	0.000
BD	6	2323.0	0.043	0.100	0.003	0.787	0.005	0.067	0.004
BE	10	2218.0	0.040	0.119	0.001	0.788	0.007	0.062	0.003
BF	14	2198.0	0.037	0.140	0.000	0.779	0.003	0.059	0.000
BG	18	1889.0	0.032	0.155	0.003	0.770	0.004	0.055	0.003
BH	22	1676.0	0.029	0.167	0.000	0.778	0.002	0.052	0.000
BI	26	1435.0	0.018	0.195	0.002	0.770	0.003	0.035	0.002
BJ	30	1120.0	0.010	0.192	0.000	0.780	0.002	0.032	0.001

Figure 10(a)

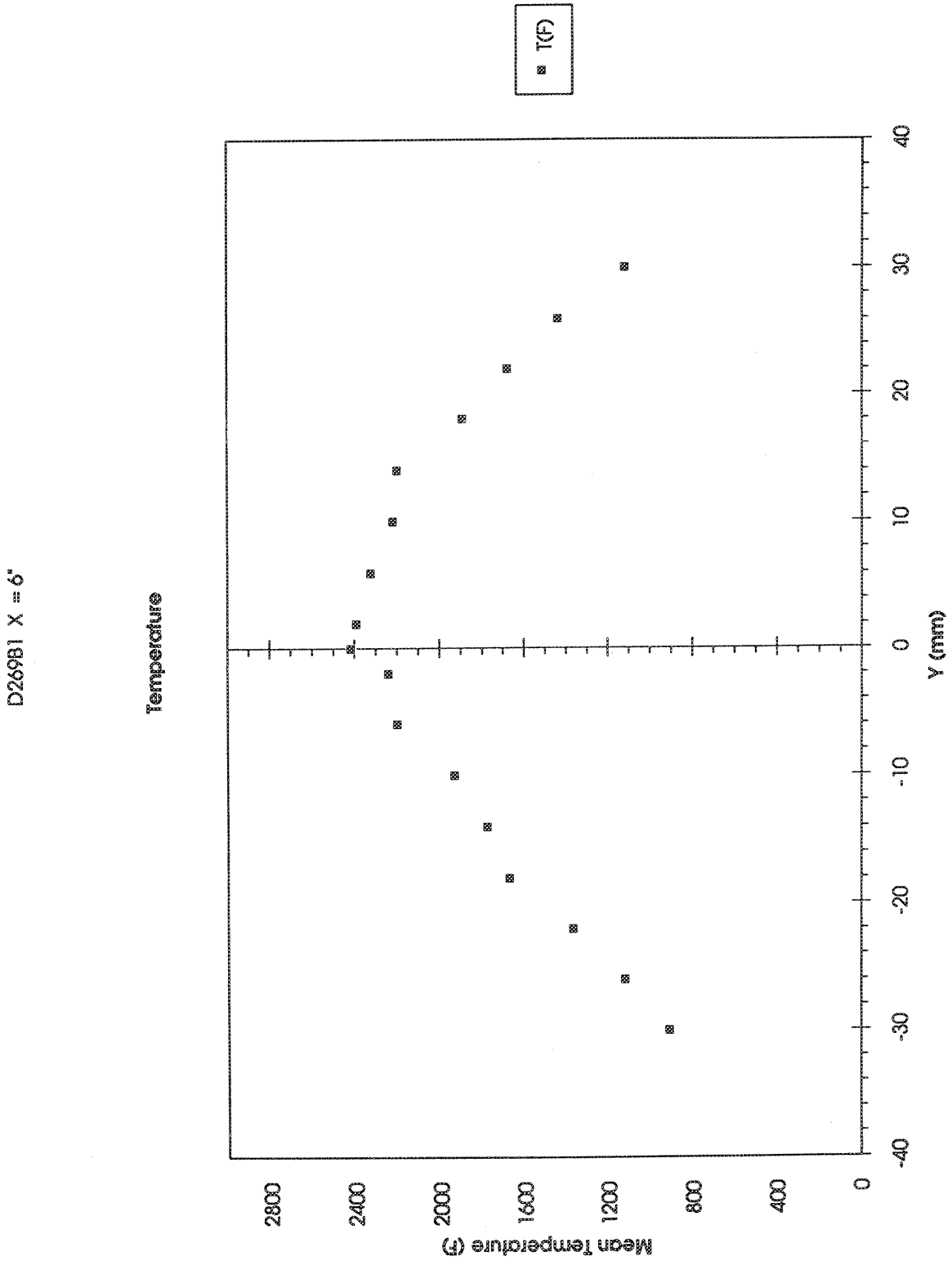
D269B1 X = 6"
Temperature
T(F)
Mean Temperature (F)
2800
2400
2000
1600
1200
800
400
0
-40
-30
-20
-10
0
10
20
30
40
Y (mm)

Figure 10(b)

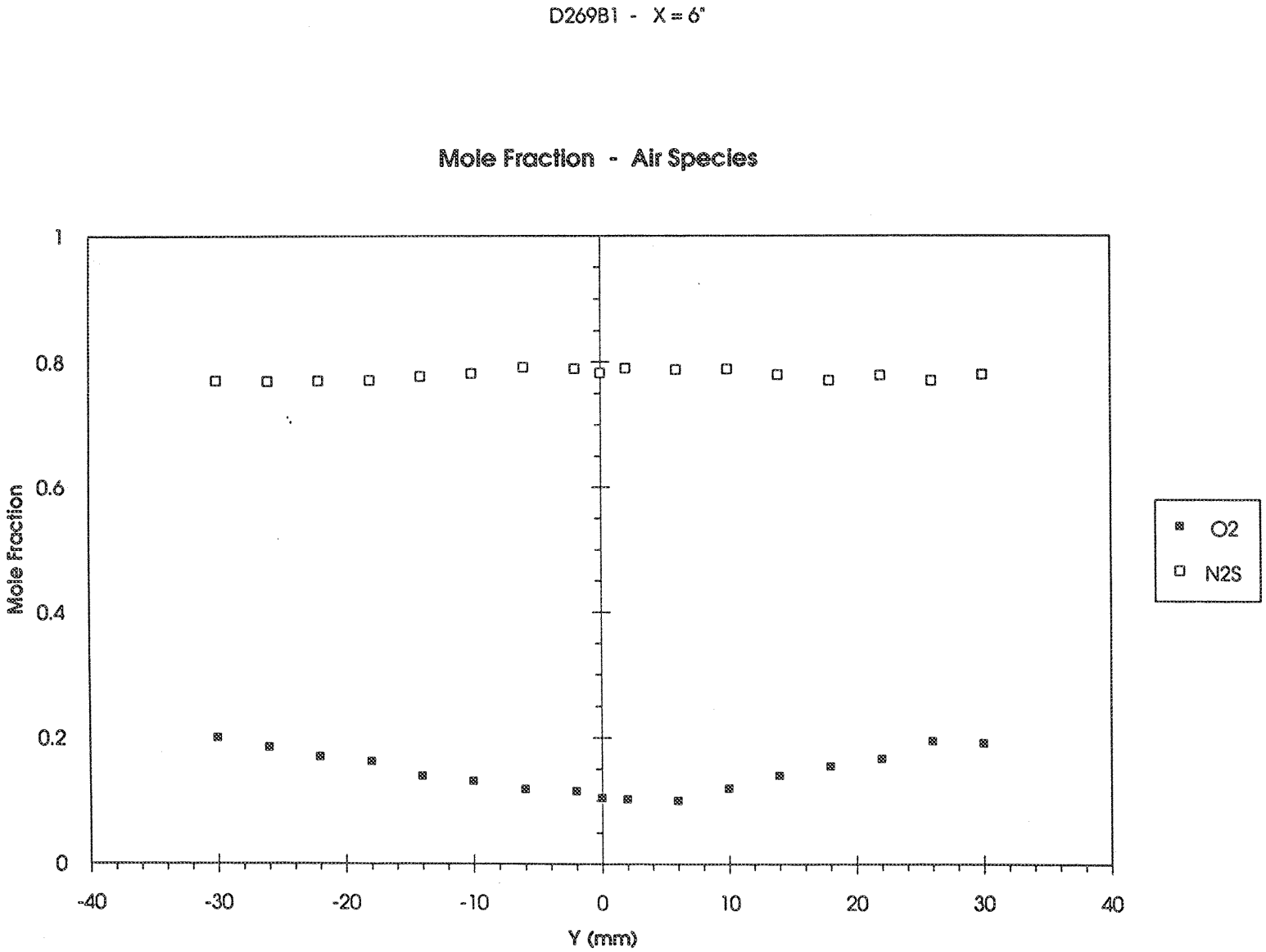
D269B1 - X = 6"
Mole Fraction - Air Species
Mole Fraction
1
0.8
0.6
0.4
0.2
0
-40
-30
-20
-10
0
10
20
30
40
Y (mm)
O2
N2S

Figure 10(c)

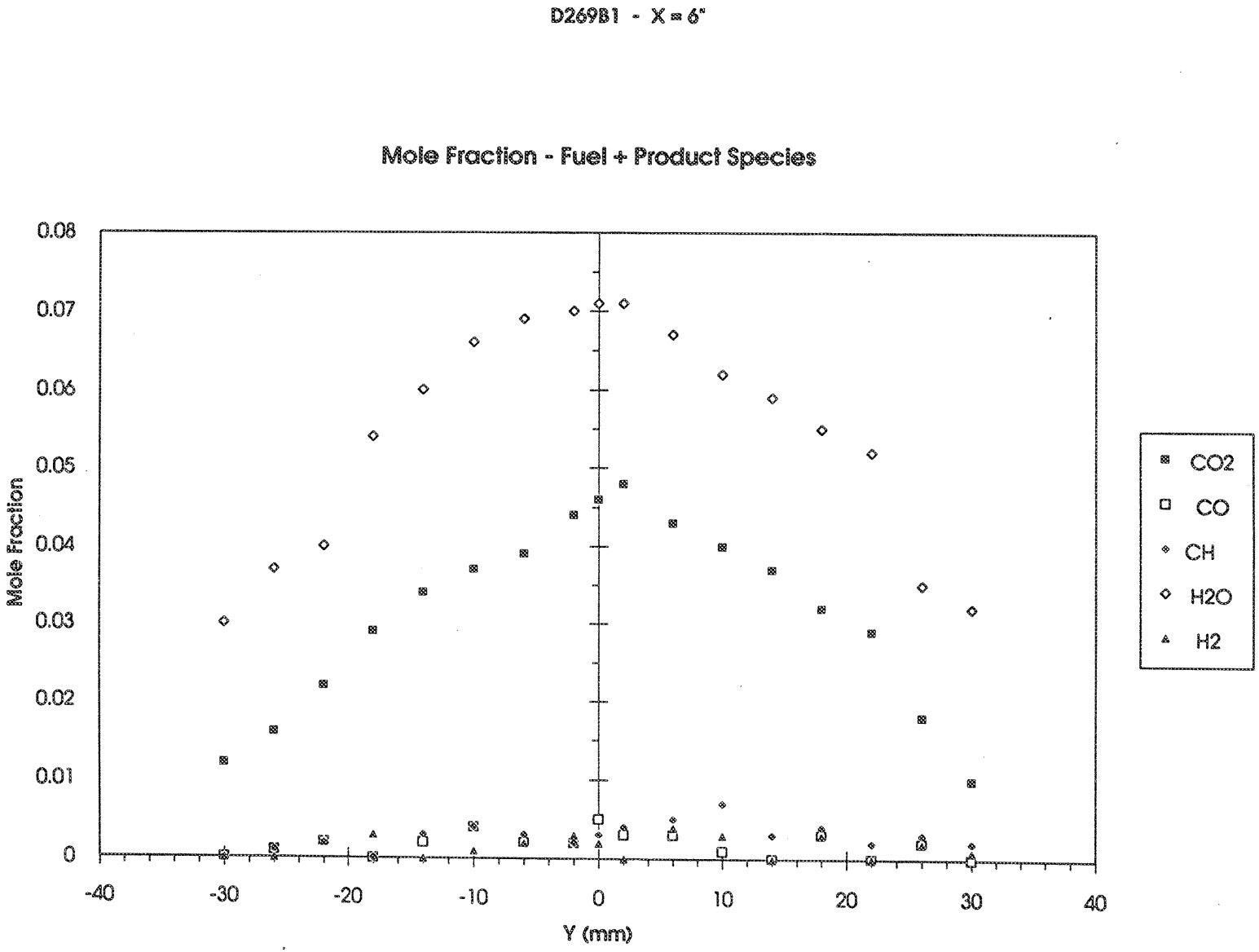
D269B1 - X = 6"
Mole Fraction - Fuel + Product Species
Mole Fraction
0.08
0.07
0.06
0.05
0.04
0.03
0.02
0.01
0
-40
-30
-20
-10
0
10
20
30
40
Y (mm)
CO2
CO
CH
H2O
H2

Figure 10(d)

10.0 APPENDIX C: PENNSYLVANIA STATE UNIVERSITY FINAL REPORT

Final Report

to

General Electric Aircraft Engines

on

Mixing and Emissions Evaluation of Lean Prevaporized Premixed (LPP) Combustion Configurations

by

D. A. Santavicca and R. L. Steinberger
The Pennsylvania State University
Department of Mechanical Engineering
University Park, PA 16802

September 1993

ABSTRACT

This final report details work carried out at Penn State to characterize fuel injection and combustor designs presented by GEAE for use in the HSCT program. The report describes the design and operation of the high pressure, high temperature flow combustor apparatus and experimental results obtained therein.

In order to achieve the overall goal of determining the effects of incomplete fuel-air mixing and vaporization on the lean limit and emissions characteristics of a lean, prevaporized, premixed combustor, the experimental measurements were carried out in two phases. First, two-dimensional exciplex fluorescence was used to characterize the degree of fuel vaporization and mixing at the combustor inlet under non-combusting conditions. These tests were conducted at a pressure of 4 atm abs, an inlet temperature of 360°C, a mixer tube velocity of 100 m/s, and an equivalence ratio of 0.8 using a mixture of tetradecane, 1 methylnapthalene, and TMPD as a fuel simulant. Two transverse injection geometries (on the centerline and at the wall) were investigated. In both cases, there was a significant amount of unvaporized fuel at the combustor entrance. Centerline injection, however, exhibited a very non-uniform distribution of fuel liquid and vapor, while wall injection yielded a much more uniform distribution of fuel across the width of the combustor entrance.

Second, lean limit and emissions measurements were made for combusting flows at a pressure of 4 atm abs, a mixer tube velocity of 100 m/s, and over a range of inlet temperatures, using Jet A as the fuel and employing both fuel injection geometries. Contrary to expectations, wall injection which produced better mixing, also yielded leaner operating limits. For a given equivalence ratio and inlet temperature, the two injection geometries also unexpectedly yielded comparable NO_x emissions; however, wall injection allowed operation at leaner equivalence ratios, thus yielding lower NO_x levels.

I. SYSTEM DESIGN AND CONSTRUCTION

A. System Overview

Over a period of several months, a system was designed to allow operation of a pre-mixed pre-vaporized continuous flow combustor test section at pressures up to 10 atm abs, at inlet air temperatures up to 1000° K (1340°F), and with flow rates permitting 100 m/sec mean velocity in the premixing section. The test section was designed to allow optical access on 4 sides around the circumference and along the entire length of the premixer-combustor.

The main portion of the apparatus consists of sections of 6" stainless steel, schedule 40 pipe, which acts as a pressure containment vessel. Figure 1 is a diagram of the system. Air is supplied by a large, Ingersoll Rand reciprocating compressor capable of supplying about 400 scfm (0.5 lb/s) at 400 psig. Air from the compressor is filtered and dried in a Hankinson Aerolescer filter and flows through a 4" stainless steel line holding a Hastings Raydist Mass Flow Meter and then to a control panel, which holds metering and shut-off valves. Upstream of the metering valve, the pressure is maintained sufficiently high to create choked conditions at the valve. System pressure is controlled by a Masoneilan Camflex valve located in the exhaust.

From the control panel, the air flows through the first section of 6" stainless steel pipe which houses the air heating unit. This unit contains three, 9 kw Watlow rod heaters, each about 144" long and each bent into a U-shape. The heaters and air flow are confined by a 3" diameter, 0.050" wall, stainless steel liner which is surrounded by ceramic insulation. The insulation used in this unit is a combination of molded insulation made in house from Fiberfrax FC-25 Tamping Mix (molded into sections about 12" long x 3" i.d. x 6" o.d.), and loose ceramic insulation (Fiberfrax short staple ceramic fiber) tamped into place. The 3" stainless steel liner had to be cut into 3 sections, each about 24" long, in order to prevent warping, which was experienced with an original 6' long liner. To improve heat transfer to the air, about 20 discs of perforated stainless steel are wired to the heaters along their length at about 3-inch intervals.

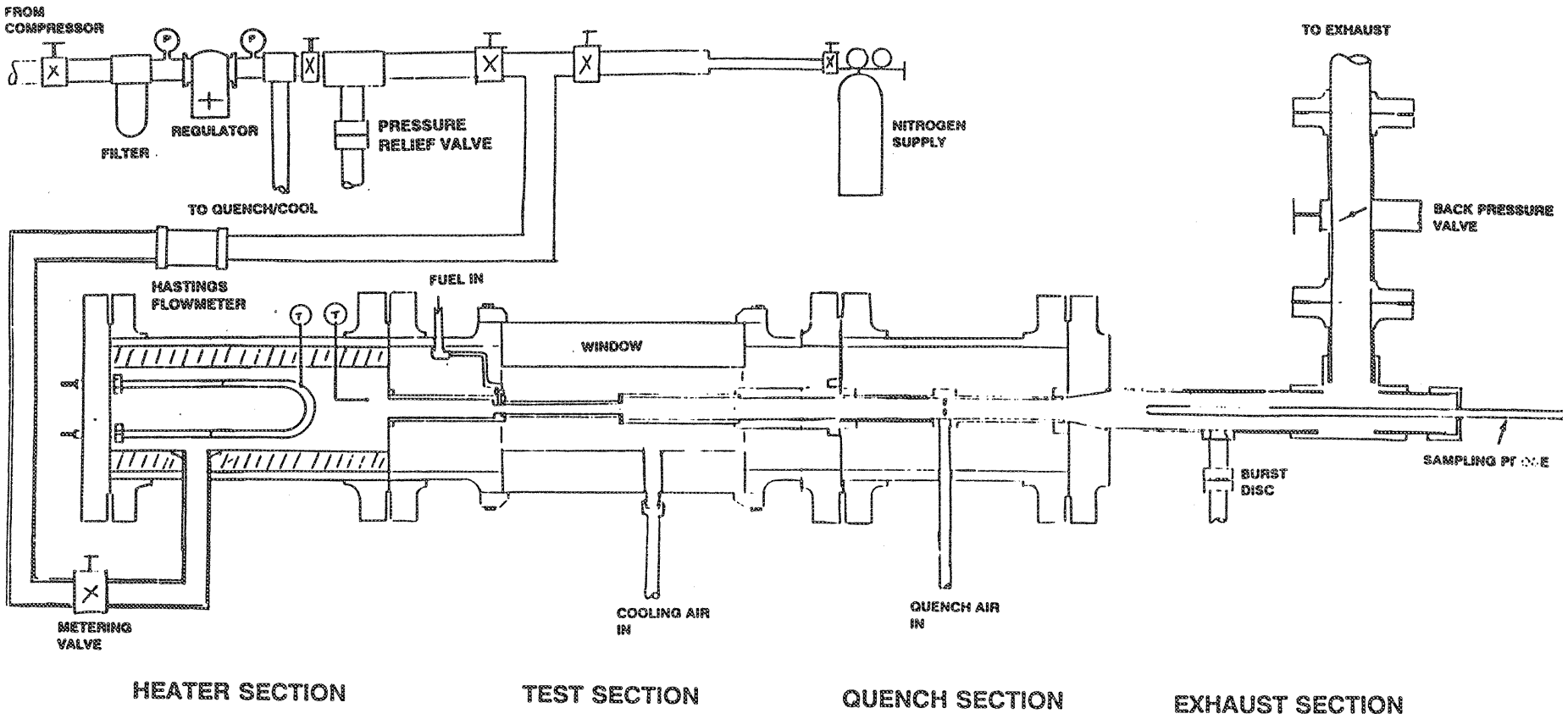

Figure 1 High Temperature, High Pressure Flow System

The next section of 6" stainless steel pipe houses the test section which is about 20" long. The 6" pipe is fitted with 4 rectangular window ports spaced at 90° intervals around the circumference. These window ports can hold quartz windows, each of which provides a viewing area of 1 1/2" x 10 1/2", or stainless steel substitutes which allow feed-throughs for instrumentation, spark ignition, etc., to the test section. The quartz windows are of a stepped design, are sealed by an O-ring, and are held in place by an aluminum retaining ring. The stainless steel window blanks are also O-ring sealed.

From the test section, air and/or exhaust gases flow into a quench section about 24" in length. The gas flow here is also confined to the inside of a 3" diameter stainless steel liner. This section is fitted with a double coil of stainless steel 1/4" o.d. tubing for water flow to enhance cooling of the exhaust gases. Because the water flow in these coils from the building water supply was inadequate to prevent boiling under combusting conditions, a pressure boost pump was introduced which maintained about 4 gal/min.

From the quench section, the exhaust flows through 1 1/2" schedule 40 stainless steel pipe, which is provided with a small nozzle for injecting a water spray transverse to the air flow to further cool it, through a Masoneilan Camflex Valve used for adjusting back pressure, and then into the building exhaust system. The exhaust section includes a 90° elbow to allow for the axial insertion and movement of a long, stainless steel, water-cooled gas sampling probe. The end of the exhaust pipe contains a few inches of fiberglass insulation which provides some sound muffling, but is really inadequate for the combustion tests. Each of the three 6" pipe sections (heater, test section, quench section) is mounted on a mobile support stand which allows for their connection and disconnection for changes in test section configuration and repairs.

B. Safety Devices

The system is fitted with several safety devices. There is a Fike burst disk assembly near the exhaust region which is set for 158 psig. Also, there is a Watts pressure relief valve assembly near

the system inlet set to open at 150 psig. There are also two pressure switches which will turn off the heaters and the fuel flow if the pressure increases beyond 145 psig or decreases below 2 psig during a test. And, there is an Omega Engineering high limit switch which will turn off power to the heaters should the heater sheath temperature exceed a set point, usually 800°C (1472°F).

C. Premixer-Combustor Test Section

The actual premixer-combustor apparatus was designed in two versions, one in quartz for use in the exciplex liquid/vapor visualization studies, and one in metal for the combustion studies. Both versions underwent several revisions before successful designs were achieved.

The quartz (fused silica) apparatus was fabricated from two tubes. The premixing section is made from 13 mm i.d. x 15 mm o.d. tubing, while the flame tube or combustion section is from 28 mm i.d. x 31 mm o.d. tubing (nominal dimensions). The two tubes were joined by flaring the smaller tube into a flat surface at right angles to the tube, and fusing this surface with the large diameter tube, thus forming the sudden expansion which serves as the flame holder. The ends of this complete quartz premixer, flame tube fit into machined parts of stainless steel. This design is shown in Figure 2. The 5" long, 1.1" i.d. stainless steel inlet section feeds the air from the heaters through a smooth rounded inlet into the quartz premixer. The downstream 5" stainless steel outlet section simply feeds the flow through the flange into the quench section of the system. Seals at both ends were achieved via compression of loose ceramic fiber insulation onto the quartz tubes. The inlet section is modular and can be fitted with various fuel injection geometries.

The combustion apparatus was revised through several designs. The first three designs made use of both hard, high-density (alumina) ceramic and low-density molded ceramic. The more rigid alumina design failed quickly, being unable to withstand the thermal shock. The low-density ceramic design, while withstanding the thermal shock better, was very susceptible to erosion in the high-speed, hot gas flow. None of the designs incorporating ceramics proved viable.

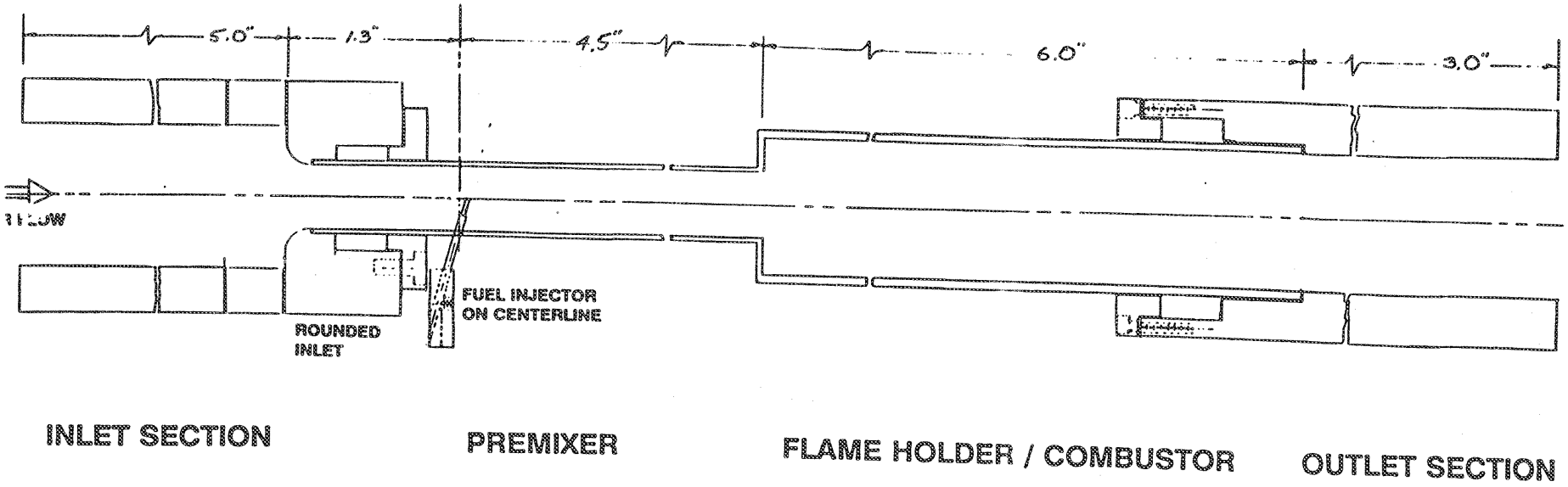

Figure 2 Quartz Test Section for Visualization Studies

The first metal flame tube was fabricated of thin-walled stainless steel tubing. Air flow which initially was used simply as a quenching flow injected into the hot exhaust stream to dilute and cool it, was re-routed through the stainless steel windows in the test section to form a cooling air stream on the flame tube exterior. However, this cooling was insufficient for the stainless tube which warped and eventually burned away over a large area.

Finally, a flame tube measuring 1.125" i.d. x 1.315" o.d. x 12" long was constructed of Haynes 230 Alloy. A spiral groove was cut in its exterior surface to enhance heat transfer. Also this tube was lengthened by about 15" so the flame tube then extended almost the entire length of the quench section. The water cooling coils surround this extension piece, and the exterior cooling air is mixed with exhaust gases at the exhaust end of the extended flame tube, near the end of the quench section. The exterior surface is cooled by the previously mentioned air flow which flows in an annulus formed by the flame tube and a length of 3" i.d. molded ceramic insulation. This design has proved very satisfactory. A cooling air flow of 3-5 times the combustion air flow was required to prevent the exterior surface temperature of the flame tube from exceeding 900°C (1650°F).

D. Fuel System

The fuel system, illustrated in Figure 3, consisted of a 2-gallon tank made of steel pipe, which was pressurized with nitrogen, thus enabling a constant and easily controlled fuel pressure. Fuel flowed from the tank through a Fischer Porter rotameter-style flow meter, an in-line 15μ filter, and a solenoid valve to a 1/16" stainless fuel line leading to a fuel injector. Early flow visualization tests incorporated a Delavan "peanut" nozzle mounted to spray axially with a 70° cone spray angle. However, most of the testing was done with a "hypo-tube" fuel injector (0.040" o.d. x 0.020" i.d.) mounted in the upstream end of the premixing section. Two mounting configurations were used: one with the tube exit flush with the inside wall of the premixer, and the other with the tube exit on the centerline of the premixer. In both cases, the axis of the tube was tilted at 15° from the vertical in the downstream direction.

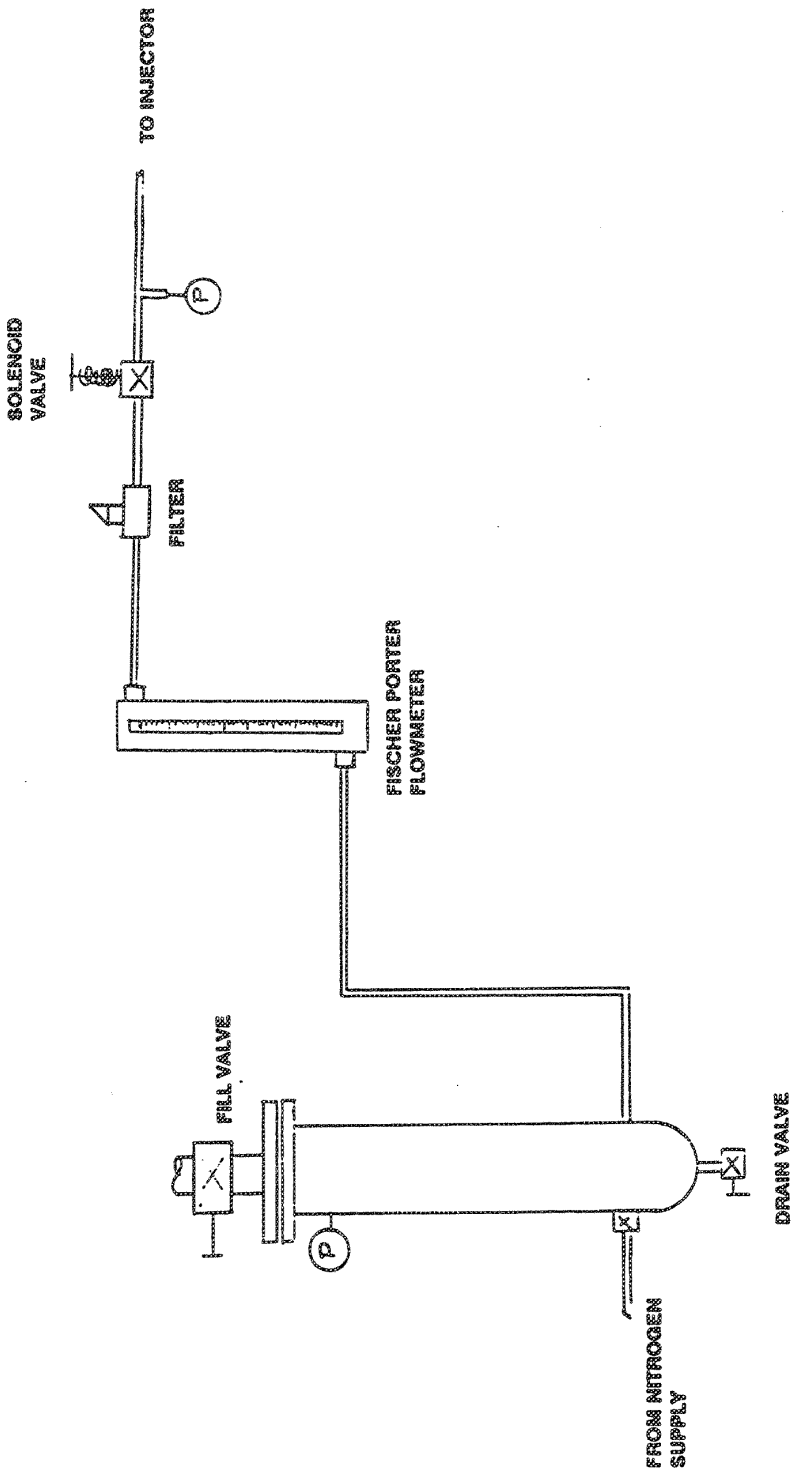

Figure 3 Fuel System

In the exciplex liquid-vapor studies, the fuel tube was mounted through a small hole in the wall of the quartz tube. The fuel in these tests was a mixture of 84% Tetradecane, 15% 1-Methyl-naphthalene and 1% N-N-N'-N'-Tetramethyl-P-phenylenediamine (TMPD), by mass.

In the combustion tests, the fuel tube was mounted through a swagelok fitting placing it at the same axial location as in the visualization tests. The fuel used was Jet A obtained from the local airport.

E. Controls and Instrumentation

A summary of the controls and instrumentation used in the apparatus is shown in Table 1. The inlet air temperature was monitored by a Type K thermocouple positioned immediately downstream of the flange separating the heater section from the test section. The temperature controller operated on the signal from this thermocouple. Thermocouples were attached using hose clamps on the sheaths of all three heaters. The signal from the heater experiencing the highest temperatures was used for the input to the High Limit Controller.

The Air Flow Meter was checked against an American Meter Corporation Diaphragm Meter with an accuracy of $\pm$ 1%. The two meters agreed to within 2% over the range of 20.0 to 80.0 scfm of air.

The Fuel Flow Meter was calibrated by timing a measured volume of liquid flow through the meter. This was done once with pure tetradecane, and twice with Jet A. The Jet A data was repeatable to within 5%.

During combustion tests in which CO, CO_2, and O_2 exhaust concentration measurements were made, the sampling probe was positioned about 1" upstream of the end of the flame tube (about 25" downstream of the flame holder). The emission instruments were operated in series with the sample flow going from the CO to the CO_2 and then to the O_2 meters.

Table 1
Instrumentation

QUANTITY OR DEVICE	INSTRUMENTATION	ACCURACY
Temperatures	Omega Type K Thermocouples	+/- 0.75%
Temperature Indicator	Omega Model 115 Digital Thermometer	+/- 2.6°C
Temperature Controller	Omega Model CN9000A	+/- 0.25% FS
High Limit Temperature Controller	Omega Model CN2091	+/- 1% FS
System Air Pressure	US Gauge Process Gauge 0-160 psig	+/- 0.5% FS
System Air Pressure Control	Masoneilan Camflex Valve	NA
Fuel Pressure	US Gauge Process Gage 0-200 psig	+/- 0.5% FS
Pressure Drop (Test Section Inlet to Outlet)	Dwyer Capsuhelic Model 2205 0-5 psid	+/- 2% FS
Pressure Switches	Barksdale Controls Model EIH-H250 145 psi inc Model EIH-H15 2 psi dec	NA
Fuel Flow Meter	Fischer Porter Model 10A6133 Rotameter	+/- 2% FS
Air Flow Meter	Teledyne Hastings Raydist Model HS-L100SF Transducer Model HAHL-100P Meter	+/- 1% FS
CO Concentration	Horiba Model PIR-2000	+/- 0.5% FS repeatability
CO_2 Concentration	Horiba Model PIR-2000	+/- 0.5% FS repeatability
O_2 Concentration	Beckman Model 755	+/- 1% FS repeatability
NO_x Concentration	Thermo Electron Model 10	+/- 1% FS

When NO_x measurements were made, no other meters were connected to the sample line. All emissions measurements were made on a dry basis, water having been removed by a desiccant in the case of CO, CO_2 and O_2, or by an ice bath condenser in the case of NO_x.

II. MIE SCATTERING EXPERIMENTS

An early version of the quartz premixer-flame tube test section was used to perform spray visualization experiments at atmospheric pressure and temperature. These experiments were conducted while the main apparatus was under construction.

A. Atmospheric Pressure/Ambient Temperature Tests

The first technique employed a 35 mm still camera using color print and slide film. The premixing section was illuminated using a pulsed Nd:YAG laser operating at 532 nm. The laser beam was formed into a sheet about 50 mm wide in the horizontal plane, while the camera viewed the Mie scattered light from the spray from the top. These experiments employed methanol as the fuel. Several experiments were performed using the still camera method.

Initially, the spray from the peanut nozzle was photographed, mostly near the nozzle exit in the premixing tube. These pictures revealed a very thick spray in this region and considerable wall wetting was noted.

The technique was then applied to the hypo-tube injector placed on the center line. In order to obtain a side view of the spray, the injector entered the quartz tube from the side, in the plane of the laser sheet, while the camera remained mounted above. In order to enhance vaporization, the quartz tube walls were heated using heated air flow from a heat gun, but no temperatures were monitored. In these tests, there seemed to be an intermittency to the spray; even with the naked eye, the spray seemed to start and stop.

As a final experiment in these preliminary atmospheric tests, aimed at verifying this intermittency, the spray from the hypo-tube injector was photographed using a Kodak Spin Physics

High Speed Video System recording at 2000 frames/sec. These sequences played back frame by frame clearly showed that at irregular intervals, the fuel actually stops flowing out of the fuel tube. Although interesting, this phenomenon was not further pursued since its relevance to fuel injection with kerosene-type fuels at operating pressures and temperatures was not clear.

B. Operating Pressure/Temperature Tests

At this point, the full apparatus became available, was assembled and modified until operation for about an hour at 45 psig, 70 scfm, and 350°C (660°F) inlet conditions was achieved without problems. The quartz premixer-flame tube test section was now one piece, as previously described.

A new recording system, consisting of a compact CCD Pulnix TM-745 video camera connected to a Sony SLV-RSVC super VHS VCR and a Sony KV20EXR20 television, was used. Two types of visualization experiments were carried out using the new apparatus and the Pulnix camera. In the first experiments, continuous illumination was provided from a spot light and the camera was allowed to record at its normal free-run framing rate wherein the effective shutter speed is 1/60 sec. Flow conditions are described in Table 2. Naked eye observation revealed a very finely atomized spray all the way down the premixing tube. Video records showed no wall wetting and no visible intermittency. In an expansion of this test, the camera was adjusted for a shutter speed of 1/2000 sec. These video records showed there actually were fluctuations in the spray, but no distinct on/off periods. There was no wall wetting. In these experiments, however, the required fuel flow rates were not achieved; this problem was eventually traced to an improperly connected swagelok fitting and was corrected.

In the next Mie scattering experiment, the video camera was employed again, but illumination was provided by the pulsed Nd:YAG laser. Flow conditions for this set of experiments are listed in Table 3. Video records of the spray were made with the camera and laser positioned to view the spray from both the top and the side, and at two axial locations: at the transition from premixer to flame tube, and about 0.5" farther downstream.

Table 2
Mie Scattering Experiments 4/2-4/4/92
Flow Conditions

System Pressure =	52 psig
Air Flow Rate =	60-62 scfm (0.076 lb/s)
Air Speed in Premixer =	121 m/s
(assuming flow coefficient = 0.86)	
Inlet Air Temperature =	360°C (680°F)
Fuel =	Jet A
Fuel Flow =	40-77 gm/min (0.0015-0.0028 lb/s)
Equivalence Ratio =	0.29-0.55
Injector =	Hypo fuel-tube positioned on centerline

Table 3
Mie Scattering Experiments 6/11-6/12/92
Flow Conditions

System Pressure =	66.3 psia
Air Flow Rate =	53.0 scfm (0.0661 lb/s)
Air Speed in Premixer =	104 m/s
(assuming flow coefficient = 0.86)	
Inlet Air Temperature =	360°C (680°F)
Fuel =	Jet A
Fuel Flow =	86.7 gm/min (0.00318 lb/s)
Equivalence Ratio =	0.70
Injector =	Hypo fuel-tube

Video records were made for two situations: the injector position on the centerline, and the injector positioned at the wall. The records are summarized in Table 4 and reviews of the video records revealed that:

1. Fine droplets exist on both sides of the transition from small diameter to large diameter in both injection geometries.
2. In the region after the transition, the droplets present in the core jet do not migrate out of the core, but rather remain confined to the core--though evaporative processes may deposit vapor everywhere--in both injector geometries.
3. The major difference in the two injector geometries is that in the case of centerline injection, the droplet density on both sides of the transition appears to be higher above the centerline than below it. This observation is apparent in the side views of the scattered light. In top views of both cases, though, the droplets appear to be fairly evenly distributed.
4. Fluctuations in the spray are apparent in all video sequences; viewing two consecutive frames shows a slightly different droplet distribution image, though all gross test conditions remain constant. No attempt was made to quantify or correlate these fluctuations.

III. EXCIPLEX LIQUID-VAPOR VISUALIZATION EXPERIMENTS

Once the flow system was proven to operate consistently at the required pressures and temperatures the exciplex visualization experiments were begun. The photophysics of the exciplex technique is described in several other references[1-4] and will not be detailed here. It is a laser fluorescence technique in which an optically active chemical mixture is substituted for the actual fuel. When this mixture is irradiated by UV laser light, the vapor component fluoresces at one wavelength and the liquid at another. By properly selecting filters, these two components of emitted light can be separated, thus allowing separate visualization of liquid and vapor. In general, the emitted light

Table 4
Video Data From 6/11-6/12/92

Date	Injector Position	Video Sequence	Axial Location	View	Observations
6/11	centerline	1	at transition premixer to flame tube	side	droplets on both sides of transition; more drops above centerline in flame tube
		2	1 cm downstream of transition	side	droplets persist but thin out; no droplets visible off core around centerline; still more drops above centerline
		3	at transition premixer to flame tube	top	droplets more evenly distributed though fluctuations are visible; no droplets visible outside core
		4	1 cm downstream of transition	top	still droplets visible, but not as dense
6/12	wall	1	at transition premixer to flame tube	top	droplets on both sides of transition evenly distributed; few droplets off axis
		2	1 cm downstream of transition	top	unchanged
		3	at transition premixer to flame tube	side	droplets seem very evenly dispersed
		4	1 cm downstream of transition	side	unchanged

intensity is proportional to the mass concentration of the respective component. The fuel substitute used here was a mixture of Tetradecane (T), 1 Methylnapthalene (MN), and NNN'N' Tetramethyl-p-phenylenediamine (TMPD). This mixture then yields a fluorescence vapor signal in the blue (380 nm) and a fluorescence liquid signal in the green (470 mm).

A. Apparatus and Procedures

A new fuel tank was constructed from 3 1/2" steel pipe to contain about 1.5 gallons of exciplex mixture, enough for about 20-30 minutes of run time under normal operating conditions.

The mixture used in all experiments was 84% T, 15% MN, and 1% TMPD by mass. Tetradecane was obtained from the Humphrey Chemical Co., while the Naphthalene and TMPD were obtained from either Aldrich Chemical Co. or Spectrum Chemical Co., and were used as received. Usually, the mixture was prepared in a 2-liter batch. Oxygen rapidly degrades TMPD and the mixture. Therefore, the fuel tank was purged with nitrogen for about 30 minutes before it was filled. Also, nitrogen was bubbled through the mixture to purge the liquids of dissolved oxygen for 15-30 minutes. The mixture was also vigorously shaken to encourage dissolving of the TMPD. Regardless of how long the mixture was shaken, some black flecks of unknown composition always remained in the mixture. Therefore, the mixture was always poured through several layers of fine nylon mesh to filter these solids out as the fuel tank was filled.

The exciplex fluorescence process is extremely susceptible to oxygen quenching. Thus, the technique must be carried out in an oxygen-free environment. For these experiments, six standard-size (1.5 $ft.^3$ @ 2500 psig) nitrogen bottles were manifolded together and a valving system was used to allow switching from air flow to nitrogen flow. The nitrogen flow was regulated by a Grove Mity-Mite Model 94 regulator down to about 175 psig to maintain choking at the flow control valve. Under normal operating conditions (about 50 scfm), six nitrogen bottles provided about 25 minutes of run time. Between the regulator and the Hastings flowmeter, the nitrogen flowed through about 30 feet of copper tubing to facilitate warming it back to near room temperature after its throttling from the gas bottles. The Hastings flowmeter has a correction factor of 1.02 for nitrogen over air. During a test, experimental conditions, including achieving steady-state inlet temperature, were stabilized using air flow. Then, by changing the states of two valves, air flow was stopped and nitrogen flow was started. Nitrogen was allowed to flow through the system for at least 1.5 minutes before taking any data. This guaranteed purging of the air remaining in the apparatus.

The fluorescence images were recorded using a Princeton Instruments Image Intensifying Camera, which makes use of a 576 x 384 pixel CCD. This camera is computer controlled and is

interfaced with a Gateway 486 33 MHz computer, where images were stored, processed and analyzed. Camera control and image processing are accomplished with Princeton Instruments' own software called CSMA (CCD Spectrometric Multichannel Analysis Software).

Exciplex fluorescence was stimulated by 355 nm light pulses (pulse duration $\approx$ 20 ns) from a Nd:YAG laser with a frequency tripling crystal, operating at a repetition rate of 10 hz. Light pulses from the laser were passed through an iris to try to eliminate as much of the stray, second harmonic green (532 nm) light as possible, then through a 65 mm focal length glass cylindrical lens to spread the circular beam into a sheet, and through a 610 mm focal length quartz spherical lens to focus the sheet down to $<$ 0.5 mm width in the test section. Also placed in the beam path was a 532 nm reflecting mirror to try to further remove any stray green laser light from the test section area where reflections and Mie scattering can overwhelm the fluorescence signals.

Mounts were built to enable the camera to be positioned above or on the side of the test section to allow top and side views. The camera and laser sheet were always at right angles. A Nikon 60 mm f/2.8 lens was used to image the test section on the camera CCD.

The vapor and liquid fluorescence signals were separated using a Corion P10-500-R-1952, 500 nm center/10 nm FWHM band pass filter for the green (liquid) signal and a Corion S25-400-R-0008, 400 nm center/25 mm FWHM band pass filter for the blue (vapor) signal.

During the experiments, one of the most persistent problems encountered was swamping of the CCD camera by a small area of high intensity light coming from the quartz test section, even without liquid flow, and passing through the green (500 nm) filter. It may be that certain impurities in the quartz fluoresce at this wavelength. Much time was spent adjusting strips of tape, which were placed on the test section windows to try to block this light. Since the windows were hot at test conditions, this was a difficult task. The effect of bright spots on the image is to greatly reduce the contrast in the less intense regions.

The procedure in a typical exciplex experiment was as follows:

1. Set up the directory structure for storing images on the computer.
2. Set the air flow to the desired value and adjust the inlet temperature set point.
3. Allow air to flow while the system heats up and reaches equilibrium.
4. View images with the CCD camera in real-time in order to focus and adjust its position.
5. Once the system is at equilibrium, position the green filter on the camera lens, and switch to nitrogen flow.
6. Having purged air from the system, begin spraying exciplex liquid, and better focus the camera on the liquid drops.
7. Record a set of liquid images.
8. Switch the filter on the camera and record a set of vapor images.

Beginning a test with 4 liters of exciplex mixture and 6 bottles of nitrogen would usually allow a set of 20-25 images (frames) to be recorded. Included in each set of liquid and vapor images, was an image under the same conditions but with no liquid flow. All exciplex images were recorded with the room lights off.

B. Results

A complete set of exciplex vapor and liquid images was obtained for two hypo-tube injector locations: at the wall and on the centerline, at an axial location about 1.3" downstream of the leading edge of the rounded inlet to the premixer. The operating conditions were the same in all cases:

System Pressure:	61-63 psia
Inlet Air Temperature:	360°C (680°F)
Air Flow Rate:	51-53 scfm (234 pph)
Premixer Air Speed: (assuming a flow coefficient of 0.86)	109 m/s
Liquid Flow Rate:	110 cc/min (11.7 pph)

The vapor and liquid images were obtained in both side and top views; the axial location of the laser and camera was always such that the transition from premixer to flame tube was in the center of the image area. Magnification was adjusted so that the diameter of the flame tube just filled the width of the image area.

Images recorded with the CCD camera are stored on disk and can be viewed and analyzed with the CSMA software. Generally, a set of five liquid or vapor images was averaged to produce a final image. Averaging means that the individual pixel intensities at each pixel location were added and the result divided by the number of images. The software then can assign colors to the various intensity levels in the image and display a false color image on the video screen. Finally, a 35 mm color print of this image was made and a set of these prints was given to GE.

In Figures 4-11, contour plots corresponding to these same test results are shown. These contour plots were generated by a separate software package which took as input an ASCII data file made up of pixel x,y locations and the corresponding pixel intensity. Contours of constant intensity (normalized by the maximum intensity in the field) are generated and plotted by the program. Figures 4-7 show liquid and vapor distributions for centerline injection, while Figures 8-11 show the distributions for wall injection.

From these tests, the following observations can be made:

1. There is significant liquid present on both sides of the transition, presumably as droplets, whether the fuel tube is on the centerline or at the wall.
2. With the fuel tube on the centerline, the side views show the liquid concentrated in the upper half of the premixer and having moved only slightly away from this line just downstream of the transition. We believe this observation to be evidence of wall wetting in the premixer due to over-penetration of the fuel jet. The vapor, too, is concentrated in the upper half of the premixer, but has spread somewhat off this line in the larger diameter flametube. Still, the dispersion is very non-uniform with the region of highest

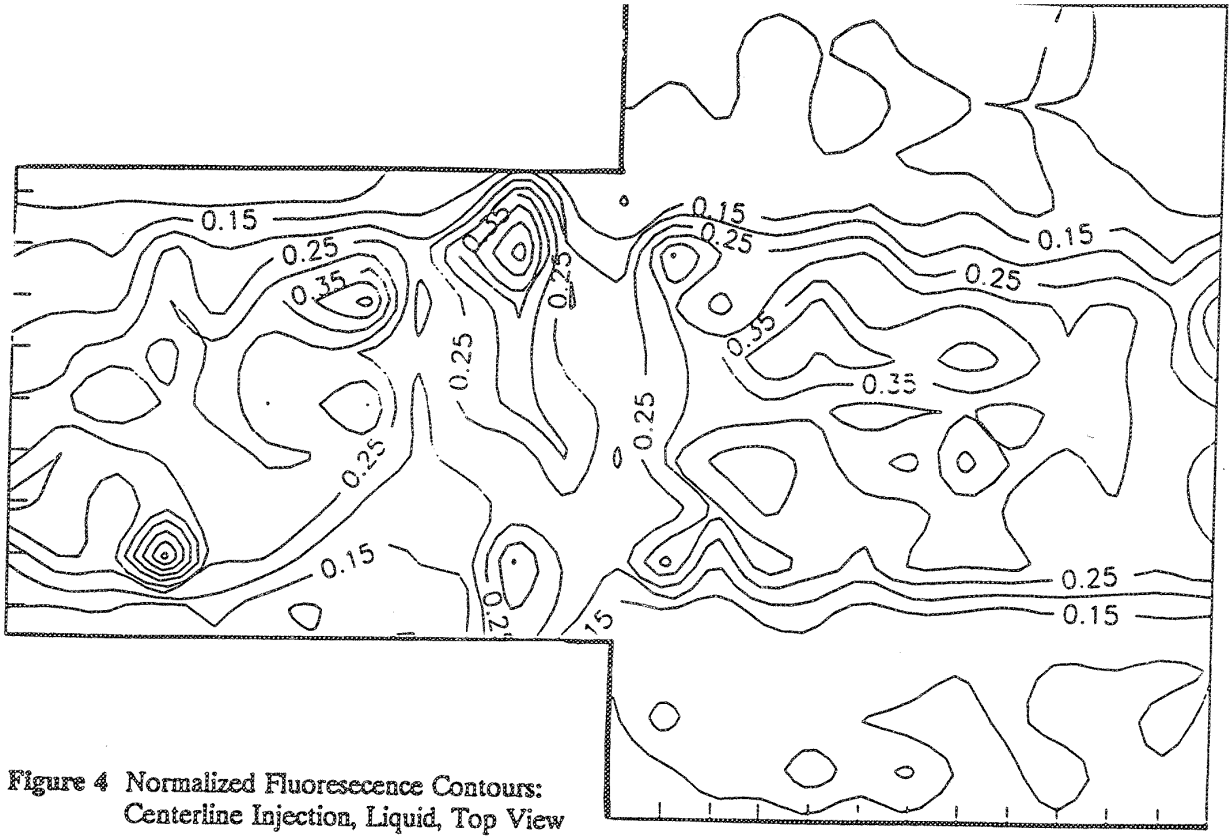

Figure 4 Normalized Fluoresecence Contours: Centerline Injection, Liquid, Top View

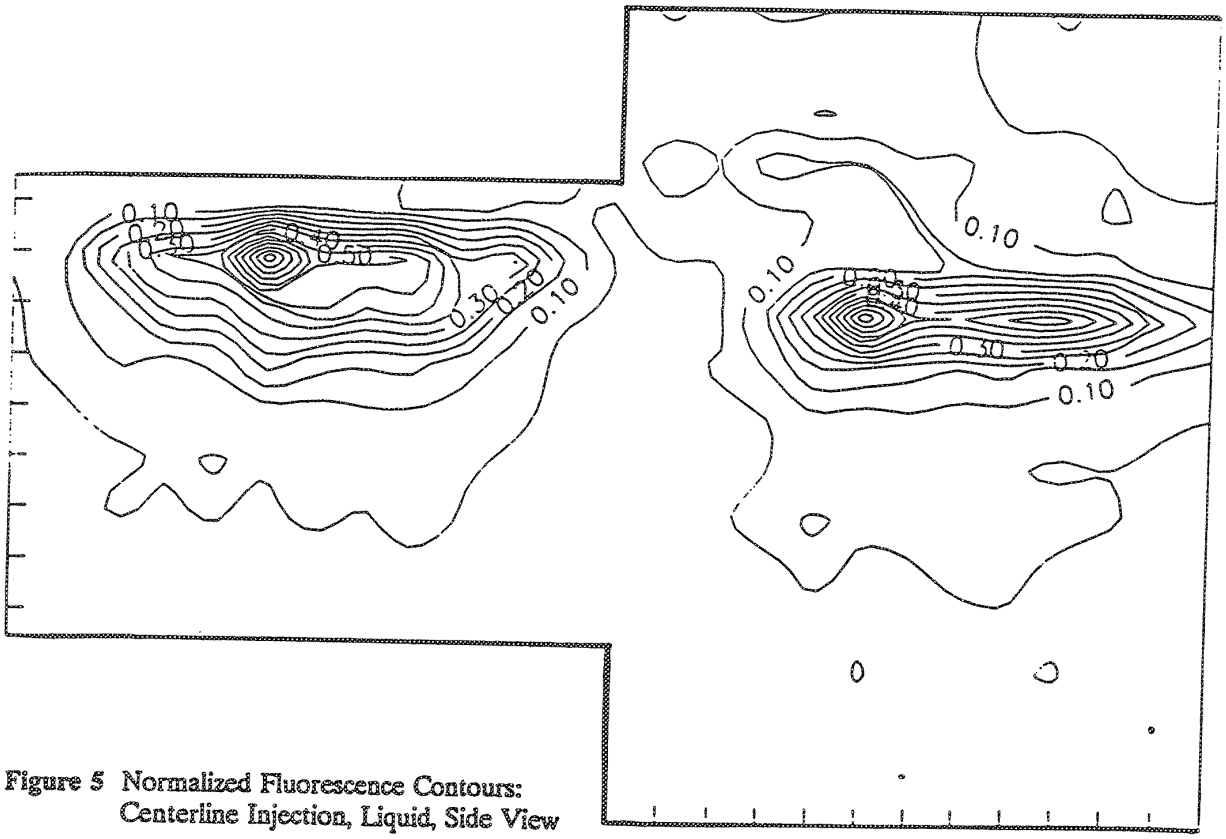

Figure 5 Normalized Fluorescence Contours: Centerline Injection, Liquid, Side View

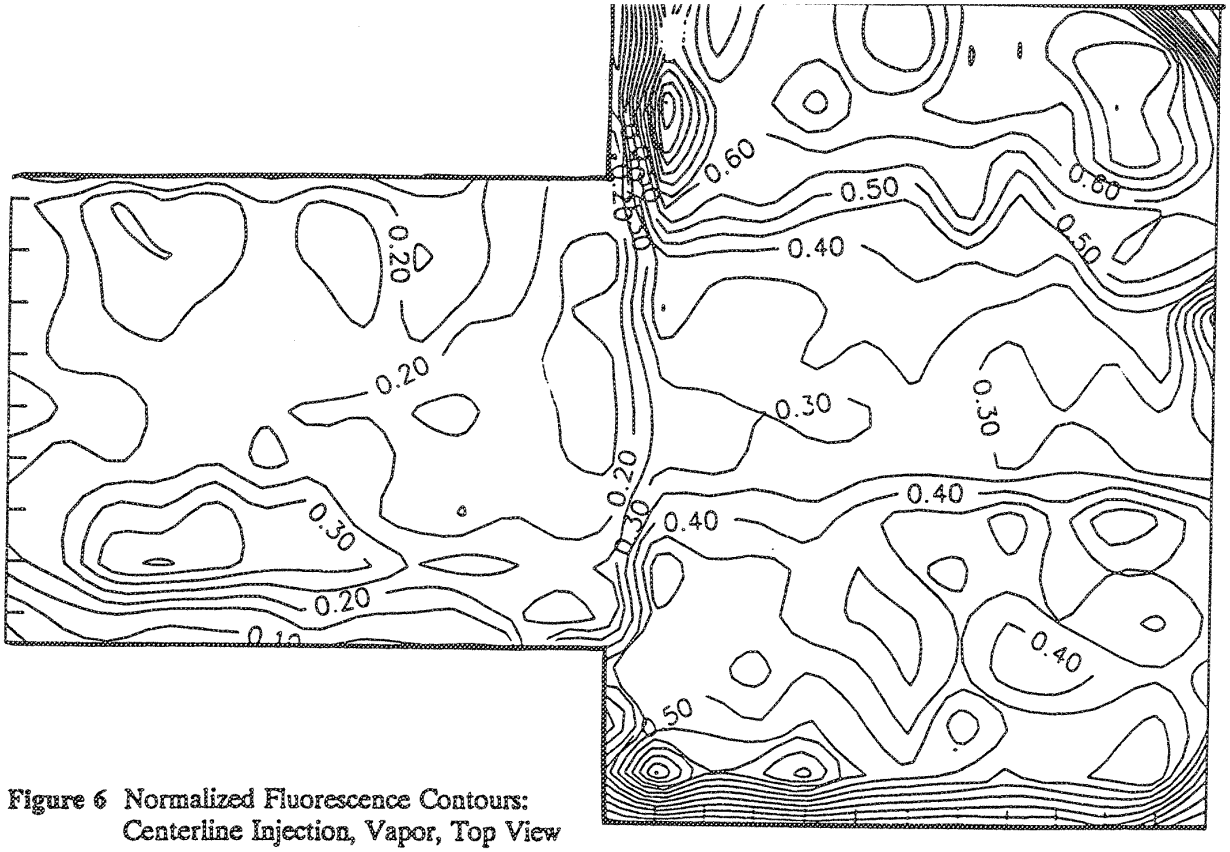

Figure 6 Normalized Fluorescence Contours: Centerline Injection, Vapor, Top View

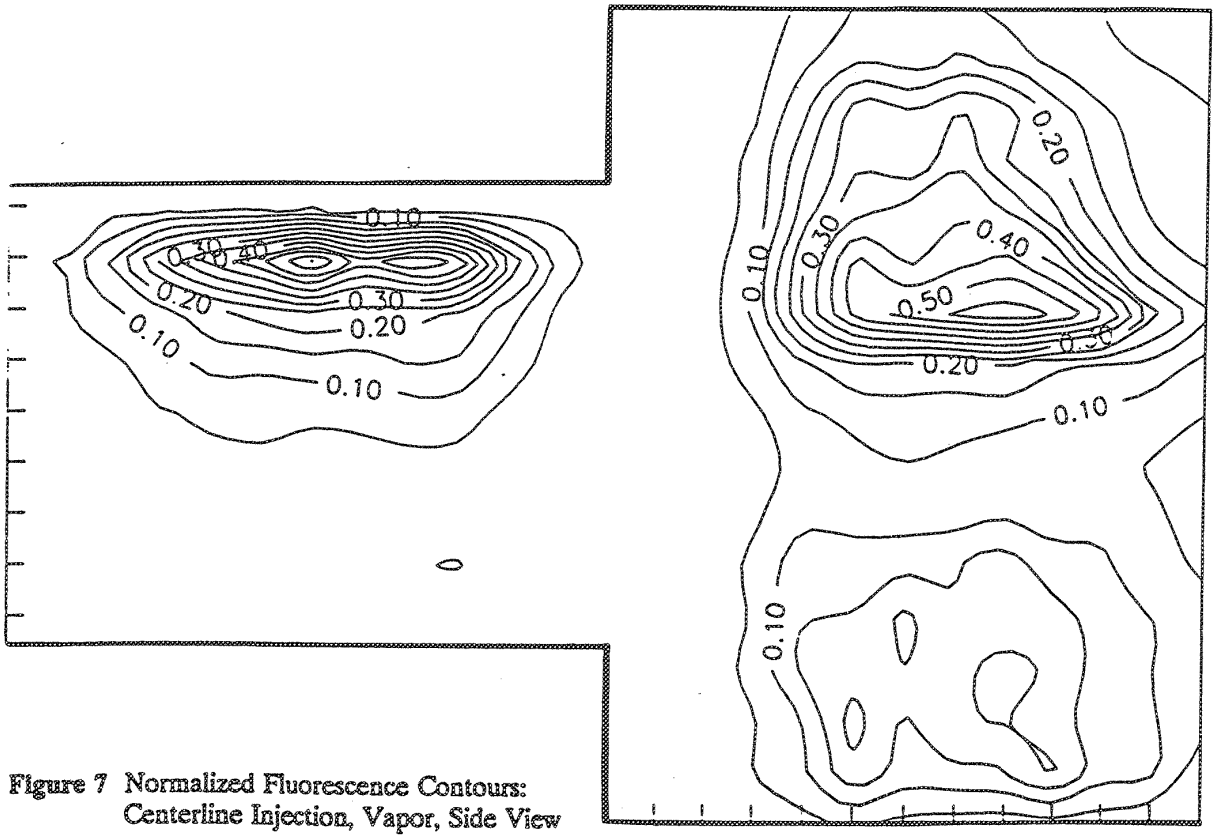

Figure 7 Normalized Fluorescence Contours: Centerline Injection, Vapor, Side View

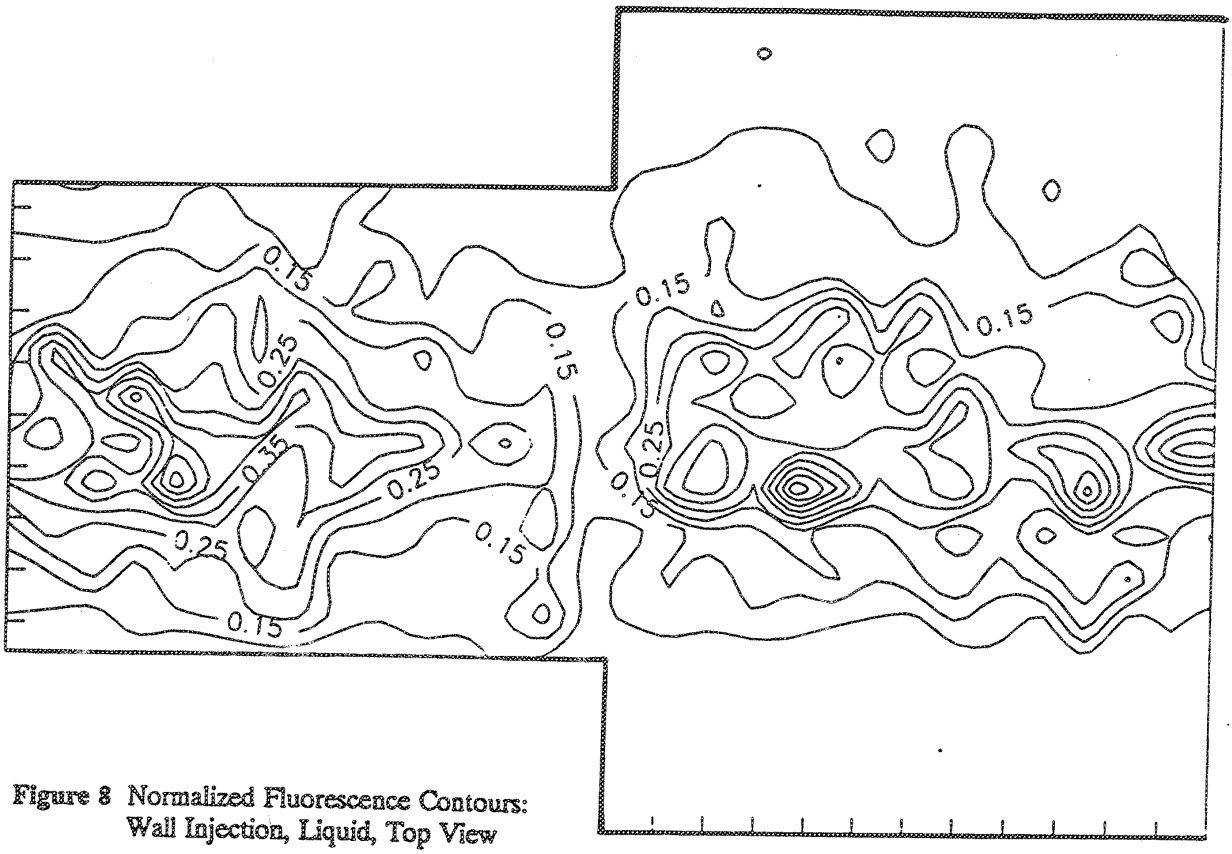

Figure 8 Normalized Fluorescence Contours: Wall Injection, Liquid, Top View

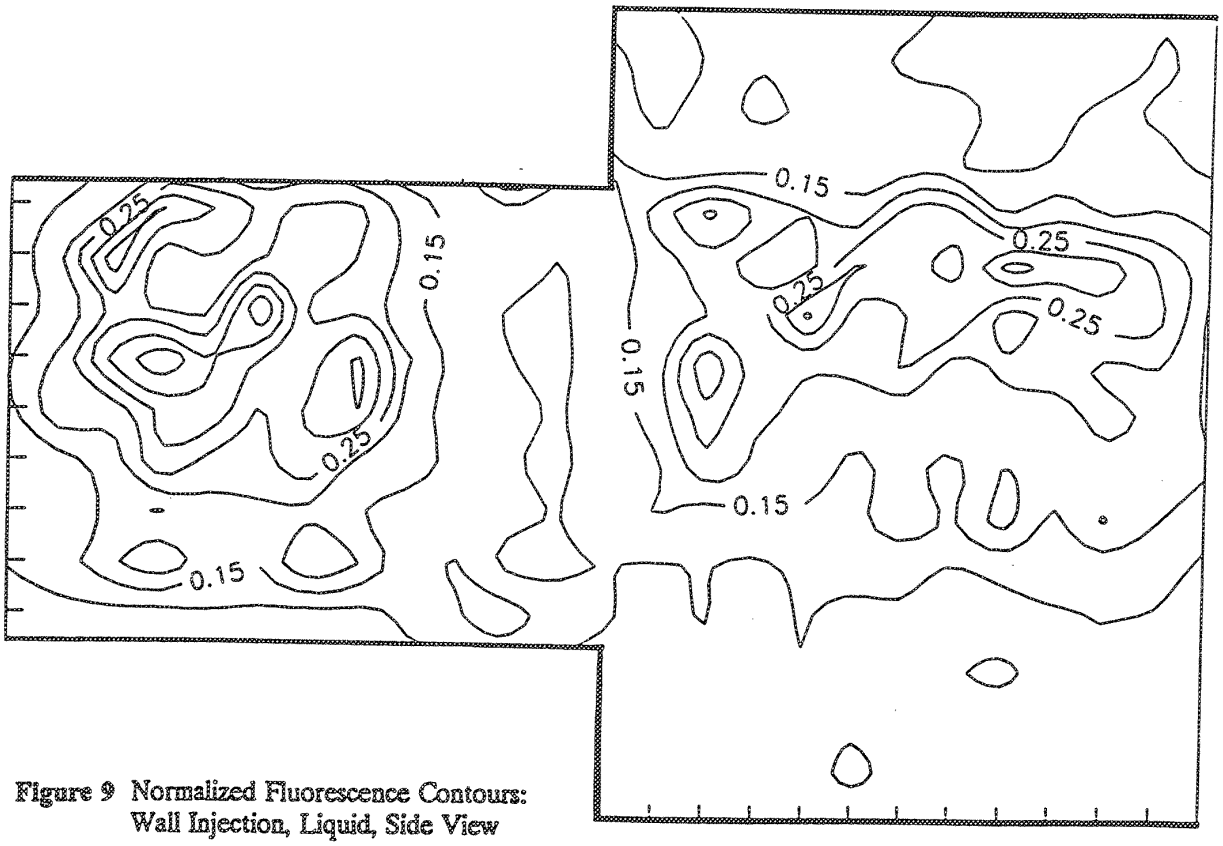

Figure 9 Normalized Fluorescence Contours: Wall Injection, Liquid, Side View

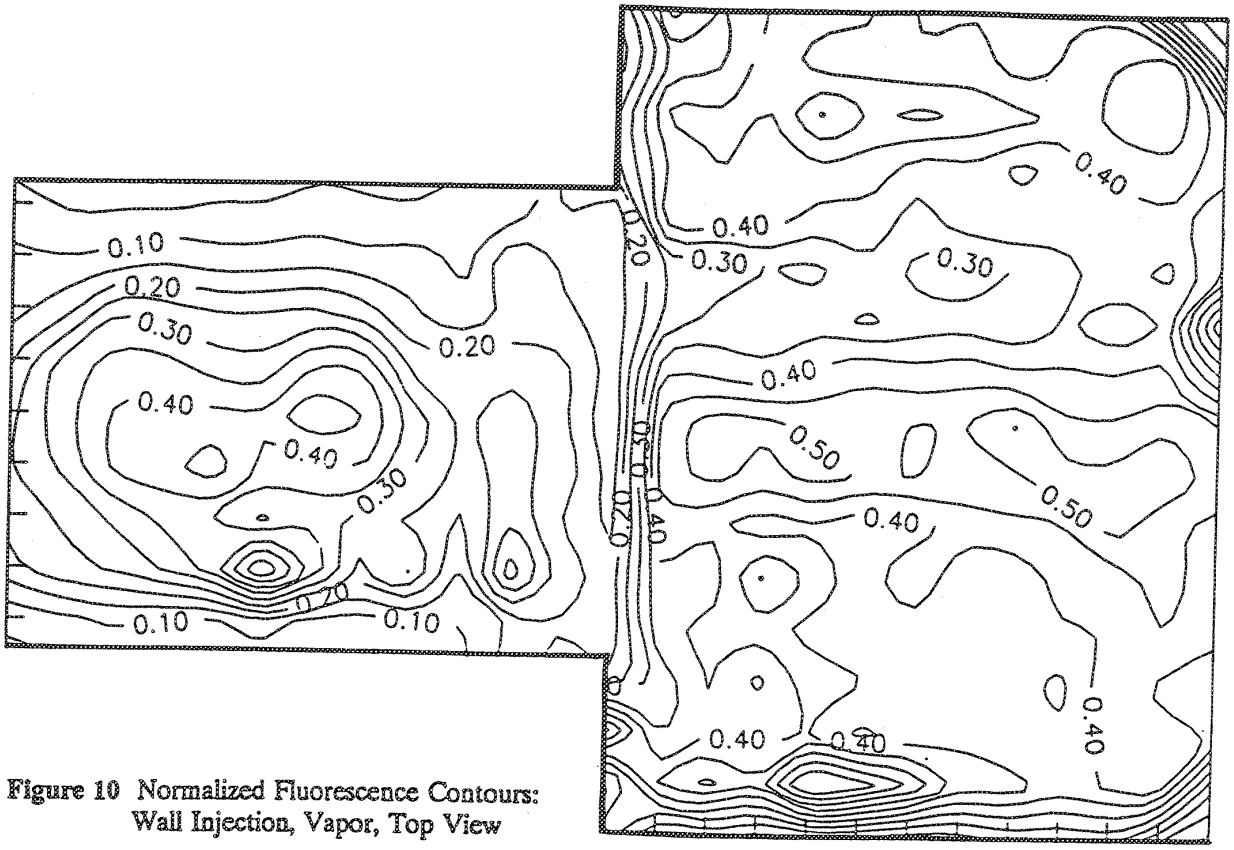

Figure 10 Normalized Fluorescence Contours: Wall Injection, Vapor, Top View

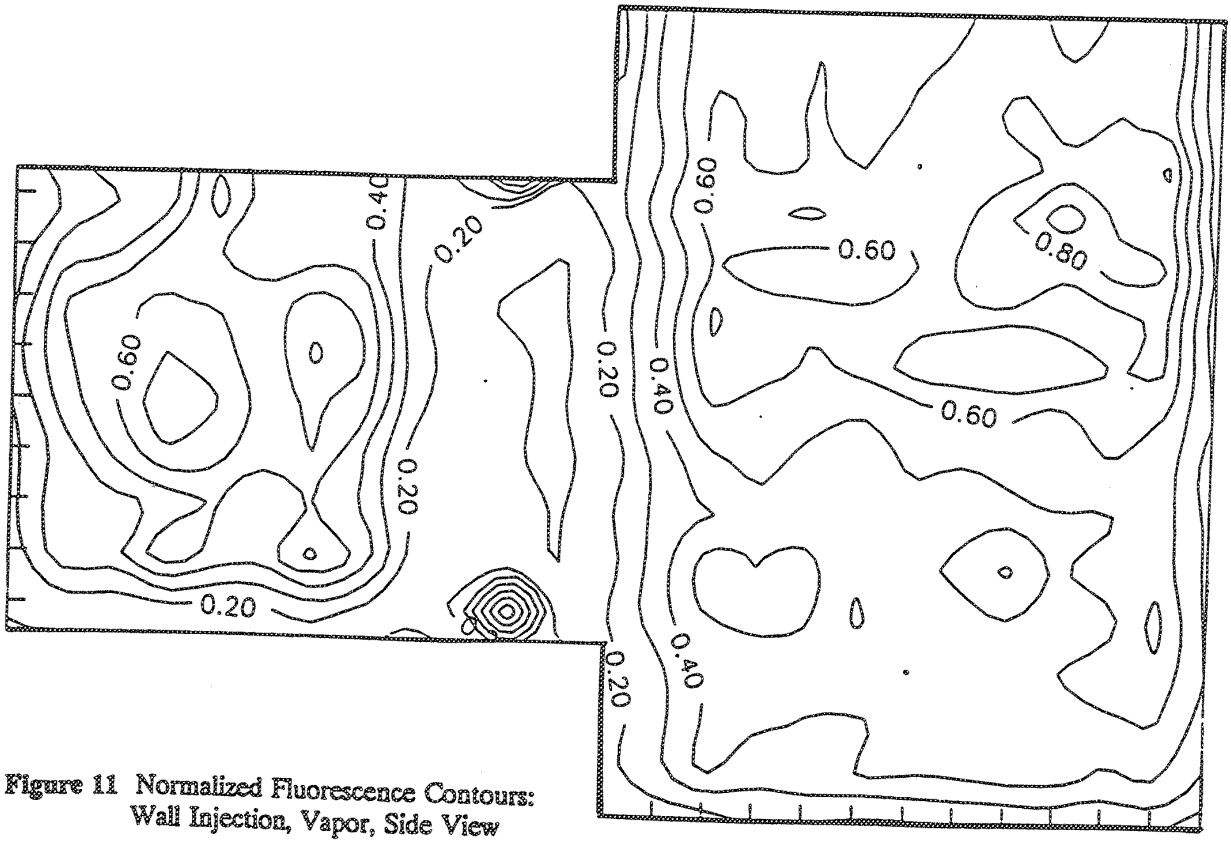

Figure 11 Normalized Fluorescence Contours: Wall Injection, Vapor, Side View

concentration of vapor lying near a line running downstream from the upper boundary of the premixer.

3. With the fuel tube at the wall, the side views show liquid and vapor on both sides of the transition, but both are much more uniformly distributed. Indeed the vapor fills the flametube region and seems very uniform.

At this point in the development of the exciplex technique, quantitative results were not possible, except to the extent that rough comparisons between two regions within a single image can be made.

C. Exciplex Calibration Experiments

In order to obtain absolute concentration information from exciplex data, a calibration curve of vapor or liquid concentration versus intensity must be obtained. For various reasons, including the fact that it is now known that the absorption coefficient for the exciplex dopants is very temperature-dependent above 500°K, it is best to obtain this calibration data *in situ*, under the same conditions which exist during an experiment. Also, laser power must be consistently maintained and variations in intensity along the laser sheet must be taken into account.

Several attempts were made to obtain this type of calibration data for the vapor component. The methodology was to try to create a uniform, completely vaporized mixture in the flameholder region and correlate the resulting fluorescent intensity with fuel flow.

For these calibration experiments, the fuel was injected via the hypo-tube at the far upstream end of the test section, ahead of the premixer, at the wall and pointing vertically upwards, transverse to the air flow. To improve the mixing, a set of Koflo static in-line mixing vanes was inserted in this upstream portion of the test section.

In order to give the exciplex mixture as much time to vaporize as possible, the camera and laser were positioned to view a region about 2.5 inches downstream of the transition from the premixer to flametube.

Laser sheet uniformity was checked and measured in the following way. A 1/4" o.d., 3/16" i.d. quartz tube about 3" long was filled with Jet A (which fluoresces brightly under UV illumination), stoppered, and attached to a rod. The rod was then inserted down the centerline of the test section so that the quartz tube was in the field of view of the camera. Then under 355 nm laser illumination, the fluorescence was recorded by the camera, producing an image of a thin line of varying intensity. Normalization of this intensity record then gave a correction factor for intensity variation along the laser sheet.

D. Results

Calibration images for several sets of experiments were analyzed for uniformity and for consistent trends. In most cases, it was found that the average intensity in one region of the field of view was quite different from that in another region. Also, in some cases, the data was not repeatable. The last data set showed the most internal consistency and incorporated the laser sheet uniformity correction. Experimental conditions were:

Date:	10/1/92
Inlet temperature:	360°C (680°F)
Air (N_2) Flow Rate:	52 scfm
System Pressure:	51 psig

For each of five fuel flow rates, a set of 5 images was recorded. These six images were averaged, and were corrected for laser sheet intensity variation. Then, a region of the image (actually the upstream half of the view area) was analyzed for its average pixel intensity, and for the standard deviation of the intensities in this region. The resulting graph of intensity versus fuel flow rate is shown in Figure 12; the data display a reasonably straight line.

These results demonstrate that we are making progress toward an exciplex calibration methodology in these experiments; however, the calibration results here cannot be applied yet to the

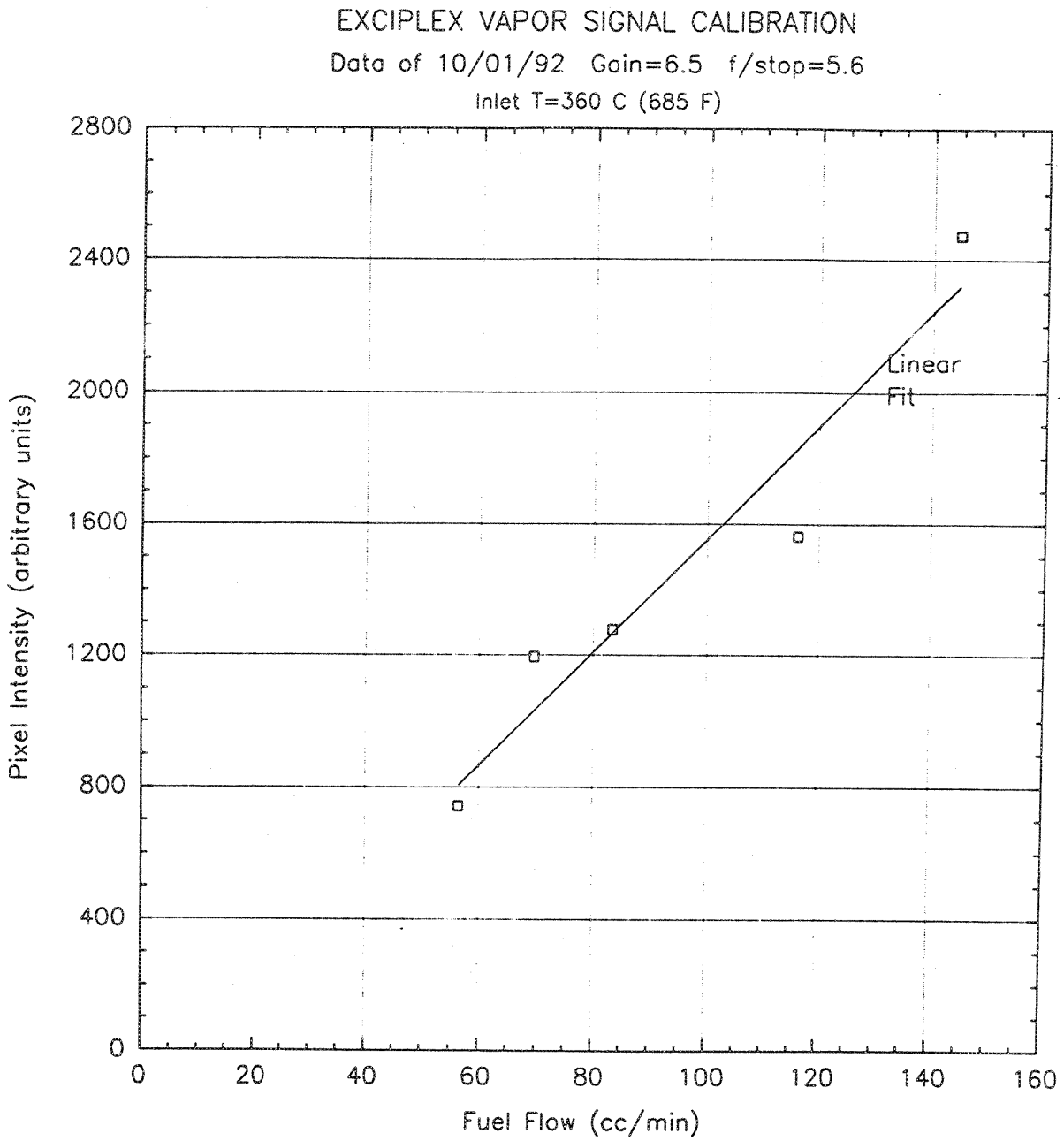
EXCIPLEX VAPOR SIGNAL CALIBRATION
Data of 10/01/92 Gain=6.5 f/stop=5.6
Inlet T=360 C (685 F)
Pixel Intensity (arbitrary units)
2800
2400
2000
1600
1200
800
400
0
Linear
Fit
0
20
40
60
80
100
120
140
160
Fuel Flow (cc/min)

Figure 12

exciplex results for several reasons. For example, the gain setting on the camera was not the same in the calibration tests as it was in the liquid-vapor visualization experiments.

The calibration experiments need to be considerably improved before applying them to exciplex results. We cannot yet be sure the fuel is entirely vaporized, and the standard deviations are too high, indicating non-uniformities persist. And we do not yet know the repeatability of these results.

IV. COMBUSTION EXPERIMENTS

The goal of the combustion experiments was to obtain lean stability limit data and emission (NO_x, CO, CO_2, O_2) data for the same injection geometries and test conditions which were studied with the exciplex technique. Several combustor designs were attempted before one which would successfully survive the combustion environment was achieved. Initially, the designs incorporated ceramic materials in order to keep the combustor adiabatic, thus simulating a real combustor situation wherein one combustor is surrounded by others. However, the final successful design was entirely metal and air cooled. A short description of each design follows.

A. Design History

The first design incorporated a hard ceramic (99.8% alumina, Vesuvius McDanel) flame tube which actually formed the liner of a stainless steel outer tube. This external tube was welded to a stainless steel pre-mixer. The alumina combustion tube extended about 6" beyond the combustion section into the quench section. Four 1/2" diameter holes were drilled circumferentially at 5 locations along this 6" extension through the tube wall to aid mixing of combustion gases with quench air in this quench region. A small hole was drilled through the outer stainless steel tube and through the alumina liner just downstream of the sudden expansion to accommodate an igniter.

The igniter was made from a four-hole, 3/16" dia. alumina tube in a stainless steel sleeve. Two platinum wires were fed through two holes in the alumina to form a spark gap, a stainless steel

tube was fed through a third hole to allow for hydrogen flow, and the fourth hole was not used. The spark-ignited hydrogen flame served as the igniter to the main flow. This method of ignition has been retained through all combustion tests.

Sustained combustion was achieved in this apparatus, but examination of it after only a few short tests revealed a broken and cracked alumina liner. It was concluded that the rigid alumina cannot stand up to the severe thermal shock encountered during ignition and combustion.

The second design incorporated low density ceramics from Zircar Products, Inc., for the combustion section. This section consisted of three ceramic tubes nested inside each other. The innermost was 1 1/8" i.d. x 2" o.d. SALI ceramic, the middle section was 2" i.d. x 3" o.d. ALC ceramic, and the outer section was 3" i.d. x 5" o.d. ASH ceramic, each cut to a 12" length and housed inside a length of steel pipe which fit inside the 6" stainless test section. However, after only three combustion tests, inspection showed that the inner SALI tube had broken in several places. Consequently, hot combustion gases had reached the stainless liner in the quench section and damaged it. Also, it was clear that the hot, high-velocity gases, easily eroded this low-density ceramic material.

At this point, the ceramic flame tube design was discarded in favor of a cooled, thin-walled (1 1/8" i.d. x 1 1/4" o.d. x 12" long) stainless steel tube. The region around the step transition was also redesigned to allow for annular cooling flow along the entire length of the flame tube. The stainless steel "window" ports in the test section were modified to accommodate hose connections and air, which previously flowed directly into the quench section was redirected through these window ports. An annular region around the flame tube was formed by retaining the outer two ceramic tubes. Air entering the test section through the window ports flowed through an annular ring of perforated stainless steel to help distribute the flow and then flowed down the length of the flame tube to cool it. A schematic drawing of this design is shown in Figure 13.

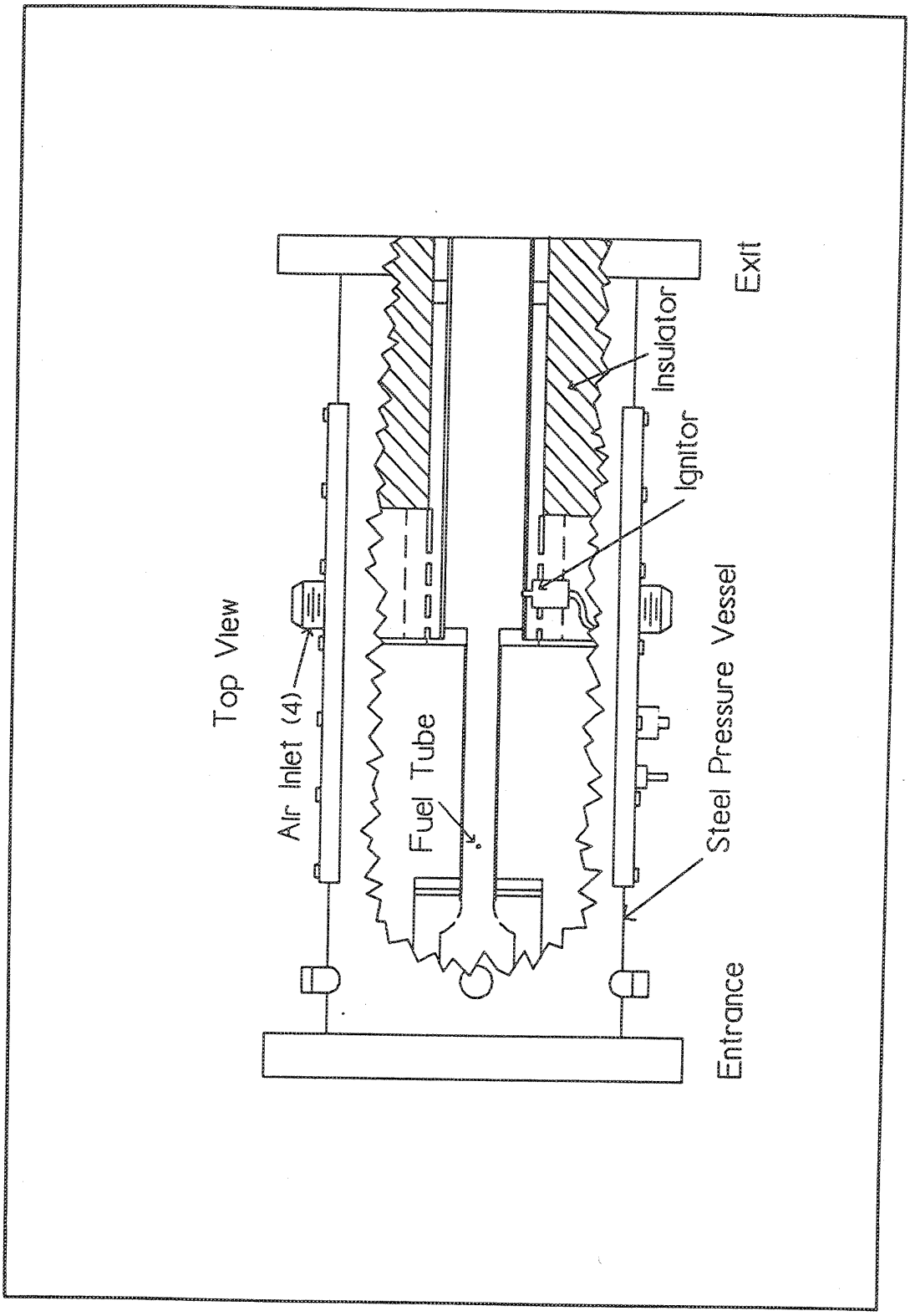

Figure 13 Cut Away View of Combustion Test Section

A number of combustion tests were made with this design. Initial inspection of the stainless tube showed it to be intact. However, at some unknown point in these tests, the flame tube badly warped, and a large hole was burned through its wall. Thus, emission data from this period could not be considered valid. We had to conclude that the stainless steel tube also was not durable enough for these conditions and that cooling of the stainless steel tube was still inadequate.

This led to the final and most successful design. The flame tube was fabricated from Haynes Alloy 230, 1" schedule 40 pipe, with the i.d. machined to 1.125". The tube was made to extend from the sudden step at the transition, nearly to the end of the quench section (a total length of about 27 1/2"); it passed inside the cooling coils in the quench section. A square cross section, spiral groove was cut in the upstream 12 inches of the flame tube in order to enhance cooling by the annular flow of cooling air. This special alloy tube was welded to the upstream premixing section using a redesigned transition piece.

In the first version of this design, a pair of Koflo static mixers was fixed in the flame tube in order to encourage mixing of the combustion gases so that the sampling probe would be sampling a uniform mixture. However, these stainless steel mixers burned up and blew out in the first test. The combustion tube itself, though, has sustained many tests in which its measured exterior wall temperature has been >800°C (1472°F) and has been relatively problem free. This configuration was used in all experiments reported here.

B. Experimental Conditions

Certain conditions remained unchanged throughout these experiments. They were:

System Pressure = 50-53 psig

Air Flow Rate = 50-52 scfm

Air Speed in Premixer (assuming a flow coefficient of 0.86) = 101 m/s @ 360°C (680°F) inlet
= 117 m/s @ 460°C (860°F) inlet

Fuel = Jet A

Injector = 0.020" i.d. x 0.040" o.d. hypo-tube positioned either at the wall or on the centerline

Sampling Probe Position = 25" downstream from the step transition between premixer and flame tube (except in special experiments during which the probe position was axially varied).

Early combustion experiments in which CO, CO_2 and O_2 levels were measured showed a discrepancy between the equivalence ratio based upon measured flow rates of fuel and air, and that calculated from measured CO, CO_2, and O_2 emissions using hydrogen, carbon and oxygen balances. This latter calculation requires certain assumptions including that there are negligible unburned hydrocarbons and nitrogen oxides in the products, that all water is removed from the products before measurements are made, and that the atomic ratio of hydrogen to carbon in the fuel is 2.0 to 1. Jet A is a mixture of hydrocarbons, but is often modeled as $C_{11}H_{22}$ in chemical calculations. However, because of this equivalence ratio discrepancy, questions remain concerning the fuel composition, and steps are being taken to define the hydrogen-to-carbon ratio. The equivalence ratio discrepancy was almost always such that the emission-based equivalence ratio was richer than the flow-based ratio. In order to be sure that air measured in the air flowmeter was not somehow lost from the combustion process, the combustor test section was tightened against leaks by welding most of it together; also, the inlet section of the premixer-combustor was screwed tightly to the flange connecting the heater section and the test section. And the fuel inlet was accomplished through a welded-on swagelok fitting.

In order to prove the tightness of the system, the following test was done. First, the Hastings Raydist Flowmeter measured flow through the pipe and hose from the compressor to the control panel, and a large Fischer-Porter rotameter measured it at the panel outlet and exhausted to the atmosphere. The two meter readings were compared over a range of 22 to 40 scfm, with the system operating at essentially 1 atm and room temperature, and found to agree to within ± 5%. Then, the heater section and the test section inlet-combustor were inserted between the two flowmeters. Again, the two readings were compared under the same operating conditions and found to agree to within ±

5%. This is certainly strong evidence that no air is lost in the test section and that the Hastings meter is measuring the entire combustion air flow.

C. CO, CO_2, O_2 Emissions Experiments

For the centerline injection case, tests were run with inlet air temperatures of 360°C (680°F) and 400°C (750°F). These results are shown in Figures 14-16. The flow-based equivalence ratio was varied from about 0.75 to about 1.05. In the tests of 3/19 and 3/22/93 (Figures 15 and 16), the agreement between flow-based and emission-based equivalence ratios is excellent; however, in the first test (Figure 14), the emission-based equivalence ratio is consistently richer than the flow-based. No explanation for this difference has been found.

For the wall injection case, one test was performed at the 360°C (680°F) inlet condition. The results of this test are shown in Figure 17, and it can be seen that there is a large discrepancy between flow- and emission-based equivalence ratios. The emission-based ratio ranges from about 0.50 to 0.85.

In order to try to find the cause of this discrepancy, additional investigations were made. First, the system was once again checked for air leaks by comparing the Hastings Flowmeter reading at the inlet to the system, to the Fischer Porter reading at the exit. These readings were found to agree to within +10% over the range of 10-44 scfm which cannot account for the large differences in equivalence ratios.

It was also thought that possibly the sampling probe was collecting a sample from a location at which the exhaust gases were not uniformly mixed. In order to check this possibility, a second investigation was run in which the CO, CO_2 and O_2 measurements were made at several axial locations inside the combustion tube upstream of the usual location for the wall injection case. These results are shown in Figures 18-21, for flow-based equivalence ratios of 0.39 and 0.51.

In Figure 18, note that the emission-based equivalence ratio is about 0.59, and the variation of the computed values at the 5 axial locations is less than 3%. In Figure 20, this variation is less than

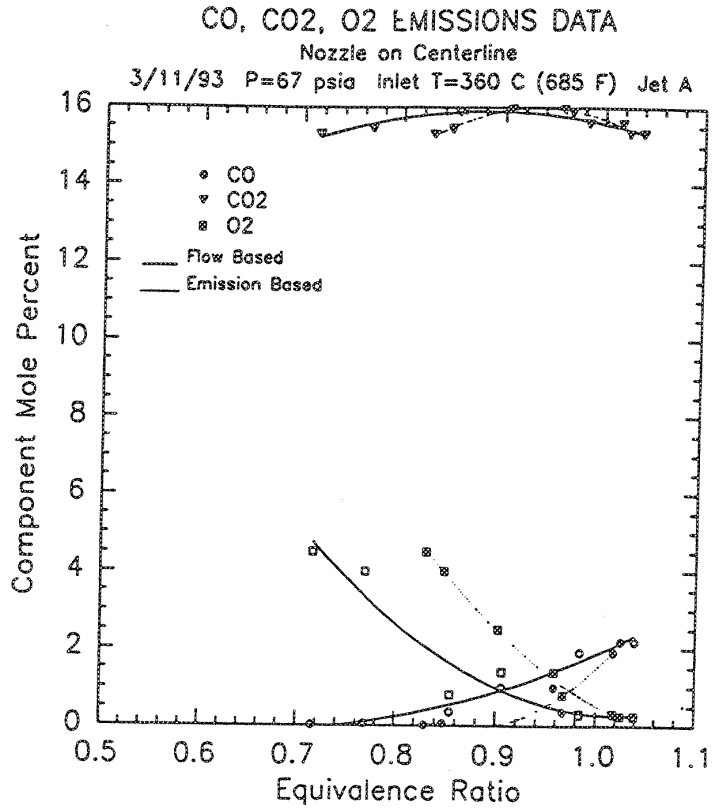

Figure 14

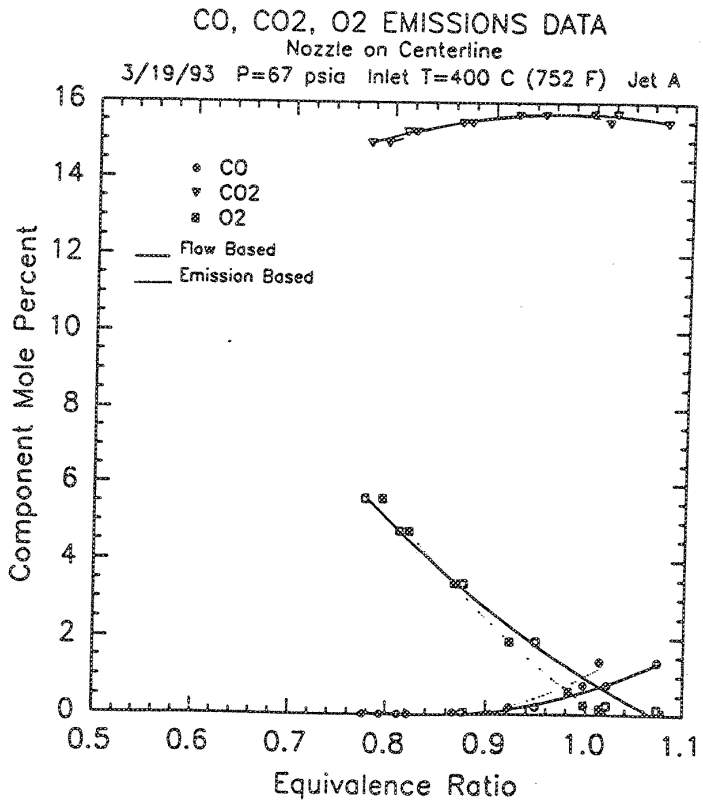

Figure 15

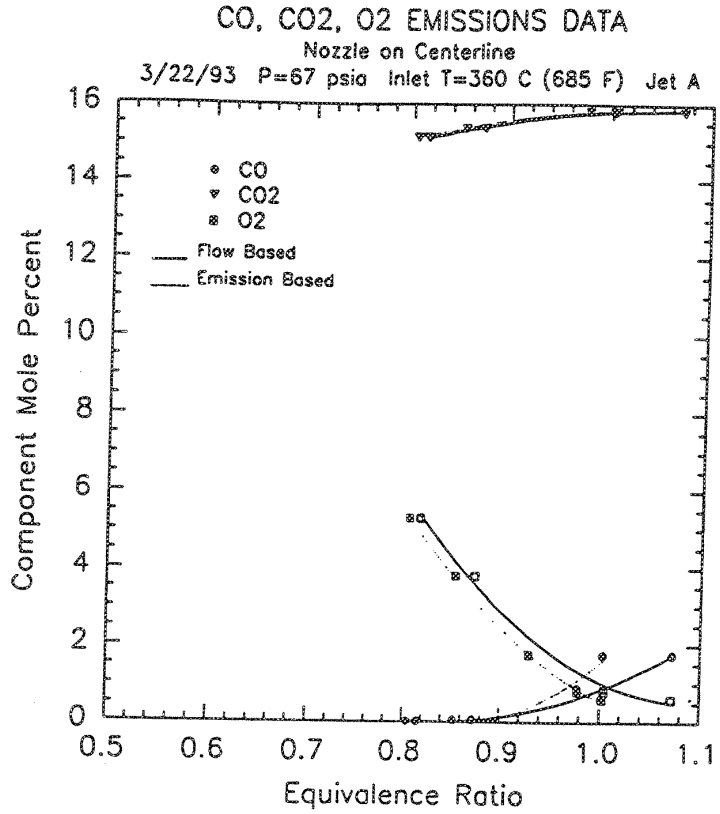

Figure 16

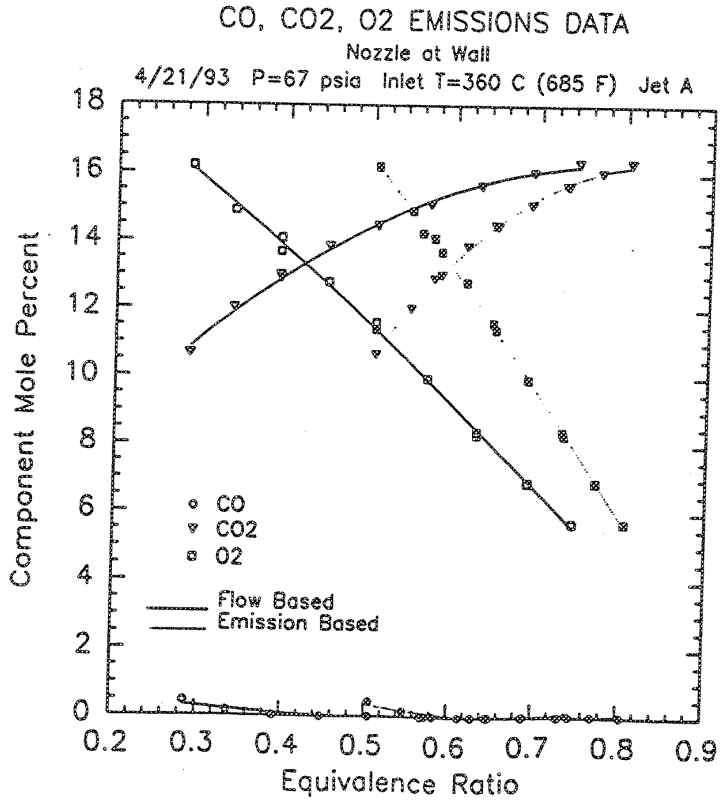

Figure 17

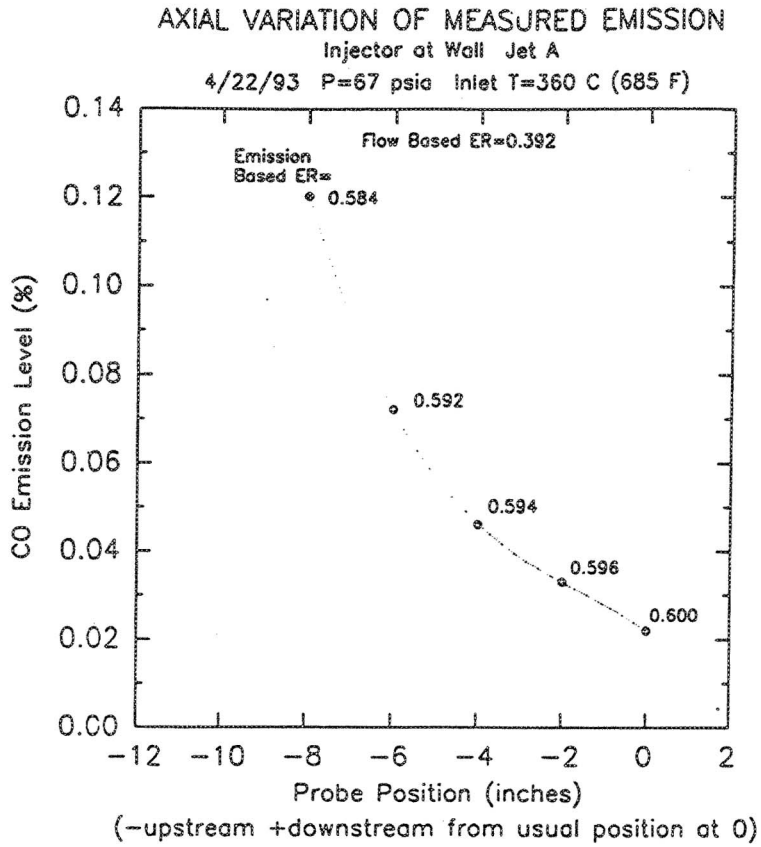

Figure 18

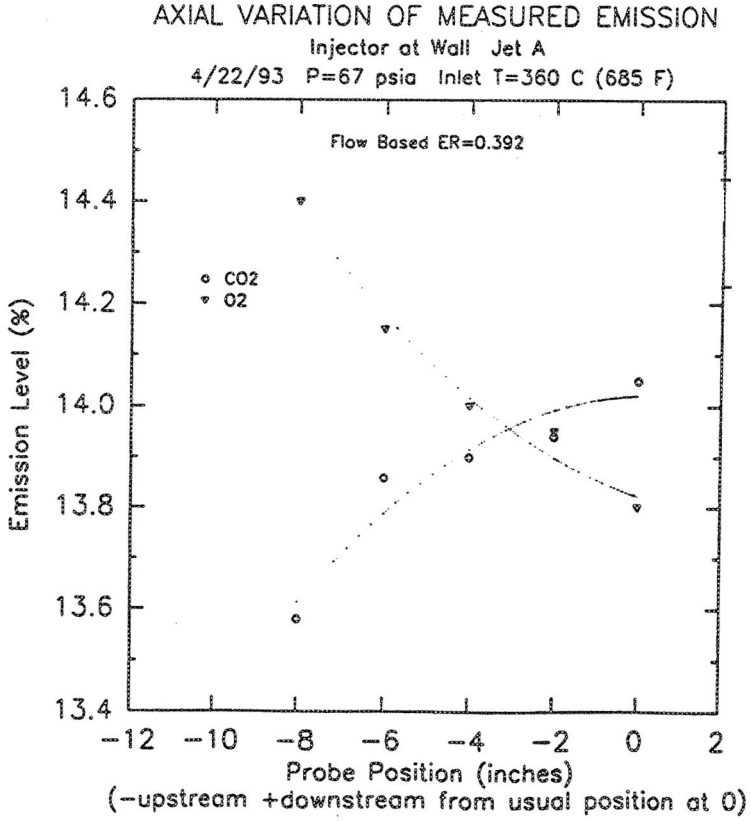

Figure 19

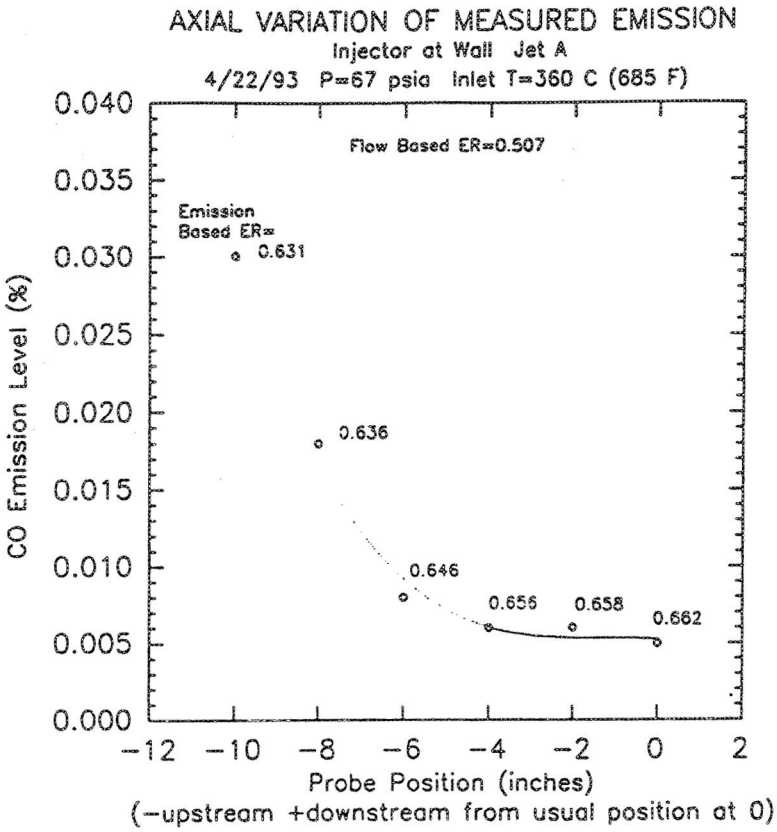

Figure 20

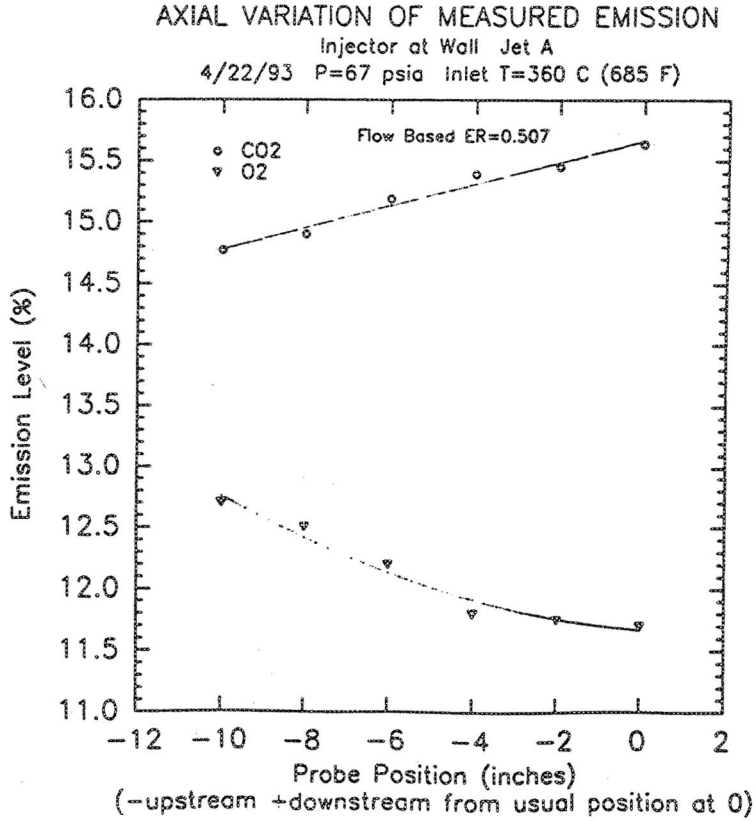

Figure 21

5%. From this evidence, it is likely that the sample is being extracted from a region, in each case, which is reasonably well mixed and uniform. At the present time, this 20-30% difference between flow-based and emission-based equivalence ratios cannot be explained and further tests must be done to uncover the problem. For example, the previously mentioned air flow meter comparisons were done with the Hastings meter at pressures lower than it experiences during combustion tests; its pressure dependence will be tested. And the fuel will be analyzed to better identify the hydrogen-to-carbon ratio.

The CO levels were generally very low, thus indicating a high combustion efficiency. For example, in the case of wall injection with an inlet temperature of 360°C, the combustion efficiency was greater than 99.9% between the equivalence ratios of 0.6 and 0.8 (emission-based); in the case of centerline injection, at 400°C inlet, the combustion efficiencies were slightly lower, at about 99.8%.

D. NO_x Emissions Experiments

With the injector on the centerline of the premixer, measurements of NO_x in the exhaust were made at inlet air temperatures of 360°C (680°F), 400°C (752°F), 430°C (806°F) and 460°C (860°F), over a (flow-based) equivalence ratio range of 0.65 to 1.05. These data are shown individually in Figures 22-25 and combined on one graph in Figure 26. Recall that when NO_x levels were measured, no other components in the exhaust were measured; the equivalence ratio in these figures is based on flowrates. In no case for centerline injection was the NO_x level ever much below 100 ppm. The higher inlet temperature cases do show slightly higher NO_x levels as might be expected.

With the injector at the wall, NO_x measurements were made at inlet temperatures of 360°C (680°F) and 460°C (860°F) over a flowrate based equivalence ratio range of 0.3 to 0.7. Results from these tests are shown in Figure 27. In these cases, the NO_x levels ranged from 20 to 200 ppm. Again, the levels are slightly increased at the higher inlet air temperatures. Results for both the centerline and wall injection NO_x levels are shown in Figure 28, for the 460°C inlet case.

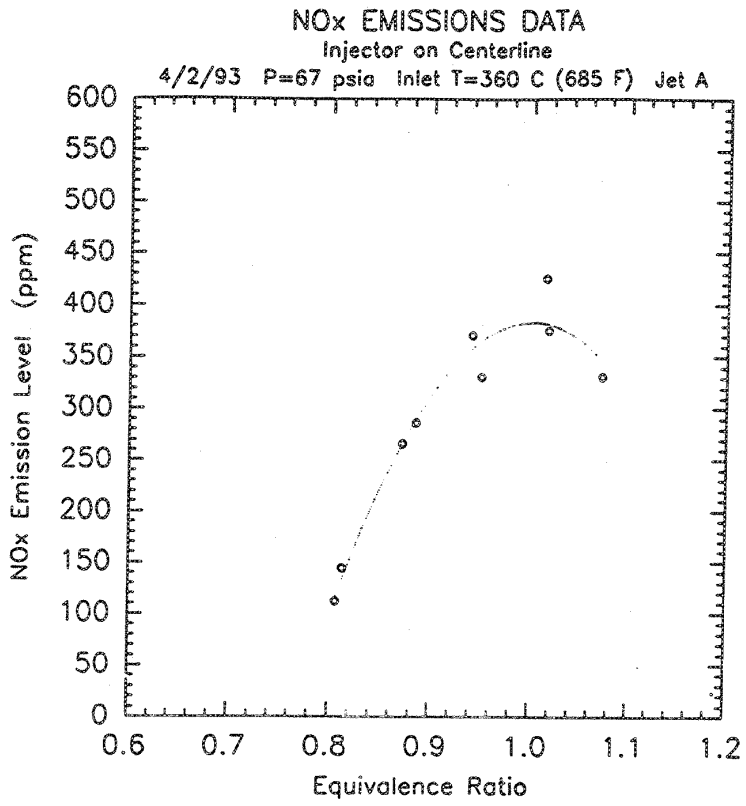

Figure 22

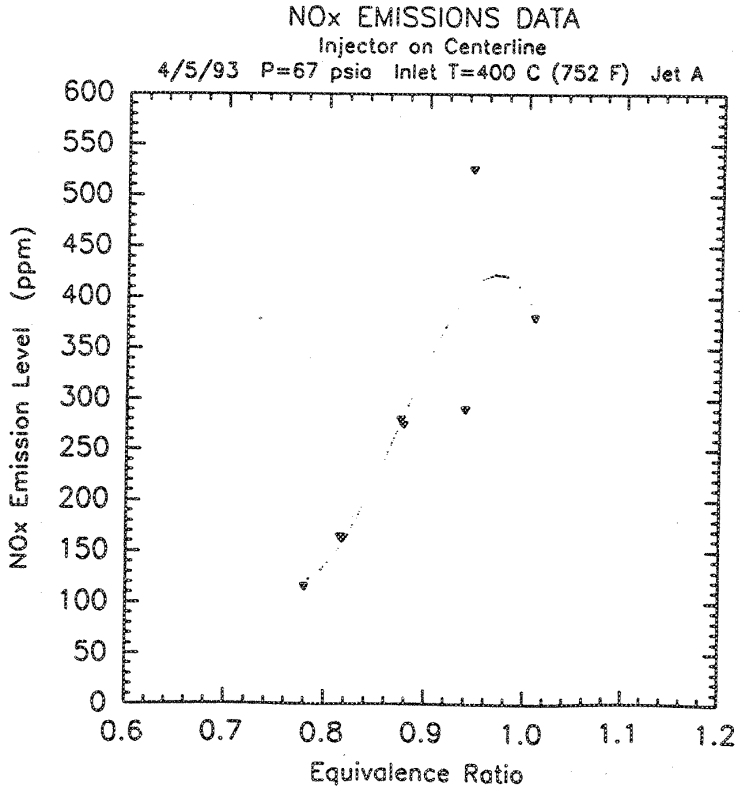

Figure 23

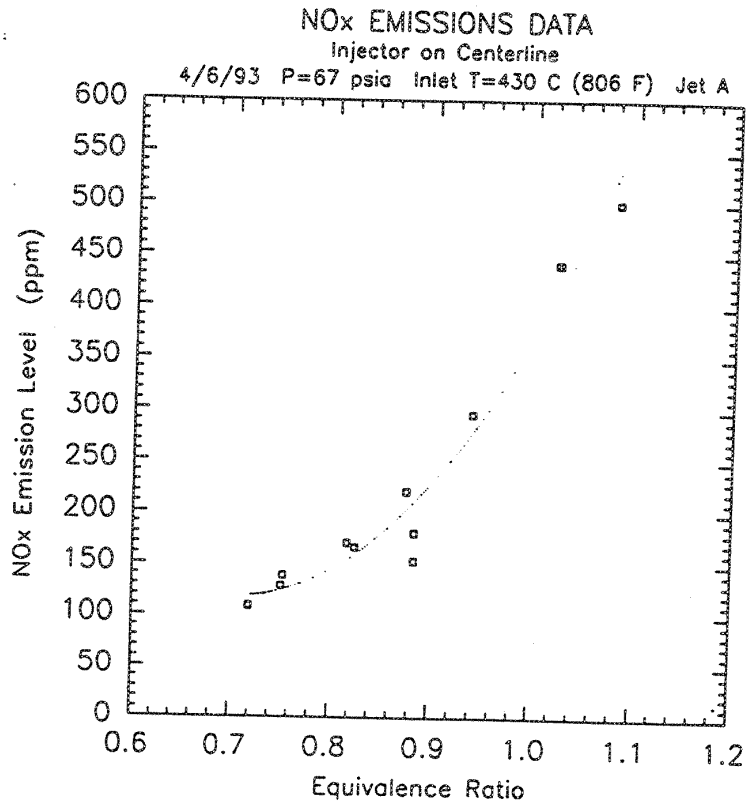

Figure 24

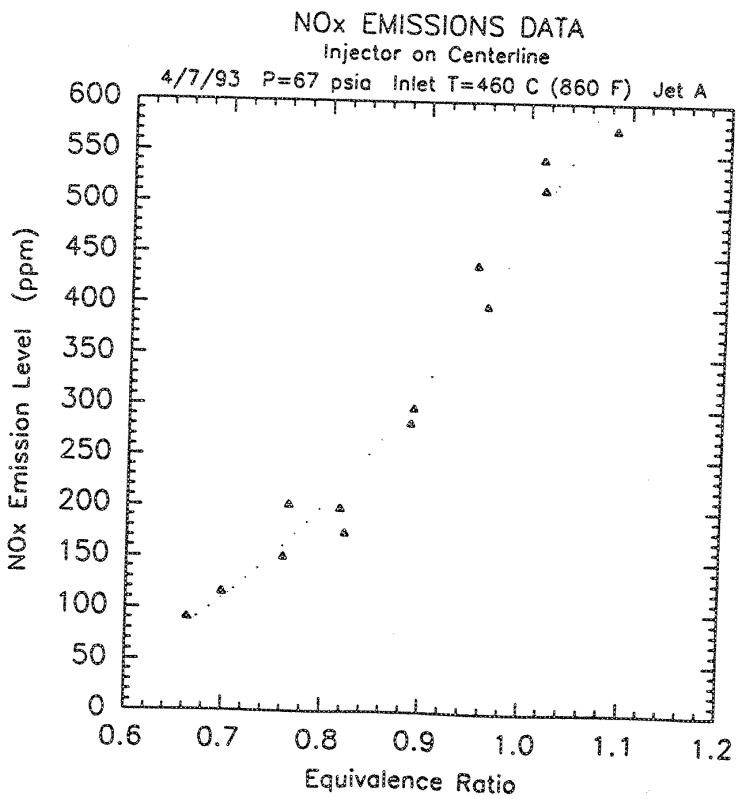

Figure 25

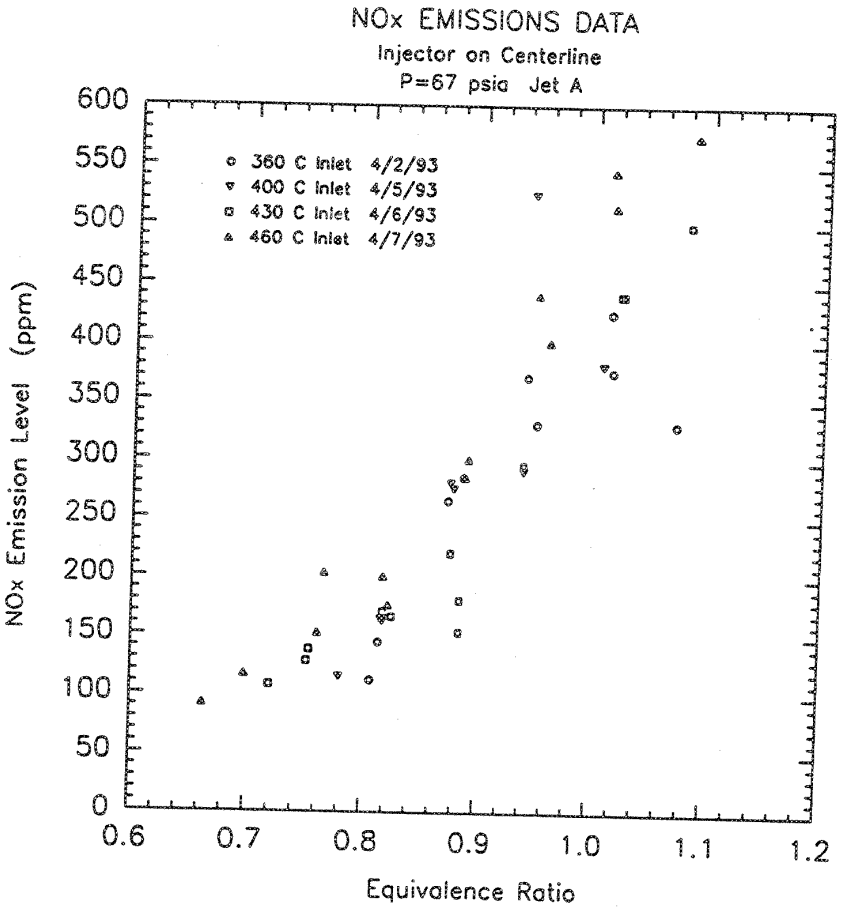
NOx EMISSIONS DATA
Injector on Centerline
P=67 psia Jet A
360 C Inlet 4/2/93
400 C Inlet 4/5/93
430 C Inlet 4/6/93
460 C Inlet 4/7/93
NOx Emission Level (ppm)
Equivalence Ratio
0
50
100
150
200
250
300
350
400
450
500
550
600
0.6
0.7
0.8
0.9
1.0
1.1
1.2

Figure 26

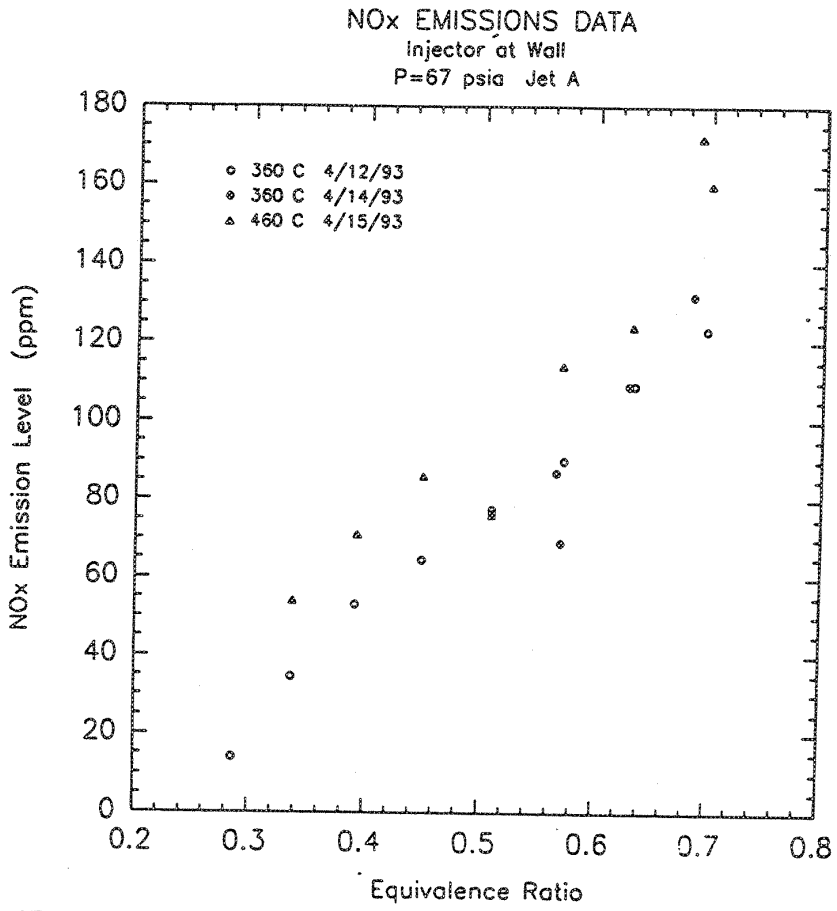
NOx EMISSIONS DATA
Injector at Wall
P=67 psia Jet A
360 C 4/12/93
360 C 4/14/93
460 C 4/15/93
NOx Emission Level (ppm)
Equivalence Ratio
0
20
40
60
80
100
120
140
160
180
0.2
0.3
0.4
0.5
0.6
0.7
0.8

Figure 27

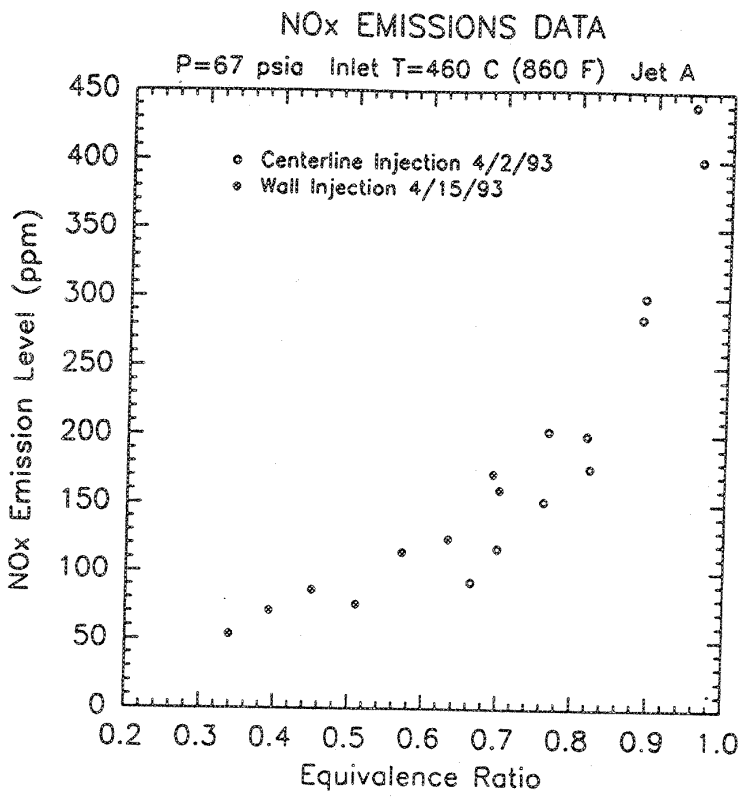

Figure 28

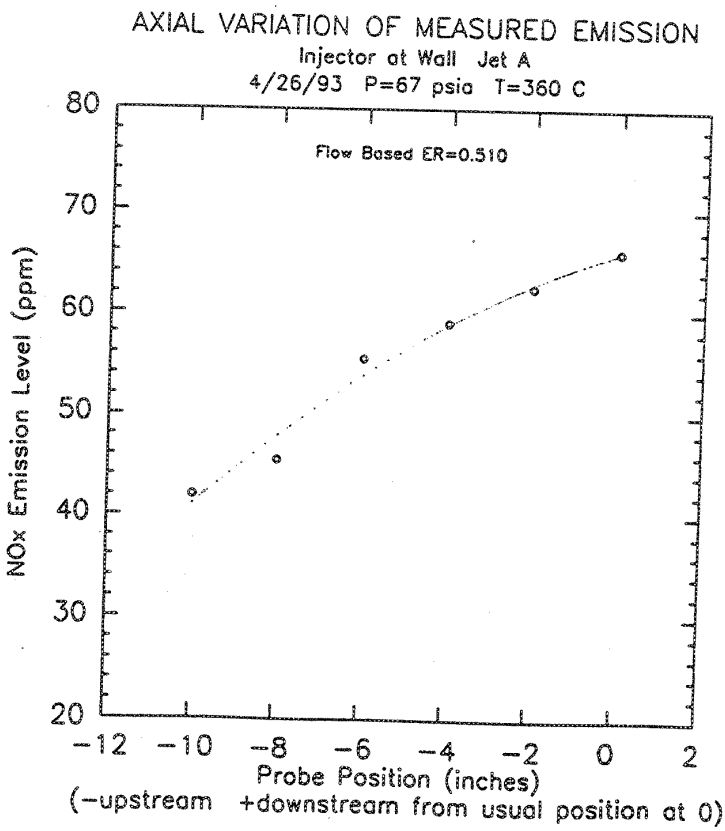

Figure 29

Surprisingly, it can be seen that the trends are such that the two injection geometries result in similar NO_x levels for a given equivalence ratio. The exciplex visualization results defined the wall injection case as yielding a more uniform distribution of both fuel liquid and fuel vapor. For a given overall equivalence ratio, a more uniform mixture at lean conditions yields reduced NO_x levels;[5-6] however, this was not observed in these experiments. Wall injection, though, did allow operation at leaner equivalence ratios, and hence, at lower NO_x levels.

In the course of making the NO_x measurements, it was not difficult to extend the measurements slightly and investigate the axial development of NO_x along the length of the combustion tube. Axial measurements of NO_x were made for one case, namely wall injection, 360°C (680°F) inlet temperature, and a flow rate based equivalence ratio of 0.51. These measurements are shown in Figure 29, and may be compared with the results shown in Figure 20 for CO under very similar conditions. It is clear in Figure 29 that NO_x is still forming, even at probe position 0, while in Figure 20, CO has reached a steady value at probe position -4 or so. Studies such as these may provide useful information applicable to determining a combustor length resulting in reduced NO_x while completing the burning of CO.

E. Lean Limit Experiments

During the NO_x emission experiments, the weak extinction limit of these flames was also measured. For both the centerline and wall injection cases, the limit was measured at 360°C (680°F), 400°C (752°F), 430°C (806°F), and 460°C (860°F) inlet air temperatures; one additional test, at 300°C (572°F), was done for wall injection.

The results for centerline injection are shown in Figure 30, and as inlet air temperature increases, the weak extinction equivalence ratio decreases almost linearly from 0.78 to 0.64 (flow-based) over this 100°C range.

A more surprising result was found for the wall injection case. Here, the weak limit was nearly constant over the inlet air temperature range considered, 300-460°C (572-860°F), varying

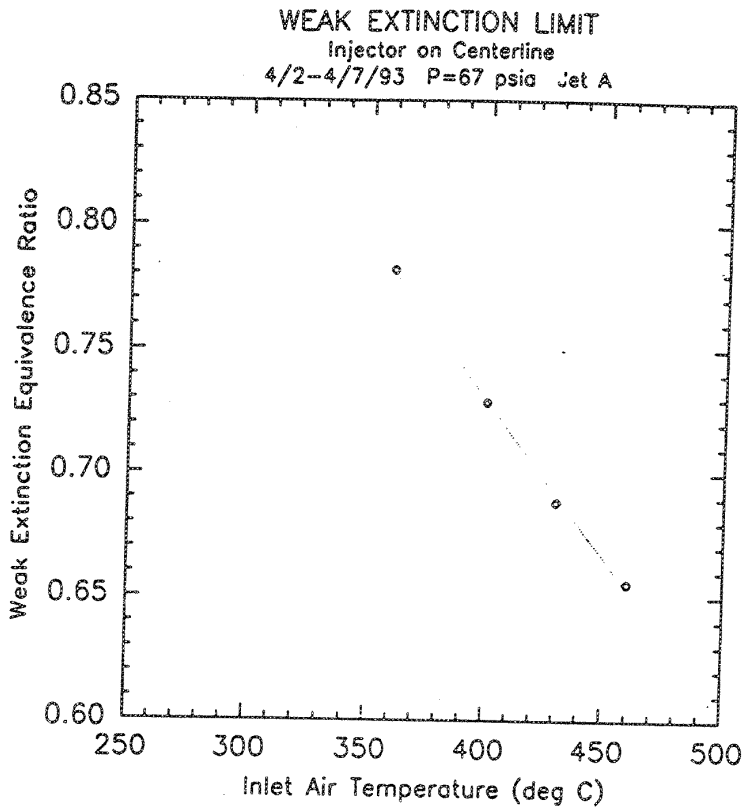

Figure 30

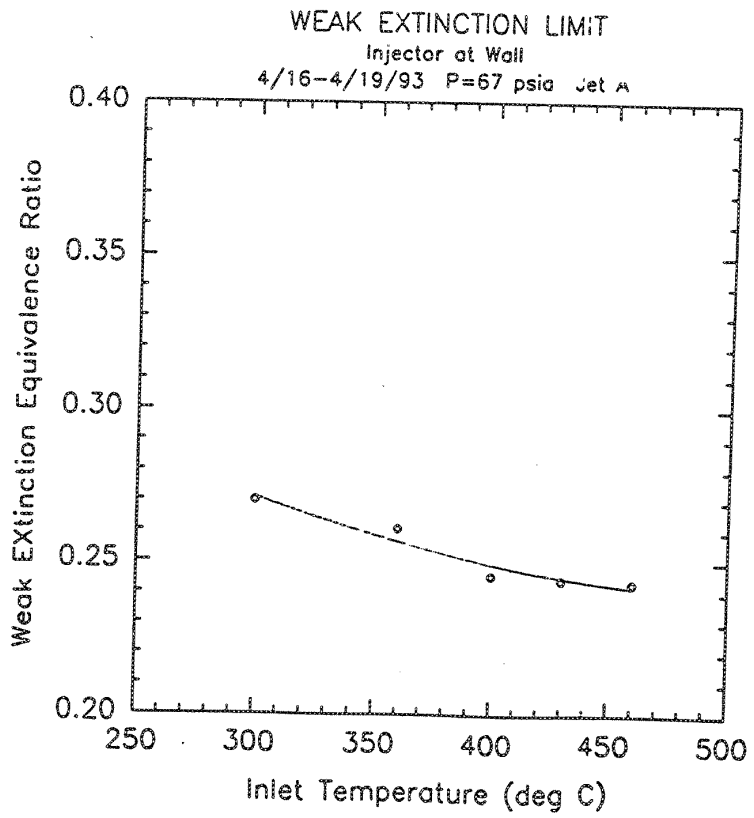

Figure 31

from 0.25 to 0.275, as seen in Figure 31. Also surprising is that these lean limits are so much lower than those for the centerline injection case. We know from the exciplex visualization results that the wall injection case yields a more uniform fuel-air mixture distribution, and it is generally accepted that improved mixing results in higher lean limit equivalence ratios.[7-12]

CONCLUSIONS

A high temperature, high pressure continuous flow combustion facility has been designed and built which has an optically accessible test section. The facility has been operated with a lean, prevaporized, premixed combustor design at a pressure of 4 atm, a velocity in the premixer of 100 m/s and over a range of inlet temperatures.

Under these test conditions, at an inlet temperature of 360°C (680°F), the degree of fuel vaporization and fuel-air mixing was qualitatively characterized using exciplex fluorescence for non-combusting flows. Two injection geometries were studied, both employing transverse injection through a hypo fuel-tube. Both had appreciable unvaporized fuel at the combustor inlet; center line injection produced a very non-uniform fuel distribution, while wall injection produced a relatively uniform distribution.

Under the same conditions, but over an inlet temperature range of 360-460° (680-860°F), lean limits and emissions were measured for combusting flows. Unexpectedly, the better mixed case had a significantly leaner limit, while NO_x emissions were comparable for the two fuel distributions. The more uniform case, however, was capable of lower NO_x emissions due to its ability to operate leaner.

REFERENCES

1. Melton, L. A. and Verdieck, J. F., "Vapor/Liquid Visualization in Fuel Sprays," *Twentieth Symposium (International) on Combustion*, The Combustion Institute, pp. 1283-1290, 1984.

2. Melton, L. A., "Spectrally Separated Fluorescence Emissions for Diesel Fuel Droplets and Vapor," *Applied Optics*, 22:14, pp. 2224-2226, July 15, 1983.

3. Rotunno, A. A., Winter, M., Dobbs, G. M., and Melton, L. A., "Direct Calibration Procedures for Exciplex-Based Vapor/Liquid Visualization for Fuel Sprays," *Combustion Science and Technology*, 71:247-261, 1990.

4. Melton, L. A., Murray, A. M., and Verdieck, J. F., "Laser Fluorescence Measurements for Fuel Sprays," *SPIE*, 'Remote Sensing,' 644, 1986.

5. Semerjian, H. G., Ball, I. C., and Vranos, A., "Pollutant Emissions from 'Partially' Mixed Turbulence Flames," *Seventeenth Symposium (International) on Combustion*, The Combustion Institute, pp. 679-687, 1979.

6. Lyons, V. J., "Fuel-Air Nonuniformity Effect on Nitric Oxide Emissions," AIAA 81-0327, *19th Aerospace Sciences Meeting*, Jan. 12-15, 1981.

7. Al Dabbagh, N. A. and Andrews, G. E., "The Influence of Premixed Combustion Flame Stabilizer Geometry on Flame Stability and Emissions," *J. of Engrg. for Power*, 103:749-758, October 1981.

8. Marek, C. J. and Papathakos, L. C., "Exhaust Emissions from a Premixing, Prevaporizing Flame Tube Using Liquid Jet A Fuel," NASATMS-3383, April 1976.

9. Roberts, P. B., Kubasco, A. J., and Sekas, N. J., "Development of a Low NO_x Lean Premixed Annular Combustor," ASME 81-GT-40, 1981.

10. Becker, B., Berenbrink, P., and Brandner, H., "Premixing Gas and Air to Reduce NO_x Emissions with Existing Proven Gas Turbine Combustion Chambers," ASME 86-GT-157, 1986.

11. Sattelmayer, Th., Felchlin, M. P., Hanman, J., Hellat, J., and Styner, D., "Second Generation Low-Emission Combustors for ABB Gas Turbines: Burner Development and Tests at Atmospheric Pressure," ASME 90-GT-162.

12. Washam, R. M., "Dry Low NO_x Combustion System for Utility Gas Turbines," ASME 83-JPGC-GT-13, 1983.

REPORT DOCUMENTATION PAGE

Form Approved
OMB No. 0704-0188

Public reporting burden for this collection of information is estimated to average 1 hour per response, including the time for reviewing instructions, searching existing data sources, gathering and maintaining the data needed, and completing and reviewing the collection of information. Send comments regarding this burden estimate or any other aspect of this collection of information, including suggestions for reducing this burden, to Washington Headquarters Services, Directorate for Information Operations and Reports, 1215 Jefferson Davis Highway, Suite 1204, Arlington, VA 22202-4302, and to the Office of Management and Budget, Paperwork Reduction Project (0704-0188), Washington, DC 20503.

1. AGENCY USE ONLY (*Leave blank*)

2. REPORT DATE
February 2005

3. REPORT TYPE AND DATES COVERED
Final Contractor Report

4. TITLE AND SUBTITLE

Low NO_x Combustor Development

5. FUNDING NUMBERS

WBS–22–714–09–46
NAS3–25951

6. AUTHOR(S)

J.A. Kastl, V. Herberling, and J.M. Matulaitis

7. PERFORMING ORGANIZATION NAME(S) AND ADDRESS(ES)

General Electric Aircraft Engines
Advanced Engineering Programs Department
One Neumann Way
Cincinnati, Ohio 45215–6301

8. PERFORMING ORGANIZATION REPORT NUMBER

E–14786

9. SPONSORING/MONITORING AGENCY NAME(S) AND ADDRESS(ES)

National Aeronautics and Space Administration
Washington, DC 20546–0001

10. SPONSORING/MONITORING AGENCY REPORT NUMBER

NASA CR—2005-213326

11. SUPPLEMENTARY NOTES

This research was originally published internally as HSR053 in August 1997. Responsible person, Diane Chapman, Ultra-Efficient Engine Technology Program Office, NASA Glenn Research Center, organization code PA, 216–433–2309.

12a. DISTRIBUTION/AVAILABILITY STATEMENT

Unclassified - Unlimited
Subject Categories: 01, 05, and 07 Distribution: Nonstandard

Available electronically at http://gltrs.grc.nasa.gov

This publication is available from the NASA Center for AeroSpace Information, 301–621–0390.

12b. DISTRIBUTION CODE

13. ABSTRACT ***(Maximum 200 words)***

The goal of these efforts was the development of an ultra-low emissions, lean-burn combustor for the High Speed Civil Transport. The HSCT Mach 2.4 FLADE C1 Cycle was selected as the baseline engine cycle. A preliminary compilation of performance requirements for the HSCT combustor system was developed. The emissions goals of the program, baseline engine cycle, and standard combustor performance requirements were considered in developing the compilation of performance requirements. Seven combustor system designs were developed. The development of these system designs was facilitated by the use of spreadsheet-type models which predicted performance of the combustor systems over the entire flight envelope of the HSCT. A chemical kinetic model was developed for an LPP combustor and employed to study NO_x formation kinetics, and CO burnout. These predictions helped to define the combustor residence time. Five fuel-air mixer concepts were analyzed for use in the combustor system designs. One of the seven system designs, one using the Swirl-Jet and Cyclone Swirler fuel-air mixers, was selected for a preliminary mechanical design study.

14. SUBJECT TERMS

High speed civil transport; Low emissions; Lean-burn combustor; Fuel-air mixers

15. NUMBER OF PAGES
260

16. PRICE CODE

17. SECURITY CLASSIFICATION OF REPORT	18. SECURITY CLASSIFICATION OF THIS PAGE	19. SECURITY CLASSIFICATION OF ABSTRACT	20. LIMITATION OF ABSTRACT
Unclassified	Unclassified	Unclassified	